SUB-MOLECULAR MECHANISM OF GENETIC EPILEPSY

EDITED BY: Weiping Liao, Qian Chen, Yuwu Jiang and Xiaorong Liu
PUBLISHED IN: Frontiers in Molecular Neuroscience

frontiers Research Topics

frontiers

ISSN 1664-8714
ISBN 978-2-88976-863-9
DOI 10.3389/978-2-88976-863-9

About Frontiers

Frontiers is more than just an open-access publisher of scholarly articles: it is a pioneering approach to the world of academia, radically improving the way scholarly research is managed. The grand vision of Frontiers is a world where all people have an equal opportunity to seek, share and generate knowledge. Frontiers provides immediate and permanent online open access to all its publications, but this alone is not enough to realize our grand goals.

Frontiers Journal Series

The Frontiers Journal Series is a multi-tier and interdisciplinary set of open-access, online journals, promising a paradigm shift from the current review, selection and dissemination processes in academic publishing. All Frontiers journals are driven by researchers for researchers; therefore, they constitute a service to the scholarly community. At the same time, the Frontiers Journal Series operates on a revolutionary invention, the tiered publishing system, initially addressing specific communities of scholars, and gradually climbing up to broader public understanding, thus serving the interests of the lay society, too.

Dedication to Quality

Each Frontiers article is a landmark of the highest quality, thanks to genuinely collaborative interactions between authors and review editors, who include some of the world's best academicians. Research must be certified by peers before entering a stream of knowledge that may eventually reach the public - and shape society; therefore, Frontiers only applies the most rigorous and unbiased reviews.
Frontiers revolutionizes research publishing by freely delivering the most outstanding research, evaluated with no bias from both the academic and social point of view. By applying the most advanced information technologies, Frontiers is catapulting scholarly publishing into a new generation.

What are Frontiers Research Topics?

Frontiers Research Topics are very popular trademarks of the Frontiers Journals Series: they are collections of at least ten articles, all centered on a particular subject. With their unique mix of varied contributions from Original Research to Review Articles, Frontiers Research Topics unify the most influential researchers, the latest key findings and historical advances in a hot research area! Find out more on how to host your own Frontiers Research Topic or contribute to one as an author by contacting the Frontiers Editorial Office: frontiersin.org/about/contact

SUB-MOLECULAR MECHANISM OF GENETIC EPILEPSY

Topic Editors:
Weiping Liao, Second Affiliated Hospital of Guangzhou Medical University, China
Qian Chen, McGovern Institute for Brain Research, School of Science, Massachusetts Institute of Technology, United States
Yuwu Jiang, First Hospital, Peking University, China
Xiaorong Liu, Guangzhou Medical University, China

Citation: Liao, W., Chen, Q., Jiang, Y., Liu, X., eds. (2022). Sub-molecular Mechanism of Genetic Epilepsy. Lausanne: Frontiers Media SA.
doi: 10.3389/978-2-88976-863-9

Table of Contents

frontiers | Frontiers in Molecular Neuroscience

TYPE Editorial
PUBLISHED 26 July 2022
DOI 10.3389/fnmol.2022.958747

OPEN ACCESS

EDITED AND REVIEWED BY
Jean-Marc Taymans,
Institut National de la Santé et de la Recherche Médicale, France

*CORRESPONDENCE
Wei-Ping Liao
wpliao@163.net

SPECIALTY SECTION
This article was submitted to Molecular Signalling and Pathways, a section of the journal Frontiers in Molecular Neuroscience

RECEIVED 01 June 2022
ACCEPTED 06 June 2022
PUBLISHED 26 July 2022

CITATION
Liao W-P, Chen Q, Jiang Y-W, Luo S and Liu X-R (2022) Editorial: Sub-molecular mechanism of genetic epilepsy.
Front. Mol. Neurosci. 15:958747.
doi: 10.3389/fnmol.2022.958747

Editorial: Sub-molecular mechanism of genetic epilepsy

Wei-Ping Liao[1,2]*, Qian Chen[3], Yu-Wu Jiang[4], Sheng Luo[1,2] and Xiao-Rong Liu[1,2]

[1]Department of Neurology, Institute of Neuroscience, The Second Affiliated Hospital of Guangzhou Medical University, Guangzhou, China, [2]Key Laboratory of Neurogenetics and Channelopathies of Guangdong Province, Ministry of Education of China, Guangzhou, China, [3]Department of Brain and Cognitive Sciences, McGovern Institute for Brain Research, Massachusetts Institute of Technology, Cambridge, MA, United States, [4]Department of Pediatrics, Peking University First Hospital, Peking, China

KEYWORDS

genetic epilepsy, sub-molecular mechanism, genotype, phenotypic variation, functional domain

Editorial on the Research Topic
Sub-molecular mechanism of genetic epilepsy

Proteins are the essential functional molecule in living organisms. A protein is featured by finely structured domains, which are encoded by genetic sequences. Variants in a gene potentially result in functional alteration of the protein and thus cause diseases. From the perspective of molecular structure, the different domains of a protein play distinct roles. Variants of different locations are thus potentially associated with various damaging effects and subsequently lead to phenotypical variation. Similarly, the bio-physical feature of the substituted amino acids caused by variants is also a determinant of the damaging effect. Such submolecular implication would be a critical factor in determining the pathogenicity of variants.

More than 4,000 genes have been associated with human diseases (https://omim.org/). A gene could be associated with a distinct phenotype, but in the majority of circumstances, it is associated with a spectrum of phenotypes that are varied in severity or other aspects, for which the underlying mechanism is mostly unknown. Previously, sub-molecular implications have been demonstrated to be a determinant of phenotypical variation in several molecules, such as sodium channel Nav1.1 (*SCN1A*) (Meng et al., 2015; Tang et al., 2020), tyrosine 3-monooxygenase/tryptophan 5-monooxygenase activation protein gamma (*YWHAG*) (Ye et al., 2021), and disheveled Egl-10 and pleckstrin domain-containing protein 5 (*DEPDC5*) (Liu et al., 2020).

The present Research Topic is dedicated to exploring the *Sub-molecular Mechanism of Genetic Epilepsy* and providing novel perspectives to understanding of the mechanisms underlying the phenotypical variation of genetic diseases. The sub-molecular implications of genetic variants are disclosed in terms of six aspects in this collection.

Functional domain and sub-molecular implication

Shu et al. identified four *de novo* missense *MAST3* variants from four patients with heterotypic neurodevelopmental disorders (NDD), including two with intellectual disability (ID) and epilepsy and two with ID and autism spectrum disorders (ASD). They created a *mast3a/b* knockout zebrafish model and observed abnormal morphology of the central nervous system. The results support the possibility that *MAST3* is a novel gene associated with NDD. Additionally, ASD-related missense variants presented higher frequencies in the DUF domain, while epilepsy-related variants exhibited higher frequencies in the STK domain, suggesting a sub-regional effect.

Bian et al. identified six hemizygous missense *SHROOM4* variants from six cases with epilepsy without ID. The *SHROOM4* gene was previously reported in patients with the Stocco dos Santos type X-linked syndromic intellectual developmental disorder (SDSX) (Hagens et al., 2006). The SDSX-related variants reported were mostly destructive or duplicative variants, while the epilepsy-related variants were all missense variants located around the N-terminal PDZ domain and the C-terminal ASD2 domain, indicating a molecular sub-regional effect.

Zou et al. identified five hemizygous missense *AFF2* mutations from five males with partial epilepsy and antecedent febrile seizures without intellectual disability or other developmental abnormalities. The *AFF2* gene is previously reported to be associated with X-linked intellectual developmental disorder 109 and ASD (Stettner et al., 2011). The ID-associated *AFF2* mutations were mostly genomic rearrangements and CCG repeats expansion mutations that caused gene silencing, whereas the mutations associated with epilepsy or ASD were all missense, suggesting the correlation between the phenotype and variant type. Furthermore, epilepsy-relative *AFF2* variants fell into the regions from N-terminal to the nuclear localization signal 1 (NLS1), while ASD-associated missense mutations were located in the regions from NLS1 to C-terminal, suggesting a sub-region effect.

Li et al. identified 12 *CACNA1A* variants and analyzed the correlation between genotype and phenotype. This study suggested that *CACNA1A* mutations were potentially associated with a spectrum of epileptic phenotypes, ranging from mild absence epilepsy to severe developmental and epileptic encephalopathy (DEE). Further analysis revealed that: 1) episodic ataxia type 2 had a tendency of higher frequency of null variants than epilepsies; 2) the missense variants in severe epileptic phenotypes were more frequently located in the pore region than those in milder epileptic phenotypes; and 3) *de novo* variants in epilepsy were more frequently associated with ID.

A functional molecular unit may be a single molecule encoded by a gene or a molecular complex consisting of several proteins encoded by different genes. Previously, the A subunit of the V1 domain of V-ATPase encoded by *ATP6V1A* was associated with DEE-93 (Fassio et al., 2018). The *ATP6V0C* gene encoded the C subunit of the V0 domain of V-ATPase. Tian Y. et al. identified *ATP6V0C* as a novel causative gene for febrile seizures (FS) and epilepsy with febrile seizures plus (EFS+), providing a novel perspective of the functional domain and sub-molecular implication.

Substituted amino acid and sub-molecular implication

Su et al. focus on the relationship between the nature of substituted amino acids and functional alteration. They identified a novel missense *SCN1A* variant (c.4868A>C/p.E1613A) in the extracellular S3-S4 loop of Nav1.1 from two cases with epilepsy. Functional studies were conducted on six mutants with all possible substitutions in the residue E1623. This study suggested the critical role of the S3–S4 loop in sodium channel function. Analysis of the correlation between the residue properties and electrophysiological alterations demonstrated that hydrophilicity of the side-chain at E1623 was potentially a crucial contributor to voltage-dependent kinetics, whereas the contributor to the channel conductance, which is closely associated with epileptogenesis, remains undetermined.

Isoforms and sub-molecular implication

Zhou et al. identified 12 *ADGRV1* variants in nine unrelated cases with FS or EFS+. Previously, the *ADGRV1* gene was reported to be associated with Usher syndrome (Weston et al., 2004). The authors reviewed all *ADGRV1* variants and analyzed the genotype-phenotype correlations of the *ADGRV1* variants in epilepsy and audio-visual disorders. This study showed that the epilepsy-related variants were monoallelic, missense, and mainly located at the CalX-β domain. Furthermore, the epilepsy-related variants mostly affected isoforms VLGR1b/1c, while the audio-visual-related variants were mainly affected isoforms VLGR1a, suggesting a potential role of isoform in phenotype variation.

Monoallelic and biallelic variants

Wang et al. identified eight pairs of compound heterozygous missense *PKD1* variants in eight patients with FS or EFS+. Dominant *PKD1* variants were reported to be associated with polycystic kidney disease (Roelfsema et al., 1997). Further analysis suggested that monoallelic mutations with haploinsufficiency of

PKD1 were potentially associated with kidney disease, compound heterozygotes with superimposed effects of two missense mutations were associated with epilepsy; whereas the homozygotes with complete loss of *PKD1* would be embryonically lethal, suggesting monoallelic variant/biallelic variant was potentially a factor in determining phenotypical variation.

Locations of the two variants in a pair of compound heterozygous variant

Luo et al. identified six pairs of compound heterozygous missense *LAMA5* variants in six unrelated infants with partial epilepsy and spasms. This article identified *LAMA5* as a novel potential epilepsy gene. Interestingly, among the biallelic variants in cases with mild phenotype, two variants of each pair were located in different structural domains or domains/links, whereas in the cases with spasms (the severer phenotype), the biallelic variants were constituted by two variants in the identical functional domains, potentially suggesting a novel perspective on sub-molecular mechanisms.

Specific genotype and sub-molecular implication

Wang et al. identified six in-frame deletion variants in *SCN1A* and performed further functional analysis. The experiments showed the complete loss of function caused by the six in-frame deletion variants, emphasizing the damaging effect of in-frame deletion variants.

Truncated C-terminal region *MN1* variants caused *MN1* C-terminal truncation (MCTT) syndrome (Mak et al., 2020). Tian Q. et al. reported a novel C-terminal null *MN1* variant (p.L1245fs) in a patient with mild developmental delay without structural brain abnormalities, expanding the clinical and genetic spectrum of MCTT.

In conclusion, this Research Topic provides novel perspectives on the mechanisms underlying phenotypical variation. Phenotypical heterogeneity is common in genetic disorders. We advocate further studies on the submolecular mechanism of genetic diseases beyond epilepsy, toward setting a submolecular stage of medicine.

Author contributions

All authors listed have made a substantial, direct, and intellectual contribution to the work and approved it for publication.

Acknowledgments

The authors would like to thank all of the authors, reviewers, and independent editors for their valuable contributions to this Research Topic.

Conflict of interest

The authors declare that the research was conducted in the absence of any commercial or financial relationships that could be construed as a potential conflict of interest.

Publisher's note

References

Fassio, A., Esposito, A., Kato, M., Saitsu, H., Mei, D., Marini, C., et al. (2018). De novo mutations of the ATP6V1A gene cause developmental encephalopathy with epilepsy. *Brain* 141, 1703–1718. doi: 10.1093/brain/awy092

Hagens, O., Dubos, A., Abidi, F., Barbi, G., Van Zutven, L., Hoeltzenbein, M., et al. (2006). Disruptions of the novel KIAA1202 gene are associated with X-linked mental retardation. *Hum. Genet.* 118, 578–590. doi: 10.1007/s00439-005-0072-2

Liu, L., Chen, Z.R., Xu, H.Q., Liu, D.T., Mao, Y., Liu, H.K., et al. (2020). DEPDC5 variants associated malformations of cortical development and focal epilepsy with febrile seizure plus/febrile seizures: the role of molecular sub-regional effect. *Front. Neurosci.* 14, 821. doi: 10.3389/fnins.2020.00821

Mak, C.C.Y., Doherty, D., Lin, A.E., Vegas, N., Cho, M.T., Viot, G., et al. (2020). MN1 C-terminal truncation syndrome is a novel neurodevelopmental and craniofacial disorder with partial rhombencephalosynapsis. *Brain* 143, 55–68. doi: 10.1093/brain/awz379

Meng, H., Xu, H.Q., Yu, L., Lin, G.W., He, N., Su, T., et al. (2015). The SCN1A mutation database: updating information and analysis of the relationships among genotype, functional alteration, and phenotype. *Hum. Mutat.* 36, 573–580. doi: 10.1002/humu.22782

Roelfsema, J.H., Spruit, L., Saris, J.J., Chang, P., Pirson, Y., Van Ommen, G.J., et al. (1997). Mutation detection in the repeated part of the PKD1 gene. *Am. J. Hum. Genet.* 61, 1044–1052. doi: 10.1086/301600

Stettner, G.M., Shoukier, M., Hoger, C., Brockmann, K., and Auber, B. (2011). Familial intellectual disability and autistic behavior caused by a small FMR2 gene deletion. *Am. J. Med. Genet. A* 155A, 2003–2007. doi: 10.1002/ajmg.a.34122

Tang, B., Li, B., Gao, L.D., He, N., Liu, X.R., Long, Y.S., et al. (2020). Optimization of in silico tools for predicting genetic variants: individualizing for genes with molecular sub-regional stratification. *Brief. Bioinform.* 21, 1776–1786. doi: 10.1093/bib/bbz115

Weston, M.D., Luijendijk, M.W., Humphrey, K.D., Moller, C., and Kimberling, W.J. (2004). Mutations in the VLGR1 gene implicate G-protein signaling in the pathogenesis of Usher syndrome type II. *Am. J. Hum. Genet.* 74, 357–366. doi: 10.1086/381685

Ye, X.G., Liu, Z.G., Wang, J., Dai, J.M., Qiao, P.X., Gao, P.M., et al. (2021). YWHAG mutations cause childhood myoclonic epilepsy and febrile seizures: molecular sub-regional effect and mechanism. *Front. Genet.* 12, 632466. doi: 10.3389/fgene.2021.632466

frontiers in Molecular Neuroscience

BRIEF RESEARCH REPORT
published: 16 December 2021
doi: 10.3389/fnmol.2021.789778

MN1 Neurodevelopmental Disease-Atypical Phenotype Due to a Novel Frameshift Variant in the *MN1* Gene

Qi Tian[1,2,3†], Li Shu[1,2†], Pu Zhang[3†], Ting Zeng[4], Yang Cao[5], Hui Xi[1], Ying Peng[1], Yaqin Wang[6], Xiao Mao[1,2*] and Hua Wang[1,2*]*

[1] Department of Medical Genetics, Maternal and Child Health Hospital of Hunan Province, Changsha, China, [2] National Health Commission Key Laboratory of Birth Defects Research, Prevention and Treatment, Hunan Provincial Maternal and Child Health Care Hospital, Changsha, China, [3] Department of Obstetrics and Gynecology, Maternal and Child Health Hospital of Hunan Province, Changsha, China, [4] The Ministry of Education and Science, Maternal and Child Health Hospital of Hunan Province, Changsha, China, [5] Department of Radiology, Chenzhou First People's Hospital, Chenzhou, China, [6] Health Management Center, The Third Xiangya Hospital, Central South University, Changsha, China

OPEN ACCESS

Edited by:
Weiping Liao,
Second Affiliated Hospital of Guangzhou Medical University, China

Reviewed by:
Junjiang Fu,
Southwest Medical University, China
Tongda Zhang,
BGI-Shenzhen, China

***Correspondence:**
Yaqin Wang
wangy11@csu.edu.cn
Xiao Mao
gbtechies@outlook.com
Hua Wang
wanghua_213@hotmail.com

†These authors share first authorship

Specialty section:
This article was submitted to Molecular Signalling and Pathways, a section of the journal Frontiers in Molecular Neuroscience

Received: 05 October 2021
Accepted: 19 November 2021
Published: 16 December 2021

Citation:
Tian Q, Shu L, Zhang P, Zeng T, Cao Y, Xi H, Peng Y, Wang Y, Mao X and Wang H (2021) MN1 Neurodevelopmental Disease-Atypical Phenotype Due to a Novel Frameshift Variant in the MN1 Gene. Front. Mol. Neurosci. 14:789778. doi: 10.3389/fnmol.2021.789778

Background: *MN1* C-terminal truncation (MCTT) syndrome is caused by variants in the C-terminal region of *MN1*, which were first described in 2020. The clinical features of MCTT syndrome includes severe neurodevelopmental and brain abnormalities. We reported on a patient who carried the *MN1* variant in the C-terminal region with mild developmental delay and normal brain magnetic resonance image (MRI).

Methods: Detailed clinical information was collected in the pedigree. Whole-exome sequencing (WES) accompanied with Sanger sequencing validation were performed. A functional study based on HEK239T cells was performed.

Results: A *de novo* heterozygous c.3734delT: p.L1245fs variant was detected. HEK239T cells transinfected with the *de novo* variant showed decreased proliferation, enhanced apoptotic rate, and MN1 nuclear aggregation.

Conclusion: Our study expended the clinical and genetic spectrum of MCTT which contributes to the genetic counseling of the *MN1* gene.

Keywords: *MN1*, *MN1* C-terminal truncation (MCTT) syndrome, neurodevelopmental outcome, developmental delay, whole-exome sequencing

INTRODUCTION

MN1 (MIM 156100) gene was initially reported to be a tumor suppressor gene associated with meningioma and myeloproliferative diseases. Mak et al. (2020) first described the *MN1* C-terminal truncation (MCTT) syndrome as causing craniofacial symptoms and severe neurodevelopmental abnormalities and brain abnormalities (Buijs et al., 1995; Lekanne Deprez et al., 1995). Another research group in the same year reported three probands with *MN1* C-terminal variants who showed consistent clinical features (Vegas et al., 2021).

There is growing evidence of genotype–phenotype correlations of *MN1*-related clinical syndrome. Different from *MN1* C-terminal variants, *MN1* N-terminal variants were reported to cause less severe clinical syndromes. Patients with variants located in the N-terminal region of *MN1* showed speech defects without significant intellectual disability, mild conductive hearing loss, and non-specific facial features (Shu et al., 2021).

Till now, atypical clinical presentations of *MN1*-related clinical syndrome caused by variants in C-terminal region have never been described. In our study, we first presented a *MN1* C-terminal frameshift deletion variant that caused mild global developmental delay, cleft palate, and dysmorphic facial features but with no hearing loss or brain magnetic resonance image (MRI) abnormalities.

MATERIALS AND METHODS

Genetic Investigation

Genomic DNA from peripheral blood leukocytes of the trio were extracted by Qiagen DNA Blood Midi/Mini Kit (Qiagen GmbH, Hilden, Germany). Data were processed preliminarily according to the protocols of whole-exome sequencing (WES) (Ulintz et al., 2019). In detail, DNA was sheared by sonication (Biorupter UCD-200, Diagenode) to approximately 200 bp. DNA fragments were repaired at the end. The sequencing adaptors were used to collect DNA fragments and the fragments (approximately 320 bp) were collected by XP beads. After amplification, the DNA fragments were captured by IDT's xGen Exome Research Panel (Integrated DNA Technologies, San Diego, CA, United States) according to the protocol. The products were eluted and collected. DNA was then amplified and purified by PCR. The enrichment of libraries was tested by qPCR, and size distribution and concentration were determined by Agilent Bioanalyzer 2100 (Agilent Technologies, Santa Clara, CA, United States). To sequence the genomic DNA of the family, WES was performed on the Illumina HiSeq 2500 system with an average coverage depth of 100× of the variants. Raw image files were processed using CASAVA v1.82 for base calling and raw data generating (Markus et al., 2020). Variants were then annotated using ANNOVAR (Wang et al., 2010).

The variants were initially filtered following HGMD and ACMG guidelines. Disease-causing mutations (DMs) and probable/possible pathological mutation (DM) in the HGMD database (Prof. version 2019.1), and pathogenic (P) and likely pathogenic (LP) variants were interpreted by ACMG guidelines. The variants were then filtered according to allele frequency, variant type, and mode of inheritance. Variants with minor allele frequencies (MAFs) <0.1%, variant depth of coverage ≥20, and alteration base depth of coverage ≥4 were chosen for further analyses. The remaining variants were further filtered according to variant type and inheritance model of the associated disease. Sanger sequencing was performed on the DNA of the proband's parents to validate the mutation found in WES.

MN1 Subcellular Localization and Aggregation in HEK293T Cells

To create N-terminal GFP-fused human *MN1* expression vector, the *MN1* (GenBank: NM_002430.3) open-reading frame

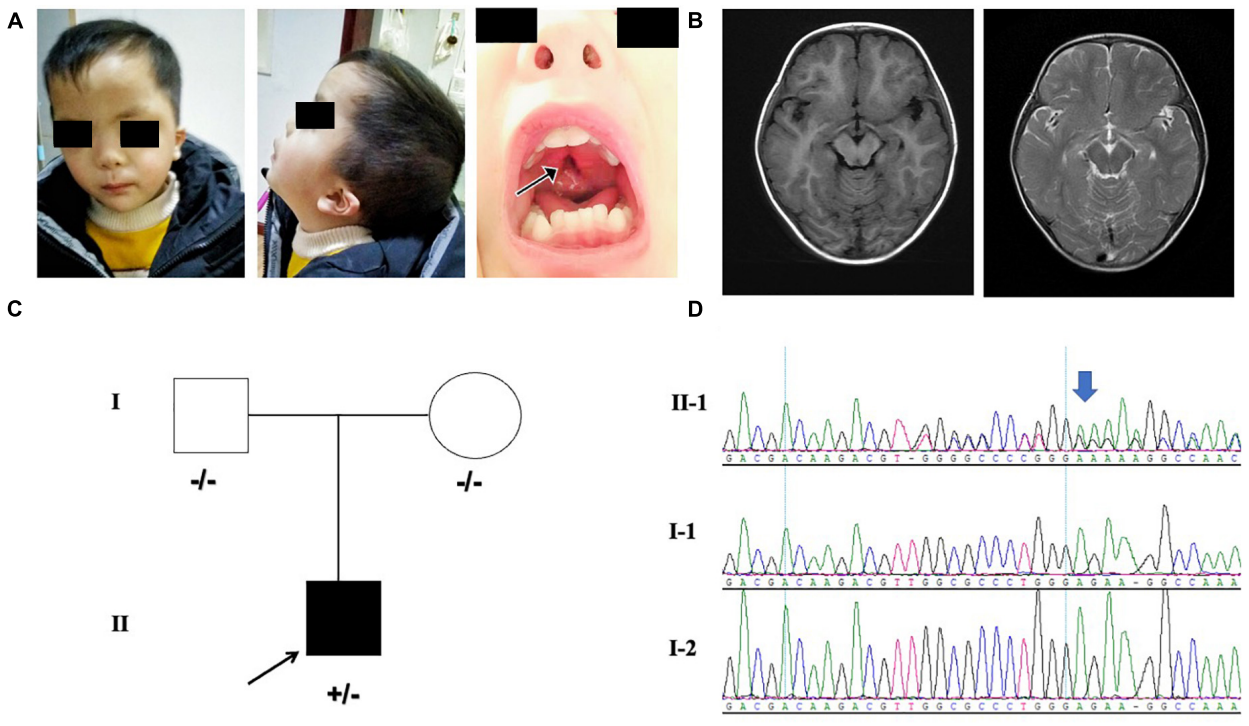

FIGURE 1 | (A) Facial features of the proband. The arrows point to the cleft palate. **(B)** MRI indicating the normal brain tissue and the protruding occipital bone (image on the left is axial T1-weighted; image on the right is axial T2-weighted) of the proband at 18-months-old. **(C)** Pedigree with *MN1* variant. Individuals with heterozygous variants are indicated by plus/minus (+/–) symbols and individuals without the variant are labeled as minus/minus (–/–) symbols. **(D)** Sanger sequencing results of *MN1* frameshift variant in family members is presented on the right.

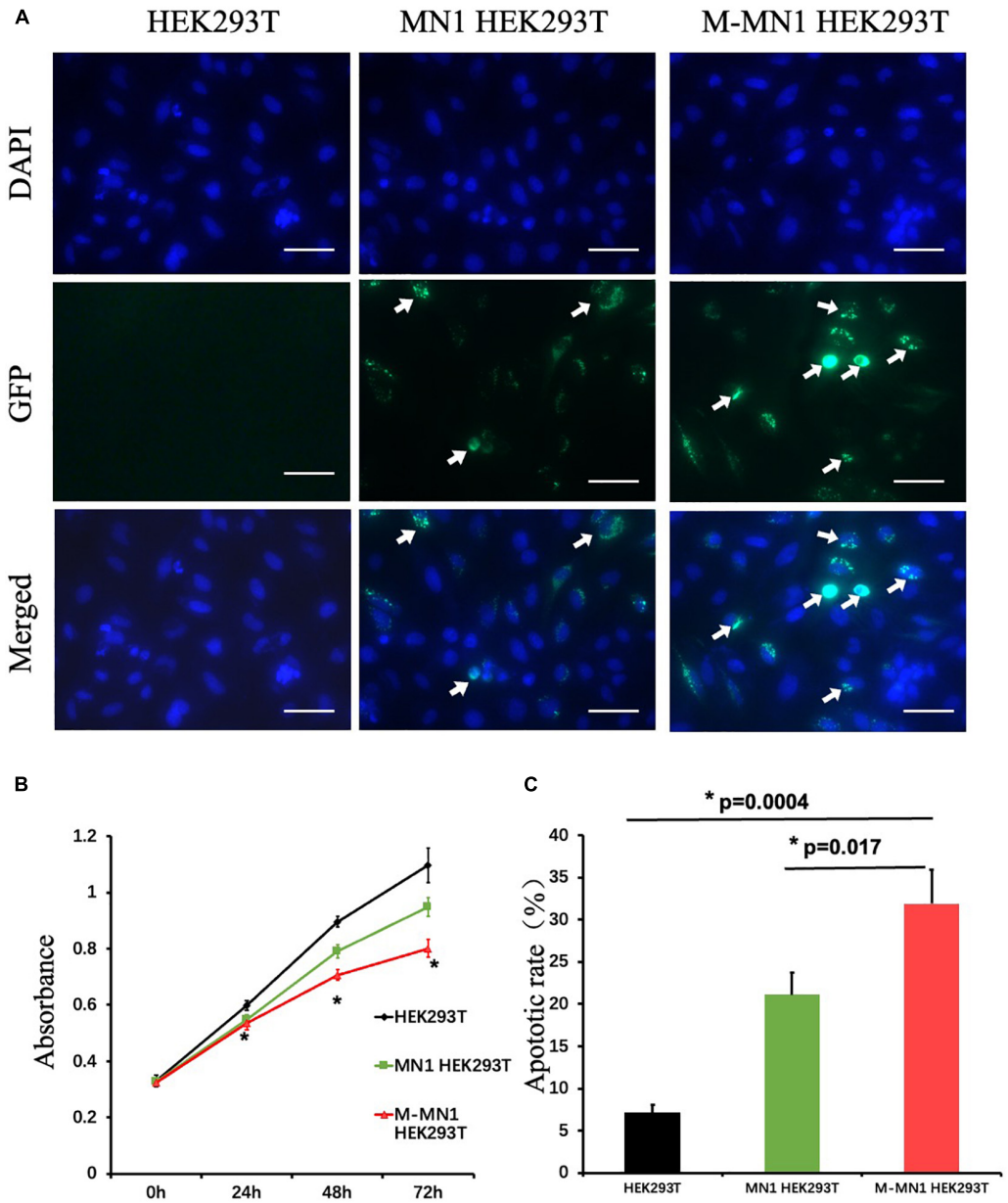

FIGURE 2 | (A) Immunofluorescence of GFP-fused MN1 and M-MN1 showing the subcellular localization and aggregation of MN1 proteins in HEK239T cells. The arrows pointed out the represented MN1 fluorescence. Scale bars represent 50 mm. **(B)** Cell proliferation at 0, 24, 48, and 72 h after transinfection. The cell numbers indicated by the absorbance at 450 nm were significantly lower in transinfected groups (*t*-test, $p = 0.017$). And the M-MN1 group had the lowest absorbance reading across all time points; at 48 and 72 h the readings of M-MN1 group were significantly lower compared to MN1 group (*t*-test, $p = 0.009$, 0.004, respectively). **(C)** Cell apoptotic rate was significantly higher in M-MN1 group compared with HEK239T and MN1 group. $^*p \leq 0.05$.

(ORF) was incorporated into DEST53 *via* the Gateway cloning system (Thermo Fisher). The mutant ORF and *MN1* was amplified with a human cDNA library (Clontech). The mutant *MN1* (M-MN1) was created by a KOD-plus-Mutagenesis Kit (TOYOBO). ViaFect Transfection Reagent (Promega) was used to transfect construct (500 ng each) into HEK239T cells. After 48 h of transfection, the cells were fixed with 2% paraformaldehyde, washed with PBS, stained with DAPI (Vector Laboratories), and then mounted onto slides. The sub-cellular localization and aggregation of MN1/M-MN1 were observed under confocal microscopy.

Cell Proliferation and Apoptosis Assay

Cell Proliferation Assay was carried out with Cell Counting Kit-8 (CCK-8, Dojindo Laboratories, Kumamoto, Japan) according to the manufacturer's protocol (Vegas et al., 2021). Cell Apoptosis Assay Kit (Solarbio, CA1020) was used to detect apoptotic rate (Xiao et al., 2019).

TABLE 1 | The clinical comparison of our patient and the patients reported previously.

Dysmorphisms	The reported patients	Our patient
Cranial shape defects	+	+
Typical facial defects	+	+
Hearing loss	+	−
Developmental delay	+	+
Feeding difficulty	+	+
Hypotonia	+	+
Brain MRI abnormality	+	−

RESULTS

Case Description

Our patient was the first child born to the non-consanguineous Chinese parents. The proband was a 3 year and 5-month-old male born at full term from a normal pregnancy. The birth weight was 2800 g and Apgar score was 9/10. The patient presented difficulties in breast feeding. He lifted his head at 7 months old and could sit with support at the age of 8 months. He stared to walk when he was 1 year and 7 months old. He had no seizures and language development delay was observed. Physical examination showed that he had facial dysmorphism, hypertelorism, auricle deformation, upper palate cleft, plagiocephaly, protruding occipital bone, and hypotonia (**Figure 1A**). Behavioral observation audiometry and auditory brainstem response were normal. The brain MRI was normal (**Figure 1B**). The developmental milestones were presented in weight/length-for-age percentiles (**Supplementary Figure 1**). A *de novo MN1* gene frameshift variant NM_002430.2: c.3734delT: p.L1245fs (chr22:28192798-28192798) was identified and proved by sanger sequencing in the pedigree (**Figures 1C,D**). The table showing the follow-up timeline is available in **Supplementary Table 1**.

Functional Study for *MN1* Variant in HEK239T Cells

GFP-fused wild-type and mutated-MN1 proteins were expressed in HEK239T cells. Both wild-type MN1 and M-MN1 were found to be aggregated and localized in the nuclear of HEK239T cells (**Figure 2A**). Intensity of M-MN1 aggregates were significantly higher than the wild-type MN1 (t-test, $p = 0.017$) (**Figure 2B**). Cell apoptotic rate were statistically higher in M-MN1 group compared with HEK239T and wild-type group (t-test, $p = 0.009$, 0.004, respectively) (**Figure 2C**).

DISCUSSION

The clinical characteristics of MCTT syndrome included craniofacial features, hearing loss, severe neurodevelopmental abnormalities, and abnormal brain MRI (Vegas et al., 2021). In our study, we identified a *de novo* frameshift deletion variant located in C-terminal of *MN1* gene in a pedigree. Our proband presented a few atypical clinical manifestations different from the reported ones (Mak et al., 2020; Miyake et al., 2020). Our patients did not show cranial shape defects, hearing loss, or brain MRI abnormalities (**Table 1**). Our patient provided evidence for *MN1* MCTT syndrome and the different clinical features of our patient may help to refine the clinical spectrum of *MN1* C-terminal variants' related syndromes.

MN1 C-terminal heterozygous variants exert a dominant-negative or gain-of-function effect on the MN1 protein (Mak et al., 2020). The variant led to increased protein MN1 stability and enhanced MN1 nuclear aggregation, which were related to the MCTT syndrome (Miyake et al., 2020). In our study, the variant was tested by functional study and the abnormal cellular functions were detected in M-MN1 group. Combining the functional studies with the genetic findings, we proved that our MN1 variant was the cause of the diseases. Further research on how different *MN1* variants lead to various clinical manifestations is needed.

Some research has revealed the molecular functions of MN1 protein. *MN1* encodes a developmentally expressed transcriptional co-regulator (Liu et al., 2008). MN1 protein may act as a transcriptional cofactor and the mutant protein could impair downstream binding transcription factors, such as Cbf-β and Runx2 (Meester-Smoor et al., 2005; Miyake et al., 2020). The clinical heterogeneities of *MN1* C-terminal variants may be due to the regulation of various corresponding downstream target genes (Lai et al., 2014). Our present study contributes to expanding the genetic and clinical spectrum of *MN1* and aid in precise genetic counseling in the future.

DATA AVAILABILITY STATEMENT

The data that support the findings of this study are available from the corresponding author (XM), upon reasonable request. Requests to access these datasets should be directed to XM (gbtechies@outlook.com).

ETHICS STATEMENT

The studies involving human participants were reviewed and approved by the Ethics Committee of the Maternal and Child Health Hospital of Hunan Province (2020-S003). Written informed consent to participate in this study was provided by the participants' legal guardian/next of kin. Written informed consent was obtained from the minor(s)' legal guardian/next of kin for the publication of any potentially identifiable images or data included in this article.

AUTHOR CONTRIBUTIONS

XM, HW, and YW designed the research. QT, LS, and TZ interpreted the data and wrote the manuscript. QT, LS, PZ, YC, HX, and YP did the follow-up study and collected, evaluated

the clinical, and genetic evidence. TZ revised the manuscript. All authors read and approved the final manuscript.

FUNDING

This work was supported by the National Natural Science Foundation of China (Nos. 81801136 and 32100162), Major Scientific and Technological Projects for Collaborative Prevention and Control of Birth Defects in Hunan Province (Nos. 2019SK1010, 2019SK1012, and 2019SK1014), the National Key R&D Program of China (No. 2019YFC1005100), the China Postdoctoral Science Foundation (No. 2019M662804), the Changsha Municipal Natural Science Foundation (No. kq2007048), Rui Xin Project of Maternal and Child Health Hospital of Hunan Province, and the Natural Science Foundation of Hunan Province (No. 2020JJ4854).

ACKNOWLEDGMENTS

We thank the families and clinical staff for participation in this study.

SUPPLEMENTARY MATERIAL

The Supplementary Material for this article can be found online at: https://www.frontiersin.org/articles/10.3389/fnmol.2021.789778/full#supplementary-material

REFERENCES

Buijs, A., Sherr, S., van Baal, S., van Bezouw, S., van der Plas, D., Geurts, et al. (1995). Translocation (12;22) (p13;q11) in myeloproliferative disorders results in fusion of the ETS-like TEL gene on 12p13 to the MN1 gene on 22q11. *Oncogene* 10, 1511–1519.

Lai, C. K., Moon, Y., Kuchenbauer, F., Starzcynowski, D. T., Argiropoulos, B., Yung, E., et al. (2014). Cell fate decisions in malignant hematopoiesis: leukemia phenotype is determined by distinct functional domains of the MN1 oncogene. *PLoS One* 9:e112671. doi: 10.1371/journal.pone.0112671

Lekanne Deprez, R. H., Riegman, P. H., Groen, N. A., Warringa, U. L., van Biezen, N. A., Molijn, A. C., et al. (1995). Cloning and characterization of MN1, a gene from chromosome 22q11, which is disrupted by a balanced translocation in a meningioma. *Oncogene* 10, 1521–1528.

Liu, W., Lan, Y., Pauws, E., Meester-Smoor, M. A., Stanier, P., Zwarthoff, E. C., et al. (2008). The Mn1 transcription factor acts upstream of Tbx22 and preferentially regulates posterior palate growth in mice. *Development* 135, 3959–3968. doi: 10.1242/dev.025304

Mak, C. C. Y., Doherty, D., Lin, A. E., Vegas, N., Cho, M. T., Viot, G., et al. (2020). MN1 C-terminal truncation syndrome is a novel neurodevelopmental and craniofacial disorder with partial rhombencephalosynapsis. *Brain* 143, 55–68. doi: 10.1093/brain/awz379

Markus, F., Angelini, C., Trimouille, A., Rudolf, G., Lesca, G., Goizet, C., et al. (2020). Rare variants in the GABAA receptor subunit epsilon identified in patients with a wide spectrum of epileptic phenotypes. *Mol. Genet. Genomic Med.* 8:e1388. doi: 10.1002/mgg3.1388

Meester-Smoor, M. A., Vermeij, M., van Helmond, M. J., Molijn, A. C., van Wely, K. H., Hekman, A. C., et al. (2005). Targeted disruption of the Mn1 oncogene results in severe defects in development of membranous bones of the cranial skeleton. *Mol. Cell Biol.* 25, 4229–4236. doi: 10.1128/MCB.25.10.4229-4236.2005

Miyake, N., Takahashi, H., Nakamura, K., Isidor, B., Hiraki, Y., Koshimizu, E., et al. (2020). Gain-of-Function MN1 truncation variants cause a recognizable syndrome with craniofacial and brain abnormalities. *Am. J. Hum. Genet.* 106, 13–25. doi: 10.1016/j.ajhg.2019.11.011

Shu, L., He, D., Wu, D., Peng, Y., Xi, H., Mao, X., et al. (2021). MN1 gene loss-of-function mutation causes cleft palate in a pedigree. *Brain* 144:e18.

Ulintz, P. J., Wu, W., and Gates, C. M. (2019). Bioinformatics analysis of whole exome sequencing data. *Methods Mol. Biol.* 1881, 277–318.

Vegas, N., Low, K., Mak, C. C. Y., Fung, J. L. F., Hing, A. V., Chung, B. H. Y., et al. (2021). Reply: MN1 gene loss-of-function mutation causes cleft palate in a pedigree. *Brain* 144:e19. doi: 10.1093/brain/awaa432

Wang, K., Li, M., and Hakonarson, H. (2010). ANNOVAR: functional annotation of genetic variants from high-throughput sequencing data. *Nucleic Acids Res.* 38:e164. doi: 10.1093/nar/gkq603

Xiao, J. M., Wang, J. J., and Sun, L. L. (2019). Effect of miR-134 against myocardial hypoxia/reoxygenation injury by directly targeting NOS3 and regulating PI3K/Akt pathway. *Acta Cir. Bras.* 34:e201900802. doi: 10.1590/s0102-865020190080000002

Conflict of Interest: The authors declare that the research was conducted in the absence of any commercial or financial relationships that could be construed as a potential conflict of interest.

Publisher's Note: All claims expressed in this article are solely those of the authors and do not necessarily represent those of their affiliated organizations, or those of the publisher, the editors and the reviewers. Any product that may be evaluated in this article, or claim that may be made by its manufacturer, is not guaranteed or endorsed by the publisher.

frontiers in Molecular Neuroscience

ORIGINAL RESEARCH
published: 10 January 2022
doi: 10.3389/fnmol.2021.797628

Critical Role of E1623 Residue in S3-S4 Loop of Nav1.1 Channel and Correlation Between Nature of Substitution and Functional Alteration

Tao Su[1,2†], Meng-Long Chen[1,2†], Li-Hong Liu[1,2], Hen Meng[1,2], Bin Tang[1,2], Xiao-Rong Liu[1,2] and Wei-Ping Liao[1,2]*

[1]Department of Neurology, Institute of Neuroscience, Second Affiliated Hospital of Guangzhou Medical University, Guangzhou, China, [2]Key Laboratory of Neurogenetics and Channelopathies of the Ministry of Education of China, Guangzhou, China

OPEN ACCESS

Edited by:
Carlos B. Duarte,
University of Coimbra, Portugal

Reviewed by:
Mohamed Chahine,
Laval University, Canada
Maurizio Taglialatela,
University of Naples Federico II, Italy

***Correspondence:**
Wei-Ping Liao
wpliao@163.net

[†]These authors have contributed equally to this work

Specialty section:
This article was submitted to Molecular Signalling and Pathways, a section of the journal Frontiers in Molecular Neuroscience

Received: 19 October 2021
Accepted: 15 December 2021
Published: 10 January 2022

Citation:
Su T, Chen M-L, Liu L-H, Meng H, Tang B, Liu X-R and Liao W-P (2022) Critical Role of E1623 Residue in S3-S4 Loop of Nav1.1 Channel and Correlation Between Nature of Substitution and Functional Alteration. Front. Mol. Neurosci. 14:797628. doi: 10.3389/fnmol.2021.797628

Objective: An overwhelming majority of the genetic variants associated with genetic disorders are missense. The association between the nature of substitution and the functional alteration, which is critical in determining the pathogenicity of variants, remains largely unknown. With a novel missense variant (E1623A) identified from two epileptic cases, which occurs in the extracellular S3-S4 loop of $Na_V1.1$, we studied functional changes of all latent mutations at residue E1623, aiming to understand the relationship between substitution nature and functional alteration.

Methods: Six latent mutants with amino acid substitutions at E1623 were generated, followed by measurements of their electrophysiological alterations. Different computational analyses were used to parameterize the residue alterations.

Results: Structural modeling indicated that the E1623 was located in the peripheral region far from the central pore, and contributed to the tight turn of the S3-S4 loop. The E1623 residue exhibited low functional tolerance to the substitutions with the most remarkable loss-of-function found in E1623A, including reduced current density, less steady-state availability of activation and inactivation, and slower recovery from fast inactivation. Correlation analysis between electrophysiological parameters and the parameterized physicochemical properties of different residues suggested that hydrophilicity of side-chain at E1623 might be a crucial contributor for voltage-dependent kinetics. However, none of the established algorithms on the physicochemical variations of residues could well predict changes in the channel conductance property indicated by peak current density.

Significance: The results established the important role of the extracellular S3-S4 loop in $Na_V1.1$ channel gating and proposed a possible effect of local conformational loop flexibility on channel conductance and kinetics. Site-specific knowledge of protein will be a fundamental task for future bioinformatics.

Keywords: missense, sodium channel, SCN1A, epilepsy, prediction

INTRODUCTION

The distinct function of a protein depends on the well-organized composition of the amino acids and intricate folding of the molecule. Gene mutations result in either gross protein malformation (referred to destructive variants), that mostly led to haploinsufficiency, such as truncation and splice-site (He et al., 2019), or residue substitution (missense). A part of genetic defects may translate into functional alterations and subsequently lead to human diseases. Advances in genetic sequencing technology have enabled the detection of numerous sequence variants in human beings. An overwhelming majority of the variants are missense (gnomAD, HGMD), which result in the substitution of the amino acid (AA) at residues. In contrast to destructive mutations that result in remarkably damaging effects on protein composition, the functional consequence of missense mutations is far more unpredictable. Our previous study demonstrated that the molecular sub-regional location of the variant plays a critical in determining the damaging effect of the mutations (Tang et al., 2020). However, the pathogenicity or functional impact of a missense mutation depends not only on its location but also potentially on the nature of amino acid substituted, such as molecular mass, polarity, and acidity. The association between the nature of substitution and the functional alteration, which remains largely unknown, is a critical aspect in exploring the molecular mechanism underlying the pathogenicity of variants.

Genetic defects in voltage-gated sodium channel ($Na_v1.1$) α subunit encoded by *SCN1A* are a major cause of epilepsy. To date, more than 1,700 *SCN1A* variants have been reported to be associated with epilepsy and other episodic disorders[1] (Meng et al., 2015). The *SCN1A* associated epilepsies compose a wide spectrum of phenotype ranging from milder febrile seizures to severe epileptic conditions, typically Dravet syndrome (DS; Claes et al., 2003; Nabbout et al., 2003; Ceulemans et al., 2004; Mulley et al., 2005; Harkin et al., 2007; Gambardella and Marini, 2009; Dravet and Oguni, 2013; Kasperaviciute et al., 2013; Gataullina and Dulac, 2017). Previous studies have demonstrated that DS or severe epilepsies are associated with destructive variants such as nonsense and frameshift variants, or missense in the pore-region that caused loss-of-function of $Na_v1.1$. Although missense variants in other regions of $Na_v1.1$ have also been reported (Meng et al., 2015), their functional relevance has not been well studied. Factors that determine the pathogenicity of *SCN1A* missense variants remain unclear.

In this study, we identified a novel distinct missense *SCN1A* variant (c.4868A>C/E1613A) in two cases with epilepsy and febrile seizures. The substitution occurs at the putative extracellular loop linking S3 and S4 in DIV. The functional role of the extracellular S3-S4 loop remains largely unknown, except that a few studies identified toxin binding sites within the loops (Rogers et al., 1996; Bosmans et al., 2008; Wang et al., 2011). To dig deep into the functional role of E1623 and the factors that influence the pathogenicity of missense variants, six E1623 mutants with all possible substitutions caused by single nucleotide variations (SNV) were artificially created using site-directed mutagenesis. We determined the electrophysiological properties of these mutants and analyzed the correlations between the residue properties and electrophysiological alterations.

MATERIALS AND METHODS

Patient and Genetic Analysis

Diagnoses and treatments of the patients were conducted in the epilepsy center of the second affiliated hospital of Guangzhou Medical University. Clinical data including medical records, standardized questionnaires, and EEG recordings were collected. The probands and relevant familial members were assessed for genetic variations using a standardized protocol after providing written informed consent. This study was approved by the Research Ethics Board of the Hospital. Genomic DNAs were prepared from ethylene diaminetetraacetic acid-treated whole blood samples. The *SCN1A* mutation was identified by direct *SCN1A* screening as in our previous report (Liao et al., 2010). The *SCN1A* mutations were described according to the nomenclature established (den Dunnen and Antonarakis, 2000), and numbering was started from the initiating ATG codon.

Bioinformatics

Na_v channel nucleotide sequences were derived from the NCBI database[2]. The NCBI database was queried with amino acid sequences of human $Na_v1.1$ to obtain the corresponding information of DNA locus and related functional regions. To determine whether other amino acid substitutions occur in the vicinity of the mutation site, information of SNPs and mutations were queried from the SNP database of the NCBI and our *SCN1A* mutation database[1]. All amino acid sequences of the Na_v families were retrieved from GenBank and saved as individual FASTA formatted files. The sequences including the S3-S4 region of DIV were subjected to multiple sequence alignment analysis by Clustal Omega with a few modifications in the color grouping. The sequence ranges of specific S3-S4 regions are in accord with that is annotated for human $Na_v1.1$ isoform1 in the NCBI database.

The high resolution cryogenic electron microscopy structure of human $Na_v1.1$ (PDB ID: 7DTD, 3.3 Å taken from the protein data bank[3]) was used as a template for subsequent modeling (Pan et al., 2021). Three-dimensional (3D) modeling of the human wild-type (WT) and mutant $Na_v1.1$ was performed using SWISS-MODEL, an automated homology modeling program[4].

The predicted effects of all latent amino acid substitutions at E1623 were scored by different established predictive tools based on different substitution score systems, including SIFT, Mutationassessor, PolyPhen, PROVEAN, I-MUTANT suite, SNAP2, and STRUM (Tang et al., 2020).

[1]http://scn1a.caae.org.cn/

[2]http://www.ncbi.nlm.nih.gov/

[3]https://www.rcsb.org/structure/7DTD

[4]http://swissmodel.expasy.org

Mutagenesis and Heterologous Expression

Plasmids containing WT full-length sequence of human $Na_v1.1$ alpha subunit (pCMV-*SCN1A*) and beta subunit 2 (pGFP-IRES-*SCN2B*) was kindly provided by professor Alfred L Jr George (Lossin et al., 2003). A full-length sequence of beta subunit 1 was constructed into a vector driving the bicistronic expression of red fluorescent protein (pDsred-IRES-*SCN1B*) in our lab. Site-directed mutagenesis at E1623 was performed using the Quick Change XL site-directed mutagenesis kit (Stratagene, La Jolla, CA) according to the manufacturer's protocols. All mutations were confirmed by DNA sequencing of the region surrounding the mutation. HEK 293T cells were grown in 1:1 Ham's F-12 and Dulbecco's modified eagle's medium (DMEM) supplemented with 10% fetal bovine serum, 100 U/ml of penicillin, and 100 μg/ml streptomycin. The cells were maintained in a humidified incubator at 37°C with 5% CO_2. Cells were then co-transfected with pCMV-*SCN1A*, and pDsred-IRES-*SCN1B* and pGFP-IRES-*SCN2B* plasmids (5 μg each) using Lipofectamine 3000 reagent Kit from Thermo Fisher Scientific. After incubation for 12–15 h, cells were replated in 35-mm culture dishes.

Electrophysiological Recordings and Analysis

Electrophysiological studies were performed 20–48 h after transfection, according to our previous report (Chen et al., 2015). Channel activity was recorded by using the conventional patch clamp technique in the whole-cell configuration with an Axopatch 200B patch-clamp amplifier (Axon Instruments). The extracellular control solution contained: 140 mM NaCl, 3 mM KCl, 1 mM $CaCl_2$, 1 mM $MgCl_2$, 10 mM HEPES, and 5 mM glucose, adjusted to pH 7.4, 310 ± 6 mOsm. The whole-cell pipette solution contained: 140 mM CsF, 1 mM EGTA, 10 mM HEPES, and 10 mM NaCl, pH 7.4, adjusted with CsOH, 310 ± 6 mOsm. Cell capacitance was calculated by integrating the area under an uncompensated capacity transient elicited by a 10-mV hyperpolarizing test pulse from a holding potential of −80 mV. Series resistance was compensated by at least 70% in all recordings. Leakage currents were subtracted by the P/N method. The pCLAMP 10.2 software (Axon Instruments) was used for the acquisition and analysis of currents. Current amplitude in response to each test pulse was normalized to the maximum. The voltage dependence of activation and inactivation was determined using standard protocols. The conductance (G) was calculated according to: $G = I_{peak}/(V_{test} - V_{rev})$, where V_{rev} is the Na^+ reversal potential, V_{test} is the command potential, and I_{peak} is the peak current amplitude. G/G_{max} was then fitted with the following Boltzmann equation: $G/G_{max} = (1 + \exp((V_m - V_{1/2})/k))^{-1}$, where G_{max} is the maximal conductance, $V_{1/2}$ is the half-activation potential, V_m is the test voltage, and k is the slope factor. From this equation, we derived parameters of the midpoint ($V_{1/2}$) and slope factor of steady-state activation and inactivation curves. Parameters for recovery of channels from fast inactivation were determined using a double pulse protocol. Channels were inactivated with −10 mV conditioning pulse for 100 ms, followed by command hyperpolarization for varying durations as a recovery period (1 ms to 1 s), and subsequent test pulse to −10 mV (for 10 ms). The normalized recovery curve was fit with a double-exponential function to obtain tau for recovery: $I/I_{max} = A1\times(1 - \exp(-t/\tau\text{-fast})) + A2\times(1 - \exp(-t/\tau\text{-slow}))$, where I is the current amplitude at the time point t after the onset of the voltage command, I_{max} is the maximal recovery current amplitude, and A is the amplitude contribution of the different recovery time constants. Time constants of recovery τ-fast and τ-slow were extracted from the equation as recovery parameters.

Statistical Analysis

Data reported throughout the text and figures are presented as means ± SEM. Statistical analyses were conducted in SPSS 19.0, using Student's *t*-test when comparisons were made between two groups or by one-way ANOVA with a *post hoc* Tukey HSD test for comparing data from multiple groups. Significance was assigned at $P < 0.05$.

RESULTS

Epilepsy-Associated Variant E1623A and the Extracellular Loop

An *SCN1A* variant c.4868A>C/p.E1623A was identified from two cases of epilepsy, including a case with de novo variant and a familial case with three individuals affected (**Figures 1A–C**). Case 1 was a 17.5-year-old boy with Dravet syndrome. The proband of case 2 was diagnosed as epilepsy with febrile seizure plus. The proband's mother and elder sister had several febrile seizures before 6 years old (clinical information refers to **Supplementary Data**). The variant occurs in exon 26 of *SCN1A* and leads to the substitution of glutamic acid by alanine at E1623 that locates in the extracellular loop linking S3-S4 in DIV of $Na_v1.1$ (**Figures 1D,E**). The E1623A is a novel missense variant despite several disease-associated or low-frequency variants flanking the site of E1623. The 3D structural modeling showed that E1623 residue and its correlated loop were located on the top of the lateral voltage-sensor domain (VSD, S4; **Figures 1F,G**).

Sequence alignments for conservation showed that the amino acid sequence of the S3–S4 loop in DIV of $Na_v1.1$ is highly conserved across species. It is noteworthy that a potential motif constituted by two residues at positions E1623 and E1626 remains evolutionarily conserved in their negative charged property (**Figure 2A**). Residues from E1623 to E1626 form a tight turn of the loop on the top of the lateral VSD (**Figure 1G**). Among different alpha subunits of Na_v family that contribute to different Na_v properties, the sequence is slightly variable, but conserved with two alternative acidic residues, glutamate or aspartate, at the equivalent position as E1623 in $Na_v1.1$ (**Figure 2B**). The other three asymmetric domains (DI-III) of human $Na_v1.1$ also showed conservation of the glutamate residue, even though they have the much shorter S3-S4 loop (**Figures 2C,D**).

Consequences of Substitutions at E1623

To understand the role of this potentially important glutamate residue on channel function and the link between residue property and functional alteration, we generated all the latent substitutions at residue E1623 caused by SNVs. The substitutions

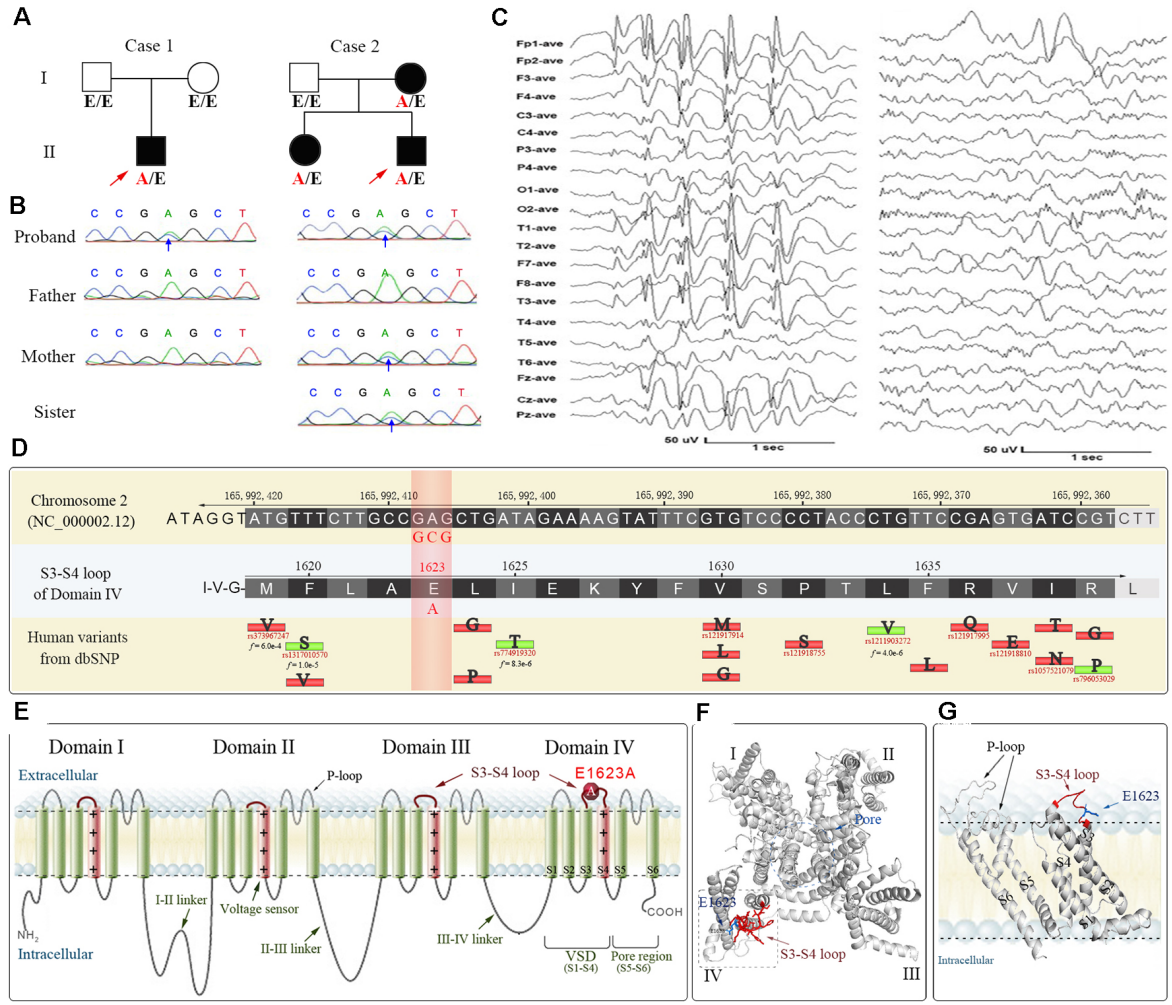

FIGURE 1 | The pedigrees, DNA chromatograms, EEG, and bioinformatical annotations of the E1623A variant of *SCN1A* gene identified from two cases of epilepsy. **(A)** Pedigrees of two cases. Case 1 was a 17.5-year-old boy with Dravet syndrome. The proband of case 2 was diagnosed as epilepsy with febrile seizure plus. His mother and elder sister had several febrile seizures before 6 years old. A/E indicates heterozygous E1623A carrier, while E/E indicates wildtype. **(B)** Sanger sequencing verification. **(C)** Representative EEG of the case 1 proband showing the generalized high amplitude sharp and slow waves (left), along with focal sharp and slow waves in the left frontal and temporal regions (right). **(D)** Collection of reference sequences and human variants within the S3-S4 extracellular loop of DIV where the E1623A occurred. The position at E1623 has not been reported with any variant according to human databases. The collected missense variants with epilepsy or non-clinical implications are indicated by red or green bars with their substituted AA abbreviations. Available minor allele frequency (*f* value) is under the reference SNP IDs. **(E)** Structure-function map of $Na_v1.1$ indicating the location of E1623A. **(F)** A top view of 3D structural modeling of the $Na_v1.1$ alpha unit shows that the S3-S4 loop and E1623 were at a distance from the central pore region. **(G)** A side view of the arrangement of the VSD highlights the extracellular S3-S4 loop and the location of E1623. The S4 helices are depicted in pink, while other helices are in green. The S3-S4 loop is highlighted in red.

included alanine (A), aspartic acid (D), glycine (G), lysine (K), glutamine (Q), and valine (V). These residues together with glutamate happen to show a spectrum of residues with different properties, such as molecular mass, polarity, and charge properties (**Figure 3**).

The WT and diverse mutant alpha-subunits, which were produced by site-directed mutagenesis, were expressed transiently in HEK293T cells. We first examined the plasma membrane expression of these mutants by Western blot and did not find any significant difference among the mutants (**Supplementary Data**). Subsequently, the mutants were subjected to examine their functional effects by using whole-cell voltage clamp recording. These mutants manifested many different amplitudes of Na^+ currents (**Figure 4A**). The peak current density of the epilepsy-associated mutant E1623A was significantly decreased ($P < 0.05$; **Figures 4B–D**), while the mutant E1623Q was slightly increased when compared with that of WT, but did not reach statistical significance ($P > 0.05$). It was noted that E1623K and E1623V also resulted in a significant decrease in current density ($P < 0.05$).

The normalized conductance-voltage (G-V, activation) curve of the E1623A showed a slight right shift compared with the WT, with a slower voltage-dependent rising. This is evident as a statistically significant difference in the parameter of

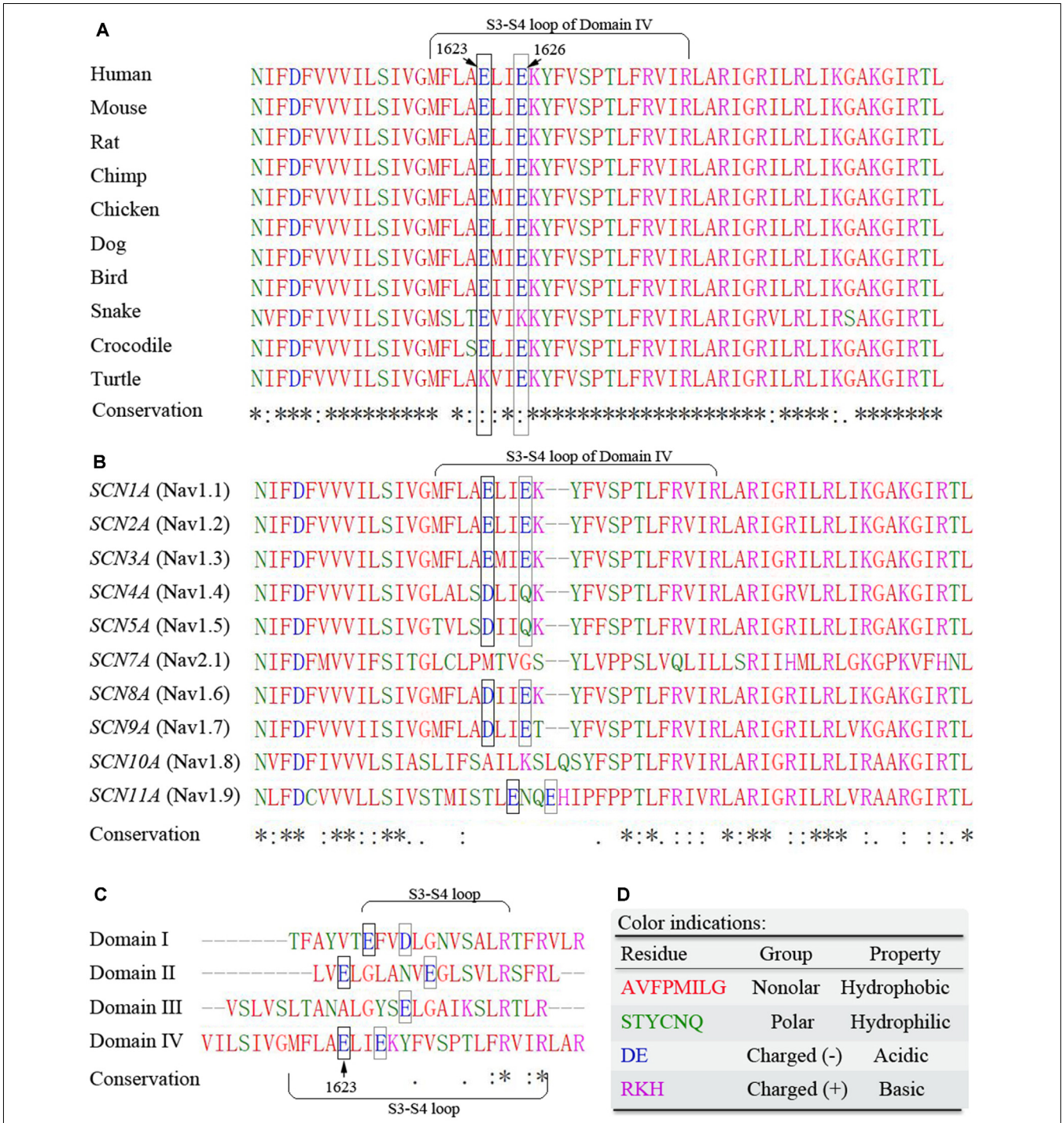

FIGURE 2 | Multiple sequence alignments of the S3-S4 extracellular loop of DIV. **(A)** Cross-species alignments show high conservation of amino acid sequence within the region. **(B)** Sequence alignments among Na_v family members indicate high conservation of two acidic residues E1623 and E1626. **(C)** Differences in sequence length and residues of the S3-S4 loop among different domains of human $Na_v1.1$ alpha unit. **(D)** Color indications. Residues are grouped by their physicochemical properties and indicated by different colors. The symbols of conservation significance are in keeping with the Clustal Omega from the NCBI website. * fully conserved; : conservation with strongly similar properties; . conservation with weakly similar properties; blank space indicates not conserved. The potentially important acidic residues are highlighted with frames.

the slope of steady-state activation between E1623A and WT (**Figure 5A**). The depolarized voltage dependence of activation may reduce the availability of the E1623A mutant channels to operate as amplifiers of subthreshold depolarization. The mutant E1623V showed similar alteration, and the other mutants caused slight alterations of activation parameters without statistical

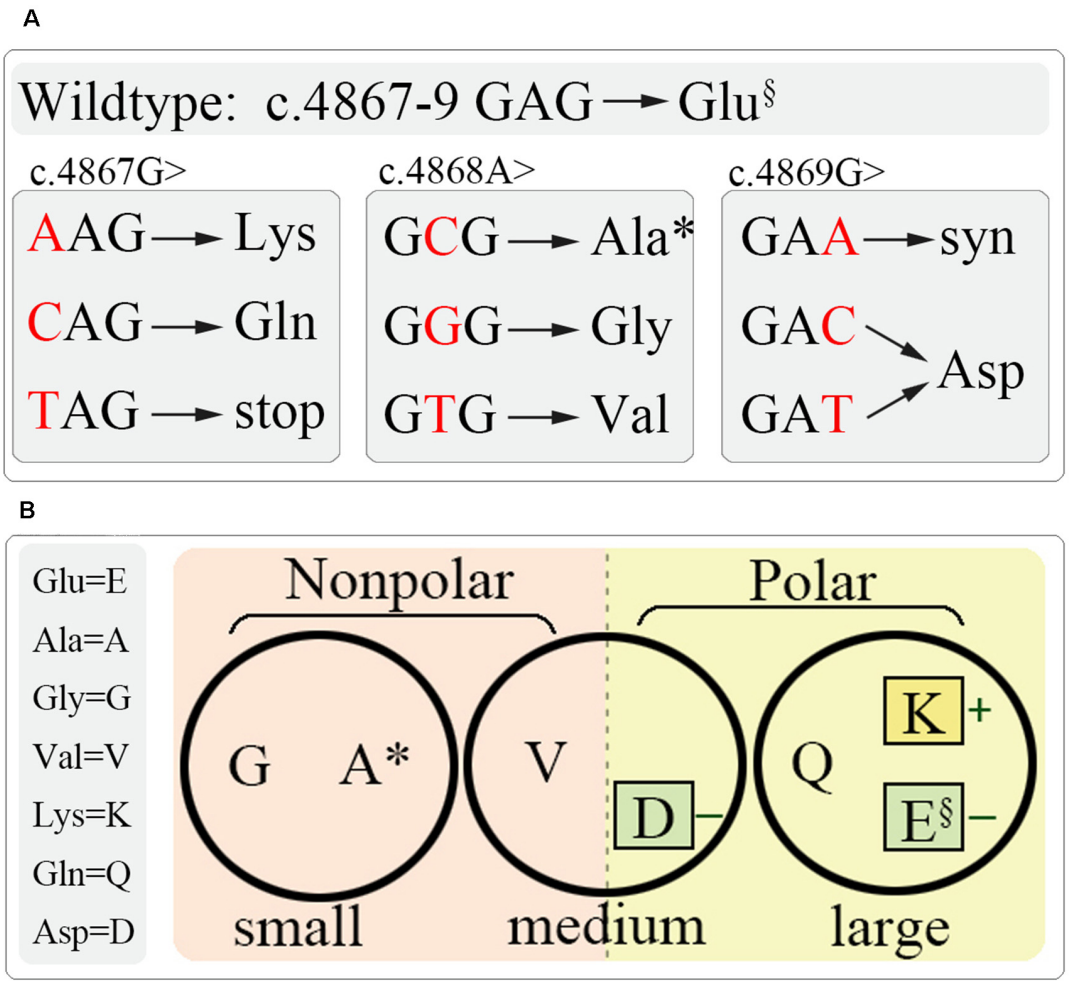

FIGURE 3 | Schematic diagram of site-directed mutagenesis at E1623. **(A)** All latent variants by single nucleotide variation at c.4867–4869. **(B)** Residue grouping according to their basic physiochemical properties, including molecular weight (circles), polar (colored squares), and charge (little colored squares). §, wild-type; *, the identified mutation.

significance. Different from a continuity of variations in the steady-state activation curves, the variants were presented as two distinct groups in fast inactivation property (**Figure 5B**). The steady-state inactivation curves of the mutants E1623A, E1623K, E1623Q, and E1623V were almost overlapped and significantly shifted in the hyperpolarizing direction, whereas the mutants E1623D and E1623G did not differ from the WT. Statistical analysis evidenced that there were two significant subsets on the potential of half-inactivation, but without difference in the slope.

Recovery from inactivation was assessed by using a standard two-pulse protocol. All examined mutants recovered fully within 1 s in this experiment. The fractional recoveries of $Na_v1.1$ peak current were plotted against the intervals on a logarithmic time scale. The WT and mutant channels exhibited significantly different kinetics (**Figure 5C**). Statistical analysis of the time constants (τ-fast and τ-slow) revealed that the E1623A mutant channel recovered from inactivation at the slowest rate among the mutants and was exclusively different from the WT. The E1623A mutant also differed significantly from the E1623D, E1623Q, E1623K, and E1623G mutants in τ-fast.

Taken together, the epilepsy-associated mutant E1623A had significant alterations in all of the four aspects of electrophysiological channel properties and presented the most apparent alteration in three of the four aspects when compared with the other potential mutants. E1623V most closely resembled E1623A, with a reduction in channel conductance and availability during activation and inactivation. E1623Q and E1623K had significant hyperdepolarization shifts only in the voltage-dependent inactivation. No significant alteration was found in either E1623D or E1623G.

Relationship Between Residue Properties and Electrophysiological Parameters

We analyzed the correlation between amino acid properties and functional alterations of $Na_v1.1$ channel (**Table 1**). The physicochemical properties including molecular size, charge, and

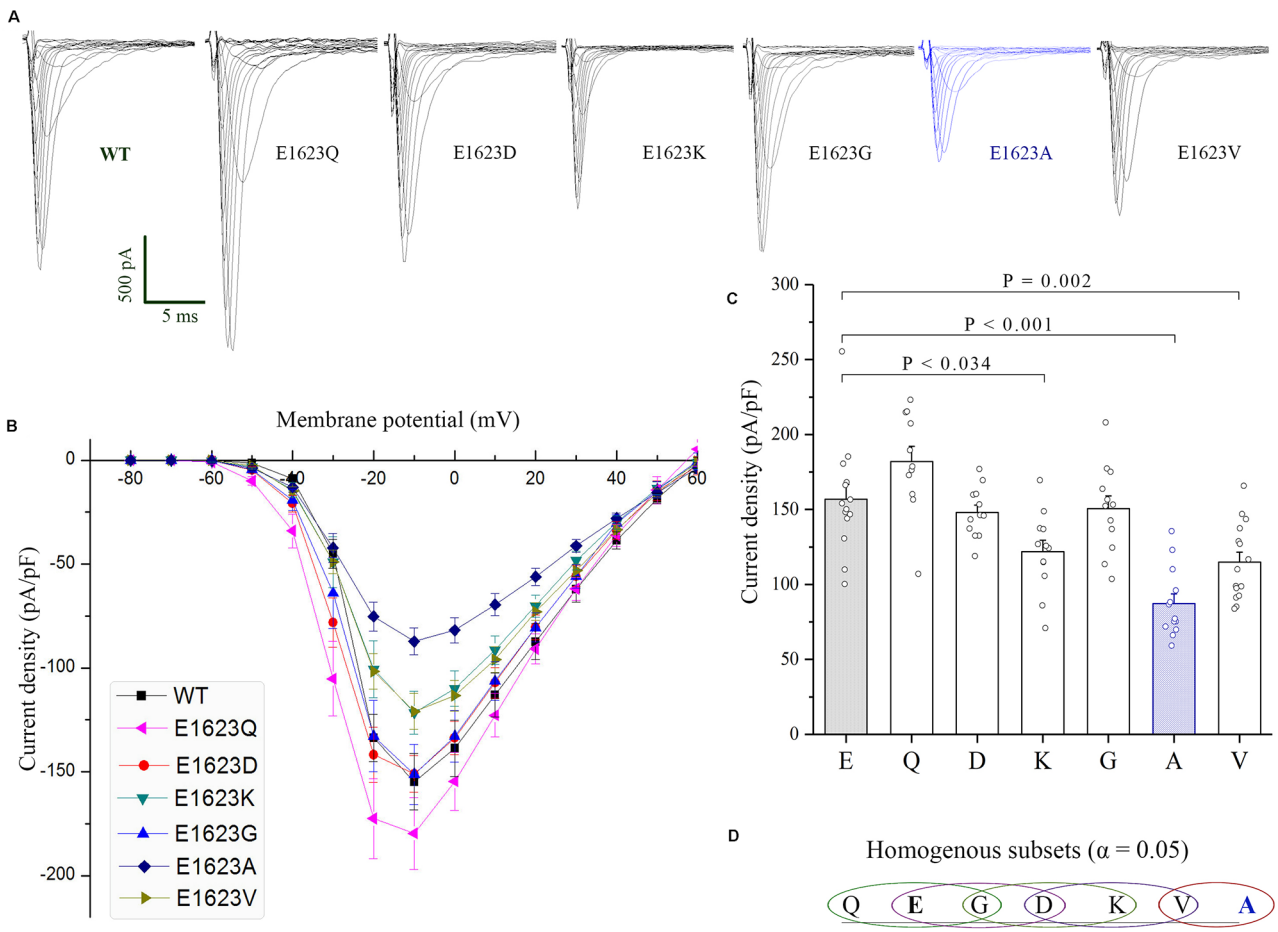

FIGURE 4 | Current densities of E1623 mutants. All variants were expressed in HEK293T cells *via* transfection. **(A)** Representative current traces elicited with 20-ms depolarizations ranging from −80 mV to +60 mV in +10 mV steps. Intervals between pulses were 10 s. The mutants were arrayed by their residue similarity to WT according to Grantham's distance. Currents are noticeably reduced in the E1623A variant. **(B)** Plots of current densities and membrane potentials. **(C)** Group data of peak current densities elicited at −10 mV. **(D)** Statistical output of homogenous subsets shows significant differences at the 0.05 level among the variants, *via* one-way ANOVA and *post hoc* Tukey HSD tests.

polarity were parameterized by their mass, isoelectric point, and hydrophobicity scale, respectively (**Supplementary Data**); and the ensemble molecular difference was assessed by the established matrices. As shown in **Table 1**, the hydrophilicity scale was significantly correlated with the channel voltage-dependent activation (slope of activation, $r = 0.770$, $P < 0.05$) and the recovery (slow recovery, $r = 0.870$, $P < 0.05$) parameters. We did not find any significant contributor to current density, which is closely related to the pathogenicity of the mutants. No quantitative correlation between residue properties and inactivation was found, either (**Table 1**).

We analyzed correlations between the predictive scores and alteration of current density. Absolute changes in average current density of the six variants at E1623 were plotted against the normalized predictive scores obtained by different in silico tools, including evolutionary conservation-based methods (e.g., SIFT and Mutationassessor), structure-based (protein stability) predicting tools (e.g., Strum and I-mutant suite), and machine-learning methods that combined comprehensive information (e.g., SNAP2 and PROVEAN; **Figure 6**). The predictive scores from SNAP2 and PROVEAN appeared to be matched better than other predictive scores ($r = 0.486$ and $r = 0.485$, respectively). However, these predictive scores did not correlate well with the alterations in current density in general.

DISCUSSION

The sodium channel plays a critical role in controlling the excitability of cells. $Na_v1.1$ appears to be a particularly important molecule since it is frequently associated with human diseases (Meisler and Kearney, 2005). Our previous study shows that $Na_v1.1$ is highly sensitive to genetic variations (Chen et al., 2015) and thus may be used as a model or an example to explore molecular bases underlying the functioning of ion channels. The present study identified a novel epilepsy-associated mutation E1623A within the extracellular S3-S4 loop of DIV, a previously unidentified functional component. Functional studies demonstrated remarkable loss-

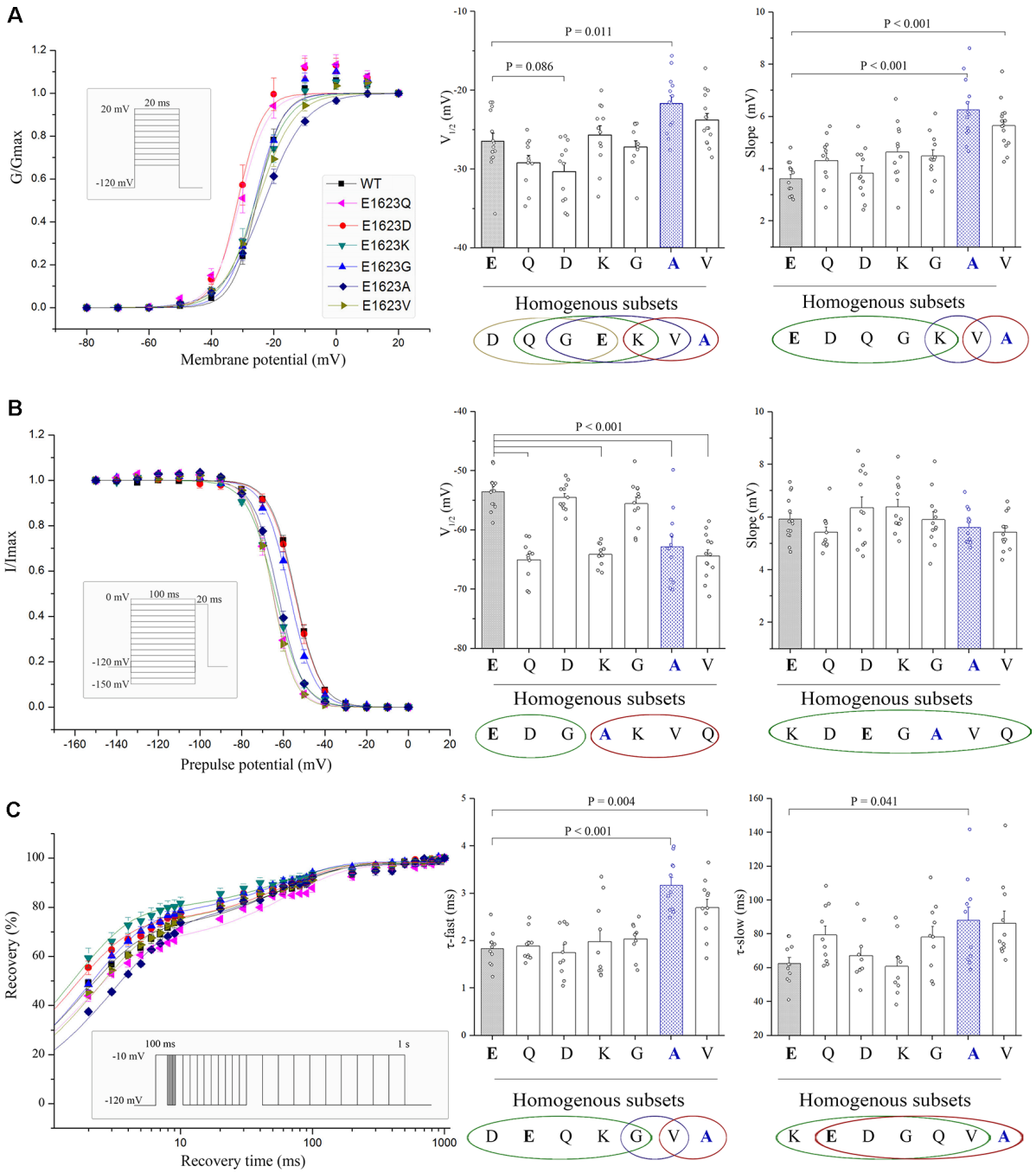

FIGURE 5 | Voltage dependence and recovery kinetics of the E1623 mutants. **(A)** Activation curves of all E1623 mutants. **(B)** Steady-state inactivation curves. For testing voltage dependent channel availability in fast inactivation, a two-pulse protocol was used. Na^+ currents were evoked by a 20-ms test pulse to −10 mV after 100-ms conditioning prepulses between −150 and 0 mV in 10-mV increments. Peak currents evoked by test pulses were measured, normalized, and plotted against the conditioning prepulse potentials. Parameters of activation and fast inactivation were estimated by fitting current-voltage relationships with the Boltzmann function. Estimated parameters including half-activation potential ($V_{1/2}$) and slope factor, were derived from the Boltzmann fits. Group data of the $V_{1/2}$ and slope are shown at the right panels. **(C)** Recovery from fast inactivation in paired stimulus experiments. Paired stimuli were applied at various inter-stimulation intervals. The recovery fractions were plotted to the intervals. The normalized recovery plots were fit with a double-exponential function to obtain parameters of τ-fast and τ-slow (shown in right panels). Statistical outputs of homogenous subsets (shown below the plots; those within the same circle are $\alpha > 0.05$) indicate significant differences among the mutants.

of-function of E1623A mutant, with characteristic alterations in activation, inactivation, and recovery properties, and confirmed the pathogenicity of E1623A. More importantly, the other substitutions at the residue E1623 also resulted in apparent

TABLE 1 | Correlation coefficients between residue similarity and functional changes.

Indices for AA differences	Conductance Peak current	Activation slope	Inactivation $V_{1/2}$	Recovery τ-fast	Recovery τ-slow
Simple property					
Volume	0.114	0.394	−0.376	0.544	0.353
Charge	0.361	0.274	0.556	0.018	−0.140
Polarity	0.482	0.770*	0.290	0.705	0.870*
Physicochemical distance					
Miyata's distance	0.258	0.599	0.039	0.577	0.626
Grantham's distance	0.392	0.720	0.083	0.688	0.730
Sneath's index	0.406	0.634	0.198	0.554	0.413
Experimental exchangeability	0.079	0.140	−0.654	0.439	0.249

*Absolute deviations of the average values of electrophysiological parameters between mutants and WT were analyzed for correlations with substitution indices. Electrophysiological parameters with statistical significance to WT were included. The single-pass algorithm of the Pearson correlation coefficient was used to estimate the individual contributions of physicochemical property to specific functional output and the predictive accuracy. Basic physicochemical properties were parameterized by molecular weight, isoelectric point, and hydrophobicity. The hydrophobicity scale of Kyte and Doolittle was adopted as the values of hydrophobicity (Kyte and Doolittle, 1982). *Significant correlation, $P < 0.05$.*

functional alterations, suggesting that the residue E1623, presumably as well as the adjacent residues within the extracellular loop, play a critical role in channel gating.

Previous studies have demonstrated that missense mutations in the central pore region of $Na_v1.1$ were exclusively associated with loss-of-function, while mutations in the other regions were associated with diverse functional alterations (Meng et al., 2015). In the present study, the novel epilepsy-associated mutation E1623A is located at the extracellular loop linking S3 and S4 in DIV. The roles of extracellular components, especially the loops that connect the transmembrane segments, in the function of $Na_v1.1$ channel complex are largely unknown. Based on topological modeling, this extracellular S3-S4 loop appears to be at a considerable distance from the central pore, and is theoretically unlikely to result in a functional change. However, both the severe clinical phenotype in our cases and the existing clinical variants within the loop indicated that the E1623 might be critical for proper channel function.

The subsequent functional studies revealed that the E1623A variant resulted in surprising abnormalities in gating properties, including channel conductance and gating kinetics. Several other potential missense mutants at E1623 also led to changes in gating properties, although to a lesser extent. It is quite interesting that the substitutions in a residue at the extracellular loop that is far apart from the central pore, lead to an overwhelming alteration in channel gating. Since E1623 is located a distance away from the central pore and appears not directly involved in ion conduction, other unknown mechanisms such as electrostatic interaction and local conformational flexibility may be involved. It has been established that sodium currents are elicited in response to changes in the membrane potential sensed by the channel voltage sensor module (S1-S4) containing the S3-S4 linker. Recent studies have uncovered intricate interactions of these elements within the Na_v channel signaling complex (Okamura et al., 2015; Catterall et al., 2017). The positive charges in the S4 segments serve as gating charges and move across the membrane electric field when activated, initiating conformational changes to open and close the channel (Yarov-Yarovoy et al., 2012). Upon opening, the upper part of the S4 approaches the pore domain. The S3-S4 loop is lying on the top of the S1-S4 bundles, extending into the extracellular space (**Figure 1**). Such location suggests that S3-S4 loops may confer local conformational flexibility and thereby impact channel functioning. In a previous study on small-conductance calcium-dependent potassium, a 3-amino acid motif within the extracellular S3-S4 loop was suggested to determine apamin blocking effects and regulate the allosteric change of gating pore (Weatherall et al., 2011). Here multiple sequence alignments of the S3-S4 loop in DIV showed a conserved residue cluster of negative charged residues glutamate ($E_{XX}E$) among Na_v superfamily members and negatively charged residues glutamate or aspartate (ExxE/DxxE) in other voltage-gated sodium channels (**Figure 2**). A similar sequence is present in the S3-S4 loops of different domains. The ExxE forms the tight turn of the loop (**Figure 1**) and is located close to the voltage-sensor. Therefore, the ExxE motif and the negatively charged acidic glutamate may be crucial for channel functioning, implying that the molecular sub-regional effect should be considered in evaluating the pathogenicity of variants.

It has been demonstrated that mutations of charged residues in S4 of all domains affected activation, whereas those in S4 segments of primarily DI and DIV had the most effects on fast inactivation (Groome and Winston, 2013). Similarly, charge-reversing mutations in S1-S3 segments alter sodium channel activation and fast inactivation, suggesting that positive charge movement across the bilayer must be facilitated by negative charges in other parts of the protein (Chowdhury and Chanda, 2012). In the voltage-gated potassium channels, similar conserved negatively charged residues in VSD have been shown to actively catalyze the transport of ionized groups through the cell membrane and control the voltage sensor operation (Starace and Bezanilla, 2004; Pless et al., 2011; Lacroix et al., 2014). These negatively charged residues are proposed to act as neutralization and electrostatic interactions with positively charged S4 residues, and thus have profound effects on activation gating (Papazian et al., 1995; Yang et al., 2009). Previously, no experimental evidence has been obtained on the role of the extracellular S3-S4 loop in sodium channel functioning. In

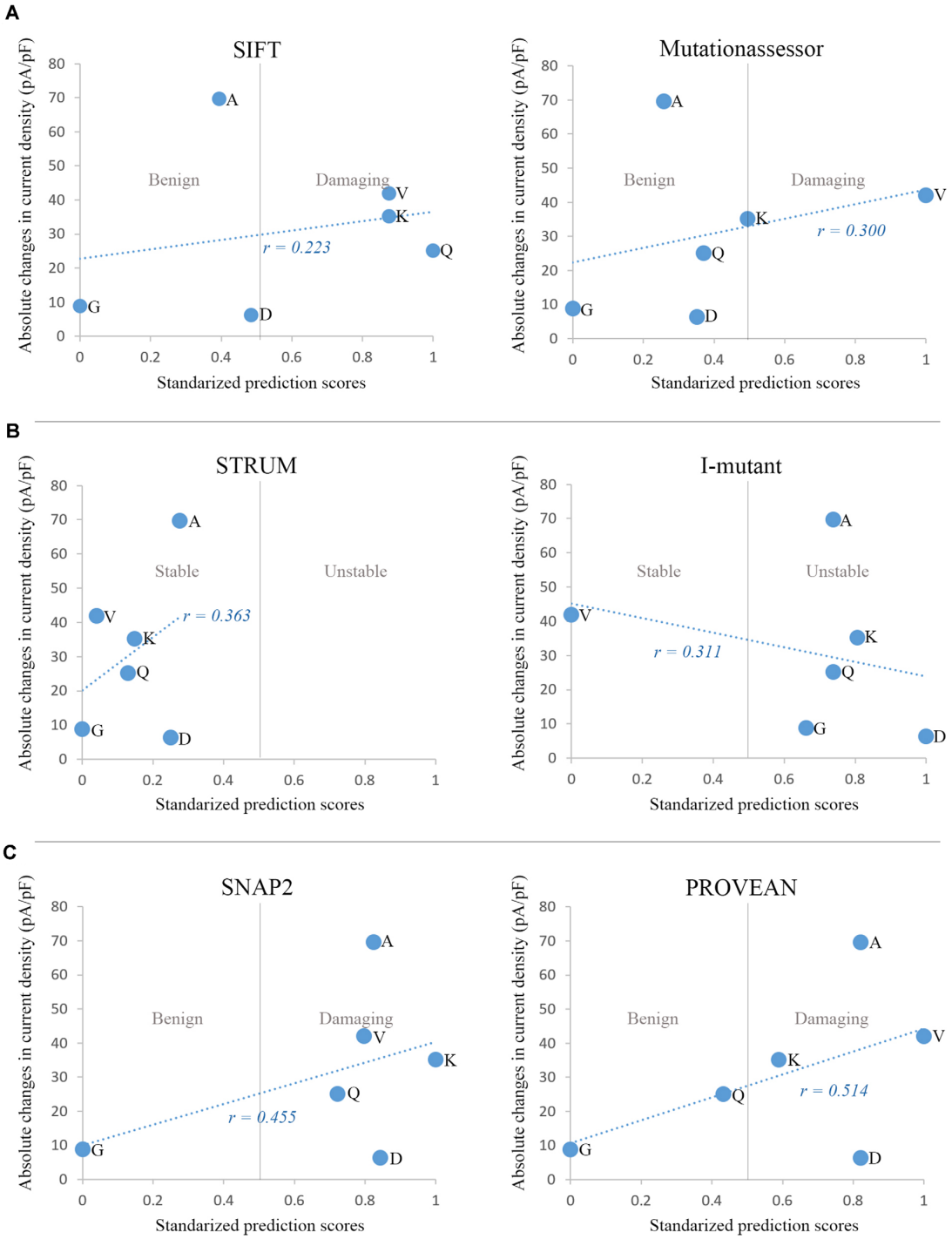

FIGURE 6 | Correlations between in silico prediction scores and functional changes in current density. **(A)** Sequence and evolutionary conservation-based methods: SIFT and Mutationassessor. **(B)** Prediction of protein stability changes by Strum and I-mutant suite. **(C)** Machine-learning methods combining comprehensive features: SNAP2 and PROVEAN. For comparison, prediction scores of the six variants from different tools were normalized to the Polyphen-2 scoring scheme, with a range from 0 to 1 and a threshold at 0.5. The minimal score with benign prediction was set as 0, and the maximal score with damaging prediction was set as 1. Scores with benign prediction were scaled to a range from 0 to 0.5, while scores of damaging variants were scaled to a range from 0.5 to 1.

the present study, the charge-reversing mutation E1623K led to significant changes in fast inactivation with a shifting of steady-state inactivation to more hyperpolarized potentials. In contrast, the negative charge-retaining mutant E1623D showed no alteration in inactivation and was mostly close to WT in fast inactivation parameters (**Figure 5**). These findings suggest

that the negative charge property of E1623 is critical in the inactivation of the sodium channel. Note that the sequence in the N-terminal part of the loop just after S3 is MFLAEL. The residues M, L, and A have high helix propensities. Replacing the E with an A may change the helix-loop-helix structure, and the S3 helical extension into the S3-S4 loop is quite likely to have some effects on the voltage-responsiveness of the S4 helix that could affect both channel activation and inactivation as observed experimentally.

Several mutants without charge-reversing or helix transformation also demonstrated apparent effects on channel activation/inactivation, suggesting much complex relationships between the residue properties of the extracellular loop and channel functioning. We analyzed the correlations between residue properties and electrophysiological alterations. Significant correlations were detected between residue polarity and channel properties (**Table 1**), indicating that hydrophobicity at the residue E1623 of the extracellular loop is a key property affecting channel functioning. Hydrophobic/polar property is a meaningful scheme clustering residue alphabets. The importance of hydrophobic interaction in protein structure owes much to the following two facts: (i) it is the driving force for protein folding (Dill, 1990); and (ii) it is an important factor for protein-protein interaction (Jones and Thornton, 1996). For hydrophilic glutamate at the extracellular site and on the top of VSDs, its hydrophilic property may play an additional role in favoring the concentration and flow of charged Na^+ through the lipid bilayer, because extracellular Na^+ is conducted as a hydrated ion (Payandeh et al., 2012).

However, we did not find any remarkable correlations between the residue properties and peak current density that reflected channel conductance. The present study revealed that the hydrophilic glutamate residue substituted by hydrophobic residues at E1623, such as E1623V and E1623A, did result in decreased current density. However, there were also polarity-altered mutants that did not affect current density, such as E1623G and E1623Q. The confounding factors for the channel conductance at E1623 may include phylogenetic and structural context, together with the elementary changes in amino acid properties. To explore the factors that contributed to channel dysfunction, we used in silico tools to score the mutants from three different perspectives, including sequence/evolutionary conservation, protein stability, and machine-learning protocol with combined comprehensive information and variant dataset of known pathogenicity, based on their working principles. The machine-learning based predictors, SNAP2 and PROVEAN, showed a relatively higher correlation coefficient between the predictive scores and channel conductance.

The conductance of $Na_v1.1$ indicated by peak current density is the most crucial property that determines macroscopic gain or loss of channel function. The common form of functional defects caused by genetic variants, identified in epilepsy patients, is loss of function or partial loss of function, featured by non-detectable or reduced sodium current in electrophysiological recordings. Changes in channel conductance determine the pathogenicity of mutations (Tang et al., 2020). In contrast, the electrophysiological parameters of voltage-dependent kinetics of the channel determine the channel characteristics and are associated with mild clinical phenotypes (Liao et al., 2010; Meng et al., 2015). Understanding what residues and functional domains would associate with channel conductance and gating kinetics would provide novel insights into the molecular basis of channel functioning and pathogenicity of variants in channels.

Theoretically, one residue is potentially subject to several different substitutions and subsequently associated with variations in channel function and phenotype, which brings challenges in clinical recognition and diagnosis of genetic disorders. The present study explored the correlation between the nature of substitution and functional alteration in sodium channel $Na_v1.1$. It would help understand the intrinsic mechanism underlying the pathogenicity of missense variants. Under the influence of some extrinsic factors, individual cases might exhibit diversity in clinical phenotype and inheritance. In our example, the case 1 and case 2 presented different epileptic phenotypes and inheritance, in which one was severe DS and de novo and the other was epilepsy with febrile seizure plus and dominantly inherited from his mother. In general, a vast majority of de novo severe mutations, especially truncations, were identified in patients with DS, while missense mutations were responsible for familial cases with milder phenotypes (Meng et al., 2015; Liu et al., 2018). This is because de novo mutations are unlikely to pass down to the offspring in patients with severe phenotypes like DS. However, the genotype-phenotype correlation is not entirely consistent. Under some circumstances, the DS-associated mutations, such as the E1623A and a previously reported p.Arg1912X truncation (Jaimes et al., 2020), might exhibit milder phenotype, and thus have the opportunity to develop into an inherited disease in pedigree. The variable disease expressivity might come from individual differences from the modulation of channel physiology, such as trafficking, posttranslational modifications, and pharmacological modulators. It remains a challenging conundrum for researchers about how biophysical alterations in a mutant $Na_v1.1$ determine their phenotypes.

Although there has been great progress in genetic sequencing and in silico prediction, variant interpretation remains a major challenge. The present study proposed not only an essential role of the extracellular S3-S4 loop at domain IV in channel functioning, but also an urge of customized predictive tools with more considerations, including 3D structure information, experimental data, and sub-regional function, etc. Different channel functional properties, such as channel conductance and voltage-dependent kinetics, are potentially affected by the distinct molecular alterations and associated with different clinical phenotypes, providing new perspectives on molecular mechanisms underlying genetic diseases.

DATA AVAILABILITY STATEMENT

The original contributions presented in the study are included in the article/**Supplementary Materials**, further inquiries can be directed to the corresponding author.

ETHICS STATEMENT

The studies involving human participants were reviewed and approved by Ethics Committee of the Second Affiliated Hospital of Guangzhou Medical University. Written informed consent to participate in this study was provided by the participants' legal guardian/next of kin. The animal study was reviewed and approved by Ethics Committee of the Second Affiliated Hospital of Guangzhou Medical University. Written informed consent was obtained from the individual(s), and minor(s)' legal guardian/next of kin, for the publication of any potentially identifiable images or data included in this article.

AUTHOR CONTRIBUTIONS

W-PL performed the conceptualization and funding acquisition. W-PL, TS, and M-LC designed research. TS, M-LC, HM, L-HL, BT, X-RL, and W-PL performed research and/or analyzed data. TS wrote the manuscript draft. W-PL contributed to critical manuscript revisions. All authors contributed to the article and approved the submitted version.

FUNDING

This work was supported by the National Natural Science Foundation of China (grant No. 81571273 and 81271197), the Science and Technology Project of Guangdong Province (grant No. 2017B09090436 and 2017B030314159), and Science and Technology Project of Guangzhou (grant No. 201904020028). The funders had no role in study design, data collection and analysis, and decision to publish or preparation of the manuscript.

ACKNOWLEDGMENTS

We are deeply grateful to the patients and clinicians who participated in this study.

SUPPLEMENTARY MATERIALS

The Supplementary Material for this article can be found online at: https://www.frontiersin.org/articles/10.3389/fnmol.2021.797628/full#supplementary-material.

REFERENCES

Bosmans, F., Martin-Eauclaire, M. F., and Swartz, K. J. (2008). Deconstructing voltage sensor function and pharmacology in sodium channels. *Nature* 456, 202–208. doi: 10.1038/nature07473

Catterall, W. A., Wisedchaisri, G., and Zheng, N. (2017). The chemical basis for electrical signaling. *Nat. Chem. Biol.* 13, 455–463. doi: 10.1038/nchembio.2353

Ceulemans, B. P., Claes, L. R., and Lagae, L. G. (2004). Clinical correlations of mutations in the SCN1A gene: from febrile seizures to severe myoclonic epilepsy in infancy. *Pediatr. Neurol.* 30, 236–243. doi: 10.1016/j.pediatrneurol.2003.10.012

Chen, Y. J., Shi, Y. W., Xu, H. Q., Chen, M. L., Gao, M. M., Sun, W. W., et al. (2015). Electrophysiological differences between the same pore region mutation in SCN1A and SCN3A. *Mol. Neurobiol.* 51, 1263–1270. doi: 10.1007/s12035-014-8802-x

Chowdhury, S., and Chanda, B. (2012). Perspectives on: conformational coupling in ion channels: thermodynamics of electromechanical coupling in voltage-gated ion channels. *J. Gen. Physiol.* 140, 613–623. doi: 10.1085/jgp.201210840

Claes, L., Ceulemans, B., Audenaert, D., Smets, K., Lofgren, A., Del-Favero, J., et al. (2003). De novo SCN1A mutations are a major cause of severe myoclonic epilepsy of infancy. *Hum. Mutat.* 21, 615–621. doi: 10.1002/humu.10217

den Dunnen, J. T., and Antonarakis, S. E. (2000). Mutation nomenclature extensions and suggestions to describe complex mutations: a discussion. *Hum. Mutat.* 15, 7–12. doi: 10.1002/(SICI)1098-1004(200001)15:1<7::AID-HUMU4>3.0.CO;2-N

Dill, K. A. (1990). Dominant forces in protein folding. *Biochemistry* 29, 7133–7155. doi: 10.1021/bi00483a001

Dravet, C., and Oguni, H. (2013). Dravet syndrome (severe myoclonic epilepsy in infancy). *Handb. Clin. Neurol.* 111, 627–633. doi: 10.1016/b978-0-444-52891-9.00065-8

Gambardella, A., and Marini, C. (2009). Clinical spectrum of SCN1A mutations. *Epilepsia* 50, 20–23. doi: 10.1111/j.1528-1167.2009.02115.x

Gataullina, S., and Dulac, O. (2017). From genotype to phenotype in Dravet disease. *Seizure* 44, 58–64. doi: 10.1016/j.seizure.2016.10.014

Groome, J. R., and Winston, V. (2013). S1–S3 counter charges in the voltage sensor module of a mammalian sodium channel regulate fast inactivation. *J. Gen. Physiol.* 141, 601–618. doi: 10.1085/jgp.201210935

Harkin, L. A., McMahon, J. M., Iona, X., Dibbens, L., Pelekanos, J. T., Zuberi, S. M., et al. (2007). The spectrum of SCN1A-related infantile epileptic encephalopathies. *Brain* 130, 843–852. doi: 10.1093/brain/awm002

He, N., Lin, Z. J., Wang, J., Wei, F., Meng, H., Liu, X. R., et al. (2019). Evaluating the pathogenic potential of genes with de novo variants in epileptic encephalopathies. *Genet. Med.* 21, 17–27. doi: 10.1038/s41436-018-0011-y

Jaimes, A., Guerrero-Lopez, R., Gonzalez-Giraldez, B., and Serratosa, J. M. (2020). De novo truncating mutation in SCN1A as a cause of febrile seizures plus (FS+). *Epileptic. Disord.* 22, 323–326. doi: 10.1684/epd.2020.1167

Jones, S., and Thornton, J. M. (1996). Principles of protein-protein interactions. *Proc. Natl. Acad. Sci. U S A* 93, 13–20. doi: 10.1073/pnas.93.1.13

Kasperaviciute, D., Catarino, C. B., Matarin, M., Leu, C., Novy, J., Tostevin, A., et al. (2013). Epilepsy, hippocampal sclerosis and febrile seizures linked by common genetic variation around SCN1A. *Brain* 136, 3140–3150. doi: 10.1093/brain/awt233

Kyte, J., and Doolittle, R. F. (1982). A simple method for displaying the hydropathic character of a protein. *J. Mol. Biol.* 157, 105–132. doi: 10.1016/0022-2836(82)90515-0

Lacroix, J. J., Hyde, H. C., Campos, F. V., and Bezanilla, F. (2014). Moving gating charges through the gating pore in a Kv channel voltage sensor. *Proc. Natl. Acad. Sci. U S A* 111, E1950–E1959. doi: 10.1073/pnas.1406161111

Liao, W. P., Shi, Y. W., Long, Y. S., Zeng, Y., Li, T., Yu, M. J., et al. (2010). Partial epilepsy with antecedent febrile seizures and seizure aggravation by antiepileptic drugs: associated with loss of function of Na(v) 1.1. *Epilepsia* 51, 1669–1678. doi: 10.1111/j.1528-1167.2010.02645.x

Liu, J., Tong, L., Song, S., Niu, Y., Li, J., Wu, X., et al. (2018). Novel and de novo mutations in pediatric refractory epilepsy. *Mol. Brain* 11:48. doi: 10.1186/s13041-018-0392-5

Lossin, C., Rhodes, T. H., Desai, R. R., Vanoye, C. G., Wang, D., Carniciu, S., et al. (2003). Epilepsy-associated dysfunction in the voltage-gated neuronal sodium channel SCN1A. *J. Neurosci.* 23, 11289–11295. doi: 10.1523/JNEUROSCI.23-36-11289.2003

Meisler, M. H., and Kearney, J. A. (2005). Sodium channel mutations in epilepsy and other neurological disorders. *J. Clin. Invest.* 115, 2010–2017. doi: 10.1172/JCI25466

Meng, H., Xu, H. Q., Yu, L., Lin, G. W., He, N., Su, T., et al. (2015). The SCN1A mutation database: updating information and analysis of the relationships among genotype, functional alteration and phenotype. *Hum. Mutat.* 36, 573–580. doi: 10.1002/humu.22782

Mulley, J. C., Scheffer, I. E., Petrou, S., Dibbens, L. M., Berkovic, S. F., and Harkin, L. A. (2005). SCN1A mutations and epilepsy. *Hum. Mutat.* 25, 535–542. doi: 10.1002/humu.20178

Nabbout, R., Gennaro, E., Dalla Bernardina, B., Dulac, O., Madia, F., Bertini, E., et al. (2003). Spectrum of SCN1A mutations in severe myoclonic epilepsy of infancy. *Neurology* 60, 1961–1967. doi: 10.1212/01.wnl.0000069463.41870.2f

Okamura, Y., Fujiwara, Y., and Sakata, S. (2015). Gating mechanisms of voltage-gated proton channels. *Annu. Rev. Biochem.* 84, 685–709. doi: 10.1146/annurev-biochem-060614-034307

Pan, X., Li, Z., Jin, X., Zhao, Y., Huang, G., Huang, X., et al. (2021). Comparative structural analysis of human Nav1.1 and Nav1.5 reveals mutational hotspots for sodium channelopathies. *Proc. Natl. Acad. Sci. U S A* 118:e2100066118. doi: 10.1073/pnas.2100066118

Papazian, D. M., Shao, X. M., Seoh, S. A., Mock, A. F., Huang, Y., and Wainstock, D. H. (1995). Electrostatic interactions of S4 voltage sensor in shaker K+ channel. *Neuron* 14, 1293–1301. doi: 10.1016/0896-6273(95)90276-7

Payandeh, J., Gamal El-Din, T. M., Scheuer, T., Zheng, N., and Catterall, W. A. (2012). Crystal structure of a voltage-gated sodium channel in two potentially inactivated states. *Nature* 486, 135–139. doi: 10.1038/nature11077

Pless, S. A., Galpin, J. D., Niciforovic, A. P., and Ahern, C. A. (2011). Contributions of counter-charge in a potassium channel voltage-sensor domain. *Nat. Chem. Biol.* 7, 617–623. doi: 10.1038/nchembio.622

Rogers, J. C., Qu, Y., Tanada, T. N., Scheuer, T., and Catterall, W. A. (1996). Molecular determinants of high affinity binding of alpha-scorpion toxin and sea anemone toxin in the S3–S4 extracellular loop in domain IV of the Na+ channel alpha subunit. *J. Biol. Chem.* 271, 15950–15962. doi: 10.1074/jbc.271.27.15950

Starace, D. M., and Bezanilla, F. (2004). A proton pore in a potassium channel voltage sensor reveals a focused electric field. *Nature* 427, 548–553. doi: 10.1038/nature02270

Tang, B., Li, B., Gao, L. D., He, N., Liu, X. R., Long, Y. S., et al. (2020). Optimization of in silico tools for predicting genetic variants: individualizing for genes with molecular sub-regional stratification. *Brief Bioinform.* 21, 1776–1786. doi: 10.1093/bib/bbz115

Wang, J., Yarov-Yarovoy, V., Kahn, R., Gordon, D., Gurevitz, M., Scheuer, T., et al. (2011). Mapping the receptor site for alpha-scorpion toxins on a Na+ channel voltage sensor. *Proc. Natl. Acad. Sci. U S A* 108, 15426–15431. doi: 10.1073/pnas.1112320108

Weatherall, K. L., Seutin, V., Liegeois, J. F., and Marrion, N. V. (2011). Crucial role of a shared extracellular loop in apamin sensitivity and maintenance of pore shape of small-conductance calcium-activated potassium (SK) channels. *Proc. Natl. Acad. Sci.* U S A 108, 18494–18499. doi: 10.1073/pnas.1110724108

Yang, Y. C., Hsieh, J. Y., and Kuo, C. C. (2009). The external pore loop interacts with S6 and S3–S4 linker in domain 4 to assume an essential role in gating control and anticonvulsant action in the Na(+) channel. *J. Gen. Physiol.* 134, 95–113. doi: 10.1085/jgp.200810158

Yarov-Yarovoy, V., DeCaen, P. G., Westenbroek, R. E., Pan, C. Y., Scheuer, T., Baker, D., et al. (2012). Structural basis for gating charge movement in the voltage sensor of a sodium channel. *Proc. Natl. Acad. Sci. U S A* 109, E93–102. doi: 10.1073/pnas.1118434109

Conflict of Interest: The authors declare that the research was conducted in the absence of any commercial or financial relationships that could be construed as a potential conflict of interest.

Publisher's Note: All claims expressed in this article are solely those of the authors and do not necessarily represent those of their affiliated organizations, or those of the publisher, the editors and the reviewers. Any product that may be evaluated in this article, or claim that may be made by its manufacturer, is not guaranteed or endorsed by the publisher.

frontiers in Molecular Neuroscience

ORIGINAL RESEARCH
published: 12 January 2022
doi: 10.3389/fnmol.2021.775479

The Role of *Microtubule Associated Serine/Threonine Kinase 3* Variants in Neurodevelopmental Diseases: Genotype-Phenotype Association

Li Shu[1,2,3†], Neng Xiao[4†], Jiong Qin[5], Qi Tian[1], Yanghui Zhang[6], Haoxian Li[6], Jing Liu[7], Qinrui Li[5], Weiyue Gu[8], Pengchao Wang[8], Hua Wang[1,2] and Xiao Mao[1,2*]*

[1] Department of Medical Genetics, Hunan Provincial Maternal and Child Health Care Hospital, Changsha, China, [2] National Health Commission Key Laboratory for Birth Defect Research and Prevention, Hunan Provincial Maternal and Child Health Care Hospital, Changsha, China, [3] Department of School of Life Sciences, Central South University, Changsha, China, [4] Department of Pediatric Neurology, Chenzhou First People's Hospital, Chenzhou, China, [5] Department of Pediatrics, Peking University People's Hospital, Beijing, China, [6] Medical Genetics Center, Jiangmen Maternity and Child Health Care Hospital, Jiangmen, China, [7] Cipher Gene LLC, Beijing, China, [8] Chigene (Beijing) Translational Medical Research Center Co., Ltd., Beijing, China

OPEN ACCESS

Edited by:
Xiaorong Liu,
Guangzhou Medical University, China

Reviewed by:
Laurence Goutebroze,
Institut National de la Santé et de la Recherche Médicale (INSERM), France
Yu Peng,
Hunan Children's Hospital, China

***Correspondence:**
Xiao Mao
gbtechies@outlook.com
Hua Wang
wanghua_213@hotmail.com

† These authors have contributed equally to this work and share first authorship

Specialty section:
This article was submitted to Molecular Signaling and Pathways, a section of the journal Frontiers in Molecular Neuroscience

Received: 14 September 2021
Accepted: 25 November 2021
Published: 12 January 2022

Citation:
Shu L, Xiao N, Qin J, Tian Q, Zhang Y, Li H, Liu J, Li Q, Gu W, Wang P, Wang H and Mao X (2022) The Role of Microtubule Associated Serine/Threonine Kinase 3 Variants in Neurodevelopmental Diseases: Genotype-Phenotype Association. Front. Mol. Neurosci. 14:775479. doi: 10.3389/fnmol.2021.775479

Objective: To prove microtubule associated serine/threonine kinase 3 (*MAST3*) gene is associated with neurodevelopmental diseases (NDD) and the genotype-phenotype correlation.

Methods: Trio exome sequencing (trio ES) was performed on four NDD trios. Bioinformatic analysis was conducted based on large-scale genome sequencing data and human brain transcriptomic data. Further *in vivo* zebrafish studies were performed.

Results: In our study, we identified four *de novo MAST3* variants (NM_015016.1: c.302C > T:p.Ser101Phe; c.311C > T:p.Ser104Leu; c.1543G > A:p.Gly515Ser; and c.1547T > C:p.Leu516Pro) in four patients with developmental and epileptic encephalopathy (DEE) separately. Clinical heterogeneities were observed in patients carrying variants in domain of unknown function (DUF) and serine-threonine kinase (STK) domain separately. Using the published large-scale exome sequencing data, higher CADD scores of missense variants in DUF domain were found in NDD cohort compared with gnomAD database. In addition, we obtained an excess of missense variants in DUF domain when compared autistic spectrum disorder (ASD) cohort with gnomAD database, similarly an excess of missense variants in STK domain when compared DEE cohort with gnomAD database. Based on Brainspan datasets, we showed that *MAST3* expression was significantly upregulated in ASD and DEE-related brain regions and was functionally linked with DEE genes. In zebrafish model, abnormal morphology of central nervous system was observed in *mast3a/b* crispants.

Conclusion: Our results support the possibility that *MAST3* is a novel gene associated with NDD which could expand the genetic spectrum for NDD. The genotype-phenotype correlation may contribute to future genetic counseling.

Keywords: *MAST3*, genetics, neurodevelopmental, epilepsy, domain

INTRODUCTION

Microtubule associated serine/threonine kinase 3 [*MAST3* (MIM 612258)] gene belongs to microtubule-associated serine/threonine kinase (MAST) family which harbors conserved protein domains including a central microtubule-associated serine-threonine kinase domain (STK) flanked by domain of unknown function (DUF) (Hain et al., 2014). *MAST3* is selectively expressed in brain especially in cerebral cortex (Garland et al., 2008) and mediated vital neuronal functions, such as neuronal survival, neurite outgrowth, and others (Delhommel et al., 2015; Khan et al., 2019).

In *MAST* gene family, *MAST1* gene has been reported to cause neurodevelopmental diseases (NDD). The representative clinical phenotypes of the patients are mega-corpus-callosum syndrome with cerebellar hypoplasia and cortical malformations (MCC-CH-CM) (MIM:618273) (McMichael et al., 2015; Tripathy et al., 2018; Ben-Mahmoud et al., 2020; Rodriguez-Garcia et al., 2020). *MAST2-4* genes have never been reported to be associated with neurological disorders until 2021. Spinelli et al. (2021) reported that patients with *de novo* variants in STK domain of *MAST3* gene showed concomitant developmental and epileptic encephalopathy (DEE) phenotypes (Spinelli et al., 2021).

In our study, we identified four *de novo* heterozygous variants in *MAST3* gene in four NDD patients using trio exome sequencing (trio ES). Genotype-phenotype correlations were observed. Together with bioinformatic analyses and functional studies on zebrafish model, our study indicated that *MAST3* variants may be related to variable neurodevelopmental phenotypes from intellectual disability (ID) with epilepsy to ID with autistic spectrum disorder (ASD).

MATERIALS AND METHODS

Trio Exome Sequencing

Genomic DNA from peripheral blood leukocytes of four trios were extracted using the Qiagen DNA Blood Midi/Mini Kit (Qiagen GmbH, Hilden, Germany). DNA was then captured using the IDT xGen Exome Research Panel (Integrated DNA Technologies, San Diego, CA, United States) and was sequenced on Novaseq 6000 platform (Illumina, San Diego, CA, United States). Sequencing reads were aligned to the human reference genome (UCSC hg19/GRCh37). Bioinformatic analyses were performed according to the standard protocol of Ulintz et al. (2019). Human population databases, such as gnomAD, ExAC, and 1000 genomes were used for variant filtration. *In silico* prediction algorithms, such as SIFT, Polyphen-2, LRT, and MutationTaster were used for variant pathogenicity. GERP++, phyloP, phastCons, and SiPhy were used for variant conservation prediction. Sanger sequencing was performed for variant validation.

Bioinformatics and Statistics

Burden Analysis

ANNOtate VARiation (ANNOVAR) was used to annotate all *MAST3* variants (Wang et al., 2010). Excess of *MAST3 de novo* variants was analyzed using two statistic models (DenovolyzeR and CH model). Briefly, we derived the expected number of *de novo* events in a given population based on the mutability of the *MAST3* and the number of probands sequenced. Then, we compared the observed number of *de novo* variants against expectation using Poisson framework (DenovolyzeR) or binormal model (CH model) (O'Roak et al., 2012; Lal et al., 2020). Correction for multiple tests was performed using Bonferroni method.

The *MAST3* expression pattern in the brain development: RNA-seq data in different developmental stages (from 8 post-conceptional weeks to 40 years) from multifarious brain regions were obtained from Brainspan.[1] RNA expression was normalized to reads per kilobase million (RPKM). Univariate linear regression was applied by using lm() function in R[2] for analyzing *MAST3* expression mode in temporal cortex (TC) and dorsolateral prefrontal cortex (DFC).

Co-expression Analysis

A gene with RPKM >0.5 in 80% of all developing cortex tissues was regarded as a cortex-expressed gene. In total, 50 known genes associated with dominant DEE syndromes were defined as known DEE gene set (Heyne et al., 2018). Furthermore, 143 known NDD genes combined 50 known DEE genes with NDD genes identified in previous research (Heyne et al., 2018). Two gene sets were both applied to calculate Spearman's correlation coefficient with all cortex-expressed genes. Next, the mean of Spearman's correlation coefficient of each cortex-expressed gene in known DEE gene set or NDD gene set was computed. Percentile of average correlation coefficient between *MAST3* and DEE gene set or NDD gene set was acquired.

Zebrafish Studies

Zebrafish Maintenance

Adult zebrafish was maintained in tanks with circulating water at 28°C on a 14/10 h light/dark cycle and fed two times a day. Zebrafish embryos were obtained by mating adult fish through standard methods (Avdesh et al., 2012). Larvae were raised in embryo media consisting of 0.03% Instant Ocean and 0.0002% methylene blue in reverse osmosis-distilled water. Transgenic line [*Tg* (*HuC:eGFP*)](Park et al., 2000) with neuron-expressing enhanced green florescent protein (eGFP) were used. All procedures were performed in accordance with the Guide for the Care and Use of Animals (National Research Council, 2011) and the guidelines and regulations of Cipher Gene, LLC.

Gene Editing and Tracking of Indels by Decomposition Assessment

The zebrafish genome has two *MAST3* orthologs: *mast3a* (ENSDARG00000061725) and *mast3b* (ENSDARG00000086505). Single guide RNA (sgRNA) targets were identified using the CHOPCHOP online tool and were obtained from GenScript. Four sgRNAs designed for each gene are as follows (PAM sequence in lowercase):

[1]http://www.brainspan.org/

[2]www.r-project.org/

cccACCCCAGATGACCTCAATCG, cccCAGATGACCTCAATCGCCTC, cccTCTCGGTTCCATCCTCGCTC, cctCTCGGTTCCATCCTCGCTCC for *mast3a*, and ccaCCAGCTTCCATACCAGCCCA, ccgAAGTTCGGAGAGCATGACTG, cctCCACGTTTATAAGACCCCGG, cccCGGTCACGTAGCCTTAGGTA for *mast3b*. The ortholog evaluation is conducted using the online tool-DIOPT Ortholog Finder. The protein identities between human MAST3 and zebrafish ortholog genes are 62% for mast3a and 63% for mast3b. The protein identity between zebrafish paralogs mast3a and mast3b is 70%. To generate mutagenesis in each targeted gene, fertilized embryos (1–2 cell stage) were injected with ∼2 nl CRISPR complexes composed of four sgRNAs (90 ng/μl for each sgRNA) and Cas9 protein (200 ng/μl). At 24 h after injection, few embryos from the injected group were pooled and sanger sequenced to verify the mutagenesis efficacy using the tracking of indels by decomposition (TIDE) online tool (Brinkman et al., 2014). *Post hoc* genotyping was performed after phenotypic studies. Individual larvae were collected for sequencing and TIDE analysis was used to confirm the mutagenesis. Larvae with TIDE efficacy <5% were excluded from phenotypic data analysis.

Imaging and Morphological Measurement

At six dpf, *Tg* (*HuC*: *eGFP*) larvae were placed in a customized mini-well (5 mm diameter and 1 mm depth) plate (one fish/well) with dorsal side up for bright-field and florescent imaging. Images were acquired with a Touptek CCD camera and Nikon SMZ800N stereo fluorescence microscope with × 1.5 magnification for bright-field imaging and × 4 magnification for florescent imaging. Images were then analyzed in Fiji (ImageJ) for body length and central nervous system (CNS) area measurements.

Statistics

Statistical analyses were performed with Prism 8 (GraphPad Software, CA, United States), using unpaired *t*-test for qualitative data. Significance for all tests was defined as $^{*}p < 0.05$; $^{**}p < 0.01$; and $^{***}p < 0.001$.

RESULTS

Clinical Presentations of Patients

The clinical features of patient 1–4 are shown in **Table 1**. Patient 1 is a 6-year-old male at present who was born at full term with normal pregnancy. At present, patient 1 has reached a normal motor developmental milestone. The 6-year-old male rarely communicate and have trouble learning to count. Patient 1 was fascinated by spinning wheels of a car, playing with hands, and repeating words of people.

Patient 2 is a four year and a half male who was born at full term without abnormality in pregnancy. At present, patients 2 is easy to fall when running and cannot get dressed. This patient does not want to play with peers and lacks eye contact.

Patient 3 is a 10-year-old male child who was born at full term with normal pregnancy. The patient 3 had seizures at the age of 3 months without inducement. Frequent nodding about 10 times a day was observed. Patient 3 began to present typical "nodding and holding ball" movements soon, accompanied by loss of consciousness, cyanosis of lips, and face. The boy was diagnosed as "infantile spasms" and given topiramate as anti-epileptic therapy. At the age of 2 years, the "nod and holding ball" movements disappeared gradually, and a new attack form appeared. Eyes staring, rigidity, and contraction of limbs, accompanied by loss of consciousness, mild cyanosis of face and lips were observed. Suspected Lennox-Gastaut syndrome (LGS) was diagnosed. After 3 months, another new attack form appeared that the patient showed sudden head tilting forward, mouth opening accompanied by salivation. The patient was diagnosed as "LGS." After 1 year of treatment with clonazepam, the patient still had many atypical absence seizures per day. The patient presented with global developmental delay and could not walk or speak words. No other neurological abnormality was observed.

Patient 4 is a 12-year-old male who was born at full term without abnormality in pregnancy. At the age of 1 year and 11 months, without inducement, generalized tonic-clonic seizure epilepsy (GTCS) was observed. Anti-epileptic drug levetiracetam was given to the patient and the seizures were relieved. At present, motor development is normal but language development is delayed.

Hence, it is reasonable to speculate that due to different protein domains in which the variants are located, these four patients showed different clinical features.

Variant Predictions

Four novel *de novo MAST3* variants were identified in proband 1–4 separately using trio-ES and Sanger validation (**Table 1** and **Figure 1**). These variants are classified as likely pathogenic by ACMG guidelines. They are absent from human population databases gnomAD, ExAC, and 1000 genomes. They are predicted to be deleterious by SIFT, Polyphen-2, LRT, MutationTaster algorithms and predicted to be conserved by GERP++, phyloP, phastCons, and SiPhy algorithms. These variants lied in protein domains DUF and STK in *MAST3* (**Figure 2A**).

Bioinformatic Analysis

De novo Microtubule Associated Serine/Threonine Kinase 3 Missense Variants in Domain of Unknown Function and Serine-Threonine Kinase Domain Exhibit Excess in Neurodevelopmental Diseases

In our study, we found a significant enrichment of *MAST3* variants (we did not include two missense variants without detailed data) (denovolyzeR: $p = 0.00152$, Bonferroni = 1; CH-model: $p = 0.001994$, Bonferroni = 1) *via* analysis of *de novo* variants by two statistic models. However, the significance did not exist after we performed a genome-wide Bonferroni correction. By combining published NDD studies with large cohorts, fifteen *de novo* missense variants (we did not include two missense variants without detailed data) were obtained from 36,347 probands (**Table 2** and **Figure 2A**). We observed significant results in two models (denovolyzeR:

TABLE 1 | Summary of genotype and phenotype information for NDD in individuals with *Microtubule associated serine/threonine kinase 3* variants.

Case index	1	2	3	4
Variant (NM_015016.1)	c.302C > T:p.Ser101Phe	c.311C > T:p.Ser104Leu	c.1547T > C:p.Leu516Pro	c.1543G > A:p.Gly515Ser
ACMG classification	Likely pathogenic (PS2, PM1, PM2)	Likely pathogenic (PS2, PM1, PM2 PP3)	Likely pathogenic (PS2, PM1, PM2)	Likely pathogenic (PS2, PM1, PM2)
Protein domain the variant located	DUF	DUF	STK	STK
Age at last examination (years)	Six	four and a half	Ten	twelve
Age at onset-seizure	NA	NA	3 months	1 year and 11 months
Gender	male	Male	Male	male
Global developmental delay/intellectual disability (diagnosed by Gessel or WAIS)	Yes	Yes	Yes	yes
Epilepsy type	NA	NA	LGS	GTCS
Epilepsy controlled	NA	NA	No	yes
ASD (diagnosed by ABC, CARS)	Yes	Yes	No	no
Hypotonia	No	No	Yes	no
Brain MRI	normal	normal	Normal	normal
EEG	NA	NA	15–25 Hz low amplitude fast waves and complex slow waves burst for 1.2 s, followed by diffuse voltage reduction for 4 s and a large number of multifocal and 1.5–2.5 Hz high amplitude spike-slow waves with sharp waves and slow waves (3 months); 15–25 Hz spikes burst intermittently for 2.5 s on the background of diffuse slow waves (2 years);20–25 Hz spikes burst for 4.5 s (2 years and 3 months)	spikes in bilateral central, parietal and temporal areas of brain

PS2, de novo (both maternity and paternity confirmed) in a patient with the disease and no family history; PM1, Located in a mutational hot spot and/or critical and well-established functional domain (e.g., active site of an enzyme) without benign variation; PM2, Absent from controls (or at extremely low frequency if recessive) in Exome Sequencing Project, 1000 Genomes Project, or Exome Aggregation Consortium; PP3, Multiple lines of computational evidence support a deleterious effect on the gene or gene product (conservation, evolutionary, splicing impact, etc.); WAIS, Wechsler Adult Intelligence Scale; ABC, Autistic Behavior Checklist; CARS, Childhood Autism Rating Scale.

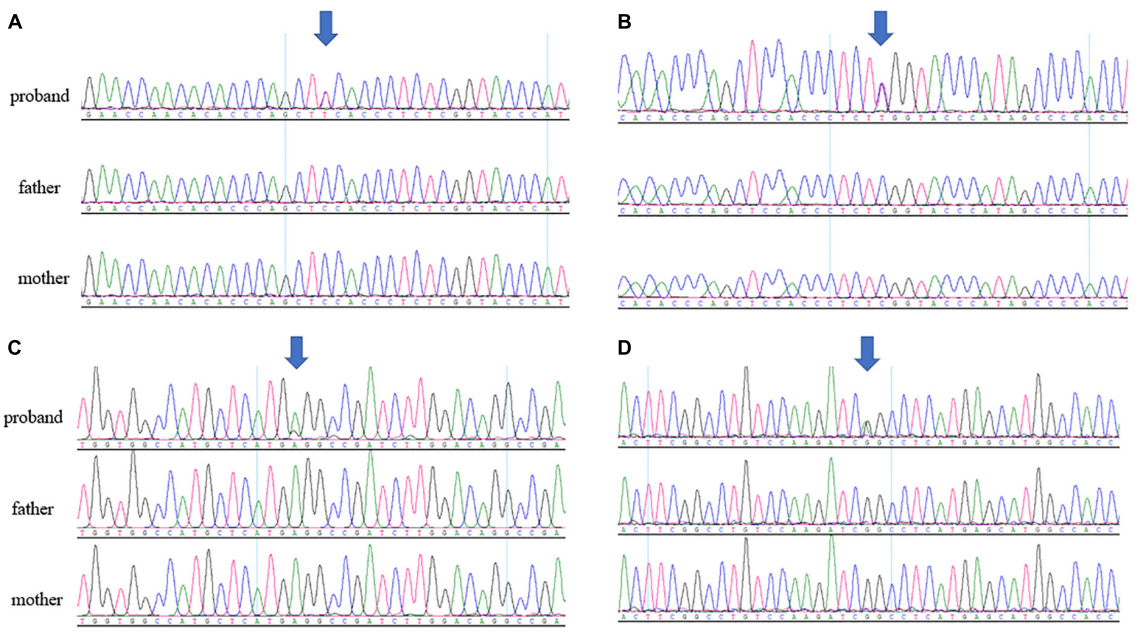

FIGURE 1 | (A) Sanger sequencing results of c.302C > T in patient 1 trio. **(B)** Sanger sequencing results of c.311C > T in patient 2 trio. **(C)** Sanger sequencing results of c.1547T > C in patient 3 trio. **(D)** Sanger sequencing results of c.1543G > A in patient 4 trio. The arrows pointed to the location of the variants.

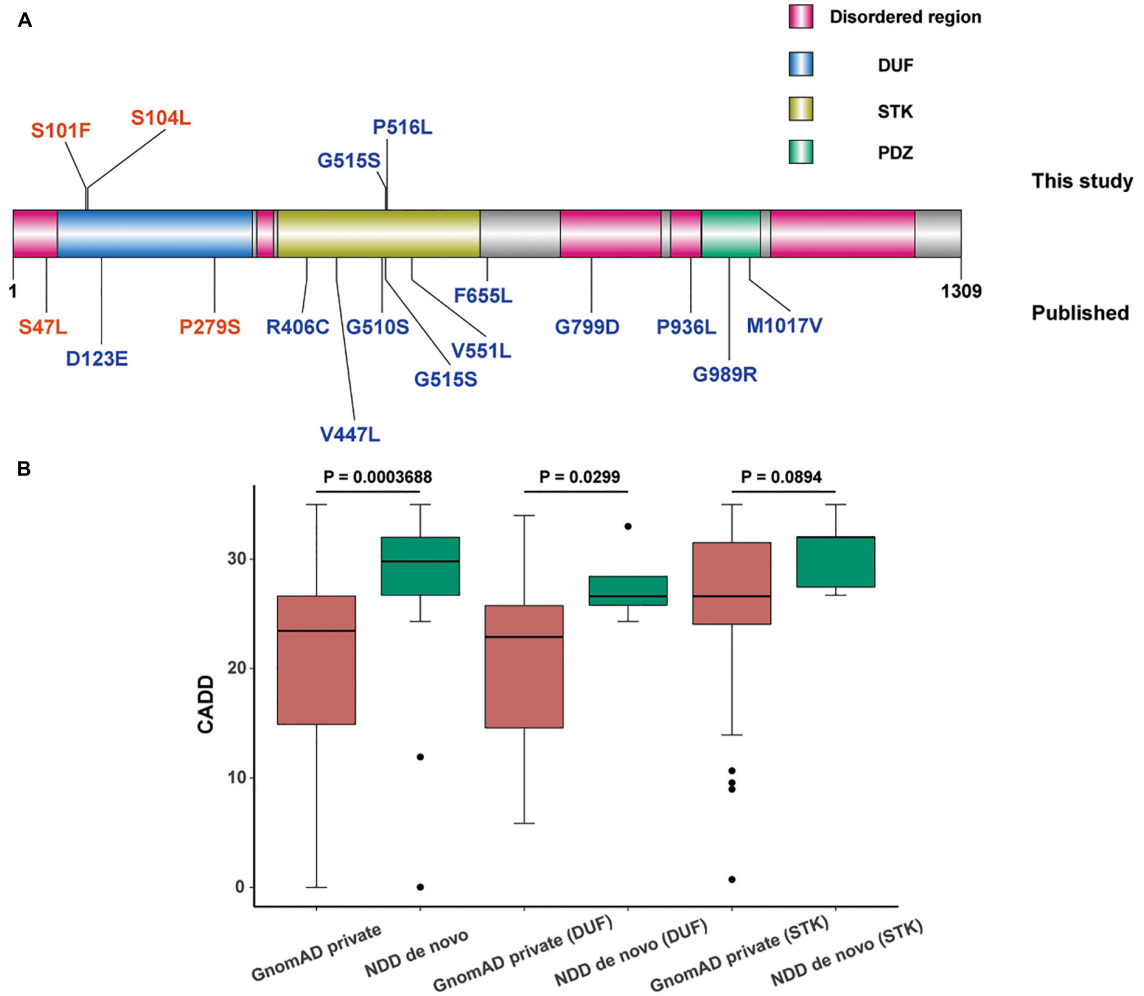

FIGURE 2 | Distribution and comparison of pathogenicity of missense mutations in domain of unknown function (DUF) and serine-threonine kinas (STK) domain of *microtubule associated serine/threonine kinase 3* (*MAST3*). **(A)** Schematic representation of missense variations in *MAST3*. Variations above and under the protein domain graph are originated from this study and published research, respectively. The colors in the *MAST3* protein represented different protein domains (pink: disordered region, blue: DUF domain, yellow: STK domain, and green: PDZ domain). The different colors of the variants showed different diseases (red, ASD; blue, DD). **(B)** Box plot of CADD of *de novo* (neurodevelopmental diseases, NDD)/private (GnomAD) missense mutations in DUF or STK domain. Higher CADD scores of missense variants in total and in DUF region of *MAST3* were found in NDD cohort compared with that in gnomAD database (p = 0.0003688, 0.0229, Wilcoxon test). Significance was lost when the same analysis was performed for STK domain variants (p = 0.0894, Wilcoxon test).

p = 4.07E-06, Bonferroni = 0.0798; CH-model: p = 2.051E-05, Bonferroni = 0.40236518). However, statistically non-significant results were found after correction in the scope of genome (corrected for ∼19,000 genes).

Interestingly, in our cohort, four *de novo MAST3* missense variants lie in DUF or STK domain separately, so we expected to further explore the domain-related clinical heterogeneity. For DUF domain (58–311 aa), higher CADD scores of missense variants in *MAST3* were found in NDD cohort compared with that in gnomAD database (p = 0.0229, Wilcoxon test) (**Figure 2B**). Significance was lost when the same analysis was performed for STK domain variants (366–645 aa) (p = 0.0894, Wilcoxon test) though it was closed to the threshold of statistical significance (**Figure 2B**). More importantly, we obtained an excess of missense variant in DUF domain when only consider ASD cohort compared with gnomAD database [2 probands in 2,210 ASD individuals vs. 48 carriers in 125,748 gnomAD samples, odds ratio (*OR*) = 2.37, p = 0.2139, Fisher's exact test]. Similarly, a higher *OR* was found in STK domain when only consider DEE cohort compared with gnomAD database (1 probands in 585 individuals vs. 51 carriers in 125,748 gnomAD samples, *OR* = 4.21, p = 0.2147, Fisher's exact test). Above insignificant p-value may be due to insufficient number of individuals carrying *MAST3* variants. These results supported our clinical data to some extent.

Spatio-Temporal Modes of *Microtubule Associated Serine/Threonine Kinase 3*

To elucidating the key role of *MAST3* in developing brain, RNA sequencing data from BrainSpan was used to find out

TABLE 2 | Summary of *Microtubule associated serine/threonine kinase 3 de novo* missense variants identified in neurodevelopmental disorders.

Index	Sample ID	gDNA change (chr19, hg19)	Function	Coding change	Protein change	SIFT	Polyphen-2	CADD	Inheritance	gnomAD (non-neuro)	PMID	Cohort size	Primary diagnosis
1	UK10K_SKUSE5080236	g.18232563C > T	Missense	c.140C > T	p.47S > L	D	D	32	*de novo*		31981491	3,899	ASD
2	9Y0069	g.18233551C > T	Missense	c.302C > T	p.101S > F	D	D	33	*de novo*		This study	585	ASD
3	DDN20002957	g.18233560C > T	Missense	c.C311T	p.S104L	D	D	26.3	*de novo*		This study (co-operation)	30,000	ASD
4	DDD4K.02825	g.18234083C > G	Missense	c.369C > G	p.123D > E	T	P	24.3	*de novo*		28135719	4,293	DD
5	1-0998-003	g.18235153C > T	Missense	c.835C > T	p.279P > S	D	D	26.9	*de novo*		28263302	1,625	ASD
6	DDD13k.01676	g.18241383C > T	Missense	c.1216C > T	p.406R > C	D	D	35	*de novo*		33057194	25,945	DD
7	117791	g.18241506G > C	Missense	c.1339G > C	p.447V > L	T	P	27.5	*de novo*		33057194	25,945	DD
8	DDD13k.00098	g.18245432G > A	missense	c.1528G > A	p.510G > S	D	D	32	*de novo*		33057194	25,945	DD
9	76597	g.18245447G > A	Missense	c.1543G > A	p.515G > S	D	D	32	*de novo*		33057194	25,945	DD
10	DD18006823	g.18245447G > A	Missense	c.G1543A	p.515G > S	D	D	32	*de novo*		This study (co-operation)	30,000	EE
11	9Y3441	g.18245451T > C	Missense	c.1547T > C	p.516L > P	D	P	26.7	*de novo*		This study	585	EE
12	96317	g.18245660G > T	Missense	c.1651G > T	p.551V > L	D	P	27.4	*de novo*		33057194	25,945	DD
13	97813	g.18248126T > C	Missense	c.1963T > C	p.655F > L	D	P	29.8	*de novo*		33057194	25,945	DD
14	2677	g.18254716G > A	Missense	c.2396G > A	p.799G > D	T	B	0.028	*de novo*		33057194	25,945	DD
15	DDD13k.00479	g.18255894C > T	Missense	c.2807C > T	p.936P > L	D	D	33	*de novo*	0.00007704	33057194	25,945	DD
16	DDD13k.03362	g.18256565G > A	Missense	c.2965G > A	p.989G > R	D	D	33	*de novo*		33057194	25,945	DD
17	3099	g.18256649A > G	Missense	c.3049A > G	p.1017M > V	T	B	11.92	*de novo*	0.00001239	33057194	25,945	DD

Isoform, NM_015016.2; ASD, Autism Spectrum Disorder; DD, Developmental Disorder; EE, Epileptic Encephalopathy; T, Tolerable; P, Possibly_damaging; B, Benign; D, Deleterious.

the spatio-temporal expression pattern of *MAST3*. We found a time-dependent upregulation *MAST3* expression in fetal brain (**Figure 3A**). Differently, high expression level was observed during post-birth periods in most brain regions (**Figure 3B**). To reveal a dynamic change of *MAST3* in DEE-related and ASD-relevant brain regions during brain development, such as TC and DFC (Ives-Deliperi and Butler, 2021; Jassim et al., 2021), a univariate linear regression analysis was applied. In TC and DFC, expression of *MAST3* was significantly upregulated during the period of embryonic development (TC: R^2 = 0.785 and p = 3.403E-05, DFC: R^2 = 0.4958 and p = 0.0016) than that during the post-natal period (TC: R^2 = 0.332 and p = 0.002961, DFC: R^2 = 0.2463 and p = 0.0362) (**Figures 3C–F**). These data implicated a potential role of *MAST3* during embryonic developing periods.

Co-expression of *Microtubule Associated Serine/Threonine Kinase 3* With Well-Established DEE/Neurodevelopmental Diseases Genes

Microtubule associated serine/threonine kinase 3 is a member of Microtubule Associated Serine/Threonine Kinase family. Regrettably, the biological function of MAST3 in NDD still remains unknown. PTEN which interacts with MAST3 from STRING database was found to be related to DEE, ASD, etc. (Hobert et al., 2014; Marchese et al., 2014).

We further explored the potentially biologic connection of *MAST3* with DEE and NDD genes using gene co-expression analysis. We wondered whether *MAST3* is highly co-expressed with DEE or NDD genes compared with other cortex-expressed genes. Spearman's correlation coefficients of all protein-coding genes with well-established DEE and NDD gene sets were calculated. *MAST3* was strongly correlated with known DEE genes (Percentile = 3.40%) compared with NDD genes (Percentile = 30.43%) (**Figures 4A,B**). In total, nine DEE/NDD genes were highly correlated with *MAST3* (Spearman's correlation coefficient > 0.7) (**Figure 4C**). Above analysis uncovered the potential relationship between *MAST3* and DEE/NDD genes.

In vivo Studies

We created zebrafish models with CRISPR/cas9-induced disruptions in *mast3a* or *mast3b*, two orthologs of human *MAST3*, to investigate the role of *MAST3* in neurodevelopment *in vivo*. The zebrafish F0 CRISPR (crispants) recapitulated the characteristic phenotypes in human NDD-abnormal brain morphology.

At six dpf, *mast3a* crispants showed normal body length (**Figures 5A,B**; n = 20 and 29 fish for cas9 control and *mast3a* crispant, respectively; unpaired t-test, p = 0.3208). Although no significant difference was observed in the whole CNS area (**Figures 5C,D**; unpaired t-test, p = 0.0844), the midbrain area was significantly increased in *mast3a* crispant vs. cas9 controls (**Figure 5E**; unpaired t-test, p = 0.0726, 0.0072, and 0.3123 for forebrain, midbrain, and hindbrain area, respectively). *Mast3b* crispants presented significantly decreased body length (**Figures 5G,H**; n = 20 and 24 fish for cas9 control and *mast3b* crispant, respectively; unpaired t-test, p = 0.0007). Although no

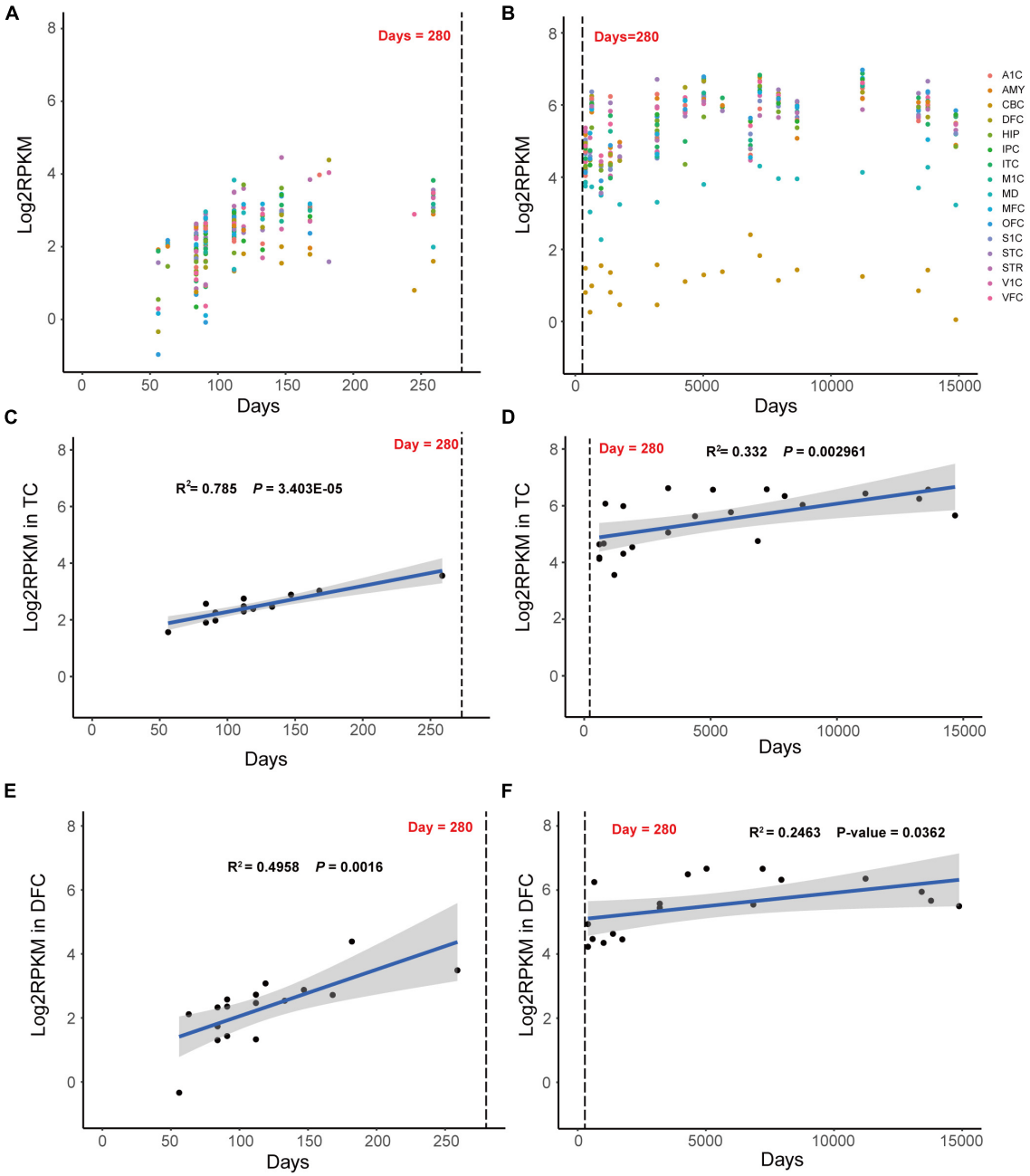

FIGURE 3 | Dynamic expression mode of *MAST3* in human development brains. **(A,B)** Expression of *MAST3* during brain development periods in different brain regions. The *x*-axis is the age of samples in days and *y*-axis is the log2-transformed RPKM of *MAST3*. A1C, primary auditory cortex; AMY, amygdaloid complex; CBC, cerebellar cortex; DFC, dorsolateral prefrontal cortex; HIP, hippocampus; IPC, inferior parietal cortex; ITC, inferolateral temporal cortex; M1C, primary motor cortex; MD, mediodorsal nucleus of thalamus; MFC, medial prefrontal cortex; OFC, orbital frontal cortex; S1C, primary somatosensory cortex; STC, superior temporal cortex; STR, striatum; V1C, primary visual cortex; VFC, ventrolateral prefrontal cortex. The dashed line indicates the birthday. **(C,D)** Expression of *MAST3* in the TC region. **(E,F)** Expression of *MAST3* in the DFC region. Univariate regression analysis was applied in prenatal brains (left) and post-natal brains (right), separately. Blue line represents the regression line and the gray region indicates 95% CI. The text shows the R^2 and *P*-value of regression.

statistically significant difference was observed in the whole CNS area (**Figures 5I,J**; unpaired *t*-test, $p = 0.1558$), the midbrain area was significantly decreased in *mast3b* crispants (**Figure 5K**; unpaired *t*-test, $p = 0.1268$, 0.0073, and 0.2807 for forebrain, midbrain, and hindbrain area, respectively). Electrophysiology and behavior studies were also conducted. No electrographic epileptiform activity or abnormal locomotion behavior was observed in the crispant larvae ($n = 38$ and 31 fish were tested for *mast3a* and *mast3b* crispants, respectively). **Figures 5F,L** showed the TIDE efficacy of the crispant larvae for phenotypic analysis.

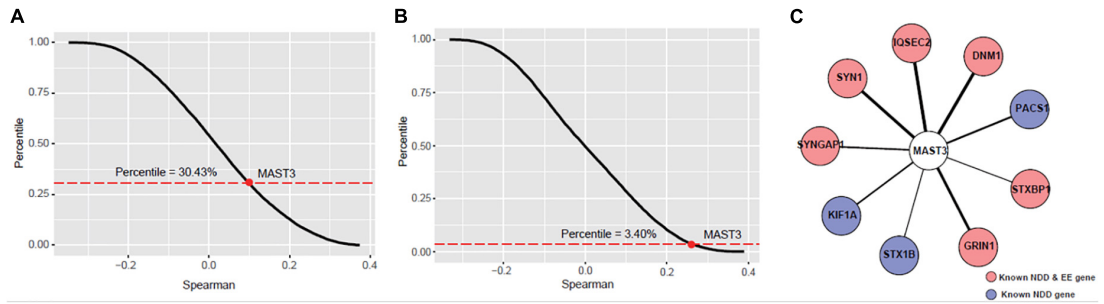

FIGURE 4 | Co-expression analyses of microtubule associated serine/threonine kinase 3 (MAST3) with EE and NDD genes. **(A,B)** The percentile of average correlation coefficient for all developing cortex expressed genes with NDD **(A)** or EE **(B)** genes. The average percentile of MAST3 was marked. **(C)** Interaction network contains nine highly co-expressed EE/NDD genes (Spearman's correlation coefficient > 0.7) with MAST3.

These results suggest that, as in humans, zebrafish *mast3a/b* is critical for brain development and possibly neuronal function.

DISCUSSION

Microtubule-associated serine/threonine kinase protein family has been proved to be highly expressed in brain and was involved in multiple critical neuronal functions (Jing et al., 2020). *De novo* variants in STK domain of *MAST3* gene has been reported to be candidate variants for Rett syndrome-like phenotypes (Iwama et al., 2019) and associated with DEE recently (Spinelli et al., 2021). In our study, combining genetic testing with bioinformatic analysis and functional studies, we reported the role of *MAST3* variants in NDD and its genotype-phenotype correlations.

We identified four *de novo* heterozygous *MAST3* variants in four unrelated patients with NDD. Although all patients showed an NDD phenotypic profile, patient 1 and 2 showed ID with ASD while patient 3 and 4 showed ID with epilepsy. Variants in *MAST3* exhibited heterogeneous clinical presentations, which probably due to different domains the variants located in **Figure 2A**.

These genotype-phenotype relationships were also supported by bioinformatic analysis based on large NDD cohorts. For DUF domain, higher CADD scores of missense variants for *MAST3* were found in NDD cohort compared with gnomAD database. More importantly, we obtained an excess of missense variants in DUF domain when compared ASD cohort with gnomAD database and similarly an excess of missense variants in STK domain when compared DEE cohort with gnomAD database. More patients with *MAST3* variants in DUF domain may yield a significant *p*-value. By applying univariate linear regression analysis using RNA sequencing data from BrainSpan, we found that in ASD-relevant brain region DFC and DEE-related brain region TC (Ives-Deliperi and Butler, 2021; Jassim et al., 2021), the expression of *MAST3* was significantly upregulated during brain development. From the co-expression analysis, nine DEE/NDD genes (*SYNGAP1, SYN1, IQSEC2, DNM1, PACS1, STXBP1, GRIN1, STX1B, and KIF1A*) were highly correlated with *MAST3*. Known NDD and/or EE genes, such as *IQSEC2, DNM1,* and *STX1B*, have all been proved to play a role in vital synaptic functions, such as synaptic vesicle recycling, excitatory synaptic transmission, and calcium-dependent synaptic vesicle release in neurodevelopment (Smirnova et al., 1996; Boumil et al., 2010; Brant et al., 2021). The mutants of these genes could cause synaptic deficit and be associated with NDD and/or EE. The *MAST3* mutations might affect the normal interactions with the nine DEE/NDD genes, cause neuronal dysfunctions thus leading to neurodevelopmental phenotypes. Although there was no supporting evidence to these functional interactions, our study provided a clue for further research.

From the functional perspective, the variants located in the domains might influence the catalytic activity of MAST3 (Iwama et al., 2019), thus affecting its interaction with different targeted proteins involved in neuronal functions (Valiente et al., 2005; Delhommel et al., 2015). It has been reported that MAST3 protein may act synergically with PTEN to moderate signal pathways in neuronal survival, neurite outgrowth, and regeneration (Khan et al., 2019). MAST3 protein could also interact with seizure related transcription factors, zif268, c-fos, c-jun, etc. (Saffen et al., 1988; Xiao et al., 1998). According to our bioinformatic analysis, *MAST3* gene was highly co-expressed with DEE or NDD genes compared with cortex-expressed other genes.

Due to the teleost-specific genome duplication (Meyer and Schartl, 1999; Howe et al., 2013), certain zebrafish gene pairs (ohnologs) have acquired different expression patterns or functions, which could be redundant function, new function, sub-function, or pseudo-function. As a result, it is not unusual to see in zebrafish study that disruptions of a/b copy of a gene show different phenotypes (Force et al., 1999; Kleinjan et al., 2008; Shin et al., 2012; Grone et al., 2016; Holt et al., 2019). In this work, brain morphological abnormality was observed in both zebrafish mast3a and mast3b crispants, so we concluded that zebrafish mast3a and mast3b are critical for brain development. Further study will be needed to elucidate how exactly these genes contribute to the brain development. In addition, human patients carrying *MAST3* missense mutations demonstrates various phenotypes, such as macrocephaly and microcephaly, which may indicate the pathological complexity (Spinelli et al., 2021). The functional study based on zebrafish model also provided evidence for *MAST3* pathogenicity by recapitulating the neurological phenotype of DEE–abnormal brain morphology. Together with the genetic and bioinformatic analysis, our work may confirm

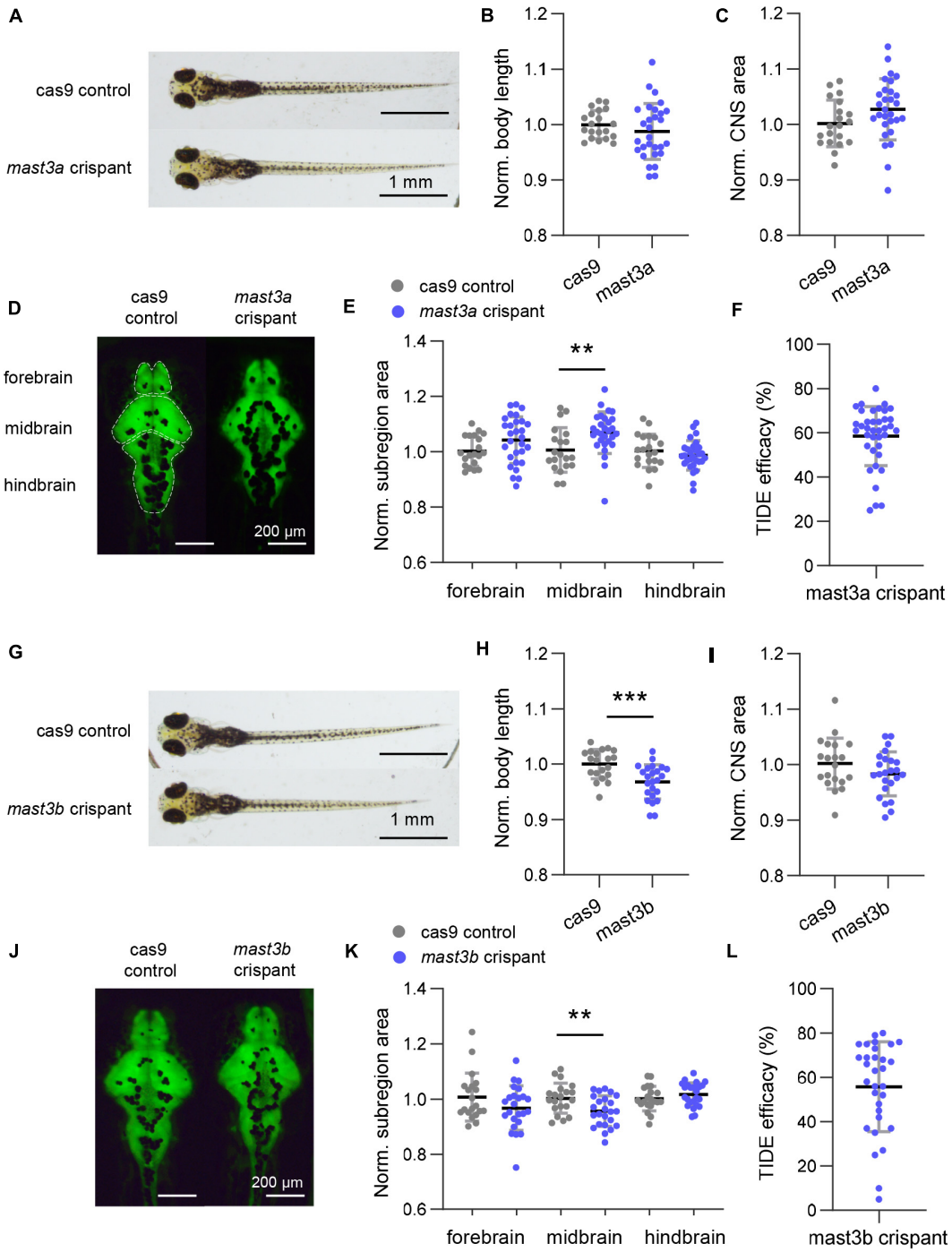

FIGURE 5 | Disruption of zebrafish *mast3a* and *mast3b* led to abnormal central nervous system (CNS) morphology. **(A)** Representative bright-field imaging of larval zebrafish at six dpf (dorsal view). Top, cas9 injected control; bottom, *mast3a* F0 CRISPR (crispant). **(B)** Measurements of body length in cas9 injected control (n = 20 fish) vs. *mast3a* crispant (n = 29 fish). Data were normalized to the average body length of cas9 control group. **(C)** Normalized CNS area in cas9 injected controls vs. *mast3a* crispants. Data were corrected by the normalized body length of individual larvae. **(D)** Representative imaging of HuC: eGFP expressed larval zebrafish shows CNS fluorescence pattern at six dpf (dorsal view). Left, cas9 injected control; right, *mast3a* crispant. White dash line highlights the CNS subregions, forebrain, midbrain, and hindbrain, for measurement. **(E)** Normalized CNS subregion area in cas9 injected control vs. *mast3a* crispant. Data were normalized to the average of each subregion area of cas9 control group, and then corrected by the normalized body length of individual larvae (gray dot, cas9 control; blue dot, *mast3a* crispant). **(F)** CRISPR efficacy calculated *via* TIDE method of individual *mast3a* crispant used in phenotypic study (n = 38 fish). **(G–L)** Data from *mast3b* crispant study (for imaging study, n = 20 fish for cas9 control, and n = 24 fish for *mast3b* crispant; n = 31 crispant for TIDE efficacy verification). Scale bars as indicated in the figure. Error bars indicate SD. Statistical significance is indicated as $^{**}p < 0.01$, and $^{***}p < 0.001$.

the pathogenicity of *MAST3* gene in NDD. However, further functional research on specific neurodevelopmental defects and larger cohorts were needed to elucidate the mechanisms underlying the genotype-phenotype correlation.

CONCLUSION

In conclusion, we first described the genotype-phenotype correlations of *MAST3* gene in NDD. The variants of DUF domain contributed to NDD with a core ASD phenotype while variants of STK contributed to NDD with a core epilepsy phenotype, therefore, conducive to future genetic counseling of *MAST3*.

DATA AVAILABILITY STATEMENT

The datasets for this article are not publicly available due to concerns regarding participant/patient anonymity. Requests to access the datasets should be directed to the corresponding authors.

ETHICS STATEMENT

The studies involving human participants were reviewed and approved by the Ethics Committee of Maternal and Child Health Hospital of Hunan Province (2020-S003). Written informed consent to participate in this study was provided by the participants' legal guardian/next of kin. Written informed consent was obtained from the individual(s), and minor(s)' legal guardian/next of kin, for the publication of any potentially identifiable images or data included in this article. The animal study was reviewed and approved by the Ethics Committee of Maternal and Child Health Hospital of Hunan Province (2020-S003).

AUTHOR CONTRIBUTIONS

XM and HW designed the research. LS and NX wrote the manuscript. YZ and HL performed the bioinformatic analysis. JQ and QL collected, evaluated the clinical, and genetic evidence. LS and JL did the functional studies on zebrafish model. QT revised the manuscript. All authors read and approved the final manuscript.

FUNDING

This work was supported by the National Natural Science Foundation of China (81801136), the Major Scientific and Technological Projects for Collaborative Prevention and Control of Birth Defects in Hunan Province (2019SK1010 and 2019SK1014), the National Key R&D Program of China (2019YFC1005100), the Hunan Provincial Science and Technology Department (2018SK2064), the Natural Science Foundation of Hunan Province, China (2021JJ40280), and the Changsha Municipal Natural Science Foundation (kq2007048).

ACKNOWLEDGMENTS

We thank all the participated patients and their families for their co-operation, as well as our co-operative organization the Chigene (Beijing) Translational Medical Research Center Co., Ltd.

REFERENCES

Avdesh, A., Chen, M., Martin-Iverson, M. T., Mondal, A., Ong, D., Rainey-Smith, S., et al. (2012). Regular care and maintenance of a zebrafish (*Danio rerio*) laboratory: an introduction. *J. Vis. Exp.* 18:e4196. doi: 10.3791/4196

Ben-Mahmoud, A., Al-Shamsi, A. M., Ali, B. R., and Al-Gazali, L. (2020). Evaluating the role of MAST1 as an intellectual disability disease gene: identification of a novel De Novo variant in a patient with developmental disabilities. *J. Mol. Neurosci.* 70, 320–327. doi: 10.1007/s12031-019-01415-8

Boumil, R. M., Letts, V. A., Roberts, M. C., Lenz, C., Mahaffey, C. L., Zhang, Z. W., et al. (2010). A missense mutation in a highly conserved alternate exon of dynamin-1 causes epilepsy in fitful mice. *PLoS Genet.* 6:e1001046. doi: 10.1371/journal.pgen.1001046

Brant, B., Stern, T., Shekhidem, H. A., Mizrahi, L., Rosh, I., Stern, Y., et al. (2021). IQSEC2 mutation associated with epilepsy, intellectual disability, and autism results in hyperexcitability of patient-derived neurons and deficient synaptic transmission. *Mol. Psychiatry* 12:43. doi: 10.1038/s41380-021-01281-0

Brinkman, E. K., Chen, T., Amendola, M., and van Steensel, B. (2014). Easy quantitative assessment of genome editing by sequence trace decomposition. *Nucleic Acids Res.* 42:e168. doi: 10.1093/nar/gku936

Delhommel, F., Chaffotte, A., Terrien, E., Raynal, B., Buc, H., Delepierre, M., et al. (2015). Deciphering the unconventional peptide binding to the PDZ domain of MAST2. *Biochem. J.* 469, 159–168. doi: 10.1042/BJ20141198

Force, A., Lynch, M., Pickett, F. B., Amores, A., Yan, Y. L., and Postlethwait, J. (1999). Preservation of duplicate genes by complementary, degenerative mutations. *Genetics* 151, 1531–1545.

Garland, P., Quraishe, S., French, P., and O'Connor, V. (2008). Expression of the MAST family of serine/threonine kinases. *Brain Res.* 1195, 12–19. doi: 10.1016/j.brainres.2007.12.027

Grone, B. P., Marchese, M., Hamling, K. R., Kumar, M. G., Krasniak, C. S., Sicca, F., et al. (2016). Epilepsy, behavioral abnormalities, and physiological comorbidities in syntaxin-binding protein 1 (STXBP1) mutant zebrafish. *PLoS One* 11:e0151148. doi: 10.1371/journal.pone.0151148

Hain, D., Langlands, A., Sonnenberg, H. C., Bailey, C., Bullock, S. L., and Muller, H. A. (2014). The *Drosophila* MAST kinase drop out is required to initiate membrane compartmentalisation during cellularisation and regulates dynein-based transport. *Development* 141, 2119–2130. doi: 10.1242/dev.104711

Heyne, H. O., Singh, T., Stamberger, H., Abou Jamra, R., Caglayan, H., Craiu, D., et al. (2018). De novo variants in neurodevelopmental disorders with epilepsy. *Nat. Genet.* 50, 1048–1053. doi: 10.1038/s41588-018-0143-7

Hobert, J. A., Embacher, R., Mester, J. L., Frazier, T. W. II, and Eng, C. (2014). Biochemical screening and PTEN mutation analysis in individuals with autism spectrum disorders and macrocephaly. *Eur. J. Hum. Genet.* 22, 273–276. doi: 10.1038/ejhg.2013.114

Holt, R. J., Young, R. M., Crespo, B., Ceroni, F., Curry, C. J., Bellacchio, E., et al. (2019). De Novo missense variants in FBXW11 cause diverse developmental phenotypes including brain, eye, and digit anomalies. *Am. J. Hum. Genet.* 105, 640–657. doi: 10.1016/j.ajhg.2019.07.005

Howe, K., Clark, M. D., Torroja, C. F., Torrance, J., Berthelot, C., Muffato, M., et al. (2013). The zebrafish reference genome sequence and its relationship to the human genome. *Nature* 496, 498–503. doi: 10.1038/nature12111

Ives-Deliperi, V., and Butler, J. T. (2021). Mechanisms of cognitive impairment in temporal lobe epilepsy: a systematic review of resting-state functional connectivity studies. *Epilepsy Behav.* 115:107686. doi: 10.1016/j.yebeh.2020.107686

Iwama, K., Mizuguchi, T., Takeshita, E., Nakagawa, E., Okazaki, T., Nomura, Y., et al. (2019). Genetic landscape of Rett syndrome-like phenotypes revealed by whole exome sequencing. *J. Med. Genet.* 56, 396–407. doi: 10.1136/jmedgenet-2018-105775

Jassim, N., Baron-Cohen, S., and Suckling, J. (2021). Meta-analytic evidence of differential prefrontal and early sensory cortex activity during non-social sensory perception in autism. *Neurosci. Biobehav. Rev.* 127, 146–157. doi: 10.1016/j.neubiorev.2021.04.014

Jing, T., Ma, J., Zhao, H., Zhang, J., Jiang, N., and Ma, D. (2020). MAST1 modulates neuronal differentiation and cell cycle exit via P27 in neuroblastoma cells. *FEBS Open Bio.* 10, 1104–1114. doi: 10.1002/2211-5463.12860

Khan, Z., Terrien, E., Delhommel, F., Lefebvre-Omar, C., Bohl, D., Vitry, S., et al. (2019). Structure-based optimization of a PDZ-binding motif within a viral peptide stimulates neurite outgrowth. *J. Biol. Chem.* 294, 13755–13768. doi: 10.1074/jbc.RA119.008238

Kleinjan, D. A., Bancewicz, R. M., Gautier, P., Dahm, R., Schonthaler, H. B., Damante, G., et al. (2008). Subfunctionalization of duplicated zebrafish pax6 genes by cis-regulatory divergence. *PLoS Genet.* 4:e29. doi: 10.1371/journal.pgen.0040029

Lal, D., May, P., Perez-Palma, E., Samocha, K. E., Kosmicki, J. A., Robinson, E. B., et al. (2020). Gene family information facilitates variant interpretation and identification of disease-associated genes in neurodevelopmental disorders. *Genome Med.* 12:28. doi: 10.1186/s13073-020-00725-6

Marchese, M., Conti, V., Valvo, G., Moro, F., Muratori, F., Tancredi, R., et al. (2014). Autism-epilepsy phenotype with macrocephaly suggests PTEN, but not GLIALCAM, genetic screening. *BMC Med. Genet.* 15:26. doi: 10.1186/1471-2350-15-26

McMichael, G., Bainbridge, M. N., Haan, E., Corbett, M., Gardner, A., Thompson, S., et al. (2015). Whole-exome sequencing points to considerable genetic heterogeneity of cerebral palsy. *Mol. Psychiatry* 20, 176–182. doi: 10.1038/mp.2014.189

Meyer, A., and Schartl, M. (1999). Gene and genome duplications in vertebrates: the one-to-four (-to-eight in fish) rule and the evolution of novel gene functions. *Curr. Opin. Cell Biol.* 11, 699–704. doi: 10.1016/s0955-0674(99)00039-3

National Research Council (2011). *Guide for the Care and Use of Laboratory Animals*, 8th Edn, Washington, DC: The National Academies Press.

O'Roak, B. J., Vives, L., Fu, W., Egertson, J. D., Stanaway, I. B., Phelps, I. G., et al. (2012). Multiplex targeted sequencing identifies recurrently mutated genes in autism spectrum disorders. *Science* 338, 1619–1622. doi: 10.1126/science.1227764

Park, H. C., Kim, C. H., Bae, Y. K., Yeo, S. Y., Kim, S. H., Hong, S. K., et al. (2000). Analysis of upstream elements in the HuC promoter leads to the establishment of transgenic zebrafish with fluorescent neurons. *Dev. Biol.* 227, 279–293. doi: 10.1006/dbio.2000.9898

Rodriguez-Garcia, M. E., Cotrina-Vinagre, F. J., Gomez-Cano, M. L. A., Martinez de Aragon, A., Martin-Hernandez, E., and Martinez-Azorin, F. (2020). MAST1 variant causes mega-corpus-callosum syndrome with cortical malformations but without cerebellar hypoplasia. *Am. J. Med. Genet. A* 182, 1483–1490.

Saffen, D. W., Cole, A. J., Worley, P. F., Christy, B. A., Ryder, K., and Baraban, J. M. (1988). Convulsant-induced increase in transcription factor messenger RNAs in rat brain. *Proc. Natl. Acad. Sci. U.S.A.* 85, 7795–7799. doi: 10.1073/pnas.85.20.7795

Shin, J., Padmanabhan, A., de Groh, E. D., Lee, J. S., Haidar, S., Dahlberg, S., et al. (2012). Zebrafish neurofibromatosis type 1 genes have redundant functions in tumorigenesis and embryonic development. *Dis. Model. Mech.* 5, 881–894. doi: 10.1242/dmm.009779

Smirnova, T., Miniou, P., Viegas-Pequignot, E., and Mallet, J. (1996). Assignment of the human syntaxin 1B gene (STX) to chromosome 16p11.2 by fluorescence in situ hybridization. *Genomics* 36, 551–553. doi: 10.1006/geno.1996.0506

Spinelli, E., Christensen, K. R., Bryant, E., Schneider, A., Rakotomamonjy, J., Muir, A. M., et al. (2021). Pathogenic MAST3 variants in the STK domain are associated with epilepsy. *Ann. Neurol.* 90, 274–284. doi: 10.1002/ana.26147

Tripathy, R., Leca, I., van Dijk, T., Weiss, J., van Bon, B. W., Sergaki, M. C., et al. (2018). Mutations in MAST1 cause mega-corpus-callosum syndrome with cerebellar hypoplasia and cortical malformations. *Neuron* 100, 1354–1368.e1355.

Ulintz, P. J., Wu, W., and Gates, C. M. (2019). Bioinformatics analysis of whole exome sequencing data. *Methods Mol. Biol.* 1881, 277–318.

Valiente, M., Andres-Pons, A., Gomar, B., Torres, J., Gil, A., Tapparel, C., et al. (2005). Binding of PTEN to specific PDZ domains contributes to PTEN protein stability and phosphorylation by microtubule-associated serine/threonine kinases. *J. Biol. Chem.* 280, 28936–28943. doi: 10.1074/jbc.M504761200

Wang, K., Li, M., and Hakonarson, H. (2010). ANNOVAR: functional annotation of genetic variants from high-throughput sequencing data. *Nucleic Acids Res.* 38:e164. doi: 10.1093/nar/gkq603

Xiao, B., Tu, J. C., Petralia, R. S., Yuan, J. P., Doan, A., Breder, C. D., et al. (1998). Homer regulates the association of group 1 metabotropic glutamate receptors with multivalent complexes of homer-related, synaptic proteins. *Neuron* 21, 707–716.

Conflict of Interest: JL was employed by the company Cipher Gene LLC. WG and PW were employed by the company Chigene (Beijing) Translational Medical Research Center Co., Ltd.

The remaining authors declare that the research was conducted in the absence of any commercial or financial relationships that could be construed as a potential conflict of interest.

Publisher's Note: All claims expressed in this article are solely those of the authors and do not necessarily represent those of their affiliated organizations, or those of the publisher, the editors and the reviewers. Any product that may be evaluated in this article, or claim that may be made by its manufacturer, is not guaranteed or endorsed by the publisher.

frontiers in Molecular Neuroscience

ORIGINAL RESEARCH
published: 14 March 2022
doi: 10.3389/fnmol.2022.828846

Clinical and Functional Features of Epilepsy-Associated In-Frame Deletion Variants in *SCN1A*

*Jing-Yang Wang[1,2,3], Bin Tang[1,2], Wen-Xiang Sheng[1,2], Li-Dong Hua[4], Yang Zeng[1,2], Cui-Xia Fan[1,2], Wei-Yi Deng[1,2], Mei-Mei Gao[1,2], Wei-Wen Zhu[3], Na He[3] and Tao Su[1,2]**

[1] Institute of Neuroscience, The Second Affiliated Hospital of Guangzhou Medical University, Guangzhou, China, [2] Key Laboratory of Neurogenetics and Channelopathies, Ministry of Education of China, Guangzhou, China, [3] Department of Neurology, The Second Affiliated Hospital of Guangzhou Medical University, Guangzhou, China, [4] Translational Medicine Center, Maternal and Child Health Research Institute, Guangdong Women and Children's Hospital, Guangzhou, China

Objective: Naturally occurring in-frame deletion is a unique type of genetic variations, causing the loss of one or more amino acids of proteins. A number of in-frame deletion variants in an epilepsy-associated gene *SCN1A*, encoding voltage gated sodium channel alpha unit 1.1 ($Na_V1.1$), have been reported in public database. In contrast to the missense and truncation variants, the in-frame deletions in *SCN1A* remains largely uncharacterized.

Methods: We summarized the basic information of forty-four *SCN1A* in-frame deletion variants and performed further analysis on six variants identified in our cases with epilepsy. Mutants of the six in-frame deletions and one truncating variant used as comparison were generated and co-transfected with beta-1 and -2 subunits in tsA201 cells, followed by patch clamp recordings.

Results: Reviewing all the in-frame deletions showed that they spread over the entire $Na_V1.1$ protein, without obvious "hot spots." The dominant type (54%) was single residue loss. There was no obvious relationship between the length or locations of deletions and their clinical phenotypes. The six in-frame deletions were two single residue deletions (p.M400del and p.I1772del), one microdeletion (p.S128_F130del) and three macrodeletions (p.T303_R322del, p.T160_Y202del, and p.V1335_V1428del). They scatter and affect different functional domains, including transmembrane helices, pore region, and P-loop. Electrophysiological recordings revealed no measurable sodium current in all of the six mutants. In contrast, the truncating mutant p.M1619Ifs*7 that loses a long stretch of peptides retains partial function.

Significance: The complete loss-of-function in these shortened, abnormal mutants indicates that $Na_V1.1$ protein is a highly accurate structure, and many of the residues have no redundancy to ion conductance. In-frame deletions caused particularly deleterious effect on protein function possibly due to the disruption of ordered residues.

Keywords: sodium channel, ***SCN1A***, epilepsy, in-frame deletion, variant

OPEN ACCESS

Edited by:
Yuwu Jiang,
Peking University First Hospital, China

Reviewed by:
Jing Peng,
Central South University, China
Nazzareno D'Avanzo,
Université de Montréal, Canada

***Correspondence:**
Tao Su
su@gzneurosci.com

Specialty section:
This article was submitted to Molecular Signalling and Pathways, a section of the journal Frontiers in Molecular Neuroscience

Received: *04 December 2021*
Accepted: *21 February 2022*
Published: *14 March 2022*

Citation:
Wang J-Y, Tang B, Sheng W-X, Hua L-D, Zeng Y, Fan C-X, Deng W-Y, Gao M-M, Zhu W-W, He N and Su T (2022) Clinical and Functional Features of Epilepsy-Associated In-Frame Deletion Variants in SCN1A. Front. Mol. Neurosci. 15:828846. doi: 10.3389/fnmol.2022.828846

INTRODUCTION

Voltage-gated sodium channels (Na_v) are responsible for the generation and propagation of action potentials in excitable membrane. These channels are complexes of one α subunit in association with two auxiliary β subunits. In humans, there are nine functional α subunits ($Na_v1.1$-$Na_v1.9$) encoded by the genes *SCN1A*-SCN11A, with different patterns of tissue expression and biophysical properties. The α subunit of ∼2000 amino acid (AA) residues is organized in four homologous domains but non-identical domains (DI-DIV), each of which contains six transmembrane segments (S1–S6) and an additional membrane re-entrant pore loop (P-loop). Four transmembrane domains (DI–DIV) are connected by intracellular loop structures (Catterall, 2000; Goldin et al., 2000; Eijkelkamp et al., 2012).

Variants in the gene *SCN1A* encoding $Na_v1.1$ α subunit have been associated with a spectrum of epilepsy disorders ranging from the relatively benign generalized epilepsy with febrile seizures plus (GEFS+) to the devastating disorder, severe myoclonic epilepsy of infancy (SMEI) (Escayg et al., 2000, 2001; Marini et al., 2009). To date, more than 1,800 epilepsy associated variants annotated for *SCN1A* have been reported in different databases, such as SCN1A database[1], the Human Gene Mutation Database (HGMD), and the ClinVar database of NCBI. Most of these are missense variants that lead to a single amino acid substitution, while there are also a significant number of in-frame deletions and premature truncations that lacks one or more amino acids. Previous studies focused on characterizing the biophysical properties of missense and truncating variants (Lossin et al., 2003; Yamakawa, 2006; Meng et al., 2015). The in-frame deletions occurred in *SCN1A* have not been well characterized, except that an in-frame deletion (p.F1289del), located at DIII S3, was reported with no measurable sodium current (Ohmori et al., 2006). The naturally occurring in-frame deletions would be unique and useful models to explore the underlying biology of $Na_v1.1$, and the genotype-phenotype relationship as well.

Here we first collected a total of 44 in-frame deletion variants in *SCN1A* from the HGMD and SCN1A database and characterized their features of clinical phenotypes and locations. To gain insights into sub-molecular gating network of $Na_v1.1$, six in-frame deletions identified in our laboratory were further subject to site-directed mutagenesis experiments to determine the functional features of the shortened $Na_v1.1$.

MATERIALS AND METHODS

Public Data Collection

All available in-frame deletion variants in *SCN1A* (a total of 44 variants) were retrieved from the SNP database of the NCBI[2], the SCN1A database (see text footnote 1) and the HGMD. The NCBI database was queried with amino acid sequences of human $Na_v1.1$ to obtain the corresponding information of DNA locus, and related functional regions.

Genetic Testing

Diagnose and treatments of the patients were conducted in our Epilepsy Center (Guangzhou, China). Clinical data including medical records, standardized questionnaires, and EEG recordings were available. The probands were assessed using a standardized protocol after providing written informed consent. This study was approved by the Research Ethics Board of the Hospital. Genomic DNAs were prepared from ethylenediaminetetraacetic acid (EDTA)-treated whole blood samples. *SCN1A* were screened for genetic abnormalities. Primers were designed to amplify all exons and the flanking intronic splice sites of the gene. The purified PCR products of polymerase chain reaction were directly sequenced. The variant was verified by a second targeted PCR and sequencing. A total of six in-frame deletion variants in *SCN1A* were identified in our genetic testing, among which three were novel and three variants (c.383 + 1A > G/p.S128_F130del, c.602 + 1G > A/p.T160_Y202del, and c.1200_1202delGAT/p.M400del) were previously reported (Depienne et al., 2009; Selmer et al., 2009).

Mutagenesis and Heterologous Expression

To reconstitute the native brain sodium channel complex, *SCN1A* was co-expressed heterologously with human accessory β1 and β2 subunits in human tsA201 cells. The expression vectors of wild-type (WT) human sodium channel $Na_v1.1$, pCMV-*SCN1A*-WT, pCD8-IRES-hβ1, and pGFP-IRES-hβ2 that express α, β1, and β2 subunits, were kindly donated by Professor Alfred L. George Jr. To improve the monitoring of transfection, pCD8-IRES-hβ1 had been modified into pDsred-IRES-hβ1 with red fluorescence; whereas pGFP-IRES-hβ2 expression is recognized by green fluorescence. The mutant vectors were generated from corresponding WT vectors using Quick-change site-directed mutagenesis (Stratagene, Cedar Creek, TX, United States) according to the manufacturer's protocol. All constructs were verified by resequencing before being transfected to human tsA201 cells. The cells were grown in 1:1 Ham's F-12 and Dulbecco's modified eagle's medium (DMEM) supplemented with 10% fetal bovine serum, 100 U/ml of penicillin, and 100 μg/ml streptomycin. The cells were maintained in a humidified incubator at 37°C with 5% CO_2. Cells were then co-transfected with pCMV-*SCN1A*, pCD8-IRES-hβ1, and pGFP-IRES-hβ2, using Lipofectamine 3000 reagent Kit from Thermo Fisher Scientific. After incubation for 12–15 h, cells were replated in 35-mm culture dishes.

Patch Clamp Analysis

Electrophysiological studies were performed 20–48 h after transfection, according to our previous report (Chen et al., 2015). Cells displaying green and red fluorescence were chosen for recording. According to our previous experience, almost all the cells (>90%) that had green and red fluorescence were

[1]http://scn1a.caae.org.cn/

[2]http://www.ncbi.nlm.nih.gov/

expressing a complex of co-transfected α, β1 and β2 subunits. Whole-cell patch clamp was performed according to previous reports. Sodium currents were recorded from tsA201 cells at room temperature (22–24°C). Series resistance (2.0–3.0 MΩ) was compensated 85–95% to assure that the command potential was reached within microseconds and with a voltage error of <4 mV. All data were acquired at 10–50 kHz and low-pass filtered at 5 kHz. The pipette solution contained (in mM): NaF 10, CsF 110, CsCl 20, EGTA 2, and HEPES 10, with a pH of 7.35 and osmolarity of 310 mOsM/kg. The extracellular solution contained (in mM): NaCl 145, KCl 4, $CaCl_2$ 1.8, $MgCl_2$ 1, and HEPES 10, with a pH of 7.35 and osmolarity of 310 mOsM/kg. Sodium currents were recorded with EPC10 amplifiers (HEKA Elektronik, Lambrecht, Germany). Sodium currents were recorded at various test potentials from a holding potential of −120 mV. The inward currents were validated by Na_v blocker tetrodotoxin. Sodium conductance (G) was calculated according to the equation $G = I_{peak}/(V_{test}\text{-}V_{rev})$, where I_{peak} is the peak inward current, V_{test} is the test potential, and V_{rev} is the reversal potential for Na^+. To compare voltage dependence of activation, data were fitted to a Boltzmann function, according to the equation $G/G_{max} = 1-1/\{1 + \exp[(V_m-V_{1/2})/k]\}$, where G_{max} is the maximum conductance, V_m is the potential of individual step pulses, $V_{1/2}$ is the average half activation potential (at which G is one-half maximal), and k is the slope factor. The voltage dependence of channel availability was assessed following a prepulse to various potentials followed by 20-ms pulse to −10 mV. The normalized current was plotted against the voltage and the inactivation curves were fit with Boltzmann functions ($I/I_{max} = 1/(1 + \exp[(V_m-V_{1/2})/k])$ to determine the voltage for half-maximal channel inactivation ($V_{1/2}$) and slope factor (k). Recovery from inactivation was determined using a two-pulse protocol. The peak current from the test pulse was normalized to the peak current from a prepulse and plotted against the recovery period. Data were fit with the two exponential function, $I/Imax = A_f\ [1-\exp(-t/\tau_f)] + A_s\ [1-\exp(-t/\tau_s)]$, where τ_f and τ_s denote time constants (fast and slow components, respectively).

Structural Modeling

The structures of the WT $Na_v1.1$ and fragmental peptides (about 600 AA, deletion locus was covered) of the deletion variants were modeled to predict the effect of deletion mutations on protein structure by using I-Tasser[3]. PyMOL 2.3 software was used for three-dimensional protein structure visualization and analysis.

Statistical Analysis

All data were analyzed using a combination of Fit master v2.53 (HEKA Electronics, Lambrecht, Germany), Excel 2003 (Microsoft, Seattle, WA, United States), and OriginPro 8.0 (OriginLab, Northampton, MA, United States) software. For statistical evaluation, results are shown as means ± SEM, and differences between WT and mutant channels were assessed by Student's *t*-test. One-way analysis of variance (ANOVA) was used to compare means among different groups. Significance was assigned at $P < 0.05$.

RESULTS

Features of In-Frame Deletion Variants in *SCN1A*

Six in-frame deletions in *SCN1A* were identified in our cases with SMEI, generalized epilepsy with febrile seizures plus (GEFS+), partial epilepsy with febrile seizures plus (PEFS+) and Lennox–Gastaut syndrome (LGS) (**Table 1**). One variant (c.383 + 1A > G/p.S128_F130) associated with

[3]https://zhanglab.ccmb.med.umich.edu/I-TASSER/

TABLE 1 | Clinical features associated with six identified in-frame deletion and one truncation variants in *SCN1A*.

Mutation	Mutation position	Age at FS/aFS onset	Seizure type	Inherited	Diagnosis	EEG	Mental retardation	AEDs	PROVEAN
c.383 + 1A > G/ p.S128_F130del	DIS1 (Intron 2)	NA	Myo, Tonic, Atonic, CPS, GTCS	*De novo*	LGS	GSW, FSW	Severe learning disability	VPA+LTG+PT(∧)	D
c.602 + 1G > A/ p.T160_Y202del	DIS2-S3 (Exon 4)	8 m/2 years	sGTCS, CPS	*De novo*	DS	FSW	Normal	VPA+TPM(↓)	D
c.909A > G/ p.T303_R322del	DIS5-S6 (Exon 6)	2 years/−	GTCS	*De novo*	FS+	NA	Normal	NA	D
c.1200_1202delGAT/ p.M400del	DIS6 (Exon 9)	8 m/−	GTCS, CPS	*De novo*	DS	GSW, FSW	Speech defect	VPA+LEV(↓)	D
c.4284 + 2T > C/ p.V1335_V1428del	DIIIS5-S6 (Exon 21)	6 m/6 m	Myo, CPS, sGTCS	Paternal	DS	GSW, FSW	Normal	VPA+TPM(∧)	D
c.5313_5315delCAT/ p.I1772del	DIVS6 (Exon 26)	7 m/3 years	GTCS, CPS	*De novo*	PEFS+	Normal	Moderate	VPA+CNZ(↓)	D
c.4853-25T > A/ p.M1619Ifs*7	DIVS3 (Exon 26)	18 m/5 years	GTCS, CPS	Maternal	PEFS+	NA	NA	NA	D

CPS, complex partial seizures; GTCS, generalized tonic-clonic seizures; Myo, myoclonic seizures; Tonic, tonic seizure; Atonic, atonic seizures; LGS, Lennox-Gastaut syndrome; GSW, generalized spike waves; FSW, focal spike waves; NA, not available; VPA, valproic acid; LTG, lamotrigine; TPM, topiramate; LEV, levetiracetam; CNZ, clonazepam; D, deleterious. (∧), *seizure-free;* (↓), *seizure remission.*

LGS and two variants (c.602 + 1G > A/p.T160_Y202del and c.1200_1202delGAT/p.M400del) associated with SMEI were reported in the ClinVar database or previous studies (Depienne et al., 2009; Selmer et al., 2009), while the other variants were novel. Residues affected by these variants are located in several distinct protein domains including the DI/S1 (c.383 + 1A > G/p.S128_F130del), DI/S2-S3 (c.602 + 1G > A/p.T160_Y202del), pore loop in DI (c.909A > G/p.T303_R322del, c.1200_1202delGAT/p.M400del), cytoplasmic DIII/S4-S5 linker to pore loops in DIII (c.4284 + 2T > C/p.V1335_V1428del), and DIV/S6 (c.5313_5315delCAT/p.I1772del) (illustrated in **Figure 1**).

We summarized all the in-frame deletion variants (a total of 44, together with the six variants identified by us) from the databases, and found that most of them (38/44) were reported as SMEI, developmental and epileptic encephalopathy (DEE) and LGS (**Table 2**). These variants spread over six functional domains of $Na_v1.1$ (**Figures 2A,B**). Approximately 54% of the in-frame deletions are single deletions of 1 AA, followed by microdeletions (2–6 AA, 30%) and macrodeletions (>6 AA, 16%) (**Figure 2C**). Almost all the single deletions are associated with SMEI, DEE, except of one in DIV/S6 presented with PEFS+ **Figure 2D**). One microdeletion located in DI S5-S6 linker is associated with febrile seizure plus (FS+). There is no clear relationship between clinical phenotypes and the length of deletions.

In-Frame Deletion Mutants Exhibit Complete Loss-of-Function

The WT and six in-frame deletion mutant alpha-subunits were expressed transiently in human tsA201 cells. We performed electrophysiological recordings for the transfected neurons and the non-transfected neurons as negative control. In contrast to the WT $Na_v1.1$ with apparent current recorded (>90 pA/pF), the six in-frame deletion mutants all exhibited tiny raw currents (usually <20 pA/pF) (**Figures 3A,B**). The tiny currents were demonstrated as endogenous current, which was also recorded in non-transfected cells. Therefore, we confirmed that the in-frame deletion mutants were not able to generate Na^+ current and fail to exhibit sufficient sodium current for biophysical analysis.

A Truncated Mutant Retains Partial Channel Function

We noticed that the in-frame deletion mutant causing a single loss of isoleucine at the S6 of DIV (I1772) resulted in complete loss-of-function. This raised an interesting question about whether a truncation mutant that was much shortened still functioned. A truncating variant c.4853-25T > A/p.M1619Ifs*7 was previously identified in our patient with PEFS+. The premature truncation is expected to have seven AA substitutions from p.M1619-E1626, with a loss of peptides from S3 of DIV to c-terminal. Interestingly, the truncated mutant exhibited partial loss-of-function, with reduced peak current density (−27.47 ± 8.46 pA/pF vs. −116.60 ± 25.60 pA/pF in the WT control, 23.6% of the WT) (**Figure 3C** and **Table 3**). The current-voltage relation analysis showed that the p.M1619Ifs*7 mutant exhibited a less steep conductance-voltage (G-V) curve with the smaller slopes of steady-state availability, but remained unchanged in the half-maximal activation and inactivation ($V_{1/2}$), suggesting a slight disruption of the voltage sensor (**Figures 3D,E** and **Table 3**). There was no significant difference in the time constants in the kinetics of recovery from inactivation (**Figure 3F** and **Table 3**).

Structure Modeling

To explore structural changes as a result of the in-frame deletions, we performed tertiary structure prediction. The comparative analysis of the predicted structures showed that the local tertiary folding differed strongly between the WT and mutants, especially for the macrodeletions (p.T303_R322del, p.T160_Y202del, and p.V1335_V1428del). The local structures of the macrodeletion mutants were deformed and the surrounding segments were relocated (**Figure 4**). The p.T160_Y202del deletion with two transmembrane segments involved has the most remarkable difference in protein folding, in which the expected segments (S2 and S3) disappear and moreover the adjacent S1 and S4 are relocated to the different sites. Both the single deletion (p.M400del) and microdeletion (p.S128_F130del) that have lost their hydrophobic residues including isoleucine, methionine and phenylalanine, were predicted to turn the coiled coil alpha helices into flexible loops. The other deletion (p.I1772del) at S6 exhibited a smaller difference in the alpha helix, but had a larger difference in the angle of the neighboring units compared to the WT.

DISCUSSION

Genetic defects in the Na_v α subunit can lead to various excitability diseases in brain, muscle, and heart, such as muscle paralysis, cardiac arrhythmias, and epileptic disorders (Meisler and Kearney, 2005; Lee et al., 2009; Remme and Bezzina, 2010; Kasperaviciute et al., 2013). The particular importance of $Na_v1.1$ channel has continually motivated researchers to identify structural or functional residues responsible for protein stability and activity. So far, more than 1800 *SCN1A* variants have been identified in epilepsy, but few studies have investigated the function of these genetic defects. Functional analysis in coding regions of $Na_v1.1$ channel might help to gain insights into the intramolecular gating network.

In this study, we report the phenotypic relevance and biophysical characterization of seven *SCN1A* variants, including six *SCN1A* in-frame deletions and one truncating variant. The six in-frame deletions scatter and affect different functional domain, including transmembrane helices, pore region, and P-loop. There are two single residue deletions (p.M400del, p.I1772del), one microdeletion (p.S128_F130del) and three macrodeletions (p.T303_R322del, p.T160_Y202del, and p.V1335_V1428del). In accordance to the features of all in-frame deletion variants summarized from public databases, the six deletion variants were associated with severe phenotypes such as SMEI, DEE, and LGS, except that two cases presented with milder phenotypes, FS+ and PEFS+. In spite of different locations, residue length of deletions, and associated phenotypes, the six in-frame deletion mutants were found to consistently lose their ion conductance, showing

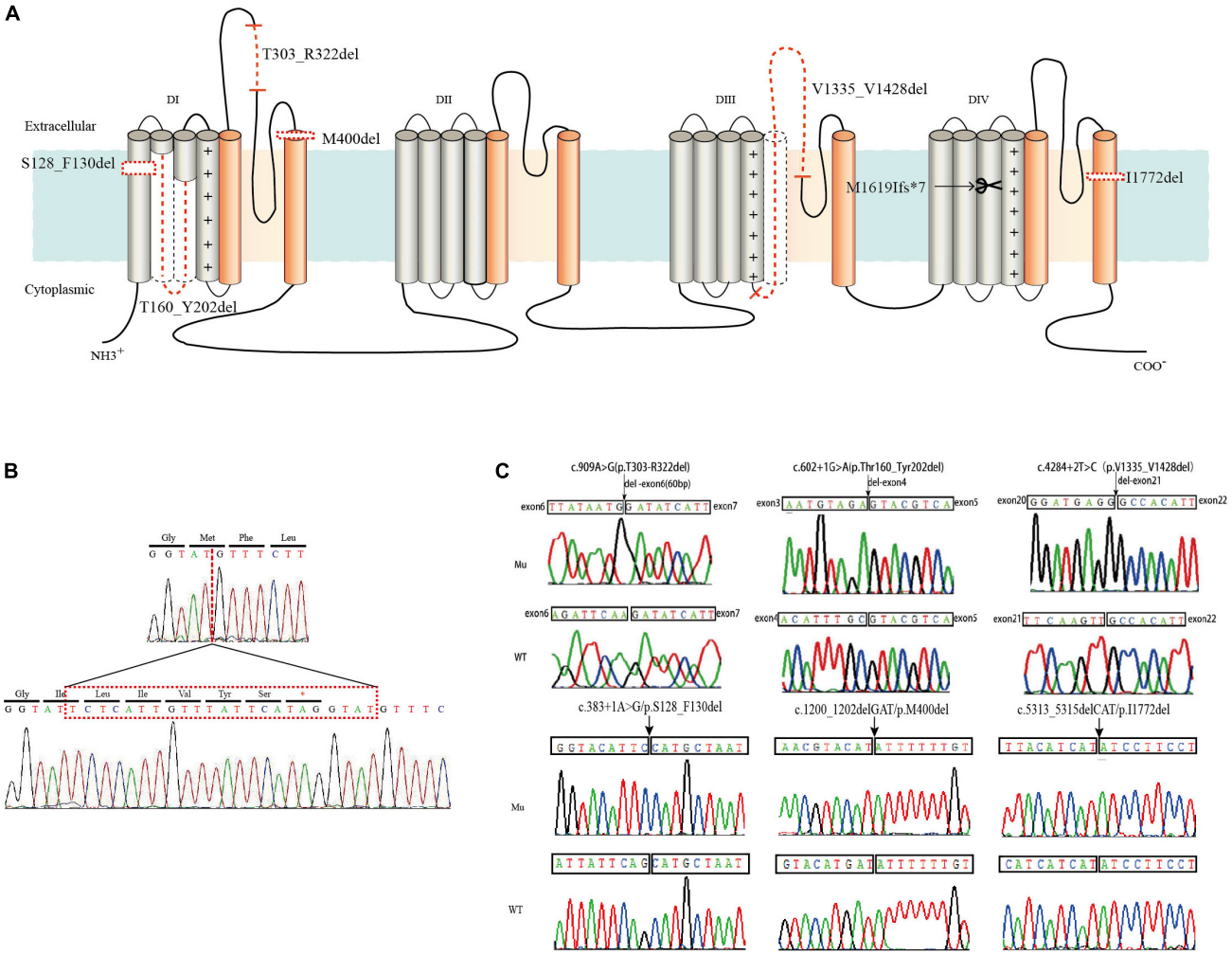

FIGURE 1 | Locations of six in-frame deletion and one truncating variants in *SCN1A* and sequence identification. **(A)** Schematic location of the variants identified. The in-frame deletion variants were marked with dotted lines and the truncating variant was marked with a scissor. **(B)** DNA sequencing of the truncating variant (c.4853-25T > A/p.M1619Ifs*7). **(C)** DNA sequencing of the in-frame deletion variants.

barely detectable inward sodium currents in the heterologous expression experiments.

It is conceivable that the macrodeletions with the loss of a large stretch of peptides would have impact on protein structure and serious functional effect. By contrast, the fact that the microdeletion and single deletion mutants also resulted in the complete loss-of-function is more striking, especially for the two single deletions (p.M400del and p.I1772del) locating at transmembrane domain DIV/S6. Analogous to p.I1772del, an in-frame deletion in the identical DIV/S6 in $Na_v1.6$ (p.I1750del), which is a spontaneous mouse variant, was reported to be associated with a chronic movement disorder with early onset tremor and adult onset dystonia (Jones et al., 2016). The removal of isoleucine in mouse $Na_v1.6$ also exhibited no measurable current in the functional studies (Jones et al., 2016). In addition, no measurable current was previously reported in a DS-associated in-frame deletion variant p.F1289del (Thompson et al., 2012), in which phenylalanine in the transmembrane segment DIII/S3 in $Na_v1.1$ was removed. In our case, the microdeletion p.S128_F130del with a combined loss of phenylalanine, leucine, and serine in S1 led to complete loss-of-function. These transmembrane residues, including isoleucine, methionine, phenylalanine and leucine are all hydrophobic and critical for the interaction between transmembrane helices and lipid membrane. However, an exceptional case was found in an in-frame deletion of leucine (p.L955del) within DII/S6 of $Na_v1.7$, which showed a gain-of-function with a robust hyperpolarizing shift of activation and slow inactivation (Yang et al., 2013). More efforts are needed to understand the functional architecture of voltage-gated sodium channels.

The variant p.T303_R322del is expected to shorten the membrane-reentrant P-loop rather than affect transmembrane helices. The P-loop is the linker between S5 and S6, forming a selectivity filter—a narrow pathway that determines which ion will pass the pore (Catterall et al., 2007; Yang et al., 2009). Functional loss in the p.T303_R322del mutant indicates the

TABLE 2 | In-frame deletion variants of *SCN1A*.

Variant	Length (AA)	Position	Phenotype	References
p.Phe17del	1	N terminal	DS	Zuberi et al., 2011
p.Thr18del	1	N terminal	DS	Djemie et al., 2016
p.Gly58_Leu61del	4	N terminal	DS	https://ncbi.nlm.nih.gov/clinvar/
p.Leu80_Asp81del	2	N terminal	DS	Usluer et al., 2016
p.Ile99_Ala104del	6	N terminal	DS	Gonsales et al., 2019
p.Leu129del	1	DI S1	DS	Mancardi et al., 2006
p.Ser128_Phe130del	3	DI S1	LGS	Selmer et al., 2009
p.Leu129_Glu158del	30	DI S1, S1-S2, S2	DS	https://.clinvar/
p.Thr160_Tyr202del	43	DI S2, S2-S3, S3	DS	https://.clinvar/
p.Glu181del	1	DI S2-S3	DS	Till et al., 2020
p.Asp208_Arg219del	12	DI S3-S4, S4	DS	de Lange et al., 2018
p.Lys246del	1	DI S4-S5	DS	Peng et al., 2019
p.Leu247del	1	DI S4-S5	Ep or NDD	Lindy et al., 2018
p.Thr303_Arg322del	20	DI S5-S6	FS+	
p.Tyr325del	1	DI S5-S6	DS	Wu et al., 2015
p.Met400del	1	DI S6	DS	Depienne et al., 2009
p.Thr775del	1	DII S1	DS	Aljaafari et al., 2017
p.Met815del	1	DII S2	DEE	https://.clinvar/
p.Gly854_Leu855del	2	DII S3-S4	DS	Zuberi et al., 2011
p.Lys868del	1	DII S4	DS	Moehring et al., 2013
p.Val896_Ala898del	3	DII S5	Ep or NDD	Lindy et al., 2018
p.Met960_Cys968del	9	DII S5-S6, S6	DS	Yang et al., 2017
p.Thr1210del	1	DII-DIII linker	DS	http://SCN1A.caae.org.cn/by_mutation.php
p.Ile1240_Asp1243del	4	DIII S1-S2	DEE	https://.clinvar/
p.Thr1247_Thr1250del	4	DIII S1-S2	DS	http://SCN1A.caae.org.cn/by_mutation.php
p.Phe1289del	1	DIII S3	DS	Depienne et al., 2009
p.Val1335_V1428del	94	DIII S4-S5, S5, S5-S6	DS	
p.Ala1429del	1	DIII S5-S6	DS	Zuberi et al., 2011
p.Asn1446_Gly2008del	563	DIII S5-S6, S6, DIII-DIV, DIV, C-terminal	DS	https://.clinvar/
p.Phe1473del	1	DIII S6	DS	Depienne et al., 2009
p.Ile1483del	1	DIII S6	DS	Depienne et al., 2009
p.Glu1503del	1	DIII-DIV linker	DS	Wang et al., 2012
p.Met1558del	1	DIV S1	DS	Fukuma et al., 2004
p.Met1559del	1	DIV S1	DS	Fukuma et al., 2004
p.Val1560_Thr1562del	3	DIV S1-S2	DS	Brunklaus et al., 2020
p.Asn1672del	1	DIV S4-S5	DS	Gertler et al., 2020
p.Gly1674_Leu1675del	2	DIV S5	Ep or NDD	Lindy et al., 2018
p.Phe1766del	1	DIV S6	DS	Fukuma et al., 2004
p.Ile1772del	1	DIV S6	PEFS+	
p.Met1807_Glu1810del	4	C terminal	DS	Fujiwara et al., 2003
p.Glu1813_Phe1815del	3	C terminal	DS	Depienne et al., 2009
p.Leu1835_Pro1837del	3	C terminal	Ep or NDD	Lindy et al., 2018
p.Thr1909del	1	C terminal	DS	Zuberi et al., 2011
p.Gln1914del	1	C terminal	Refractory epilepsy	Liu et al., 2018

DS, Dravet syndrome (SMEI); Ep, epilepsy; NDD, neurodevelopmental disorders; LGS, Lennox–Gastaut syndrome; PEFS+, partial epilepsy with febrile seizures plus; FS+, Febrile seizures plus.

non-redundant role of the P-loop for ion conductance. In support of this postulation, it was shown that a five amino acids in-frame deletion of P-loop in a p.R1370-L1374del of $Na_v1.7$, which is associated with channelopathy-associated insensitivity to pain disorder, also resulted in a normally expressed but non-functional channel (Cox et al., 2010). Likewise in $Na_v1.5$, a heterozygous

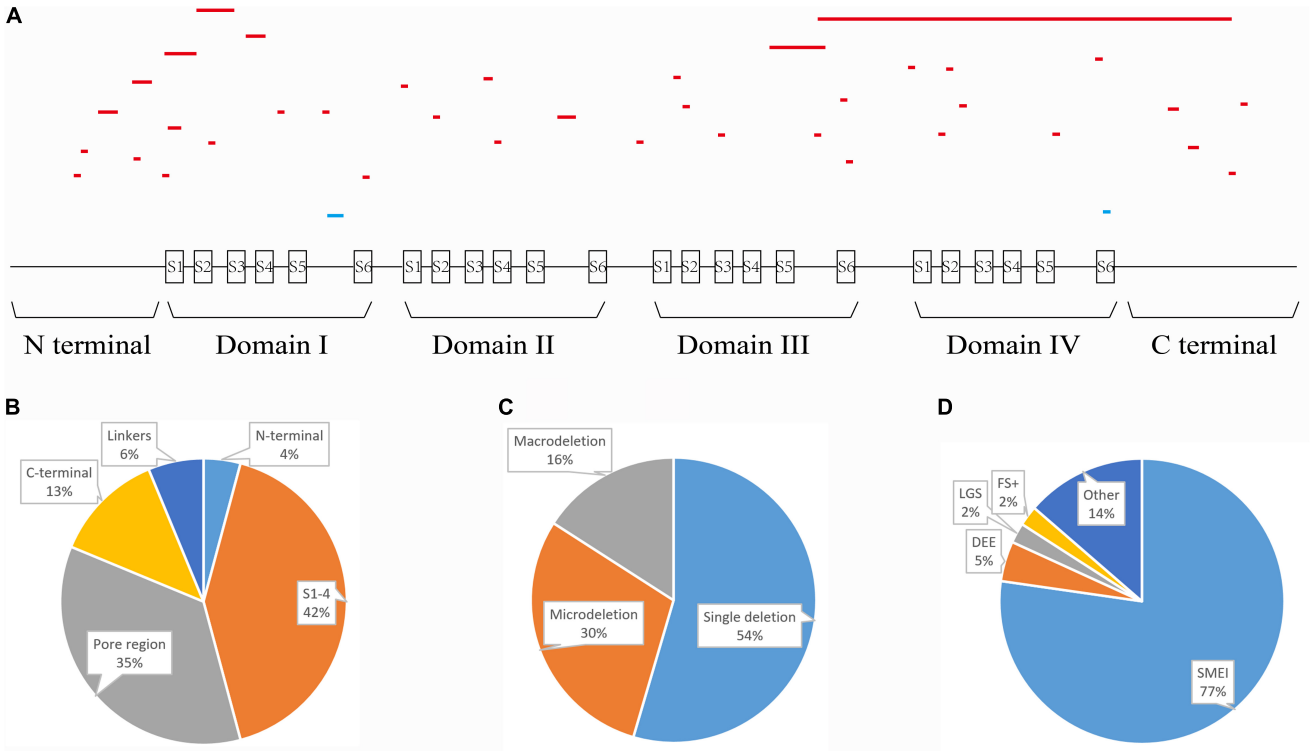

FIGURE 2 | Statistics of all in-frame deletions in *SCN1A*. **(A)** Schematic picture showing the length, location, and phenotypes of the 44 variants. Lines indicate different variants. Severe phenotypes (SMEI, DEE, and LGS) were highlighted as red, while mild phenotypes (PEFS+ and FS+) were blue. **(B)** Distribution of the variants on different functional domains. **(C)** The proportions of single deletion, microdeletions, and macrodeletions. **(D)** Phenotypic spectrum.

in-frame deletion p.N1380del that was associated with cardiac conduction disturbance and ventricular tachycardia exhibited no detectable current (Yang et al., 2017), even though only a single amino acid was removed. Together with previous experimental mutagenesis and clinical studies (Terlau et al., 1991; Favre et al., 1996; Ishii et al., 2017), it has well established that P-loops are critical determinants of catalytic permeation properties of Na^+ channels, but their precise structure-function and deletion-phenotype relationships remain largely unknown.

The most puzzling result in the study is that the truncating mutant (p.M1619Ifs*7), that is expected to delete the S4–S6 pore-forming segments in DIV and the whole C-terminal tail, retained partial channel function. According to several expression and functional studies in the truncated Na_v, most of the truncation variants would fail to produce functional channel (e.g., $hNa_v1.1$-p.R1234*), except those occurring at the C-terminal tail (e.g., $hNa_v1.1$-p.R1892*, $hNa_v1.5$-p.R1860Gfs*12) (Sugawara et al., 2003; Bechi et al., 2012; Brunklaus et al., 2020). However, the Na^+ current in the p.M1619Ifs*7 transfected cell was observed in this study, although the current remarkably decreased to 24% of the WT. The evidence proved that the truncated channel without last pore-forming segments still retained the basic biophysics of $Na_v1.1$. A possible explanation could be that new assembly of the remaining segments is capable of forming a functional channel.

Several mechanisms might underlie the non-functional $Na_v1.1$ channel. First, as Na_v channel opening is determined by a series of gating checkpoints in the transmembrane and cytosolic regions, disruptions caused by missense or deletion variants at these gating checkpoints would definitely impact on the functioning of $Na_v1.1$ channel. For example, the residues in the pore regions are highly conservative and determine ion selectivity and permeation, and the voltage-sensing domains determine the right response to membrane potential. Secondly, integrity of the functional motifs that determine mRNA expression, splicing, and protein trafficking has been destroyed. Thirdly, a local misfolding of residues disturbs the topology of the adjoining functional motifs and misleads gating motions. In our study, p.T303_R322del, p.M400del, p.V1335_V1428del, and p.I1772del affect the integrity of the pore-forming regions. This is consistent with the roughly loss-of-function changes found in missense variants in these gate checkpoints (Ohmori et al., 2006). However, both p.S128_F130del and p.T160_Y202del transformed the α helices into flexible loops according to the structural modeling (**Figure 4**), which would have impacts on overall arrangements of different segments. As functional motifs of a protein are usually a fixed order of the residues, deletions could be at higher risk of disrupting the order, thereby causing more deleterious effects on function or structure, when compared to missense or truncation mutations.

It has been suggested that changes in amino acid sequence have variable functional effects on sodium channels, with a mixture of loss-of-function and gain-of-function effects

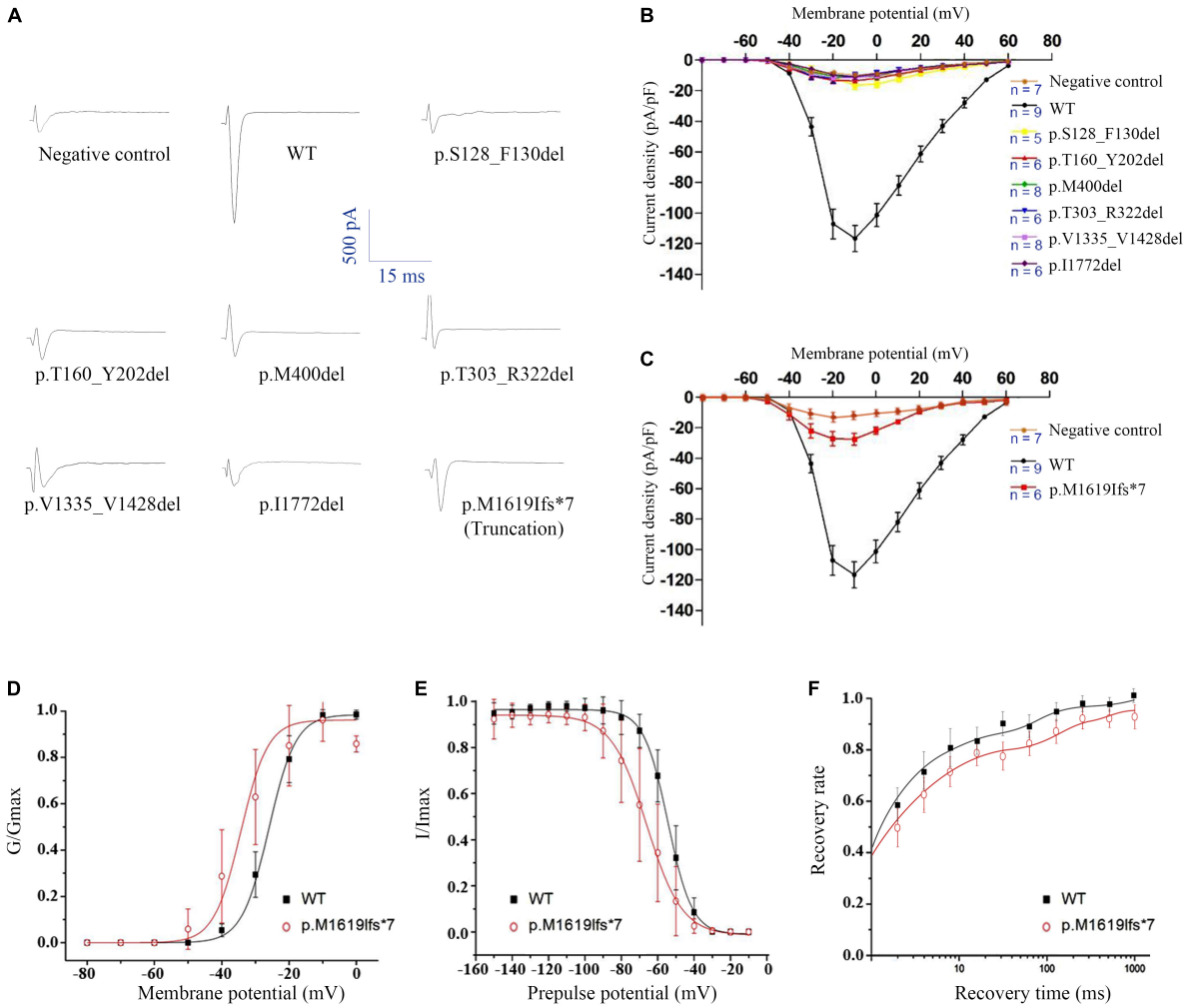

FIGURE 3 | Electrophysiological analysis of the *SCN1A* in-frame deletion and truncated mutants. **(A)** Representative traces of sodium current evoked at 0 mV. **(B)** Current-voltage relationship of six in-frame deletion mutants. **(C)** Current-voltage relationship of the truncated mutant. **(D)** G-V activation curve, **(E)** steady-state inactivation curve, and **(F)** recovery from inactivation, all for the truncated mutant p.Met1619Ilefs*7. Non-transfected cells were used as negative control.

TABLE 3 | Biophysical parameters of truncating mutant p.Met1619Ilefs*7.

		WT (*n* = 9)	p.Met1619Ilefs*7 (*n* = 6)
Current density (−10 mv)	pA/pF	−116.60 ± 25.60	−27.47 ± 8.46§
Voltage-dependence of activation	$V_{1/2}$ (mV)	−26.10 ± 4.70	−32.32 ± 25.86
	k	4.50 ± 0.15	7.31 ± 0.73§§
Voltage-dependence of fast inactivation	$V_{1/2}$ (mV)	−54.42 ± 15.78	−66.03 ± 31.03
	k	6.60 ± 0.25	9.70 ± 0.42§§
Recovery from fast inactivation	τ_f (ms)	1.06 ± 0.96	1.24 ± 1.11
	τ_s (ms)	23.94 ± 9.43	168.86 ± 103.49

Compared with the WT, $^{\S}P < 0.050$, $^{\S\S}P < 0.001$.

(Yamakawa, 2006; Gataullina and Dulac, 2017). The SMEI-associated *SCN1A* variants seem to be more closely correlated with haploinsufficiency for $Na_v1.1$, which caused by deleterious nonsense and frameshift variants in *SCN1A* (Gambardella and Marini, 2009; de Jonghe, 2011), and missense variants exhibiting remarkably attenuated or barely detectable sodium currents (Sugawara et al., 2003). Studies on heterozygous *SCN1A*$^{\pm}$ mice demonstrated that substantially reduced Na^+ current density with a loss of sustained high-frequency firing of action potentials were found in hippocampal and cortical interneurons, possibly responsible for the spontaneous seizure phenotypes in the *SCN1A*$^{\pm}$ mice (Yu et al., 2006). In agreement with the previous

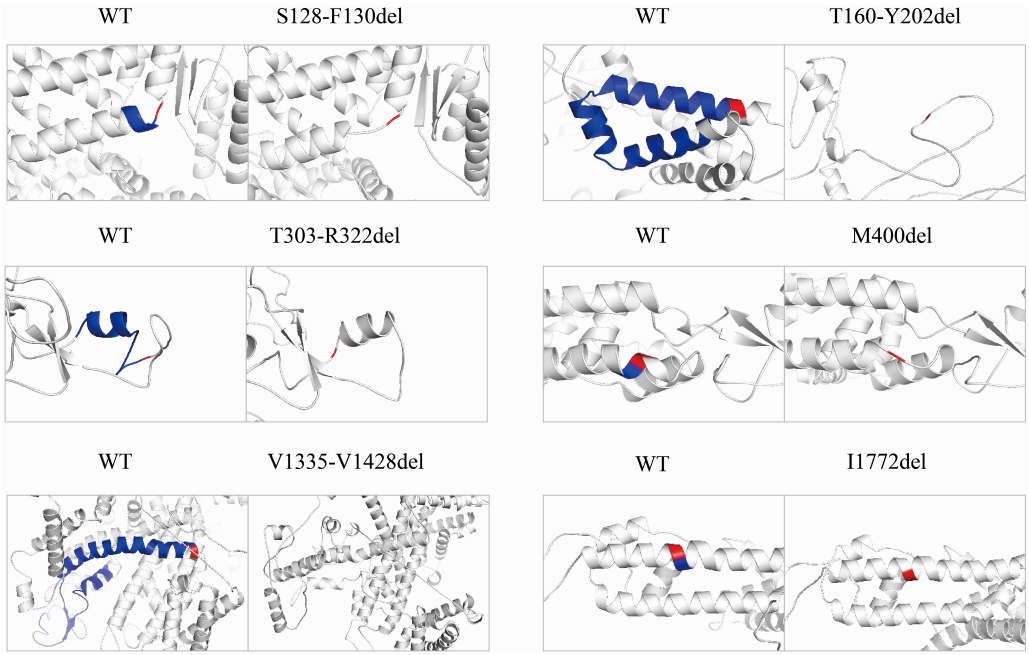

FIGURE 4 | Pairwise comparison of the predicted local structure features between wild-type and in-frame deletions. Location of deleted residues is indicated in blue, and their next residues are in red.

result, the six in-frame deletion mutants in this study were non-functional and mostly associated with SMEI, except that two variants, p.T160_Y202del and p.I1772del, which affect pore regions, were associated with FS+ and PEFS+, respectively. The variable phenotypes might be explained by the role of genetic modifiers and molecular interactions. It remains a challenging conundrum for researchers about how the common loss-of-function in $Na_v1.1$ results in different phenotypes.

This study provides some new insights into the effect of in-frame deletion on the biological functions of $Na_v1.1$, suggesting a complete loss-of-function of channel and their associations with clinical phenotypes including SMEI, FS+, and PEFS+. However, we only characterized the functional properties in the six out of 44 in-frame deletions identified to date. With more deletion variants identified and functionally characterized, the relationship among deletion pattern, functional changes, and clinical phenotypes would become more clear.

DATA AVAILABILITY STATEMENT

The original contributions presented in the study are included in the article/supplementary material, further inquiries can be directed to the corresponding author/s.

ETHICS STATEMENT

The studies involving human participants were reviewed and approved by Ethics Committee of The Second Affiliated Hospital of Guangzhou Medical University. Written informed consent to participate in this study was provided by the participants' legal guardian/next of kin.

AUTHOR CONTRIBUTIONS

TS and NH contributed to the conceptualization and funding acquisition. TS and J-YW designed the study, while the other authors performed the experiments and/or analyzed the data, and contributed to the manuscript draft. All authors contributed to the article and approved the submitted version.

FUNDING

This work was funded by the National Natural Science Foundation of China (Grant Nos. 81271197 to TS, 81971216 to NH, and 82171439 to Yi-Wu Shi), Science and Technology Project of Guangdong Province (Grant No. 2017B030314159 to Wei-Ping Liao), Guangdong Basic and Applied Basic Research Foundation (Grant Nos. 2020A1515011048 to NH and 2021A1515010986 to Yi-Wu Shi), and Science and Technology Project of Guangzhou (Grant Nos. 201904010292 to NH and 201904020028 to Wei-Ping Liao). The funders had no role in study design, data collection and analysis, and decision to publish or preparation of the manuscript.

ACKNOWLEDGMENTS

We are deeply grateful to the patients and clinicians who participated in this study.

REFERENCES

Aljaafari, D., Fasano, A., Nascimento, F. A., Lang, A. E., and Andrade, D. M. (2017). Adult motor phenotype differentiates Dravet syndrome from Lennox-Gastaut syndrome and links SCN1A to early onset parkinsonian features. *Epilepsia* 58, e44–e48. doi: 10.1111/epi.13692

Bechi, G., Scalmani, P., Schiavon, E., Rusconi, R., Franceschetti, S., and Mantegazza, M. (2012). Pure haploinsufficiency for Dravet syndrome Na(V)1.1 (SCN1A) sodium channel truncating mutations. *Epilepsia* 53, 87–100. doi: 10.1111/j.1528-1167.2011.03346.x

Brunklaus, A., Du, J., Steckler, F., Ghanty, I. I., Johannesen, K. M., Fenger, C. D., et al. (2020). Biological concepts in human sodium channel epilepsies and their relevance in clinical practice. *Epilepsia* 61, 387–399. doi: 10.1111/epi.16438

Catterall, W. A. (2000). From ionic currents to molecular mechanisms: the structure and function of voltage-gated sodium channels. *Neuron* 26, 13–25. doi: 10.1016/s0896-6273(00)81133-2

Catterall, W. A., Cestele, S., Yarov-Yarovoy, V., Yu, F. H., Konoki, K., and Scheuer, T. (2007). Voltage-gated ion channels and gating modifier toxins. *Toxicon* 49, 124–141. doi: 10.1016/j.toxicon.2006.09.022

Chen, Y. J., Shi, Y. W., Xu, H. Q., Chen, M. L., Gao, M. M., Sun, W. W., et al. (2015). Electrophysiological differences between the same pore region mutation in SCN1A and SCN3A. *Mol. Neurobiol.* 51, 1263–1270. doi: 10.1007/s12035-014-8802-x

Cox, J. J., Sheynin, J., Shorer, Z., Reimann, F., Nicholas, A. K., Zubovic, L., et al. (2010). Congenital insensitivity to pain: novel SCN9A missense and in-frame deletion mutations. *Hum. Mutat.* 31, E1670–E1686. doi: 10.1002/humu.21325

de Jonghe, P. (2011). Molecular genetics of Dravet syndrome. *Dev. Med. Child. Neurol.* 53, 7–10. doi: 10.1111/j.1469-8749.2011.03965.x

de Lange, I. M., Koudijs, M. J., VanTSlot, R., Gunning, B., Sonsma, A. C. M., Van Gemert, L., et al. (2018). Mosaicism of de novo pathogenic SCN1A variants in epilepsy is a frequent phenomenon that correlates with variable phenotypes. *Epilepsia* 59, 690–703. doi: 10.1111/epi.14021

Depienne, C., Trouillard, O., Saint-Martin, C., Gourfinkel-An, I., Bouteiller, D., Carpentier, W., et al. (2009). Spectrum of SCN1A gene mutations associated with Dravet syndrome: analysis of 333 patients. *J. Med. Genet.* 46, 183–191. doi: 10.1136/jmg.2008.062323

Djemie, T., Weckhuysen, S., von Spiczak, S., Carvill, G. L., Jaehn, J., Anttonen, A. K., et al. (2016). Pitfalls in genetic testing: the story of missed SCN1A mutations. *Mol. Genet. Genomic Med.* 4, 457–464. doi: 10.1002/mgg3.217

Eijkelkamp, N., Linley, J. E., Baker, M. D., Minett, M. S., Cregg, R., Werdehausen, R., et al. (2012). Neurological perspectives on voltage-gated sodium channels. *Brain* 135, 2585–2612. doi: 10.1093/brain/aws225

Escayg, A., De Waard, M., Lee, D. D., Bichet, D., Wolf, P., Mayer, T., et al. (2000). Coding and noncoding variation of the human calcium-channel beta4-subunit gene CACNB4 in patients with idiopathic generalized epilepsy and episodic ataxia. *Am. J. Hum. Genet.* 66, 1531–1539. doi: 10.1086/302909

Escayg, A., Heils, A., MacDonald, B. T., Haug, K., Sander, T., and Meisler, M. H. (2001). A novel SCN1A mutation associated with generalized epilepsy with febrile seizures plus–and prevalence of variants in patients with epilepsy. *Am. J. Hum. Genet.* 68, 866–873. doi: 10.1086/319524

Favre, I., Moczydlowski, E., and Schild, L. (1996). On the structural basis for ionic selectivity among Na+, K+, and Ca2+ in the voltage-gated sodium channel. *Biophys. J.* 71, 3110–3125. doi: 10.1016/S0006-3495(96)79505-X

Fujiwara, T., Sugawara, T., Mazaki-Miyazaki, E., Takahashi, Y., Fukushima, K., Watanabe, M., et al. (2003). Mutations of sodium channel alpha subunit type 1 (SCN1A) in intractable childhood epilepsies with frequent generalized tonic-clonic seizures. *Brain* 126, 531–546. doi: 10.1093/brain/awg053

Fukuma, G., Oguni, H., Shirasaka, Y., Watanabe, K., Miyajima, T., Yasumoto, S., et al. (2004). Mutations of neuronal voltage-gated Na+ channel alpha 1 subunit gene SCN1A in core severe myoclonic epilepsy in infancy (SMEI) and in borderline SMEI (SMEB). *Epilepsia* 45, 140–148. doi: 10.1111/j.0013-9580.2004.15103.x

Gambardella, A., and Marini, C. (2009). Clinical spectrum of SCN1A mutations. *Epilepsia* 50, 20–23.

Gataullina, S., and Dulac, O. (2017). From genotype to phenotype in Dravet disease. *Seizure* 44, 58–64. doi: 10.1016/j.seizure.2016.10.014

Gertler, T. S., Calhoun, J., and Laux, L. (2020). A single-center, retrospective analysis of genotype-phenotype correlations in children with Dravet syndrome. *Seizure* 75, 1–6. doi: 10.1016/j.seizure.2019.12.009

Goldin, A. L., Barchi, R. L., Caldwell, J. H., Hofmann, F., Howe, J. R., Hunter, J. C., et al. (2000). Nomenclature of voltage-gated sodium channels. *Neuron* 28, 365–368.

Gonsales, M. C., Montenegro, M. A., Preto, P., Guerreiro, M. M., Coan, A. C., Quast, M. P., et al. (2019). Multimodal Analysis of SCN1A missense variants improves interpretation of clinically relevant variants in dravet syndrome. *Front. Neurol.* 10:289. doi: 10.3389/fneur.2019.00289

Ishii, A., Watkins, J. C., Chen, D., Hirose, S., and Hammer, M. F. (2017). Clinical implications of SCN1A missense and truncation variants in a large Japanese cohort with Dravet syndrome. *Epilepsia* 58, 282–290. doi: 10.1111/epi.13639

Jones, J. M., Dionne, L., Dell'Orco, J., Parent, R., Krueger, J. N., Cheng, X., et al. (2016). Single amino acid deletion in transmembrane segment D4S6 of sodium channel Scn8a (Nav1.6) in a mouse mutant with a chronic movement disorder. *Neurobiol. Dis.* 89, 36–45. doi: 10.1016/j.nbd.2016.01.018

Kasperaviciute, D., Catarino, C. B., Matarin, M., Leu, C., Novy, J., Tostevin, A., et al. (2013). Epilepsy, hippocampal sclerosis and febrile seizures linked by common genetic variation around SCN1A. *Brain* 136, 3140–3150. doi: 10.1093/brain/awt233

Lee, S. C., Kim, H. S., Park, Y. E., Choi, Y. C., Park, K. H., and Kim, D. S. (2009). Clinical Diversity of SCN4A-Mutation-associated skeletal muscle sodium channelopathy. *J. Clin. Neurol.* 5, 186–191. doi: 10.3988/jcn.2009.5.4.186

Lindy, A. S., Stosser, M. B., Butler, E., Downtain-Pickersgill, C., Shanmugham, A., Retterer, K., et al. (2018). Diagnostic outcomes for genetic testing of 70 genes in 8565 patients with epilepsy and neurodevelopmental disorders. *Epilepsia* 59, 1062–1071. doi: 10.1111/epi.14074

Liu, J., Tong, L., Song, S., Niu, Y., Li, J., Wu, X., et al. (2018). Novel and de novo mutations in pediatric refractory epilepsy. *Mol. Brain* 11:48.

Lossin, C., Rhodes, T. H., Desai, R. R., Vanoye, C. G., Wang, D., Carniciu, S., et al. (2003). Epilepsy-associated dysfunction in the voltage-gated neuronal sodium channel SCN1A. *J. Neurosci.* 23, 11289–11295. doi: 10.1523/JNEUROSCI.23-36-11289.2003

Mancardi, M. M., Striano, P., Gennaro, E., Madia, F., Paravidino, R., Scapolan, S., et al. (2006). Familial occurrence of febrile seizures and epilepsy in severe myoclonic epilepsy of infancy (SMEI) patients with SCN1A mutations. *Epilepsia* 47, 1629–1635. doi: 10.1111/j.1528-1167.2006.00641.x

Marini, C., Scheffer, I. E., Nabbout, R., Mei, D., Cox, K., Dibbens, L. M., et al. (2009). SCN1A duplications and deletions detected in Dravet syndrome: implications for molecular diagnosis. *Epilepsia* 50, 1670–1678. doi: 10.1111/j.1528-1167.2009.02013.x

Meisler, M. H., and Kearney, J. A. (2005). Sodium channel mutations in epilepsy and other neurological disorders. *J. Clin. Invest.* 115, 2010–2017. doi: 10.1172/JCI25466

Meng, H., Xu, H. Q., Yu, L., Lin, G. W., He, N., Su, T., et al. (2015). The SCN1A mutation database: updating information and analysis of the relationships among genotype, functional alteration, and phenotype. *Hum. Mutat.* 36, 573–580. doi: 10.1002/humu.22782

Moehring, J., von Spiczak, S., Moeller, F., Helbig, I., Wolff, S., Jansen, O., et al. (2013). Variability of EEG-fMRI findings in patients with SCN1A-positive Dravet syndrome. *Epilepsia* 54, 918–926. doi: 10.1111/epi.12119

Ohmori, I., Kahlig, K. M., Rhodes, T. H., Wang, D. W., and George, A. L. Jr. (2006). Nonfunctional SCN1A is common in severe myoclonic epilepsy of infancy. *Epilepsia* 47, 1636–1642. doi: 10.1111/j.1528-1167.2006.00643.x

Peng, J., Pang, N., Wang, Y., Wang, X. L., Chen, J., Xiong, J., et al. (2019). Next-generation sequencing improves treatment efficacy and reduces hospitalization in children with drug-resistant epilepsy. *CNS Neurosci. Ther.* 25, 14–20. doi: 10.1111/cns.12869

Remme, C. A., and Bezzina, C. R. (2010). Sodium channel (dys)function and cardiac arrhythmias. *Cardiovasc. Ther.* 28, 287–294. doi: 10.1111/j.1755-5922.2010.00210.x

Selmer, K. K., Lund, C., Brandal, K., Undlien, D. E., and Brodtkorb, E. (2009). SCN1A mutation screening in adult patients with Lennox-Gastaut syndrome features. *Epilepsy. Behav.* 16, 555–557. doi: 10.1016/j.yebeh.2009.08.021

Sugawara, T., Tsurubuchi, Y., Fujiwara, T., Mazaki-Miyazaki, E., Nagata, K., Montal, M., et al. (2003). Nav1.1 channels with mutations of severe myoclonic

epilepsy in infancy display attenuated currents. *Epilepsy. Res.* 54, 201–207. doi: 10.1016/s0920-1211(03)00084-6

Terlau, H., Heinemann, S. H., Stuhmer, W., Pusch, M., Conti, F., Imoto, K., et al. (1991). Mapping the site of block by tetrodotoxin and saxitoxin of sodium channel II. *FEBS Lett.* 293, 93–96. doi: 10.1016/0014-5793(91)81159-6

Thompson, C. H., Porter, J. C., Kahlig, K. M., Daniels, M. A., and George, A. L. Jr. (2012). Nontruncating SCN1A mutations associated with severe myoclonic epilepsy of infancy impair cell surface expression. *J. Biol. Chem.* 287, 42001–42008. doi: 10.1074/jbc.M112.421883

Till, A., Zima, J., Fekete, A., Bene, J., Czako, M., Szabo, A., et al. (2020). Mutation spectrum of the SCN1A gene in a Hungarian population with epilepsy. *Seizure* 74, 8–13. doi: 10.1016/j.seizure.2019.10.019

Usluer, S., Salar, S., Arslan, M., Yis, U., Kara, B., Tekturk, P., et al. (2016). SCN1A gene sequencing in 46 Turkish epilepsy patients disclosed 12 novel mutations. *Seizure* 39, 34–43. doi: 10.1016/j.seizure.2016.05.008

Wang, J. W., Shi, X. Y., Kurahashi, H., Hwang, S. K., Ishii, A., Higurashi, N., et al. (2012). Prevalence of SCN1A mutations in children with suspected Dravet syndrome and intractable childhood epilepsy. *Epilepsy. Res.* 102, 195–200. doi: 10.1016/j.eplepsyres.2012.06.006

Wu, Y. W., Sullivan, J., McDaniel, S. S., Meisler, M. H., Walsh, E. M., Li, S. X., et al. (2015). Incidence of Dravet Syndrome in a US Population. *Pediatrics* 136, e1310–e1315.

Yamakawa, K. (2006). Na channel gene mutations in epilepsy–the functional consequences. *Epilepsy. Res.* 70, S218–S222. doi: 10.1016/j.eplepsyres.2005.11.025

Yang, Y., Estacion, M., Dib-Hajj, S. D., and Waxman, S. G. (2013). Molecular architecture of a sodium channel S6 helix: radial tuning of the voltage-gated sodium channel 1.7 activation gate. *J. Biol. Chem.* 288, 13741–13747. doi: 10.1074/jbc.M113.462366

Yang, Y. C., Hsieh, J. Y., and Kuo, C. C. (2009). The external pore loop interacts with S6 and S3-S4 linker in domain 4 to assume an essential role in gating control and anticonvulsant action in the Na(+) channel. *J. Gen. Physiol.* 134, 95–113. doi: 10.1085/jgp.200810158

Yang, Z., Lu, D., Zhang, L., Hu, J., Nie, Z., Xie, C., et al. (2017). p.N1380del mutation in the pore-forming region of SCN5A gene is associated with cardiac conduction disturbance and ventricular tachycardia. *Acta Biochim. Biophys. Sin.* 49, 270–276. doi: 10.1093/abbs/gmx003

Yu, F. H., Mantegazza, M., Westenbroek, R. E., Robbins, C. A., Kalume, F., Burton, K. A., et al. (2006). Reduced sodium current in GABAergic interneurons in a mouse model of severe myoclonic epilepsy in infancy. *Nat. Neurosci.* 9, 1142–1149. doi: 10.1038/nn1754

Zuberi, S. M., Brunklaus, A., Birch, R., Reavey, E., Duncan, J., and Forbes, G. H. (2011). Genotype-phenotype associations in SCN1A-related epilepsies. *Neurology* 76, 594–600. doi: 10.1212/WNL.0b013e31820c309b

Conflict of Interest: The authors declare that the research was conducted in the absence of any commercial or financial relationships that could be construed as a potential conflict of interest.

Publisher's Note: All claims expressed in this article are solely those of the authors and do not necessarily represent those of their affiliated organizations, or those of the publisher, the editors and the reviewers. Any product that may be evaluated in this article, or claim that may be made by its manufacturer, is not guaranteed or endorsed by the publisher.

frontiers in Molecular Neuroscience

ORIGINAL RESEARCH
published: 30 March 2022
doi: 10.3389/fnmol.2022.795840

AFF2 Is Associated With X-Linked Partial (Focal) Epilepsy With Antecedent Febrile Seizures

Dongfang Zou[1,2,3†], Bing Qin[4†], Jie Wang[2,3], Yiwu Shi[2,3], Peng Zhou[2,3], Yonghong Yi[2,3], Jianxiang Liao[1] and Xinguo Lu[1*]*

[1] Epilepsy Center and Department of Neurology, Shenzhen Children's Hospital, Shenzhen, China, [2] Department of Neurology, Institute of Neuroscience, The Second Affiliated Hospital of Guangzhou Medical University, Guangzhou, China, [3] Key Laboratory of Neurogenetics and Channelopathies of Guangdong Province and the Ministry of Education of China, Guangzhou, China, [4] Epilepsy Center and Department of Neurosurgery, The First Affiliated Hospital of Jinan University, Guangzhou, China

Objective: *AFF2* mutations were associated with X-linked intellectual developmental disorder-109 and in males with autism spectrum disorder (ASD). The relationship between *AFF2* and epilepsy has not been defined.

Method: Trios-based whole-exome sequencing was performed in a cohort of 372 unrelated cases (families) with partial (focal) epilepsy without acquired causes.

Results: Five hemizygous missense *AFF2* mutations were identified in five males with partial epilepsy and antecedent febrile seizures without intellectual disability or other developmental abnormalities. The mutations did not present in the controls of general populations with an aggregate frequency significantly higher than that in the control populations. Previously, intellectual disability-associated *AFF2* mutations were genomic rearrangements and CCG repeat expansion mutations mostly, whereas the mutations associated with partial epilepsy were all missense. Missense *AFF2* mutations associated with epilepsy fell into the regions from N-terminal to the nuclear localization signal 1 (NLS1), while ASD-associated missense mutations fell in the regions from NLS1 to C-terminal.

Conclusion: *AFF2* is potentially a candidate causative gene of X-link partial epilepsy with antecedent febrile seizures. The genotype–phenotype correlation and molecular sub-regional effect of *AFF2* help in explaining the mechanisms underlying phenotypic variations.

Keywords: epilepsy, *AFF2* gene, whole-exome sequencing, intellectual disability, autism spectrum disorder

OPEN ACCESS

Edited by:
Qian Chen,
Massachusetts Institute of Technology, United States

Reviewed by:
Qiongxiang Zhai,
Guangdong Academy of Medical Sciences, China
Dong Zhou,
Sichuan University, China

***Correspondence:**
Jianxiang Liao
liaojianxiang@vip.sina.com
Xinguo Lu
szluxg20@163.com

[†] These authors have contributed equally to this work

Specialty section:
This article was submitted to Molecular Signaling and Pathways, a section of the journal Frontiers in Molecular Neuroscience

Received: *15 October 2021*
Accepted: *08 February 2022*
Published: *30 March 2022*

Citation:
Zou D, Qin B, Wang J, Shi Y, Zhou P, Yi Y, Liao J and Lu X (2022) AFF2 Is Associated With X-Linked Partial (Focal) Epilepsy With Antecedent Febrile Seizures. Front. Mol. Neurosci. 15:795840. doi: 10.3389/fnmol.2022.795840

INTRODUCTION

AFF2 (OMIM* 300806) (also known as *FMR2* gene), which encodes AF4/FMR2 family member 2, is a transcriptional factor and RNA-binding protein that plays an important role in transcriptional regulation, RNA splicing, mRNA processing, and nuclear speckle organization (Bensaid et al., 2009). *AFF2* is highly conserved and abundantly expressed in human brain (Gecz et al., 1997), being essential for brain development. Homozygous *AFF2* knock-out mice showed abnormal central nervous system synaptic transmission, abnormal excitatory postsynaptic potential, and premature

death.[1] Previous studies have identified *AFF2* mutations in the etiology of X-linked intellectual developmental disorder-109 (MRX109), a form of mildly to moderately impaired intellectual development associated with learning difficulties, communication deficits, attention problems, hyperactivity, and autistic behavior (Knight et al., 1993, 1996; Mulley et al., 1995; Gecz, 2000), in which epileptic seizures were occasionally observed (Lo Nigro et al., 2000; Lesca et al., 2003). Several point mutations were also identified in patients with autism spectrum disorder (ASD) (Mondal et al., 2012; Jiang et al., 2013; Yuen et al., 2017). The relationship between *AFF2* and epilepsy has not been defined. In the present study, trios-based whole-exome sequencing (WES) was performed in a cohort of cases (families) of partial (focal) epilepsy without acquired causes. Five missense mutations of *AFF2* were identified in five unrelated individuals of partial epilepsy without intellectual disability or other developmental abnormalities.

MATERIALS AND METHODS

Participants

A total of 372 cases (families) with partial epilepsy without acquired causes were recruited, including 323 cases from the Epilepsy Center of the Second Affiliated Hospital of Guangzhou Medical University in China between January 2013 and July 2020, and 49 cases from Shenzhen Children's Hospital and the First Affiliated Hospital of Jinan University in China between January 2018 and July 2020. The probands included 230 males and 142 females and were subjected to trios-based WES for potential genetic etiology of epilepsy. The complete pedigree and clinical data of the probands were collected, including detailed clinical phenotypes, age of seizure onset, seizure type, seizure course and frequency, family history, treatment, prognosis, general and neurological examination, and brain magnetic resonance imaging (MRI). 24-h video electroencephalography (EEG) was performed on all patients, at the age ranging from 4 to 23 years (mean age, 10.2 years), and EEG was analyzed by at least two qualified electroencephalographers. The developmental and intellectual states of all patients (at the age range, 3–24 years; mean age, 10.4 years) were evaluated, including language, fine and gross motor, and adaptive social skills and performance at school or work. Gesell development scale, Wechsler intelligence scale for children-V, and Wechsler adult intelligence scale were utilized in the neuropsychological evaluation of the participants according to their ages. Seizure type and epilepsy syndrome were classified according to the criteria of the Commission on Classification and Terminology of International League of Against Epilepsy (ILAE) (No Author, 1985, 1989; Berg et al., 2010; Scheffer et al., 2017). The inclusion criteria were: (1) diagnosis of partial epilepsy based on ILAE criteria, characterized by focal seizures or focally originated focal to bilateral tonic-clonic seizures; (2) EEG examination presented focal discharges, including unilateral, bilateral, and multiple focal discharges with normal background. The exclusion criteria were: (1) diagnosis of generalized epilepsy based on ILAE criteria; (2) individuals with acquired causes, including brain tumors, head trauma, immune encephalitis, central nervous system infections, and cerebrovascular diseases.

This study was based on the guidelines of the International Committee of Medical Journal Editors concerning patient consent for research or participation. Written informed consent was obtained from all individuals or their legal guardians. The present study was approved by the Ethics Committee of the Second Affiliated Hospital of Guangzhou Medical University.

Whole Exome Sequencing

Blood samples were obtained from all individuals and their parents. Genomic DNA was extracted from the peripheral blood using Qiagen Flexi Gene DNA kit (Qiagen, Hilden, Germany), according to the protocol of the manufacturer. Trio-based WES was conducted on the MGI 2000 platform by BGI-Shenzhen (Shenzhen, China) performing pair-end reads, 100 bp sequencing with 100–150 times average depth and more than 98% coverage of the target region. Deep sequencing data were aligned to the reference GRCh37 build (hg19) and variants were called according to the standard procedures as previously reported (Wang et al., 2018; Cai et al., 2019; Shi et al., 2019). We adopted a case-by-case analytical approach to identify candidate causative mutations in each trio. Firstly, we prioritized the rare variants with a minor allele frequency < 0.005 in the 1,000 Genomes Projects, Exome Aggregation Consortium, and Genome Aggregation Database (gnomAD). Secondly, we retained potentially pathogenic mutations, including frameshift, nonsense, canonical splice site, initiation codon, and missense mutations predicted as being damaging by 21 algorithms *in silico* prediction.[2] Finally and importantly, potential disease-causing variants were screened under five models: (1) epilepsy-associated gene model; (2) *de novo* autosomal dominant model; (3) autosomal recessive inheritance model, including compound heterozygous and homozygous variants; (4) X-linked inheritance model; (5) co-segregation model. To identify novel epilepsy-associated genes, we put the known epilepsy-associated genes (Wang et al., 2017) aside. The genes with repetitively identified *de novo* variants, bi-allelic variants, hemizygous variants, and variants with segregations, were selected for further studies to define the gene-disease association. *AFF2* appeared as a candidate gene with recurrent hemizygous variants in this cohort of partial epilepsy and was subjected to further analysis in this study. The other potential candidate genes were not included in the present study. The candidate pathogenic variants were validated by Sanger sequencing. All variants in *AFF2* were annotated to the reference transcript NM_002025.4. Conservation of the mutated positions was evaluated by generating multiple sequence alignments of different species.

Molecular and Genotype-Phenotype Correlation Analysis

To predict the effect of missense mutations on molecular structure, a protein model was established by Phyre2 (V 2.0).[3]

[1] http://www.informatics.jax.org/allele/MGI:2182641

[2] http://varcards.biols.ac.cn/

[3] http://www.sbg.bio.ic.ac.uk/~phyre2/html/page.cgi?id=index

PyMOL 1.7 was used to visualize and analyze the three-dimensional protein structure and alteration of hydrogen bonds. Amino acids were annotated to the reference protein NP_002016. To evaluate the genotype-phenotype correlation, we reviewed all the relevant literature about *AFF2* mutations reported previously, including point mutations, genomic rearrangements, and CCG repeat expansion variants, as well as all the phenotypes of the mutations. All the mutations were retrieved from PubMed[4] and Human Gene Mutation Database[5] up to December 2020.

Statistical Analysis

R statistical software (v3.4.1) and SPSS version 22.0 (SPSS, Inc., Chicago, IL, United States) were used for statistical analyses. Fisher's exact test was applied to access the frequencies of *AFF2* mutations in the case cohort and the control populations. A p-value < 0.05 was considered statistically significant.

RESULTS

Identification of *AFF2* Mutations

Five hemizygous missense *AFF2* variants were identified in five unrelated individuals with partial epilepsy, including c.230A > T/p.N77I, c.391C > T/p.H131Y, c.1540C > T/p.R514C, c.2009G > A/p.R670H, and c.2074C > G/p.P692A. All variants originated from their asymptomatic mothers (**Figures 1A,B** and **Table 1**). No *AFF2* variants were found in their fathers. The amino acid sequence alignment indicated that N77I, R514C, and R670H were located at residuals of highly conserved across various species ("highly conserved" means the fraction of the AFF2 residues conserved for the used species is 100%); while H131Y and P692A were located at residuals of less conserved according to the sequence alignment ("less conserved" means the fraction is less than 100%) (**Figure 1C**). None of the five cases was identified to have other pathogenic or likely pathogenic variants in the known genes associated with seizure disorders (Wang et al., 2017), neither other pathogenic nor likely pathogenic variants were found in the *de novo* autosomal dominant, autosomal recessive inheritance, and co-segregation model.

We compared the aggregate frequency of the five hemizygous *AFF2* mutations in this cohort with that in the populations in gnomAD, or controls of gnomAD, according to the aggregate variant analysis method suggested by ClinGen (Strande et al., 2017). Five mutant alleles in a total of 230 alleles (230 males in the 372 cases) were detected in this cohort. Mutation R514C had an extremely low frequency (9.95e-06) but was not present in the controls of gnomAD-East Asian and gnomAD-all population, part of the allele frequency was from the 1000G data. The other four mutations in *AFF2* had no allele frequency in gnomAD databases (**Table 2**). The differences in aggregate frequencies of the mutant alleles between this cohort in male cases and the male controls in gnomAD (general population, East-Asian population) were statistically significant (5/230 vs. 0/46329 in the male controls of gnomAD-all population, $p = 2.82 \times 10^{-12}$; 5/230 vs. 0/3058 in the male controls of gnomAD-East Asian population, $p = 1.61 \times 10^{-6}$, respectively) (**Table 2**).

Clinical Features of the Cases With *AFF2* Mutations

AFF2 mutations were identified in five unrelated male epilepsy patients with focal seizures and/or focal discharges, ranging in age from 5 to 27 years. The clinical features of the five cases were summarized in **Table 1**. The age of febrile seizures onset ranged from 10 months to 2 years, and the afebrile seizures started from 5 to 9 years. All the cases presented with infrequent focal impaired awareness seizures, and the cases with mutation R670H (Case 4) and P692A (Case 5) also had focal to bilateral tonic-clonic seizures. Except for the case with mutation P692A (Case 5), the other four cases exhibited antecedent febrile seizures or prolonged febrile seizures, and they developed afebrile seizures later with an intermission of 4–7 years. The interictal EEG recording showed epileptiform discharges, including bilateral, unilateral, and multiple discharges, predominantly at frontal, central, and temporal lobe, predominantly during sleeping. Trends of generalization were also observed in the case with mutation R514C (Case 3) (**Figure 1D**). The ictal EEG of the case with mutation N77I (Case 1) showed an onset originated from the left mid-central area, and the case with mutation R514C (Case 3) demonstrated a seizure originated from the left hemisphere. Brain MRIs of all the cases were normal. According to the results of the relevant developmental scales, all individuals presented normal development and intellectual ability. The epilepsy of the five cases was controlled with one or two antiepileptic drugs. The cases with mutation N77I (Case 1) and R514C (Case 3) achieved seizure free with monotherapy of lamotrigine (6–7 mg/kg/d). The cases with H131Y (Case 2) and R670H (Case 4) had seizure reductions with valproate (20–25 mg/kg/d) at first and became seizure free after the add-on of oxcarbazepine (20–25 mg/kg/d). The case with P692A (Case 5) had seizure reduction of more than 60% with initial valproate (20 mg/kg/d) and got seizures controlled on the combined use of lamotrigine (5 mg/kg/d).

Molecular Effect of *AFF2* Mutations

The length of amino acid of FMR2 is 1311, including two bipartite NLSs (nuclear localization signals)–NLS1 (RKEPRPNIPLAPEKKK) at amino acid position 681–696 and NLS2 (KPAPKGKRKHKPIEVAEKIPEKK) at position 846–868. Additionally, a large serine-rich domain locates at protein position 481–502, which overlaps with the regions involved in transcription activation, and a large alanine-threonine-rich domain is at position 979–1032, being unique to the FMR2 (Gecz et al., 1997). N-terminal domain of the protein includes amino acids 1–541, which is known to have transactivation activity (Hillman and Gecz, 2001), whereas C-terminal domain comprises amino acids 633–1272, being responsible for localization of the protein in nuclear speckles (Bensaid et al., 2009). In the present study, mutations N77I, H131Y, and R514C were located in the N-terminal domain. P692A was located in the NLS1 domain, while R670H was located in the N-terminal frank of NLS1 (**Figure 2A**).

[4]https://pubmed.ncbi.nlm.nih.gov/

[5]http://www.hgmd.cf.ac.uk/ac/index.php

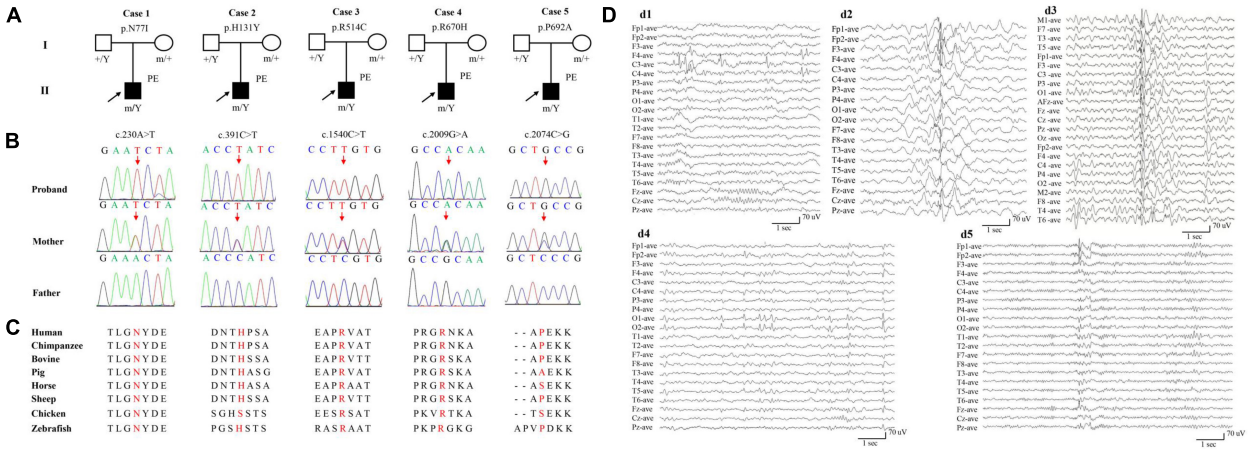

FIGURE 1 | Genetic and electroencephalograms (EEG) of the cases with *AFF2* mutations. **(A)** Pedigrees of the five cases with *AFF2* mutations and their corresponding phenotypes. PE, partial epilepsy. **(B)** DNA sequence chromatogram of the *AFF2* mutations. Arrows indicate the positions of the mutations. **(C)** The amino acid sequence alignment of the five missense mutations shows that residues N77I, R514C, and R670H were highly conserved across various species. Residues H131Y and P692A were less conserved. **(D)** Changes of interictal EEG in the cases with *AFF2* mutations. **(d1)** Interictal EEG of case 1 showed bilateral frontal-central spike and slow waves (obtained at the age of 8 years). **(d2)** Interictal EEG of case 2 showed bilateral frontal and anterior-temporal spike and slow waves (at the age of 9 years). **(d3)** Interictal EEG of case 3 showed spike and slow waves predominant at left hemisphere (at the age of 5 years). **(d4)** Interictal EEG of case 4 showed sharp waves predominant at bilateral occipital regions (at the age of 3 years). **(d5)** Interictal EEG of case 5 showed spike and slow waves predominant at bilateral frontal regions (at the age of 17 years).

The molecular effect of the five missense mutations was analyzed by protein modeling using PHYRE2[6] and PyMOL with the templates available (**Figure 2B**). The protein modeling showed that mutations N77I and H131Y resulted in alteration of hydrogen bonds and potentially affected the protein steric configuration. Originally, residue N77 formed three hydrogen bonds with residue D79, E80, and M81, respectively. When asparagine was replaced by isoleucine at residue N77, the hydrogen bond with D79 was destroyed (**Figure 2Bb1**). Residue H131 formed two hydrogen bonds with residue T130 and one hydrogen bond with residue N129. When histidine was replaced by tyrosine at residue H131, the hydrogen bonds with residue T130 were destroyed (**Figure 2Bb2**). There was no hydrogen bond formed with other surrounding residues at residue C514 (**Figure 2Bb3**). Mutation R670H and P692A showed no hydrogen bond altered at the residues (**Figures 2Bb4,b5**).

Genotype-Phenotype Correlation and Molecular Sub-Regional Implication

We reviewed the previous studies through PubMed and Human Gene Mutation Database and analyzed the relationship between genotype and phenotype of *AFF2* mutations. Previously, 33 *AFF2* mutations that were associated with diseases of the central nervous system have been reported (**Supplementary Table 1**), including 8 missense mutations, 6 destructive (null) mutations (2 nonsense, 1 small deletion, and 3 small insertions), and 19 genomic rearrangements (15 gross deletions, 3 gross insertions, and 1 complex rearrangement). Additionally, 28 cases/families with CCG repeat expansion ($\geq$ 200 repeats or $>$ 5.2 Kb) in 5′-UTR have been published. The missense mutations were identified in 6 cases with ASD (6/8) and 2 cases with intellectual disability (2/8, one of whom accompanied with epilepsy). The destructive mutations were associated with ASD (5/6) mostly, and a case with intellectual disability (1/6). The genomic rearrangements were all associated with intellectual disability, among which 15 cases accompanied with developmental delay (15/19), 9 cases with epilepsy (9/19), and 1 case with ASD (1/19). Similarly, the CCG repeat variants were all associated with intellectual disability (**Figure 2C** and **Supplementary Table 1**).

In this study, the 5 cases who presented partial epilepsy all harbored missense mutations (5/5, 100%). In contrast, among the patients with ASD, six cases harbored missense mutations (6/11, 54.5%) and five cases harbored truncated mutations (5/11, 45.5%). In the patients with intellectual disability, missense mutations accounted for 4.0% (2/50), truncating mutation accounted for 2.0% (1/50), genomic rearrangements accounted for 38.0% (19/50), and CCG repeat variants accounted for 56.0% (28/50) of the cases. The proportion of missense mutations in epilepsy without intellectual disability and ASD was 100%, which was significantly higher than that in intellectual disability ($p < 0.001$) (**Figure 2C**).

Our previous studies showed that the molecular sub-regional location of the missense mutations was associated with the phenotypic variation and considered to be a critical factor to determine the pathogenicity of variants (Liu et al., 2020; Tang et al., 2020). We thus analyzed the molecular sub-regional implications of *AFF2* variants on phenotype variation. The missense mutations with epilepsy in the present study fell into the regions from the N-terminal to the NLS1, whereas the missense mutations with ASD fell in the regions from the NLS1 to the C-terminal, with several mutations overlapped around the NLS1 (**Figure 2A**).

[6]http://www.sbg.bio.ic.ac.uk/~phyre2/html/page.cgi?id=index

TABLE 1 | Clinical features of the cases with *AFF2* mutations.

	Case 1	Case 2	Case 3	Case 4	Case 5
AFF2 mutations (NM_002025.4)	c.230A > T/p.N77I	c.391C > T/p.H131Y	c.1540C > T/p.R514C	c.2009G > A/p.R670H	c.2074C > G/p.P692A
Diagnosis	PE	PE	PE	PE	PE
Gender	Male	Male	Male	Male	Male
Present age	8 yr	9 yr	5 yr	10 yr	27 yr
FS onset age	14 mo	2 yr	18 mo	10 mo	—
aFS onset age	7 yrs	9 yrs	5 yrs	7 yrs	8 yrs
Intermission from FS to EP	6 yrs	7 yrs	4 yrs	7 yrs	—
Seizure type	FS, CPS	FS, CPS	FS, CPS	FS, CPS, sGTCS	CPS, sGTCS
Seizure frequency	FS once, CPS 2 times/mo	FS once, CPS 3 times/mo	FS 4 times, CPS 4–5 times/yr	Prolonged FS 2 times/yr, CPS/sGTCS 3–4 times/yr	CPS 5–6 times/mo, sGTCS 1–2 times/yr
Seizure timing	Nocturnal	Diurnal	Diurnal	Diurnal and nocturnal	Diurnal and nocturnal
Family history of seizure	None	None	None	None	None
Ictal EEG	Generalized spike and spike-slow wave originated from the left mid-central with a partial seizure	NA	Generalized slow wave originated from the left hemisphere with a partial seizure	NA	NA
Interictal EEG	Bilateral spike and slow waves predominantly in the frontal and central areas	Bilateral spike and slow waves predominantly in the frontal and anterior-temporal areas	Spike and slow waves predominantly in the left hemisphere	Bilateral sharp waves predominantly in the occipital areas	Bilateral spike and slow waves predominantly in the frontal areas
Brain MRI	Normal	Normal	Normal	Normal	Normal
Intelligence	Normal	Normal	Normal	Normal	Normal
Developmental delay	No	No	No	No	No
Treatment	LTG	VPA, OXC	LTG	VPA, OXC	VPA, LTG
Seizure outcome	Free for 1 yr	Free for 1 yr	Free for 1 yr	Free for 1 yr	Free for 5 yrs

aFS, afebrile seizures; CPS, complex partial seizure; EEG, electroencephalogram; EP, epilepsy; FS, febrile seizures; LTG, lamotrigine; MRI, magnetic resonance imaging; mo, month; NA, not available; OXC, oxcarbazepine; PE, partial epilepsy; sGTCS, secondary generalized tonic-clonic seizure; VPA, valproate; yr, year.

TABLE 2 | Analysis of the aggregate frequency of *AFF2* mutations identified in this study.

	Allele count/number in this study (%)	Allele count/number in male controls of gnomAD-all populations (%)	Allele count/number in male controls of gnomAD-East Asian populations (%)
Identified *AFF2* mutations			
chrX:147743478 (c.230A > T/p.N77I)	1/230 (0.43)	-/-	-/-
chrX:147743639(c.391C > T/p.H131Y)	1/230 (0.43)	-/-	-/-
chrX:148035252(c.1540C > T/p.R514C)	1/230 (0.43)	-/-	-/-
chrX:148037584(c.2009G > A/p.R670H)	1/230 (0.43)	-/-	-/-
chrX:148037649(c.2074C > G/p.P692A)	1/230 (0.43)	-/-	-/-
Total	5/230 (2.17)	0/46329 (0)	0/3058 (0)
***p*-value**		2.82×10^{-12}	1.61×10^{-6}
OR (95% CI)		Inf (186.76–Inf)	Inf (12.33–Inf)

p-values and odds ratio were estimated with two-sided Fisher's exact test.
CI, confidence interval; gnomAD, Genome Aggregation Database; OR, odds ratio.
Ref: Cai et al. (2015).

DISCUSSION

AFF2 is a large gene containing 22 exons and spanning about 500 kb that is located on chromosome Xq28. FMR2, the *AFF2* encoded protein, has five annotated isoforms. The longest one is composed of 1,311 amino acids and contains two nuclear localization signals (Gecz et al., 1997). FMR2 acts as a transcriptional factor and RNA-binding protein, playing an

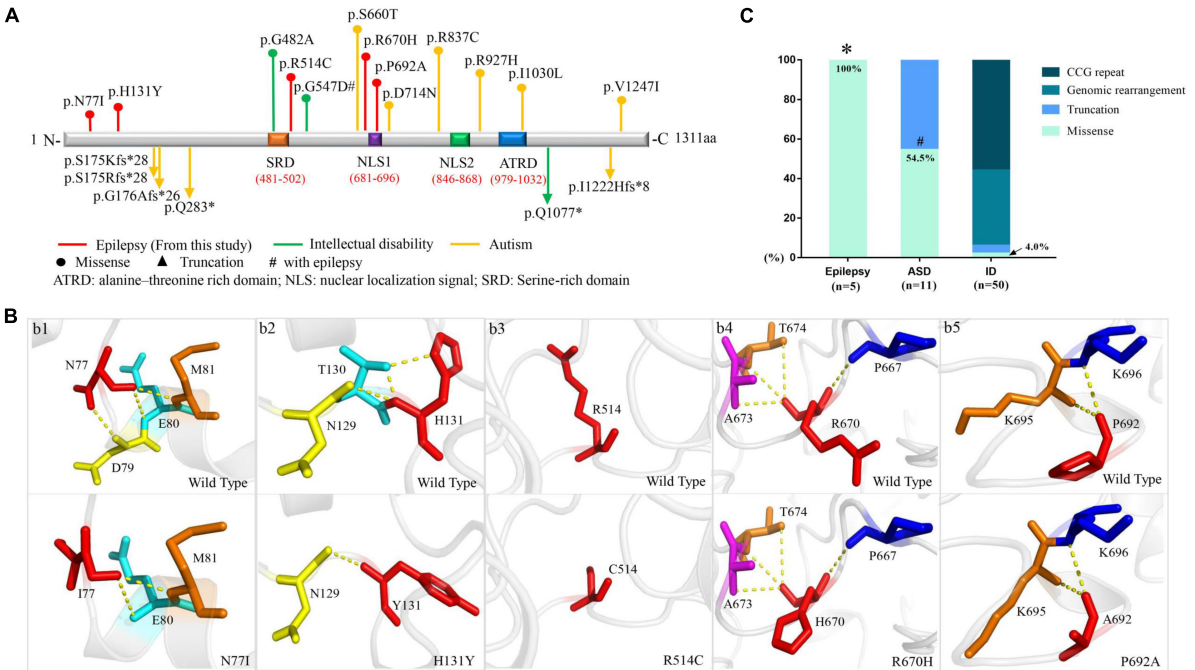

FIGURE 2 | Schematic presentation of FMR2 structure and genotype-phenotype correlation of *AFF2*. **(A)** Schematic diagram of missense and destructive *AFF2* mutations and their locations on FMR2 protein. Missense mutations were shown at the top of the structural diagram. Destructive mutations were shown at the bottom. **(B)** Schematic illustration of the changes in hydrogen bonds. The residues where the mutations occurred are shown as red rods. The hydrogen bonds are shown as yellow spheres. **(C)** Genotypes of *AFF2* in epilepsy, autism spectrum disorder (ASD), and intellectual disability (ID). *The proportion of missense mutations in epilepsy is significantly higher than that in ID ($p < 0.001$) through Fisher's exact test. #The proportion of missense mutations in ASD is significantly higher than that in ID ($p < 0.001$) through Fisher's exact test.

essential role for transcriptional regulation and RNA splicing in nuclear speckle (Bensaid et al., 2009). In the present study, five novel missense *AFF2* mutations were identified in five male individuals with partial epilepsy and antecedent febrile seizures. The mutations were inherited from their asymptomatic mothers, consistent with an X-linked inheritance pattern. This study suggests that *AFF2* is potentially a candidate causative gene of X-link partial epilepsy with antecedent febrile seizures. The molecular sub-regional effect of *AFF2* helps in explaining the mechanisms underlying phenotypic variations.

Homozygous knock-out of *Aff2* in the mice model resulted in premature death with incomplete penetrance. The survival mice showed impaired learning and memory abilities and increased long-term potentiation—similar features as human intellectual disability (Gu et al., 2002), supporting the view that FMR2 is responsible for intellectual disability. Previous studies showed that intellectual disability associated *AFF2* mutations were genomic rearrangements and CCG repeat expansion mostly (**Figure 2C** and **Supplementary Table 1**), suggesting a pathogenic role of loss-of-function of *AFF2* in intellectual disability. Epileptic seizures were also observed in patients with genomic rearrangements (Wolff et al., 1997; Moore et al., 1999), suggesting that loss-of-function of *AFF2* would be potentially associated with epilepsy. In the present study, the patients presented good responses to antiepileptic drugs and become seizure free. These findings suggested that missense *AFF2* mutations were potentially associated with epilepsy with favorable outcomes without intellectual disability.

Apart from epilepsy, missense *AFF2* mutations have also been identified in patients with ASD (Mondal et al., 2012; Jiang et al., 2013). Further analysis revealed that missense *AFF2* mutations with epilepsy in this study mainly fell into the regions from the N-terminal to the NLS1, whereas the missense mutations with ASD mainly fell in the regions from the NLS1 to the C-terminal (**Figure 2A**). This evidence suggested a molecular sub-regional effect of *AFF2* mutations, as that in several genes reported previously (Liu et al., 2020; Tang et al., 2020). FMR2 is a multifunctional protein connecting transcriptional regulation and RNA splicing and plays an important role in regulating gene expression in the cell nucleus (Gecz, 2000). The protein shuttles between speckles and splicing sites, where it can pick up cargo RNAs and transfer them to the nucleolus for subsequent modifications (Bensaid et al., 2009). A previous study showed that FMR2 acted as a potent transcription activator and could regulate transcription via its N-terminal region (Hillman and Gecz, 2001). On the other hand, FMR2 protein is also an RNA binding protein, co-localizing with the splicing factor SC35 in nuclear speckles and is involved in splicing of *FMR1* pre-mRNA through its specific interaction with G-quadruplex RNA-forming structure via its C-terminal domain (Lamond and Spector, 2003). The G-quadruplex structure was known to work as an exonic splicing enhancer which could control splicing efficiency (Bensaid et al., 2009). Therefore, the N-terminal region of FMR2 was closely associated with transcription and C-terminal region was able to modulate splicing, providing a molecular basis of the sub-regional effect

of *AFF2* mutations and potentially explaining the underlying mechanisms of phenotypic variations.

In this study, the cases all presented with partial epilepsy. *AFF2* is ubiquitously expressed in multiple human brain tissues (Gecz et al., 1997) and is more abundant in the frontal cortex, anterior cingulate cortex, hippocampus, and the amygdala, which may provide an anatomical basis for the phenotype of partial epilepsy. Moreover, four cases presented with antecedent febrile seizures at the average age of 16.5 months (from 10 months to 2 years old). The intermission from febrile seizures to epilepsy was 4–7 years. It is notable that *AFF2* is significantly expressed in the fetal and adult brain (Gecz et al., 1997). The data from Unigene database in NCBI showed that the expression of *AFF2* was high in blastocyte and fetus, with an intermission in early life, and then increased again in adults (**Supplementary Figure 1**). The intermission of gene expression was consistent with the intermission between febrile seizures and epilepsy presented in the patients. The relationship between gene expression and occurrence of phenotype potentially implies clinical significance in evaluation of the course and outcome of the illness.

There were several limitations in this study. First, the functional consequences of these missense variants warrant further validation by experimental studies. Second, previous studies revealed that some of the *AFF2* mutations associated with intellectual disability were CCG repeat expansion, which were not included in the present study. Third, a previous study reported that a missense mutation of *AFF2* was identified in a 6-year-old boy with focal epilepsy and moderate intellectual disability, but without febrile seizures (Zhang et al., 2015). The study indicated that missense *AFF2* mutations could also lead to other phenotypes such as intellectual disability, possibly associated with the molecular sub-regional location. Further studies are required to verify the association. Last, the sample size was limited with geographical limitations. Larger cohorts are required for validation by multicenter research.

CONCLUSION

This study identified five missense *AFF2* mutations in five unrelated males with partial epilepsy and antecedent febrile seizures without intellectual disability or other developmental abnormalities. The frequency of the identified mutant alleles in this cohort was significantly higher than that in the control populations in gnomAD. Further analysis revealed that the *AFF2* mutations associated with partial epilepsy in this study were all missense, in contrast, intellectual disability-associated mutations were genomic rearrangements and CCG repeat expansion mostly. These findings suggested *AFF2* was potentially a candidate causative gene of X-link partial epilepsy with antecedent febrile seizures. The genotype-phenotype correlation and molecular sub-regional effect of *AFF2* help in explaining the mechanisms underlying phenotypic variations.

DATA AVAILABILITY STATEMENT

The datasets presented in this study can be found in online repositories. The names of the repository/repositories and accession number(s) are the following: Genbank (https://www.ncbi.nlm.nih.gov/nuccore/) with accession numbers: GenBank MZ958719–MZ958733.

ETHICS STATEMENT

The studies involving human participants were reviewed and approved by the Ethics Committee of the Second Affiliated Hospital of Guangzhou Medical University. Written informed consent to participate in this study was provided by the participants' legal guardian/next of kin.

AUTHOR CONTRIBUTIONS

XL designed the study, administered the project, and revised the manuscript. JL designed the study and contributed to data interpretation. DZ completed collection of the clinical data, analysis of the data, and draft of the manuscript. XL and DZ completed the recruitment of the patients and contributed to data interpretation. BQ, JL, and YY contributed to data analysis and interpretation. JW, PZ, and YS performed data analysis and provided technical assistance. All authors have read and approved the final manuscript.

FUNDING

This work was supported by grants from the National Natural Science Foundation of China (Grant Nos. 81871015 and 81870903), the Natural Science Foundation of Guangdong Province (2020A1515010108), the Science and Technology Project of Guangzhou (Grant Nos. 201904020028 and 201904010275), the Science and Technology Project of Guangdong Province (Grant Nos. 2017B09090436 and 2017B030314159), the Multi-Center Clinical Research Fund Project of the Second Affiliated Hospital of Guangzhou Medical University (Grant Nos. DZX-002 and 2020-LCYJ-DZX-03), the Sanming Project of Medicine in Shenzhen (Grant No. SZSM201812005), the Shenzhen Fund for Guangdong Provincial High-level Clinical Key Specialties (Grant No. SZGSP012), and the Shenzhen Key Medical Discipline Construction Fund (Grant No. SZXK033).

ACKNOWLEDGMENTS

We are deeply grateful to the patients and clinicians who participated in this work.

SUPPLEMENTARY MATERIAL

The Supplementary Material for this article can be found online at: https://www.frontiersin.org/articles/10.3389/fnmol.2022.795840/full#supplementary-material

REFERENCES

Bensaid, M., Melko, M., Bechara, E. G., Davidovic, L., Berretta, A., Catania, M. V., et al. (2009). FRAXE-associated mental retardation protein (FMR2) is an RNA-binding protein with high affinity for G-quartet RNA forming structure. *Nucleic Acids Res.* 37, 1269–1279. doi: 10.1093/nar/gkn1058

Berg, A. T., Berkovic, S. F., Brodie, M. J., Buchhalter, J., Cross, J. H., van Emde Boas, W., et al. (2010). Revised terminology and concepts for organization of seizures and epilepsies: report of the ILAE Commission on Classification and Terminology, 2005-2009. *Epilepsia* 51, 676–685. doi: 10.1111/j.1528-1167.2010.02522.x

Cai, K., Wang, J., Eissman, J., Wang, J., Nwosu, G., Shen, W., et al. (2019). A missense mutation in SLC6A1 associated with Lennox-Gastaut syndrome impairs GABA transporter 1 protein trafficking and function. *Exp. Neurol.* 320:112973. doi: 10.1016/j.expneurol.2019.112973

Cai, N., Bigdeli, T. B., Kretzschmar, W., Li, Y., Liang, J., Song, L., et al. (2015). Sparse whole-genome sequencing identifies two loci for major depressive disorder. *Nature* 523, 588–591.

Gecz, J. (2000). The FMR2 gene, FRAXE and non-specific X-linked mental retardation: clinical and molecular aspects. *Ann. Hum. Genet.* 64, 95–106. doi: 10.1017/S0003480000007983

Gecz, J., Bielby, S., Sutherland, G. R., and Mulley, J. C. (1997). Gene structure and subcellular localization of FMR2, a member of a new family of putative transcription activators. *Genomics* 44, 201–213. doi: 10.1006/geno.1997.4867

Gu, Y., McIlwain, K. L., Weeber, E. J., Yamagata, T., Xu, B., Antalffy, B. A., et al. (2002). Impaired conditioned fear and enhanced long-term potentiation in Fmr2 knock-out mice. *J. Neurosci.* 22, 2753–2763. doi: 10.1523/JNEUROSCI.22-07-02753.2002

Hillman, M. A., and Gecz, J. (2001). Fragile XE-associated familial mental retardation protein 2 (FMR2) acts as a potent transcription activator. *J. Hum. Genet.* 46, 251–259. doi: 10.1007/s100380170074

Jiang, Y. H., Yuen, R. K., Jin, X., Wang, M., Chen, N., Wu, X., et al. (2013). Detection of clinically relevant genetic variants in autism spectrum disorder by whole-genome sequencing. *Am. J. Hum. Genet.* 93, 249–263. doi: 10.1016/j.ajhg.2013.06.012

Knight, S. J., Flannery, A. V., Hirst, M. C., Campbell, L., Christodoulou, Z., Phelps, S. R., et al. (1993). Trinucleotide repeat amplification and hypermethylation of a CpG island in FRAXE mental retardation. *Cell* 74, 127–134. doi: 10.1016/0092-8674(93)90300-f

Knight, S. J., Ritchie, R. J., Chakrabarti, L., Cross, G., Taylor, G. R., Mueller, R. F., et al. (1996). A study of FRAXE in mentally retarded individuals referred for fragile X syndrome (FRAXA) testing in the United Kingdom. *Am. J. Hum. Genet.* 58, 906–913.

Lamond, A. I., and Spector, D. L. (2003). Nuclear speckles: a model for nuclear organelles. *Nat. Rev. Mol. Cell. Biol.* 4, 605–612. doi: 10.1038/nrm1172

Lesca, G., Biancalana, V., Brunel, M. J., Quack, B., Calender, A., and Lespinasse, J. (2003). Clinical, cytogenetic, and molecular description of a FRAXE French family. *Psychiatr Genet.* 13, 43–46. doi: 10.1097/00041444-200303000-00007

Liu, L., Chen, Z. R., Xu, H. Q., Liu, D. T., Mao, Y., Liu, H. K., et al. (2020). DEPDC5 variants associated malformations of cortical development and focal epilepsy with febrile seizure plus/febrile seizures: the role of molecular sub-regional effect. *Front. Neurosci.* 14:821. doi: 10.3389/fnins.2020.00821

Lo Nigro, C., Faravelli, F., Cavani, S., Perroni, L., Novello, P., Vitali, M., et al. (2000). FRAXE mutation in a mentally retarded subject and in his phenotypically normal twin brother. *Eur. J. Hum. Genet.* 8, 157–162. doi: 10.1038/sj.ejhg.5200425

Mondal, K., Ramachandran, D., Patel, V. C., Hagen, K. R., Bose, P., Cutler, D. J., et al. (2012). Excess variants in AFF2 detected by massively parallel sequencing of males with autism spectrum disorder. *Hum. Mol. Genet.* 21, 4356–4364. doi: 10.1093/hmg/dds267

Moore, S. J., Strain, L., Cole, G. F., Miedzybrodzka, Z., Kelly, K. F., and Dean, J. C. (1999). Fragile X syndrome with FMR1 and FMR2 deletion. *J. Med. Genet.* 36, 565–566.

Mulley, J. C., Yu, S., Loesch, D. Z., Hay, D. A., Donnelly, A., Gedeon, A. K., et al. (1995). FRAXE and mental retardation. *J. Med. Genet.* 32, 162–169. doi: 10.1136/jmg.32.3.162

No Author (1985). Proposal for classification of epilepsies and epileptic syndromes. Commission on classification and terminology of the international league against Epilepsy. *Epilepsia* 26, 268–278. doi: 10.1111/j.1528-1157.1985.tb05417.x

No Author (1989). Proposal for revised classification of epilepsies and epileptic syndromes. Commission on classification and terminology of the international league against Epilepsy. *Epilepsia* 30, 389–399. doi: 10.1111/j.1528-1157.1989.tb05316.x

Scheffer, I. E., Berkovic, S., Capovilla, G., Connolly, M. B., French, J., Guilhoto, L., et al. (2017). ILAE classification of the epilepsies: position paper of the ILAE Commission for classification and terminology. *Epilepsia* 58, 512–521. doi: 10.1111/epi.13709

Shi, Y. W., Zhang, Q., Cai, K., Poliquin, S., Shen, W., Winters, N., et al. (2019). Synaptic clustering differences due to different GABRB3 mutations cause variable epilepsy syndromes. *Brain* 142, 3028–3044. doi: 10.1093/brain/awz250

Strande, N. T., Riggs, E. R., Buchanan, A. H., Ceyhan-Birsoy, O., DiStefano, M., Dwight, S. S., et al. (2017). Evaluating the clinical validity of gene-disease associations: an evidence-based framework developed by the clinical genome resource. *Am. J. Hum. Genet.* 100, 895–906. doi: 10.1016/j.ajhg.2017.04.015

Tang, B., Li, B., Gao, L. D., He, N., Liu, X. R., Long, Y. S., et al. (2020). Optimization of in silico tools for predicting genetic variants: individualizing for genes with molecular sub-regional stratification. *Brief Bioinform.* 21, 1776–1786. doi: 10.1093/bib/bbz115

Wang, J., Lin, Z. J., Liu, L., Xu, H. Q., Shi, Y. W., Yi, Y. H., et al. (2017). Epilepsy-associated genes. *Seizure* 44, 11–20. doi: 10.1016/j.seizure.2016.11.030

Wang, J. Y., Zhou, P., Wang, J., Tang, B., Su, T., Liu, X. R., et al. (2018). ARHGEF9 mutations in epileptic encephalopathy/intellectual disability: toward understanding the mechanism underlying phenotypic variation. *Neurogenetics* 19, 9–16. doi: 10.1007/s10048-017-0528-2

Wolff, D. J., Gustashaw, K. M., Zurcher, V., Ko, L., White, W., Weiss, L., et al. (1997). Deletions in Xq26.3-q27.3 including FMR1 result in a severe phenotype in a male and variable phenotypes in females depending upon the X inactivation pattern. *Hum. Genet.* 100, 256–261. doi: 10.1007/s004390050501

Yuen, R. K. C., Merico, D., Bookman, M., Howe, J. L., Thiruvahindrapuram, B., Patel, R. V., et al. (2017). Whole genome sequencing resource identifies 18 new candidate genes for autism spectrum disorder. *Nat. Neurosci.* 20, 602–611. doi: 10.1038/nn.4524

Zhang, Y., Kong, W., Gao, Y., Liu, X., Gao, K., Xie, H., et al. (2015). Gene mutation analysis in 253 chinese children with unexplained epilepsy and intellectual/developmental disabilities. *PLoS One* 10:e0141782. doi: 10.1371/journal.pone.0141782

Conflict of Interest: The authors declare that the research was conducted in the absence of any commercial or financial relationships that could be construed as a potential conflict of interest.

frontiers | Frontiers in Molecular Neuroscience

ORIGINAL RESEARCH
published: 29 April 2022
doi: 10.3389/fnmol.2022.828891

Dysfunction of the Hippocampal-Lateral Septal Circuit Impairs Risk Assessment in Epileptic Mice

Yi Cao[1,2†], Chongyang Sun[1†], Jianyu Huang[1,3], Peng Sun[1,4], Lulu Wang[1], Shuyu He[5], Jianxiang Liao[6], Zhonghua Lu[1], Yi Lu[1] and Cheng Zhong[1]**

[1] Guangdong Provincial Key Laboratory of Brain Connectome and Behavior, CAS Key Laboratory of Brain Connectome and Manipulation, The Brain Cognition and Brain Disease Institute, Shenzhen Institute of Advanced Technology, Chinese Academy of Sciences, Shenzhen-Hong Kong Institute of Brain Science-Shenzhen Fundamental Research Institutions, Shenzhen, China, [2] Division of Life Sciences and Medicine, School of Life Sciences, University of Science and Technology of China, Hefei, China, [3] Key Laboratory of Industrial Microbiology, College of Biotechnology, Tianjin University of Science and Technology, Tianjin, China, [4] College of Electronic and Information Engineering, Hebei University, Baoding, China, [5] Shenzhen Children's Hospital, China Medical University, Shenzhen, China, [6] Epilepsy Center, Shenzhen Children's Hospital, Shenzhen, China

OPEN ACCESS

Edited by:
Yuwu Jiang,
Peking University First Hospital, China

Reviewed by:
Lucas Alberto Mongiat,
Bariloche Atomic Centre (CNEA), Argentina
Ling-Qiang Zhu,
Huazhong University of Science and Technology, China

***Correspondence:**
Cheng Zhong
cheng.zhong@siat.ac.cn
Yi Lu
luyi@siat.ac.cn

[†] These authors have contributed equally to this work

Specialty section:
This article was submitted to Molecular Signalling and Pathways, a section of the journal Frontiers in Molecular Neuroscience

Received: 04 December 2021
Accepted: 29 March 2022
Published: 29 April 2022

Citation:
Cao Y, Sun C, Huang J, Sun P, Wang L, He S, Liao J, Lu Z, Lu Y and Zhong C (2022) Dysfunction of the Hippocampal-Lateral Septal Circuit Impairs Risk Assessment in Epileptic Mice.
Front. Mol. Neurosci. 15:828891.
doi: 10.3389/fnmol.2022.828891

Temporal lobe epilepsy, a chronic disease of the brain characterized by degeneration of the hippocampus, has impaired risk assessment. Risk assessment is vital for survival in complex environments with potential threats. However, the underlying mechanisms remain largely unknown. The intricate balance of gene regulation and expression across different brain regions is related to the structure and function of specific neuron subtypes. In particular, excitation/inhibition imbalance caused by hyperexcitability of glutamatergic neurons and/or dysfunction of GABAergic neurons, have been implicated in epilepsy. First, we estimated the risk assessment (RA) by evaluating the behavior of mice in the center of the elevated plus maze, and found that the kainic acid-induced temporal lobe epilepsy mice were specifically impaired their RA. This experiment evaluated approach-RA, with a forthcoming approach to the open arm, and avoid-RA, with forthcoming avoidance of the open arm. Next, results from free-moving electrophysiological recordings showed that in the hippocampus, ∼7% of putative glutamatergic neurons and ∼15% of putative GABAergic neurons were preferentially responsive to either approach-risk assessment or avoid-risk assessment, respectively. In addition, ∼12% and ∼8% of dorsal lateral septum GABAergic neurons were preferentially responsive to approach-risk assessment and avoid-risk assessment, respectively. Notably, during the impaired approach-risk assessment, the favorably activated dorsal dentate gyrus and CA3 glutamatergic neurons increased (∼9%) and dorsal dentate gyrus and CA3 GABAergic neurons decreased (∼7%) in the temporal lobe epilepsy mice. Then, we used RNA sequencing and immunohistochemical staining to investigate which subtype of GABAergic neuron loss may contribute to excitation/inhibition imbalance. The results show that temporal lobe epilepsy mice exhibit significant neuronal loss and reorganization of neural networks. In particular, the dorsal dentate gyrus and CA3 somatostatin-positive neurons and dorsal lateral septum

cholecystokinin-positive neurons are selectively vulnerable to damage after temporal lobe epilepsy. Optogenetic activation of the hippocampal glutamatergic neurons or chemogenetic inhibition of the hippocampal somatostatin neurons directly disrupts RA, suggesting that an excitation/inhibition imbalance in the dHPC dorsal lateral septum circuit results in the impairment of RA behavior. Taken together, this study provides insight into epilepsy and its comorbidity at different levels, including molecular, cell, neural circuit, and behavior, which are expected to decrease injury and premature mortality in patients with epilepsy.

Keywords: temporal lobe epilepsy, risk assessment, forthcoming approach, hippocampus, E/I imbalance, lateral septum

INTRODUCTION

Epilepsy is a common brain disorder with repeated seizures and is often comorbid with other neuropsychiatric disorders (Moshe et al., 2015; Kanner, 2016; Hermann et al., 2021). Previous research has shown that epileptic patients have a higher risk of premature mortality due to external causes, including falls and drowning (Fazel et al., 2013). Risk assessment (RA) plays a key role in survival, and its impairment may lead to injury or even death (Gross and Canteras, 2012; McNaughton and Corr, 2018). When there is ambiguity and conflict between the internal approach and avoidance tendencies, RA is likely to arise primarily. Previous studies have suggested that individuals with epilepsy have RA impairment, but the results are controversial (Kubova et al., 2004; O'Loughlin et al., 2014). However, there is little knowledge of the underlying neural mechanisms involved in RA dysfunction in epileptic individuals.

Temporal lobe epilepsy (TLE) is one of the most common and refractory epilepsies in adults and represents pathological alterations in the hippocampal structures (Tellez-Zenteno et al., 2005; Curia et al., 2008; Ren and Curia, 2021). The hippocampus (HPC) performs a broad range of brain functions, especially contextual cognitive behaviors. To obtain information about a novel environment with potential threats and to support the following choice between approach and avoidance, RA is necessary (Gross and Canteras, 2012; McNaughton and Corr, 2018). In a conflict context, for example, rodents in the elevated plus maze (EPM), RA behaviors were observed as crouch-sniff and stretch-attend in the center zone. RA behavior was considered as both a cognitive and emotional process. It is generally considered that the ventral hippocampal neurons participate in the modulation of anxiety behaviors, while the dorsal hippocampal neurons play an important role in coding spatial information (Fanselow and Dong, 2010). Recent studies have revealed that the dorsal hippocampus also regulates mild anxiogenic contextual exploration (Dong et al., 2021) and ambiguous threat context (Besnard et al., 2020). As the HPC and its downstream region represent diverging patterns of coding of RA information, which correlated with subsequent behaviors, including approach and avoidance of the open arm (Jacinto et al., 2016), it should be confirmed whether the abnormal hippocampal network contributes to the impairment of RA in TLE.

In TLE, the HPC of both human patients and animal models showed obvious neuronal loss and network reorganization. Importantly, this alteration shows high neuronal heterogeneity (Lothman et al., 1995; Mangan et al., 1995) which often induces an excitation and inhibition (E/I) imbalance. The E/I imbalance in TLE not only contributes to seizures, but is also related to other brain dysfunctions, such as unconsciousness (Motelow et al., 2015). During seizures, the E/I imbalance, typically as the hyperexcitability of glutamatergic neurons and/or the reduced inhibition of GABAergic neurons, causes epileptic waveforms and propagates from the hippocampus downstream (Krook-Magnuson et al., 2013; Levesque et al., 2016; Lu et al., 2016). Furthermore, selective loss of dentate hilar somatostatin-positive (SOM+) neurons was observed, whereas loss of cholecystokinin-positive (CCK+) or parvalbumin-positive (PV+) neurons was not significant in TLE (Sun et al., 2007; Benini et al., 2011). Therefore, we hypothesized that profound loss and dysfunction of hippocampal GABAergic neurons in TLE may result in an imbalance of E/I and contribute to impaired RA behavior.

Both hippocampal dentate gyrus /hilus (DGH) GABAergic neurons and glutamatergic neurons have been found to play different roles in EPM (Botterill et al., 2021; Wang et al., 2021). Ventral hippocampal vasoactive intestinal polypeptide positive (VIP+) GABAergic neurons can distinguish the open and closed arms in EPM more strongly than PV+ or SOM+ interneurons (Lee et al., 2019). However, the subtype of GABAergic neurons that preferentially respond to the central zone remains unknown. Many hippocampal downstream regions have been suggested to be involved in RA, including the prefrontal cortex, amygdala, and lateral septum (LS) (Xia and Kheirbek, 2020). The LS, in which more than 95% of neurons are GABAergic interneurons, is a vital relay between the hippocampus and other regions and has been implicated in a wide variety of functions (Wirtshafter and Wilson, 2021), including emotional, motivational, and spatial behavior, as well as RA behavior (Motta et al., 2017; McNaughton and Corr, 2018). Dysfunction of the hippocampal-lateral section (HPC-LS) is suggested to be involved in epilepsy (Motelow et al., 2015). Thus, an investigation into the cellular

Abbreviations: TLE, temporal lobe epilepsy; WT, wild type; RA, risk assessment; dHPC, dorsal hippocampus; HPC, hippocampus; EPM, elevated plus maze; E/I, excitation and inhibition; SOM+, somatostatin-positive; CCK+, cholecystokinin-positive; PV+, parvalbumin-positive; VIP+, vasoactive intestinal polypeptide positive; LS, lateral septum; HPC-LS, hippocampal-lateral section; dDG/CA3, dorsal dentate gyrus and CA3; ns, no significant; N.R., no response.

mechanism of E/I imbalance in HPC degeneration in impaired RA is necessary.

Herein, we show that kainic acid (KA)-induced epilepsy preferentially has an impairment of RA. Through extracellular electrophysiological recordings, we found that hippocampal dorsal dentate gyrus and CA3 (dDG/CA3) neurons participate in response to RA, in which a subpopulation of them is specifically activated by approach-RA and another subpopulation is specifically activated by avoid-RA. Epileptic mice show E/I imbalance of dDG/CA3 in the approach-RA, where the approach-RA specifically activated glutamatergic neurons increased, whereas the approach-RA-specifically activated GABAergic neurons decreased. In addition, in the LS, the approach-RA specifically activated GABAergic neurons decreased. Moreover, our results imply that the decreased dDG/CA3 GABAergic neurons are SOM+ neurons, while the decreased LS GABAergic neurons are CCK+ neurons. Taken together, the epilepsy-induced impairment of RA due to dysfunction of the dDG/CA3-LS circuit, which shortens the approach-RA duration. Meanwhile, when they approached the threat with inadequate RA, they were more likely to be injured.

MATERIALS AND METHODS

Animals

Adult male C57/BL6J mice (18–22 g; 6–8 weeks old) were purchased from the Guangdong Medical Laboratory Animal Center (Guangdong Province, China). Adult Sst-IRES-Cre knock-in mice (Jackson Laboratory, repository number 013044), expressing Cre recombinase in somatostatin-expressing neurons, and CCK-IRES-Cre knock-in mice (Jackson Laboratory, repository number 012706) expressing Cre recombinase in cholecystokinin positive neurons, were bred, identified, and provided by the Shenzhen Institute of Advanced Technology using specific criteria (18–22 g; 6–8 weeks old). Animals were housed under the following laboratory conditions: ambient temperature, 24 ± 1°C; humidity, 50–60%; 12-h light/dark cycle beginning at 8 a.m.; food and water *ad libitum*. All experiments were performed in accordance with protocols approved by the Ethics Committee for Animal Research, Shenzhen Institute of Advanced Technology, Chinese Academy of Sciences (SIAT-IACUC-20210617-NS-NTPZX-ZC-A0893-03).

Fabrication of Electrode Arrays

Microwire electrode arrays, each containing 10 stereotrodes (20 channels), were fabricated from 17.78 μm diameter formvar-coated nickel-chromium wires (California Fine Wire Company, Grover Beach, CA, United States). Each stereotrode was threaded through a silica tube (TSP100170, Polymicro Technologies, Phoenix, AZ, United States). Each stereotrode was wrapped around two adjacent pins of a standard electrode connector (A79026, Omnetics connector, Minneapolis, MN, United States). Silver microwires (*OD* = 200 μm, 99.95% pure) were then soldered to four pins on the outer side of the connector as ground and reference, respectively. Acrylic resin was used for the encapsulation. Electrode tips were plated with platinum to reduce impedance to 300–800 kΩ (at 1 kHz in PBS) before use. The electrode arrays were fabricated as previously described by Sun et al. (2022).

Surgery

Mice (8-week-old, male) were treated with atropine (0.2 mg/kg) 15 min before the experiment to overcome breathing problems. General anesthesia was achieved by intraperitoneal administration of urethane (1.5 g/kg). After the animal's head was fixed in a standard stereotaxic frame, the cranium was exposed through a small midline scalp incision. A small craniotomy was performed with a high-speed dental drill, and the tips of the 34-gage needle (Hamilton) were directed toward the brain at the following stereotaxic coordinates: at anteroposterior (AP) −1.8 mm, mediolateral (ML) −2.0 mm, and dorsoventral −1.8 (DV) mm and then 650 nL (0.3 mg/mL in 0.1M) of KA solution was injected into the dorsal hippocampus using a micropump. After 8–12 weeks of injection, the KA-induced chronic temporal lobe epilepsy model was established as previously described (Krook-Magnuson et al., 2013; Moura et al., 2020).

For chemogenetic testing, the virus was carefully drawn up into a 10 μL Hamilton syringe with 34-gage needle by automatically raising the plunger. The virus [200 nL rAAV-EF1α-DIO-hM4D(Gi)-mCherry] was injected into the dCA3 area of the brain (AP, −2.00 mm; ML, ±1.50 mm; DV, −2.00 mm) of SOM-cre mice at a rate of 100 nL min^{-1}, followed by a 9 min pause. For optogenetic testing, the virus (300 nL AAV-CaMKII-ChR2-mCherry) was injected into C57/BL6J mice. After 3 weeks of viral proliferation, an optical fiber (diameter, 200 μm) was inserted into the dCA3 area of the brain for optical stimulation. After the procedure, all animals were allowed to recover for a week in their home cages with free access to food and water.

For electrode implantation, a neural electrode was directed toward the brain at the following stereotaxic coordinates after the craniotomy: the tips of the stereotrodes at AP +0.74 mm, ML −0.75 mm, and DV −2.80 mm in a 10° angle for dLS recording and at AP −2.00 mm, ML −1.90 mm, and DV −2.00 mm for dCA3 recording. After the procedure, all animals were allowed to recover for a week in their home cages.

Elevated-Plus Maze Test

The elevated plus maze (EPM) test was performed at least one week after the mice recovered from the implantation surgery. The EPM consisted of 2 opposing closed arms (sidewalls, 30 × 5 × 25 cm) and 2 opposing open arms (open platforms, 30 × 5 cm) connected by a central stage (5 × 5 cm). The EPM was set 1 m from the floor. Before each trial, all arms and center stages were cleaned with 20% alcohol. The mice were placed individually on the central platform and allowed to explore for 10 min. For the chemogenetic experiments, the designer receptor ligand clozapine-N-oxide (CNO) was dissolved in 100% saline at a concentration of 0.10 mg/mL and administered intraperitoneally at a dose of 1 mg/kg 30 min before the commencement of behavioral testing. For the optogenetic experiments, blue light at a wavelength of 473 nm was delivered

at a power of 10 mW in cycling stimulation mode (5 ms pulses at 20 Hz, 5 min off, 5 min on) *via* an optical fiber.

Electrophysiological Recording

Electrophysiological signals were recorded using a 64-channel neural acquisition processor (Plexon, Dallas, TX, United States). Neural electrophysiological data acquired in this study were sampled at 40 kHz and bandpass filtered in the range of 300–5000 Hz. Synchronized mouse behavior was recorded using a digital video camera (Plexon, Dallas, TX, United States).

Data Analysis

Data analyses were performed using Offline Sorter (Offline sorter application version 4.6.0), NeuroExplorer (NeuroExplorer version 5.310), and custom software written in MATLAB. Multi-unit recordings were high-pass filtered (300 Hz) with a Bessel filter for the detection of spikes. Individual spikes were detected by setting a threshold at $-5 \times$ standard deviations (SD), and spike waveforms were measured within a 1400 μs time window beginning 300 μs before threshold crossing. Single units were isolated using the first three principal components. To characterize putative GABAergic and glutaminergic neurons, two features of the extracellular waveform, the peak-to-peak time, and the half-width of the spikes, were calculated. Neurons with narrow peaks were regarded as putative GABAergic neurons, whereas neurons with wide peaks were regarded as putative glutamatergic neurons (Courtin et al., 2014; Lu et al., 2016). For the peri-event raster plot, RA-induced neural activity was calculated from 9 s segments of continuous neural recordings (from 6 s before to 3 s after RA onset) using a *z*-score transformation (bin = 0.5 s). *Z*-score values were calculated by subtracting the average baseline firing rate over the 6 s preceding RA onset and dividing by the baseline SD.

Transcriptomic Sequencing

All animals recruited in this cohort arrived at our facility at the same time and completed the experimental procedures, including KA injection and sample collection, on the same day (**Supplementary Table 1**). Both wild type (WT) and TLE mice were euthanized in the same time window (3–4 p.m., 20-week-old, male) with a lethal dose of pentobarbital. Brains were extracted from the skull, and the hippocampus and lateral septum tissues were dissected, collected on ice, and frozen quickly. Total RNA from the hippocampus and lateral septum of the WT and TLE mice was utilized for library construction for sequencing by using the Illumina whole transcriptome RNA sequencer. All experimental protocols and transcriptome analyses were performed by trained technicians (**Supplementary Figure 3**).

All sequencing adapters were removed by running the Cutadapt. Quality control on FastQ files was checked by the FastQC application. All reads were aligned to UCSC genome browser (Mus musculus NCBIM37) by using HISAT2. We used HTSeq statistics to compare read count values for each gene as the original expression of the gene. Read counts are positively correlated with the true level of gene expression, as well as the length and sequencing depth of the gene. To make the level of gene expression comparable between different genes and samples, we used fragments per kilo bases per million fragments (FPKM) to standardize the expression (Normalization). We used DESeq to analyze the differences in gene expression, and the screening of the differentially expressed gene conditions was: expression difference multiples $|\log2\text{FoldChange}| > 1$, the significance P-value < 0.05. The R language ggplots2 software package was used to map the volcano of the differentially expressed genes. The volcanic map shows the distribution of genes, multiple gene expression differences, and significant results; under normal circumstances, the difference in gene distribution should be roughly symmetrical, the left side is Case compared to Control down gene, and the right side is compared to Case Control up gene. Genes that had no reads across all samples were discarded by the DESeq analysis.

Histology

Briefly, the mice were perfused transcardially with 0.1 mol/L phosphate buffered saline (PBS) followed by 4% paraformaldehyde in 0.1 mol/L PBS, and the brains were removed and fixed at 4°C overnight, transferred to 30% sucrose in 0.1 M PBS 3 days, and then stored at −80°C. For immunostaining, 35 μm sections were cut using a cryostat (CM1950, Leica, Wetzlar, Germany). Subsequently, neurons were incubated overnight at 4°C with primary antibodies against somatostatin (Millipore, ab5494, 1:100, Darmstadt, Germany), neurotensin (Abcam, ab233107, 1:250, Cambridge, England), VIP (Abcam, ab272726, 1:250, Cambridge, England), and CCK (ImmunoStar, 20078, 1:250, Hudson, WI, United States) diluted in PBS containing 10% normal goat serum based on the antibody used. After extensive washing with PBS, secondary antibodies were added for 1 h at room temperature. Nuclei were counterstained with DAPI. Subsequently, the coverslips were washed with PBS and mounted onto glass slides with Southern Biotech fluorescence mounting medium.

Microscopy and Quantitative Image Analysis

Fluorescence images were obtained using an Olympus VS120 microscope with UPLSAPO 10X and UPLSAPO 20X. Images containing 4–5 sections were used for the analysis of fluorescence intensities, counting of neurons, or the number of fluorescent spots in the case of *in situ* proximity ligation assay (PLA). The laser intensities and detector gain were adjusted such that all signals were below saturation. Images were analyzed using the Olympus CellSens Dimension Desktop 1.18.

Statistics

Data were analyzed using two-tailed two-sample *t*-tests with the Origin software. All data are presented as the mean ± SD. Significance levels are indicated as follows: $^{*}\ p < 0.05$, $^{**}\ p < 0.01$, and $^{***}\ p < 0.001$. The statistical details are shown in the respective figure legends.

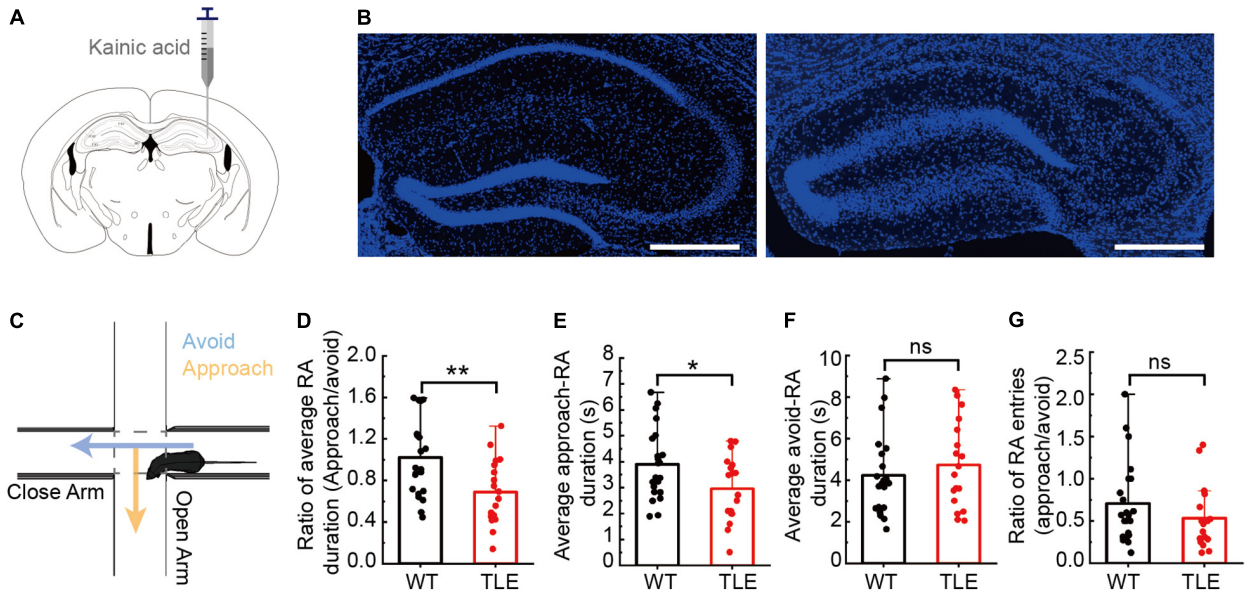

FIGURE 1 | Kainic acid-induced TLE mice showed impairments in the hippocampal cytoarchitecture and RA behavior. **(A)** Schematic diagram of intrahippocampal kainic acid injection in C57/BL6J mice. **(B)** Comparison of hippocampal subfields between WT and TLE mice. Scale bar, 500 μm. **(C)** Schematic diagram of elevated plus maze test and a typical RA. **(D)** Ratio between average of approach-RA duration and average of avoid-RA duration. **(E)** Average of approach-RA duration. **(F)** Average of avoid-RA duration. **(G)** Ratio between approach-RA and avoid-RA entries (WT, $n = 22$; TLE, $n = 18$; ns is no significant difference; error bars represent s.d; $^{*}p < 0.05$; $^{**}p < 0.01$, t test).

RESULTS

Heightened Approach-Risk Assessment Behavior of Kainic Acid-Induced Temporal Lobe Epilepsy Mice in Elevated Plus Maze

To obtain a stable mouse model of chronic temporal lobe epilepsy, we used an intrahippocampal kainic acid injection strategy (**Figure 1A**). In the KA-injected group, the CA1 sector exhibited severe neuronal loss, whereas, in the control group, layers of the CA1 and CA3 sectors and the dentate gyrus appeared intact (**Figure 1B** and **Supplementary Figure 2**, $p < 0.0001$). Stable hippocampal sclerosis in TLE mice demonstrated the efficiency of the KA-induced TLE mouse model. To investigate whether the impairment of the hippocampus cast a shadow on the RA, we used EPM and focused on a typical RA behavior with a forthcoming approach or avoidance (**Figure 1C**). Here, we defined approach-RA as that with a forthcoming approach to the open arm, and avoid-RA that with a forthcoming avoidance of the open arm. Compared with WT mice, the TLE mice showed a significant decrease in approach-RA duration (WT: 3.90 ± 1.37, TLE: 2.96 ± 1.26, $p = 0.0307$, **Figure 1E**) but not avoid-RA duration (WT: 4.23 ± 1.93, TLE: 4.74 ± 2.08, $p = 0.4341$, **Figure 1F**). Moreover, the ratio between approach-RA duration and avoid-RA duration even altered more significantly (WT: 1.02 ± 0.38, TLE: 0.69 ± 0.31, $p = 0.0051$, **Figure 1D**). The ratio between entries of approach-RA and avoid-RA did not significantly differ (WT: 0.64 ± 0.59, TLE: 0.71 ± 0.49, $p = 0.7042$, **Figure 1G**). These results indicated that the TLE mice spent less time in approach-RA and decreased latency from the close arm to the open arm, which led to more vulnerable animals. Taken together, intrahippocampal KA injection-induced TLE mice exhibited neuronal degeneration, DG dispersion, and reorganization of the hippocampal structure, and significantly destroyed RA, facing potential threat.

Excitation and Inhibition Imbalance of Dorsal Dentate Gyrus and CA3-dLS in Approach-Risk Assessment

Considered patterns of hippocampal oscillation predicting approach-RA and avoid-RA has been reported (Jacinto et al., 2016), to confirm whether the hippocampal neurons can also predict approach-RA and avoid-RA, we recorded and analyzed the electrophysiological signals in dDG/CA3 and dLS during EPM. We found that the amounts of glutamatergic and GABAergic neurons were activated by RA (**Figure 2A**), most of which were positively responsive to both approach-RA and avoid-RA (**Figure 2C**). However, there are subpopulations of RA-activated neurons that preferentially respond to either approach-RA or avoid-RA (**Figures 2D,E**). In this study, we found that some of RA-inhibited neurons exhibited a phasic increase of firing rate before RA (in close arm, duration, ∼2–3 s) and subsequently a decrease of firing rate during RA (in center zone) (**Figure 2B** and **Supplementary Figure 1**). Thus, we considered the RA-inhibited neurons as another behavior-related neurons, and did not discuss in current study. The selectively responsive neurons may contribute to the changed pattern of theta oscillations to predict the forthcoming approach or avoid.

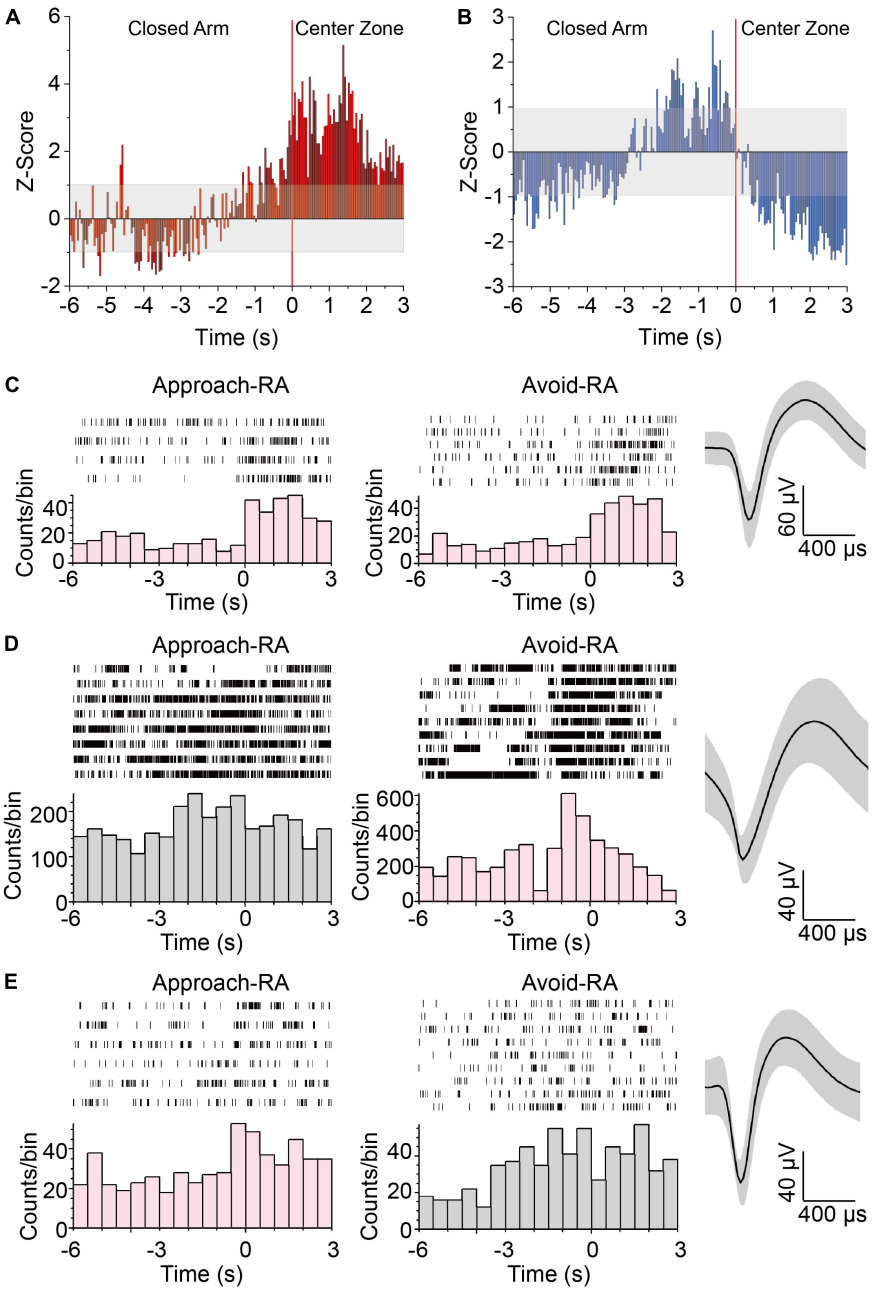

FIGURE 2 | Neurons in HPC responding to approach-RA or avoid-RA selectively. **(A,B)** *Z*-scored peri-RA time histograms aligned with onset of RA. **(A)** $n = 57$ cells from 5 mice. **(B)** $n = 60$ cells from 5 mice. **(C)** Representative raster plots and waveforms of dDG/CA3 neurons positively responsive to RA. **(D)** Representative raster plots and waveforms of dDG/CA3 neurons positively responsive to avoid RA. **(E)** Representative raster plots and waveforms of dDG/CA3 neurons positively responsive to approach RA. Each row in the raster represents a single trial of RA behavior. Averaged spike waveforms of the representative neuron were provided at the left panels. Bin = 0.5 s.

To elucidate the role of responsive neurons in the impaired RA of TLE mice, we examined all neurons recorded from unbiased populations of dDG/CA3 or dLS in WT and TLE mice. During RA, the proportion of inhibited dDG/CA3 putative glutamatergic neurons showed no obvious change between TLE (41%) and WT (42%) mice, whereas the proportion of excited dDG/CA3 putative glutamatergic neurons decreased by 16% in TLE mice (WT, 36%; TLE, 20%) (**Figures 3A,B**). The proportion of excited putative GABAergic neurons in the HPC was 22% lower in the TLE group than the WT group (WT, 65%; TLE, 43%) (**Figures 3C,D**), and RA was found to inhibit putative GABAergic neurons in the HPC by 12% (WT, 15%; TLE, 27%). Therefore, both types of RA-excited HPC neurons were decreased in TLE mice, which may play a role in the impaired RA of epileptic mice.

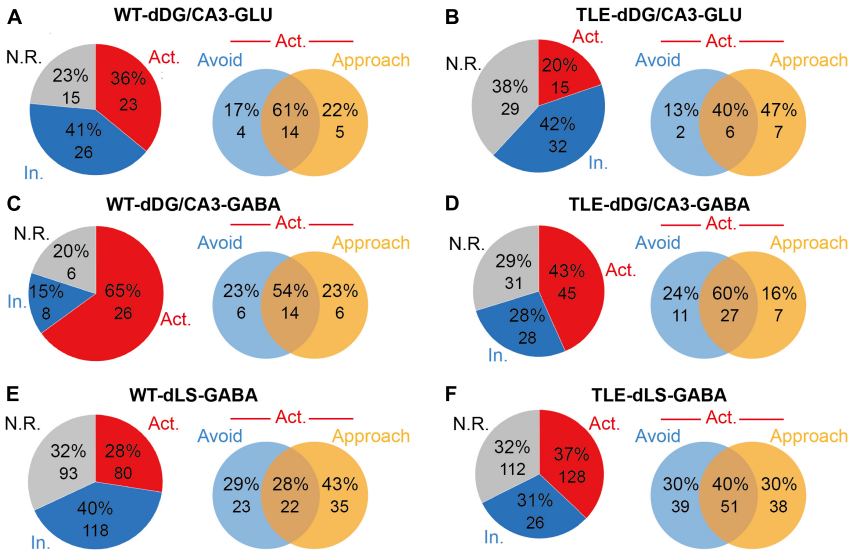

FIGURE 3 | Electrophysiological analysis showed E/I imbalance in TLE mice. **(A)** Neuronal response types of putative glutamatergic neurons to RA in dDG/CA3 of WT mice [Red, excited (Act.); blue, inhibited (In.); gray, no response (N.R.). *n* = 64 cells from 5 mice]. Venn diagram shows the distribution of approached RA-excited only, avoid RA-excited only or dual-excited putative glutamatergic neurons in dDG/CA3 of WT mice at RA. **(B)** Neuronal response types of putative glutamatergic neurons to RA in dDG/CA3 of TLE mice (Red, excited; blue, inhibited; gray, no response; *n* = 76 cells from 5 mice). Venn diagram shows the distribution of approached RA-excited only, avoid RA-excited only or dual-excited putative glutamatergic neurons in dDG/CA3 of TLE mice at RA. **(C)** Neuronal response types of putative GABAergic neurons to RA in dDG/CA3 of WT mice (Red, excited; blue, inhibited; gray, no response; *n* = 40 cells from 17 mice). Venn diagram shows the distribution of approached RA-excited only, avoid RA-excited only or dual-excited putative glutamatergic neurons in dDG/CA3 of WT mice at RA. **(D)** Neuronal response types of putative GABAergic neurons to RA in dDG/CA3 of TLE mice (Red, excited; blue, inhibited; gray, no response; *n* = 104 cells from 15 mice). Venn diagram shows the distribution of approached RA-excited only, avoid RA-excited only or dual-excited putative glutamatergic neurons in dDG/CA3 of TLE mice at RA. **(E)** Neuronal response types of putative GABAergic neurons to RA in dDG/CA3 of WT mice (Red, excited; blue, inhibited; gray, no response; *n* = 291 cells from mice). Venn diagram shows the distribution of approached RA-excited only, avoid RA-excited only or dual-excited putative glutamatergic neurons in dLS of WT mice at RA. **(F)** Neuronal response types of putative GABAergic neurons to RA in dDG/CA3 of TLE mice (Red, excited; blue, inhibited; gray, no response; *n* = 346 cells from mice). Venn diagram shows the distribution of approached RA-excited only, avoid RA-excited only or dual-excited putative glutamatergic neurons in dLS of TLE mice at RA.

Of note, when compared with the avoid-RA selectively responsive neurons, the approach-RA selectively excited dDG/CA3 putative glutamatergic neurons increased (WT, 22%; TLE, 47%), for which the percentage was defined as either approach-RA selectively excited neurons divided by all RA-excited neurons, or avoid-RA selectively excited neurons divided by all excited neurons (**Figures 3A,B**). On the other hand, the proportion of approach-RA selectively excited dDG/CA3 putative GABAergic neurons showed a slight unexpected decrease (WT, 23%; TLE, 16%) while the proportion for avoid-RA remained unchanged (**Figures 3C,D**). Taken together, in the TLE-impaired approach-RA, the E/I balance changed markedly, and the approach-RA preferentially activated glutamatergic neurons increased, whereas the approach-RA preferentially activated GABAergic neurons decreased.

Similarly, the proportion of RA-excited putative GABAergic neurons in the LS was slightly increased (WT, 28%; TLE, 37%), while the approach-RA selectively excited putative GABAergic neurons in the LS (WT, 43%; TLE, 30%) decreased more than those for avoid-RA (WT, 29%; TLE, 30%) (**Figures 3E,F**). Taken together, these findings suggest that in TLE mice, approach-RA selectively activated neurons were changed more significantly in both the dDG/CA3 and the dLS. In particular, approach-RA selectively responsive neurons displayed an E/I imbalance in the dDG/CA3. Therefore, the RA-recruited neuronal network in the dDG/CA3-dLS areas of the brain may be vulnerable to epilepsy due to degeneration and reorganization.

Translational Signatures Imply Apoptosis, Impairment of Neurogenesis, and Migration

To investigate the causes of impaired dysfunction of hippocampus and lateral septum neurons at the molecular level, we used RNA-seq technology to characterize the transcriptome of dHPC and LS of TLE mice (**Supplementary Table 1**). The normalized expression analysis of all samples from both the TLE and WT groups was used to visualize the differences in expression of all detected genes in both dHPC and LS. As expected, a large number of genes were expressed at higher levels in the dHPCs of TLE mice (**Figure 4A**). Similarly, we found differentially expressed genes in the LS (**Figure 4B**). To further explore the link between the impaired approach-RA and the change in transcription in TLE mice, we examined gene expression for Gene Ontology terms. Most of the genes examined showed similar expression between TLE and WT mice. However, several genes were upregulated or downregulated in neurogenesis, migration,

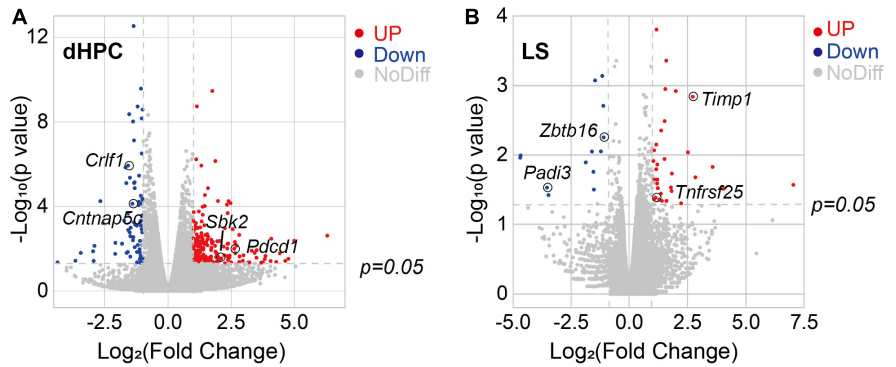

FIGURE 4 | Kainic acid-induced TLE mice showed transcriptome alterations in the hippocampus and lateral septum. **(A)** Volcano plot of relative RNA expression in DG/CA3 from TLE mice as compared to WT mice. **(B)** Volcano plot of relative RNA expression in dLS from TLE mice as compared to WT mice [Genes in upper left and right quadrants are significantly differentially expressed. Red dots, up-regulation (dHPC, 65 genes; LS, 34 genes), blue dots, down-regulation (dHPC, 224 genes; LS, 11 genes). WT, $n = 4$ mice; TLE, $n = 6$ mice. $p < 0.05$].

TABLE 1 | Representative dysregulated genes in HPC and LS of TLE mice.

Brain region	ID	Chromosome	Name	Fold change	Description
HPC	ENSMUSG00000009900	11	Wnt3a	–, 0	wingless-type MMTV integration site family, member 3A
	ENSMUSG00000054409	15	Crlf1	–, 0.336	cytokine receptor-like factor 1
	ENSMUSG00000041911	2	Dlx1	–, 0.494	distal-less homeobox 1
	ENSMUSG00000021676	13	Iqgap2	–, 0.313	IQ motif containing GTPase activating protein 2
	ENSMUSG00000038048	17	Cntnap5c	–, 0.377	contactin associated protein-like 5C
	ENSMUSG00000069310	13	H3c3	+, infinite	H3 clustered histone 3
	ENSMUSG00000043557	17	Mdga1	–,0.488	MAM domain containing glycosylphosphatidylinositol anchor 1
	ENSMUSG00000026285	1	Pdcd1	+, 6.157	programmed cell death 1
	ENSMUSG00000030433	7	Sbk2	+, 5.395	SH3-binding domain kinase family, member 2
LS	ENSMUSG00000026343	1	Gpr39	+, infinite	G protein–coupled receptor 39
	ENSMUSG00000024793	4	Tnfrsf25	+, 2.191	tumor necrosis factor receptor superfamily, member 25
	ENSMUSG00000066687	9	Zbtb16	–, 0.464	zinc finger and BTB domain containing 16
	ENSMUSG00000001131	X	Timp1	+, 6.603	tissue inhibitor of metalloproteinase 1
	ENSMUSG00000025328	4	Padi3	–, 0.087	peptidyl arginine deiminase, type III

and apoptosis in dHPC, as well as migration and apoptosis in LS (**Table 1**).

For example, Wnt3a acts through canonical Wnt signaling to drive embryonic development, stem cell differentiation, and promote neural circuit formation, as well as neurogenesis in the hippocampus (Rash et al., 2013; Harada et al., 2019). Here, Wnt3a expression was not detected in the TLE hippocampus, suggesting that neurogenesis was disrupted. In addition, Crlf1 is also considered to play a crucial role during neuronal development (Johnson et al., 2010) and Dlx1 was found to participate in the differentiation of interneurons (He et al., 2001; Cobos et al., 2006), such as bipolar cells in the developing retina; thus, their downregulation may be related to neurogenesis dysfunction, especially E/I imbalance. Moreover, we found through the immunostaining of BrdU+ neurons in the HPC that the number of newborn neurons was significantly decreased in TLE mice (**Supplementary Figure 4**), which confirmed that there was an impairment of neurogenesis due to TLE. In short, downregulation of neurogenesis may result in an E/I imbalance and subsequently contribute to impaired RA.

The Iqgap2 gene encodes a protein that interacts with components of the cytoskeleton, which is related to cell–cell adhesion, cell migration, and cell signaling, as well as crosstalk with the Wnt pathway (Smith et al., 2015). The Cntnap5c gene is a contactin-associated protein that is important for cell adhesion and intercellular communication in the nervous system (Hirata et al., 2016). Mdga1 encodes a glycosylphosphatidylinositol (GPI)-anchored cell surface glycoprotein that is suggested to play a role in neuronal migration, axon outgrowth, and axon-target recognition (Litwack et al., 2004). Furthermore, the Mdga1 and Cntnap5c genes were found to be crucial for balancing excitatory and inhibitory neurotransmission (Elegheert et al., 2017; Tong et al., 2019). Taken together, the downregulation of Iqgap2, Cntnap5c, and Mdga1 confirmed that in TLE, there is DG dispersion, neuronal reorganization, as well as neuronal disconnection and E/I imbalance.

Pdcd1 encodes programmed cell death protein 1, which indicates cell death of the nervous tissue following chronic injury (Pu et al., 2018). Tnfrsf25 gene production is known as death receptor 3, which is involved in the regulation of

apoptosis, and is increased in slowly expanding lesions (Jackle et al., 2020). Timp1 mRNA was found after neuronal injury, and the Timp1 gene product was considered to have an anti-apoptotic function (Huang et al., 2011). Zbtb16 is involved in cell cycle progression and is used as a boundary cell marker (Takahashi and Osumi, 2011). Moreover, Zbtb16 was shown to be downregulated after nerve injury (Zhang et al., 2019). Thus, the decrease in Pdcd1 gene transcription confirmed neuronal loss in the TLE hippocampus; both Timp1 and Tnfrsf25 increase, Zbtb16 decrease may also be related to dLS neuron apoptosis and neuronal dysfunction.

Notably, Gpr39 was reported to be related to neurotensin receptors (NTSR) (Popovics and Stewart, 2011). In our study, we found that Gpr39 transcription was increased. Taken together, the transcriptome analysis results revealed that gene dysfunction contributed to neuronal loss, neural network reorganization, and downregulation of neurogenesis in TLE dHPC and may cause E/I imbalance and risk assessment impairments. Interestingly, dLS also exhibited the dysregulation of related genes, indicating that intrahippocampal kainic acid injection can result in dLS-related circuit reorganization.

Degeneration of Dorsal Dentate Gyrus and CA3 Somatostatin-Positive Neurons and dLS Cholecystokinin-Positive Neurons May Contribute to Excitation and Inhibition Imbalance

To examine the effect of KA injection on hippocampal and lateral septal GABAergic neurons, we performed immunostaining for SOM+ and PV+ in dDG/CA3 and NTSR+, CCK+, and VIP+ in the dLS. The SOM+ neurons in dDG/CA3 were significantly decreased in TLE mice compared with WT mice, whereas PV+ neurons showed no significant change (SOM+, $p = 0.0002626$; **Figures 5A,B**). However, morphological changes in PV+ neurons were observed, indicating the alteration of PV+ neurons function (**Supplementary Figure 5**). The loss of SOM+ neurons may contribute to E/I imbalance in the HPC and impaired RA. In dLS, NTSR+ neurons were significantly increased, in accordance with transcription-related results, whereas CCK+ neurons decreased (NTSR+, $p = 0.00912$, CCK+, $p = 0.0042$; **Figures 5C,D**), which may be due to decreased GABAergic neurons in the dLS and impaired RA. Therefore, GABAergic neurons in both the dHPC and dLS were altered in TLE mice, and different subtypes showed different vulnerabilities. These GABAergic neurons may have a complicated involvement in the E/I imbalance and RA impairment.

Manipulation of Dorsal Dentate Gyrus and CA3 CaMKII+ or Somatostatin-Positive Neurons Is Sufficient to Impair Risk Assessment

Our electrophysiological and histological data indicated that SOM+ neurons in the HPC were decreased in KA-induced TLE mice, which may contribute to RA impairment. Therefore, we hypothesized that the direct inhibition of SOM+ neurons in the HPC *in vivo* would be sufficient to alter RA. To investigate this hypothesis, we used chemogenetic in combination with the EPM. To selectively inhibit SOM+ neurons in the HPC, we bilaterally expressed hM4Di in these neurons (**Figure 6A**). As compared to the group without clozapine-N-oxide (CNO) administration, the CNO administration group showed a significant decrease in the ratio of the average approach- and avoid-RA durations (**Figure 6B**). These results showed that the inhibition of dHPC SOM+ neurons led to an impairment in RA behavior. Furthermore, the inhibition of SOM+ neurons caused an increase in the ratio of approach- to avoid-RA entries, suggesting that after RA, the animals have a higher probability of exploring the open arm than the closed arm (**Figure 6E**). Taken together, these results imply that these animals are more likely susceptible to danger.

Interestingly, the inhibition of SOM+ neurons in the HPC led to an increased average duration of avoid-RA (**Figure 6D**), while did not affect average duration of approach-RA (**Figure 6C**). It is widely accepted that closed arms are relatively safe compared with open arms. To further investigate the meaning of the average duration of avoid-RA, we noted that both the entries and total duration of avoid-RA had decreased consistently (**Supplementary Figures 6A–D**), suggesting that the CNO administration group suppressed the preference of the closed arm (safe zone). These results further substantiate the notion that selective inhibition of the SOM+ neurons in the HPC leads to RA impairment in mice after CNO administration.

To further investigate whether the activation of glutamatergic neurons in the HPC impairs RA, we selectively applied optogenetic activation to these neurons in the EPM (**Figure 6F**). The optogenetic activation showed no effect on the avoid-RA (**Figure 6I** and **Supplementary Figures 6G,H**), while the ratio of approach- and avoid-RA was no significant difference (**Figures 6G,J**). However, both of the average and total approach-RA duration were significantly decreased (**Figure 6H** and **Supplementary Figures 6E,F**). Taken together, the chemogenetic inhibition and optogenetic activation results, which were similar to the TLE mice, confirmed that the E/I imbalance of HPC contributed to impairment of RA behavior. Moreover, the heterogeneous loss of neurons, which may be modulated by dysregulation of apoptosis, neurogenesis and migration, was related to the E/I imbalance in KA-induced TLE mice.

DISCUSSION

The current study confirms and extends previous studies on the epilepsy-induced impairment of RA and the future exploratory outcome, in which E/I imbalance in dDG/CA3 and alteration of dLS contributed. Animal behavior in the EPM can be quantified as anxiety, exploration, and RA. Recent studies have suggested that animals with epilepsy have impaired RA (Kubova et al., 2004; O'Loughlin et al., 2014), and we found that the impaired RA led to epileptic mice preferentially approaching potential threats. Previous studies have shown that the hippocampus and its broad of downstream participate in regulating behavior in EPM (Lee et al., 2019; Besnard et al., 2020; Xia and Kheirbek, 2020; Botterill et al., 2021; Dong et al., 2021; Wang et al., 2021), in

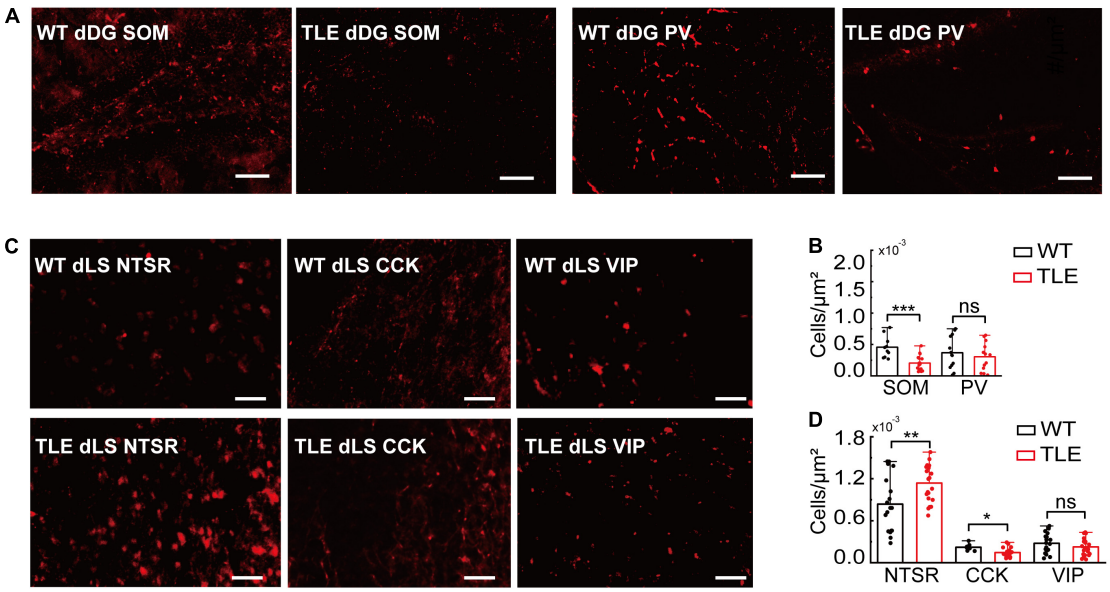

FIGURE 5 | Comparison of GABAergic neurons subtypes in WT vs. TLE. **(A)** Representative images of immunostaining of PV+ and SOM+ neurons in dDG of WT and TLE mice. Scale bar, 200 μm. **(B)** The densities of SOM+ and PV+ neurons in dDG/CA3 (SOM+: WT, n = 6 mice, TLE, n = 6 mice; PV+: WT, n = 6 mice, TLE, n = 5 mice). **(C)** Representative images of immunostaining of NTSR+, CCK+, and VIP+ neurons in dLS of WT and TLE mice. Scale bar, 200 μm. **(D)** The densities of NTSR+, CCK+, and VIP+ neurons in dLS (NTSR+: WT, n = 11 mice, TLE, n = 10 mice; CCK+: WT, n = 6 mice, TLE, n = 9 mice, VIP+: WT, n = 11 mice, TLE, n = 6 mice) (Error bars represent s.d; $^{*}p < 0.05$; $^{**}p < 0.01$, $^{***}p < 0.001$, t-test).

which RA behavior plays a key role in future outcomes (Jacinto et al., 2016; Motta et al., 2017; Blanchard, 2018; McNaughton and Corr, 2018). In this study, we confirmed that dDG/CA3 neurons are involved in RA behavior. Moreover, subpopulations of activated neurons preferentially responded to either approach-RA or avoid-RA. In epileptic mice, the impaired approach-RA was attributed to the E/I imbalance of dDG/CA3. In addition, a decrease in the approach-RA-specifically activated GABAergic neurons may also contribute toward it.

Risk assessment is considered a core component of the defense survival system, especially when dealing with ambiguous or mild threats (Gross and Canteras, 2012; Blanchard, 2018). Therefore, an animal's behavior in the central stage of the EPM is considered to be RA (Rodgers and Dalvi, 1997), which can help an animal detect potential threats, while the animal's internal state, such as anxiety, can also affect its RA behavior (Blanchard et al., 2011). Previous studies have shown that hippocampal neuronal activity changes as the experimental subject moves to different regions of the EPM (open or closed arms), focusing on anxiety behavior (Adhikari et al., 2011; Felix-Ortiz et al., 2013; Padilla-Coreano et al., 2016; Lee et al., 2019). Moreover, hippocampal neurons also participate in RA behavior (Motta et al., 2017; McNaughton and Corr, 2018), and hippocampal theta oscillations are recruited in RA, and their pattern can predict future exploratory outcomes, including approach and avoidance to the open arms (Jacinto et al., 2016. Here, we directly demonstrate, at the neuronal level, that among the RA-activated dDG/CA3 neurons, ∼22% of glutamatergic and ∼23% of GABAergic neurons are preferentially responsive to approach-RA, while ∼17% of glutamatergic and ∼23% of GABAergic neurons are preferentially responsive to avoid-RA. Notably, several studies have dissected the RA mechanism focusing on the ventral hippocampus because it is more involved in emotions, such as anxiety (Felix-Ortiz et al., 2013). As the RA stands at the interface of cognition and emotion (Blanchard, 2018), we determined that the dorsal hippocampal dDG/CA3 also processed the RA information. In the future, depending on the activity of the dDG/CA3 neurons, we may predict the following behavioral outcomes. In addition, the dLS, as the key node between the hippocampus and subcortical regions, is also engaged in RA (Motta et al., 2017). We further discovered that dLS neurons could specifically activate either approach-RA or avoid-RA, similar to dDG/CA3 neurons.

Epileptic animals were found to have reduced RA, which may be related to the impairment of fear and anxiety (O'Loughlin et al., 2014). Here, we evaluated RA and analyzed the approach-RA and avoid-RA behaviors, and more accurately revealed that the duration of approach-RA in epileptic mice was reduced significantly, but not in the avoid-RA. Thus, the epileptic mice are specifically impaired with approach-RA, so that they may have a tendency to underestimate the potential threat. Notably, we observed that a few epileptic mice fell from the open arm in the EPM (these samples were excluded from our results), but no WT mice were found to fall. It has been reported that epileptic patients have a higher risk of premature mortality due to external causes (Fazel et al., 2013), and our results imply that the impairment of estimating the potential risk may contribute to it.

Recurrent seizures lead to significant structural and functional disability of the involved brain regions, including dysconnectivity of the cortex and hippocampus (Fadaie et al., 2021). As a result,

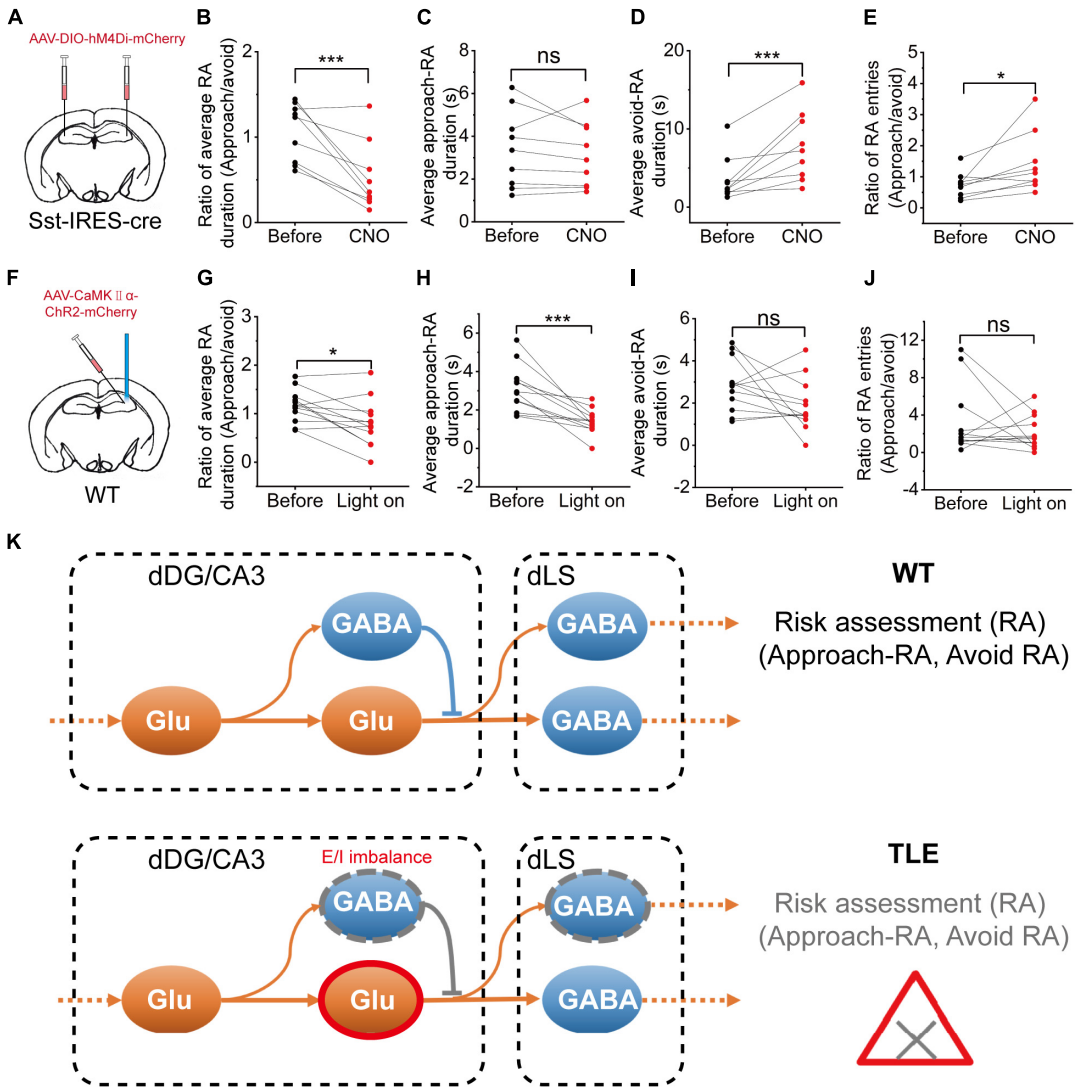

FIGURE 6 | Chemogenetic inhibition of hippocampal SOM+ neurons or optogenetic activation of CaMKII+ neurons impaired the RA of mice. **(A)** Diagram showing the chemogenetic inhibition of CA3 SOM+ neurons; **(B)** Ratio between the mean approach- and avoid-RA durations; **(C)** Average approach-RA duration; **(D)** Average avoid-RA duration; **(E)** Ratio between approach- and avoid-RA entries (before CNO, $n = 9$; CNO, $n = 9$; error bars represent standard deviation (s.d.); $^{*}p < 0.05$; $^{***}p < 0.001$, paired t-test); **(F)** Diagram of the experimental setup for optogenetic stimulations; **(G–J)** Optogenetic activation of hippocampal glutamatergic neurons; **(G)** Ratio between the mean approach- and avoid-RA durations; **(H)** Average approach-RA duration; **(I)** Average avoid-RA duration; **(J)** Ratio between approach- and avoid-RA entries (before light, $n = 12$; light on, $n = 12$; error bars represent standard deviation (s.d.); $^{***}p < 0.001$, paired t-test); and **(K)** A supposed model of neural E/I imbalance mechanism in impairment of approach-RA in TLE. ns, no significant difference.

it is widely accepted that this can lead to brain disorders with broad cognitive impairments (Fadaie et al., 2021). Seizures in TLE disable the function of the hippocampus and its downstream brain regions, including the LS, entorhinal cortex, and broad cortex areas (Motelow et al., 2015; Lu et al., 2016). KA-induced TLE rodents show obvious hippocampal apoptosis, similar to epileptic patients. Moreover, the loss of GABAergic neurons is even more severe (Wyeth et al., 2020). In the present study, we found that an increase in the dDG/CA3 glutamatergic neurons and a decrease in dDG/CA3 and dLS GABAergic neurons in the HPC of the mice with TLE resulted in the impairment of approach-RA, but not avoid-RA. Interestingly, our results also suggested that approach-RA-activated dDG/CA3 glutamatergic neurons increased in accordance with hyperexcitation of glutamatergic neurons in seizures in a previous study (Krook-Magnuson et al., 2013). In summary, our results suggest that in recurrent seizures, the E/I imbalance of the hippocampus induces inhomogeneous neuronal lesions and induces dysfunction of RA.

In TLE, different types of GABAergic neurons suffer heterogeneous damage, such as SOM+ neurons optionally located in the hilus, which are more vulnerable than PV+ neurons in HPC both in animals and humans (Swartz et al., 2006; Marx et al., 2013). In this study, we confirmed that the SOM+ neurons were significantly degenerated compared with

PV+ neurons. The VIP+ GABAergic neurons were found to preferentially innervate inhibitory interneurons, such as CCK+, SOM+, and PV+ neurons, highlighting their central role in disinhibitory modulation in HPC (Kullander and Topolnik, 2021). In addition, the VIP+ neurons were found to code information of the open and closed arms in the EPM (Lee et al., 2019). CCK+ neurons are involved in relevant behavioral functions, such as memory, cognition, anxiety, and reward, by regulating their cognitive components (Ballaz and Bourin, 2021). Herein, we found that the number of dLS CCK+ neurons in TLE was significantly decreased, but not in NTSR+ or VIP+ neurons. Direct manipulation of glutamatergic or GABAergic neurons in the HPC results in the impairment of RA, and may also can the animal to underestimate a potential threat. As such, we hypothesized that the activation of dDG/CA3 glutamatergic neurons and the loss of dDG/CA3 SOM+ neurons contributed to E/I imbalance and impairment of RA in mice with TLE (**Figure 6K**).

It is known that epilepsy not only induces hippocampal neurodegeneration, hyper synchronicity, and E/I imbalance, but also leads to the formation of abnormal hippocampal circuitry reorganization, such as granule cell dispersion. The hippocampus has a complex brain structure with a special regular organization. Based on this, the hippocampus is a super plastic structure, which is critical for a broad function of cognition, emotion, and motivation, while it is vulnerable to damage, especially in epilepsy. Thus, the TLE-induced reorganization and disconnection of the hippocampus may cause approach-RA, even though approach-RA-related neurons did not degenerate. In addition, we found that hippocampal PV+ neurons have altered morphology, so that the disconnection of PV+ neurons may contribute to impaired approach-RA. In the DG, axons of the entorhinal cortex project onto dentate granule cells (glutamatergic neurons) and onto GABAergic interneurons (including PV+ and SOM+ cells) as well as mossy cells (glutamatergic neurons) in the hilus. Furthermore, the DG/hilus are considered as a gate, in which hilar mossy cells play a critical role and are vulnerable to excitotoxicity in TLE (Goldberg and Coulter, 2013). Thus, TLE may decrease the inhibition of survival of GABAergic neurons. In summary, the reorganization of the DG-CA3 network, both the rearrangement of mossy fiber sprouting and PV+ neurons, may also contribute to the E/I imbalance, then selectively damage the approach-RA function.

Specifically, adult hippocampal neurogenesis has been discovered, and these newborn neurons are important for hippocampal functions (Anacker and Hen, 2017). With the discovery of adult neurogenesis and its understanding, the role of neurogenesis in epilepsy needs to be addressed. After seizures, dentate neurogenesis increase has been reported (Goldberg and Coulter, 2013), whereas others have found that neurogenesis is disrupted (Lauren et al., 2013; Marucci et al., 2013). Our results suggest that neurogenesis in the epileptic hippocampus was abnormal, as evidenced by the downregulation of related transcriptional signals, such as Wnt3a, Crlf1, and Dlx1. In accordance with a study on chronic epilepsy, we suppose that an increase in neurogenesis may occur in the acute phase, but a decrease in neurogenesis occurs in the chronic phase (Huang et al., 2015). Furthermore, newborn neurons were thought to inhibit mature granule cells, as silencing them affected the animal's stress-related behaviors (Anacker et al., 2018). Future studies should investigate whether the impairment of neurogenesis affects RA in TLE.

In conclusion, we found a decrease in the capacity of RA in epileptic animals, which may lead epileptic individuals to underestimate the potential threat and ultimately cause injury. There were subpopulations of neurons in both the hippocampus and the lateral septum that could specifically actively respond to approach-RA, while maintaining a certain balance between excitatory and inhibition. However, in epileptic animals, these neurons are altered, and the E/I balance is disrupted. Transcriptome and immunohistochemical staining showed that neurons in the hippocampus and LS were lost, and neural networks were reorganized. In particular, dDG/CA3 SOM+ neurons and dLS CCK+ neurons are selectively vulnerable to damage in the TLE, whereas the dCA3/DG glutamatergic neurons are considered to be overexcited (Goldberg and Coulter, 2013). In the present study, we demonstrated that when combined with the manipulation of CaMKII+ and SOM+ neurons, an E/I imbalance of the dCA3/DG-dLS circuit contributes to the impairment of RA behavior and alternates the future exploratory outcome during epileptic individuals facing potential threat. The understanding of epileptic-induced impaired risk assessment at multiple levels would shed light on the understanding of E/I balance in brain function and provide a potential paradigm for related studies.

DATA AVAILABILITY STATEMENT

The raw data supporting the conclusions of this article will be made available by the authors, without undue reservation.

ETHICS STATEMENT

The animal study was reviewed and approved by Shenzhen Institute of Advanced Technology, Chinese Academy of Sciences.

AUTHOR CONTRIBUTIONS

CZ, YL, CS, and YC were responsible for the conception of the study, design of experiments, and interpretation of the data. CS, YC, JH, and LW acquired the data. CZ, CS, YC, JH, PS, SH, and JL analyzed the data. CZ, CS, and YC wrote the manuscript. YL commented on this manuscript. All authors contributed to the manuscript and approved the submitted version.

FUNDING

This work was supported by National Natural Science Foundation of China (Nos. 31871080, 32171024, 32071035, and T2122021), CAS Key Laboratory of Brain Connectome and Manipulation (2019DP173024), Guangdong Natural Science

Fund for Distinguished Young Scholars (2020B1515020042), the Special Support Project for Outstanding Young Scholars of Guangdong Province (2019TQ05Y177), Shenzhen Government Basic Research Grant (JCYJ20200109150818777), and Shenzhen Engineering Lab of Brain Activity Mapping Technologies.

ACKNOWLEDGMENTS

We thank Dr. Kang Huang for assisting with electrophysiological data analysis. We also thank Bingfeng Liu for the animal feeding.

SUPPLEMENTARY MATERIAL

The Supplementary Material for this article can be found online at: https://www.frontiersin.org/articles/10.3389/fnmol.2022.828891/full#supplementary-material

Supplementary Figure 1 | Neuronal classification and activity responses. **(A)** HPC neurons (n = 180 neurons from 5 mice) were classified by valley-to-peak time and spike half-width when the mice entered the food zone; blue, putative GABAergic neurons; red, putative glutamatergic neurons; **(B)** Quantified neuronal responses to approach-RA, where blue hollow rectangle = no response GABAergic neurons, red hollow rectangle = no response glutamatergic neurons, blue triangle = approach-RA excited GABAergic neurons, red triangle = approach-RA excited glutamatergic neurons, blue circle = approach-RA inhibited GABAergic neurons, and red circle = approach-RA inhibited glutamatergic neurons; and **(C)** Representative raster plots and waveforms of dDG/CA3 neurons responding negatively to RA, in which RA-inhibited neurons exhibited a phasic increase in the firing rate before RA (in close arm, duration, ∼2–3 s) and a subsequent decrease of the firing rate during RA (in center zone).

Supplementary Figure 2 | The DAPI positive cells were reduced. The ratios were the fluorescence positive area (DAPI+ signal) divided area of ROI (region of interest) in dDG/CA3. WT, n = 22 slices from 6 mice, TLE, n = 27 slices from 6 mice. Error bars represent s.d. $^{***}p < 0.001$. Two-sample t-test.

Supplementary Figure 3 | Overview of RNA sequencing flow diagram. Wild-type 6-week-old C57BL/6J male mice were obtained and housed for 2-week environmental acclimation. Half of the wild-type 8-week-old mice were subjected to KA-injection. All mice were housed to 20-week-old for sampling.

Supplementary Figure 4 | Comparison of BrdU+ neurons in WT vs. TLE. **(A)** Representative images of immunostaining of BrdU+ neurons in dDG of WT and TLE mice. Scale bar, 50 μm. **(B)** The number of BrdU+ neurons in dDG (BrdU+: WT, n = 14 slices from 2 mice, TLE, n = 8 slices from 3 mice) (Error bars represent s.d; $^{**}p < 0.01$, two-sample t test).

Supplementary Figure 5 | Morphological changes in PV+ neurons. Representative confocal images at 40× showed that the morphology of PV+ neurons cell body altered in dDG/CA3 of TLE mice. Scale bar, 20 μ m.

Supplementary Figure 6 | Chemogenetics inhibition of hippocampal SOM+ neurons or optogenetic activation of hippocampal glutamatergic neurons impaired the RA. **(A–D)** Chemogenetics inhibition of hippocampal SOM+ neurons. **(A)** The approach-RA duration. **(B)** The approach-RA entries. **(C)** The avoid-RA duration. **(D)** The avoid-RA entries (before CNO, n = 9; CNO administration, n = 9). **(E–H)** Optogenetic activation of hippocampal glutamatergic neurons. **(E)** The approach-RA duration. **(F)** The approach-RA entries. **(G)** The avoid-RA duration. **(H)** The avoid-RA entries (before light, n = 12; light on, n = 12) (ns is no significant difference; error bars represent s.d; $^{*}p < 0.05$; $^{***}p < 0.001$, paired-t test).

REFERENCES

Adhikari, A., Topiwala, M. A., and Gordon, J. A. (2011). Single units in the medial prefrontal cortex with anxiety-related firing patterns are preferentially influenced by ventral hippocampal activity. *Neuron* 71, 898–910. doi: 10.1016/j.neuron.2011.07.027

Anacker, C., and Hen, R. (2017). Adult hippocampal neurogenesis and cognitive flexibility – linking memory and mood. *Nat. Rev. Neurosci.* 18, 335–346. doi: 10.1038/nrn.2017.45

Anacker, C., Luna, V. M., Stevens, G. S., Millette, A., Shores, R., Jimenez, J. C., et al. (2018). Hippocampal neurogenesis confers stress resilience by inhibiting the ventral dentate gyrus. *Nature* 559, 98–102. doi: 10.1038/s41586-018-0262-4

Ballaz, S. J., and Bourin, M. (2021). Cholecystokinin-mediated neuromodulation of anxiety and schizophrenia: a "Dimmer-switch" hypothesis. *Curr. Neuropharmacol.* 19, 925–938. doi: 10.2174/1570159X18666201113145143

Benini, R., Longo, D., Biagini, G., and Avoli, M. (2011). Perirhinal cortex hyperexcitability in pilocarpine-treated epileptic rats. *Hippocampus* 21, 702–713. doi: 10.1002/hipo.20785

Besnard, A., Miller, S. M., and Sahay, A. (2020). Distinct dorsal and ventral hippocampal ca3 outputs govern contextual fear discrimination. *Cell Rep.* 30, 2360–2373. doi: 10.1016/j.celrep.2020.01.055

Blanchard, D. C. (2018). Risk assessment: at the interface of cognition and emotion. *Curr. Opin. Behav. Sci.* 24, 69–74. doi: 10.1016/j.cobeha.2018.03.006

Blanchard, D. C., Griebel, G., Pobbe, R., and Blanchard, R. J. (2011). Risk assessment as an evolved threat detection and analysis process. *Neurosci. Biobehav. Rev.* 35, 991–998. doi: 10.1016/j.neubiorev.2010.10.016

Botterill, J. J., Vinod, K. Y., Gerencer, K. J., Teixeira, C. M., LaFrancois, J. J., and Scharfman, H. E. (2021). Bidirectional regulation of cognitive and anxiety-like behaviors by dentate gyrus mossy cells in male and female mice. *J. Neurosci.* 41, 2475–2495. doi: 10.1523/JNEUROSCI.1724-20.2021

Cobos, I., Long, J. E., Thwin, M. T., and Rubenstein, J. L. (2006). Cellular patterns of transcription factor expression in developing cortical Interneurons. *Cereb. Cortex* 16, I82–I88. doi: 10.1093/cercor/bhk003

Courtin, J., Chaudun, F., Rozeske, R. R., Karalis, N., Gonzalez-Campo, C., Wurtz, H., et al. (2014). Prefrontal parvalbumin interneurons shape neuronal activity to drive fear expression. *Nature* 505, 92–96. doi: 10.1038/nature12755

Curia, G., Longo, D., Biagini, G., Jones, R. S. G., and Avoli, M. (2008). The pilocarpine model of temporal lobe epilepsy. *J. Neurosci. Methods* 172, 143–157.

Dong, W. X., Chen, H. B., Sit, T., Han, Y. C., Song, F., Vyssotski, A. L., et al. (2021). Characterization of exploratory patterns and hippocampal-prefrontal network oscillations during the emergence of free exploration. *Sci. Bull.* 66, 2238–2250. doi: 10.1016/j.scib.2021.05.018

Elegheert, J., Cvetkovska, V., Clayton, A. J., Heroven, C., Vennekens, K. M., Smukowski, S. N., et al. (2017). Structural mechanism for modulation of synaptic neuroligin-neurexin signaling by mdga proteins. *Neuron* 95, 896–913.e10.

Fadaie, F., Lee, H. M., Caldairou, B., Gill, R. S., Sziklas, V., Crane, J., et al. (2021). Atypical functional connectome hierarchy impacts cognition in temporal lobe epilepsy. *Epilepsia* 62, 2589–2603. doi: 10.1111/epi.17032

Fanselow, M. S., and Dong, H. W. (2010). Are the dorsal and ventral hippocampus functionally distinct structures? *Neuron* 65, 7–19. doi: 10.1016/j.neuron.2009.11.031

Fazel, S., Wolf, A., Langstrom, N., Newton, C. R., and Lichtenstein, P. (2013). Premature mortality in epilepsy and the role of psychiatric comorbidity: a total population study. *Lancet* 382, 1646–1654. doi: 10.1016/S0140-6736(13)60899-5

Felix-Ortiz, A. C., Beyeler, A., Seo, C., Leppla, C. A., Wildes, C. P., and Tye, K. M. (2013). BLA to vHPC inputs modulate anxiety-related behaviors. *Neuron* 79, 658–664. doi: 10.1016/j.neuron.2013.06.016

Goldberg, E. M., and Coulter, D. A. (2013). Mechanisms of epileptogenesis: a convergence on neural circuit dysfunction. *Nat. Rev. Neurosci.* 14, 337–349. doi: 10.1038/nrn3482

Gross, C. T., and Canteras, N. S. (2012). The many paths to fear. *Nat. Rev. Neurosci.* 13, 651–658. doi: 10.1038/nrn3301

Harada, H., Farhani, N., Wang, X. F., Sugita, S., Charish, J., Attisano, L., et al. (2019). Extracellular phosphorylation drives the formation of

neuronal circuitry. *Nat. Chem. Biol.* 15, 1030–1031. doi: 10.1038/s41589-019-0345-z

He, W. L., Ingraham, C., Rising, L., Goderie, S., and Temple, S. (2001). Multipotent stem cells from the mouse basal forebrain contribute GABAergic neurons and oligodendrocytes to the cerebral cortex during embryogenesis. *J. Neurosci.* 21, 8854–8862. doi: 10.1523/JNEUROSCI.21-22-08854.2001

Hermann, B. P., Struck, A. F., Busch, R. M., Reyes, A., Kaestner, E., and McDonald, C. R. (2021). Neurobehavioural comorbidities of epilepsy: towards a network-based precision taxonomy. *Nat. Rev. Neurol.* 17, 731–746. doi: 10.1038/s41582-021-00555-z

Hirata, H., Umemori, J., Yoshioka, H., Koide, T., Watanabe, K., and Shimoda, Y. (2016). Cell adhesion molecule contactin-associated protein 3 is expressed in the mouse basal ganglia during early postnatal stages. *J. Neurosci. Res.* 94, 74–89. doi: 10.1002/jnr.23670

Huang, B., Zhao, X., Zheng, L. B., Zhang, L., Ni, B., and Wang, Y. W. (2011). Different expression of tissue inhibitor of metalloproteinase family members in rat dorsal root ganglia and their changes after peripheral nerve injury. *Neuroscience* 193, 421–428. doi: 10.1016/j.neuroscience.2011.07.031

Huang, C., Fu, X. H., Zhou, D., and Li, J. M. (2015). The role of wnt/beta-catenin signaling pathway in disrupted hippocampal neurogenesis of temporal lobe epilepsy: a potential therapeutic target? *Neurochem. Res.* 40, 1319–1332. doi: 10.1007/s11064-015-1614-1

Jacinto, L. R., Cerqueira, J. J., and Sousa, N. (2016). Patterns of theta activity in limbic anxiety circuit preceding exploratory behavior in approach-avoidance conflict. *Front. Behav. Neurosci.* 10:171. doi: 10.3389/fnbeh.2016.00171

Jackle, K., Zeis, T., Schaeren-Wiemers, N., Junker, A., van der Meer, F., Kramann, N., et al. (2020). Molecular signature of slowly expanding lesions in progressive multiple sclerosis. *Brain* 143, 2073–2088. doi: 10.1093/brain/awaa158

Johnson, K. J., Robbins, A. K., Wang, Y. P., McCahan, S. M., Chacko, J. K., and Barthold, J. S. (2010). Insulin-like 3 exposure of the fetal rat gubernaculum modulates expression of genes involved in neural pathways. *Biol. Reprod.* 83, 774–782. doi: 10.1095/biolreprod.110.085175

Kanner, A. M. (2016). Management of psychiatric and neurological comorbidities in epilepsy. *Nat. Rev. Neurol.* 12, 106–116. doi: 10.1038/nrneurol.2015.243

Krook-Magnuson, E., Armstrong, C., Oijala, M., and Soltesz, I. (2013). On-demand optogenetic control of spontaneous seizures in temporal lobe epilepsy. *Nat. Commun.* 4:1376. doi: 10.1038/ncomms2376

Kubova, H., Mares, P., Suchomelova, L., Brozek, G., Druga, R., and Pitkanen, A. (2004). Status epilepticus in immature rats leads to behavioural and cognitive impairment and epileptogenesis. *Eur. J. Neurosci.* 19, 3255–3265. doi: 10.1111/j.0953-816X.2004.03410.x

Kullander, K., and Topolnik, L. (2021). Cortical disinhibitory circuits: cell types, connectivity and function. *Trends Neurosci.* 44, 643–657. doi: 10.1016/j.tins.2021.04.009

Lauren, H. B., Ruohonen, S., Kukko-Lukjanov, T. K., Virta, J. E., Gronman, M. A., Lopez-Picon, F. R., et al. (2013). Status epilepticus alters neurogenesis and decreases the number of GABAergic neurons in the septal dentate gyrus of 9-day-old rats at the early phase of epileptogenesis. *Brain Res.* 1516, 33–44. doi: 10.1016/j.brainres.2013.04.028

Lee, A. T., Cunniff, M. M., See, J. Z., Wilke, S. A., Luongo, F. J., Ellwood, I. T., et al. (2019). VIP interneurons contribute to avoidance behavior by regulating information flow across hippocampal-prefrontal networks. *Neuron* 102, 1223–1234.e4. doi: 10.1016/j.neuron.2019.04.001

Levesque, M., Avoli, M., and Bernard, C. (2016). Animal models of temporal lobe epilepsy following systemic chemoconvulsant administration. *J. Neurosci. Methods* 260, 45–52. doi: 10.1016/j.jneumeth.2015.03.009

Litwack, E. D., Babey, R., Buser, R., Gesemann, M., and O'Leary, D. D. M. (2004). Identification and characterization of two novel brain-derived immunoglobulin superfamily members with a unique structural organization. *Mol. Cell. Neurosci.* 25, 263–274. doi: 10.1016/j.mcn.2003.10.016

Lothman, E. W., Rempe, D. A., and Mangan, P. S. (1995). Changes in excitatory neurotransmission in the CA1 region and dentate gyrus in a chronic model of temporal lobe epilepsy. *J. Neurophysiol.* 74, 841–848. doi: 10.1152/jn.1995.74.2.841

Lu, Y., Zhong, C., Wang, L., Wei, P., He, W., Huang, K., et al. (2016). Optogenetic dissection of ictal propagation in the hippocampal-entorhinal cortex structures. *Nat. Commun.* 7:10962.

Mangan, P. S., Rempe, D. A., and Lothman, E. W. (1995). Changes in inhibitory neurotransmission in the CA1 region and dentate gyrus in a chronic model of temporal lobe epilepsy. *J. Neurophysiol.* 74, 829–840. doi: 10.1152/jn.1995.74.2.829

Marucci, G., Giulioni, M., Rubboli, G., Paradisi, M., Fernandez, M., Del Vecchio, G., et al. (2013). Neurogenesis in temporal lobe epilepsy: relationship between histological findings and changes in dentate gyrus proliferative properties. *Clin. Neurol. Neurosurg.* 115, 187–191. doi: 10.1016/j.clineuro.2012.05.012

Marx, M., Haas, C. A., and Haussler, U. (2013). Differential vulnerability of interneurons in the epileptic hippocampus. *Front. Cell. Neurosci.* 7:167. doi: 10.3389/fncel.2013.00167

McNaughton, N., and Corr, P. J. (2018). Survival circuits and risk assessment. *Curr. Opin. Behav. Sci.* 24, 14–20. doi: 10.1016/j.cobeha.2018.01.018

Moshe, S. L., Perucca, E., Ryvlin, P., and Tomson, T. (2015). Epilepsy: new advances. *Lancet* 385, 884–898. doi: 10.1016/s0140-6736(14)60456-6

Motelow, J. E., Li, W., Zhan, Q., Mishra, A. M., Sachdev, R. N., Liu, G., et al. (2015). Decreased subcortical cholinergic arousal in focal seizures. *Neuron* 85, 561–572. doi: 10.1016/j.neuron.2014.12.058

Motta, S. C., Carobrez, A. P., and Canteras, N. S. (2017). The periaqueductal gray and primal emotional processing critical to influence complex defensive responses, fear learning and reward seeking. *Neurosci. Biobehav. Rev.* 76, 39–47. doi: 10.1016/j.neubiorev.2016.10.012

Moura, D. M. S., Brandao, J. A., Lentini, C., Heinrich, C., Queiroz, C. M., and Costa, M. R. (2020). Evidence of progenitor cell lineage rerouting in the adult mouse hippocampus after status epilepticus. *Front. Neurosci.* 14:571315. doi: 10.3389/fnins.2020.571315

O'Loughlin, E. K., Pakan, J. M., McDermott, K. W., and Yilmazer-Hanke, D. (2014). Expression of neuropeptide Y1 receptors in the amygdala and hippocampus and anxiety-like behavior associated with Ammon's horn sclerosis following intrahippocampal kainate injection in C57BL/6J mice. *Epilepsy Behav.* 37, 175–183. doi: 10.1016/j.yebeh.2014.06.033

Padilla-Coreano, N., Bolkan, S. S., Pierce, G. M., Blackman, D. R., Hardin, W. D., Garcia-Garcia, A. L., et al. (2016). Direct ventral hippocampal-prefrontal input is required for anxiety-related neural activity and behavior. *Neuron* 89, 857–866. doi: 10.1016/j.neuron.2016.01.011

Popovics, P., and Stewart, A. J. (2011). GPR39: a Zn2+-activated G protein-coupled receptor that regulates pancreatic, gastrointestinal and neuronal functions. *Cell. Mol. Life Sci.* 68, 85–95. doi: 10.1007/s00018-010-0517-1

Pu, S. F., Li, S. Y., Xu, Y. M., Wu, J. Z., Lv, Y. Y., and Du, D. P. (2018). Role of receptor-interacting protein 1/receptor-interacting protein 3 in inflammation and necrosis following chronic constriction injury of the sciatic nerve. *Neuroreport* 29, 1373–1378. doi: 10.1097/WNR.0000000000001120

Rash, B. G., Tomasi, S., Lim, H. D., Suh, C. Y., and Vaccarino, F. M. (2013). Cortical gyrification induced by fibroblast growth factor 2 in the mouse brain. *J. Neurosci.* 33, 10802–10814. doi: 10.1523/JNEUROSCI.3621-12.2013

Ren, E., and Curia, G. (2021). Synaptic reshaping and neuronal outcomes in the temporal lobe epilepsy. *Int. J. Mol. Sci.* 22:3860. doi: 10.3390/ijms22083860

Rodgers, R. J., and Dalvi, A. (1997). Anxiety, defence and the elevated plus-maze. *Neurosci. Biobehav. Rev.* 21, 801–810. doi: 10.1016/s0149-7634(96)00058-9

Smith, J. M., Hedman, A. C., and Sacks, D. B. (2015). IQGAPs choreograph cellular signaling from the membrane to the nucleus. *Trends Cell Biol.* 25, 171–184. doi: 10.1016/j.tcb.2014.12.005

Sun, C. S., Mtchedlishvili, Z., Bertram, E. H., Erisir, A., and Kapur, J. (2007). Selective loss of dentate hilar interneurons contributes to reduced synaptic inhibition of granule cells in an electrical stimulation-based animal model of temporal lobe epilepsy. *J. Comp. Neurol.* 500, 876–893. doi: 10.1002/cne.21207

Sun, C. Y., Cao, Y., Huang, J. Y., Huang, K., Lu, Y., and Zhong, C. (2022). Low-cost and easy-fabrication lightweight drivable electrode array for multiple-regions electrophysiological recording in free-moving mice. *J. Neural Eng.* 19:016003. doi: 10.1088/1741-2552/ac494e

Swartz, B. E., Houser, C. R., Tomiyasu, U., Walsh, G. O., DeSalles, A., Rich, J. R., et al. (2006). Hippocampal cell loss in posttraumatic human epilepsy. *Epilepsia* 47, 1373–1382. doi: 10.1111/j.1528-1167.2006.00602.x

Takahashi, M., and Osumi, N. (2011). Pax6 regulates boundary-cell specification in the rat hindbrain. *Mech. Dev.* 128, 289–302. doi: 10.1016/j.mod.2011.04.001

Tellez-Zenteno, J. F., Dhar, R., and Wiebe, S. (2005). Long-term seizure outcomes following epilepsy surgery: a systematic review

and meta-analysis. *Brain* 128, 1188–1198. doi: 10.1093/brain/awh449

Tong, D. L., Chen, R. G., Lu, Y. L., Li, W. K., Zhang, Y. F., Lin, J. K., et al. (2019). The critical role of ASD-related gene CNTNAP3 in regulating synaptic development and social behavior in mice. *Neurobiol. Dis.* 130:104486. doi: 10.1016/j.nbd.2019.104486

Wang, K. Y., Wu, J. W., Cheng, J. K., Chen, C. C., Wong, W. Y., Averkin, R. G., et al. (2021). Elevation of hilar mossy cell activity suppresses hippocampal excitability and avoidance behavior. *Cell Rep.* 36:109702. doi: 10.1016/j.celrep.2021.109702

Wirtshafter, H. S., and Wilson, M. A. (2021). Lateral septum as a nexus for mood, motivation, and movement. *Neurosci. Biobehav. Rev.* 126, 544–559. doi: 10.1016/j.neubiorev.2021.03.029

Wyeth, M., Nagendran, M., and Buckmaster, P. S. (2020). Ictal onset sites and gamma-aminobutyric acidergic neuron loss in epileptic pilocarpine-treated rats. *Epilepsia* 61, 856–867. doi: 10.1111/epi.16490

Xia, F., and Kheirbek, M. A. (2020). Circuit-based biomarkers for mood and anxiety disorders. *Trends Neurosci.* 43, 902–915. doi: 10.1016/j.tins.2020.08.004

Zhang, F. C., Gu, X. K., Yi, S., and Xu, H. (2019). Dysregulated transcription factor TFAP2A after peripheral nerve injury modulated schwann cell phenotype. *Neurochem. Res.* 44, 2776–2785. doi: 10.1007/s11064-019-02898-y

Conflict of Interest: The authors declare that the research was conducted in the absence of any commercial or financial relationships that could be construed as a potential conflict of interest.

Publisher's Note: All claims expressed in this article are solely those of the authors and do not necessarily represent those of their affiliated organizations, or those of the publisher, the editors and the reviewers. Any product that may be evaluated in this article, or claim that may be made by its manufacturer, is not guaranteed or endorsed by the publisher.

frontiers | Frontiers in Molecular Neuroscience

ORIGINAL RESEARCH
published: 04 May 2022
doi: 10.3389/fnmol.2022.860662

CACNA1A Mutations Associated With Epilepsies and Their Molecular Sub-Regional Implications

Xue-Lian Li[1,2†], Zong-Jun Li[1†], Xiao-Yu Liang[1], De-Tian Liu[1], Mi Jiang[1], Liang-Di Gao[1], Huan Li[1], Xue-Qing Tang[1], Yi-Wu Shi[1], Bing-Mei Li[1], Na He[1], Bin Li[1], Wen-Jun Bian[1], Yong-Hong Yi[1], Chuan-Fang Cheng[1,3] and Jie Wang[1]* for the China Epilepsy Gene 1.0 Project*

[1] Key Laboratory of Neurogenetics and Channelopathies of the Ministry of Education of China, Department of Neurology, Institute of Neuroscience, The Second Affiliated Hospital of Guangzhou Medical University, Guangzhou, China, [2] Department of Neurology, The Affiliated Yuebei People's Hospital of Shantou University Medical College, Shaoguan, China, [3] Department of Cardiology, The Second Affiliated Hospital of Guangzhou Medical University, Guangzhou Medical University, Guangzhou, China

OPEN ACCESS

Edited by:
Yuwu Jiang,
Peking University First Hospital, China

Reviewed by:
Huanghe Yang,
Duke University, United States
Martin Heine,
Johannes Gutenberg University Mainz, Germany

***Correspondence:**
Chuan-Fang Cheng
chuanfangcheng@163.com
Jie Wang
wangjie2014010@163.com

[†]These authors have contributed equally to this work

Specialty section:
This article was submitted to Molecular Signalling and Pathways, a section of the journal Frontiers in Molecular Neuroscience

Received: *23 January 2022*
Accepted: *05 April 2022*
Published: *04 May 2022*

Citation:
Li X-L, Li Z-J, Liang X-Y, Liu D-T, Jiang M, Gao L-D, Li H, Tang X-Q, Shi Y-W, Li B-M, He N, Li B, Bian W-J, Yi Y-H, Cheng C-F and Wang J (2022) CACNA1A Mutations Associated With Epilepsies and Their Molecular Sub-Regional Implications. Front. Mol. Neurosci. 15:860662. doi: 10.3389/fnmol.2022.860662

Purpose: Previously, mutations in the voltage-gated calcium channel subunit alpha1 A (*CACNA1A*) gene have been reported to be associated with paroxysmal disorders, typically as episodic ataxia type 2. To determine the relationship between *CACNA1A* and epilepsies and the role of molecular sub-regional on the phenotypic heterogeneity.

Methods: Trio-based whole-exome sequencing was performed in 318 cases with partial epilepsy and 150 cases with generalized epilepsy. We then reviewed all previously reported *CACNA1A* mutations and analyzed the genotype-phenotype correlations with molecular sub-regional implications.

Results: We identified 12 *CACNA1A* mutations in ten unrelated cases of epilepsy, including four *de novo* null mutations (c.2963_2964insG/p.Gly989Argfs*78, c.3089 + 1G > A, c.4755 + 1G > T, and c.6340-1G > A), four *de novo* missense mutations (c.203G > T/p.Arg68Leu, c.3965G > A/p.Gly1322Glu, c.5032C > T/p.Arg1678Cys, and c.5393C > T/p.Ser1798Leu), and two pairs of compound heterozygous missense mutations (c.4891A > G/p.Ile1631Val& c.5978C > T/p.Pro1993Leu and c.3233C > T/p.Ser1078Leu&c.6061G > A/p.Glu2021Lys). The eight *de novo* mutations were evaluated as pathogenic or likely pathogenic mutations according to the criteria of American College of Medical Genetics and Genomics (ACMG). The frequencies of the compound heterozygous *CACNA1A* mutations identified in this cohort were significantly higher than that in the controls of East Asian and all populations ($P = 7.30 \times 10^{-4}$, $P = 2.53 \times 10^{-4}$). All of the ten cases were ultimately seizure-free after antiepileptic treatment, although frequent epileptic seizures were observed in four cases. Further analysis revealed that episodic ataxia type 2 (EA2) had a tendency of higher frequency of null mutations than epilepsies. The missense mutations in severe

epileptic phenotypes were more frequently located in the pore region than those in milder epileptic phenotypes ($P = 1.67 \times 10^{-4}$); *de novo* mutations in the epilepsy with intellectual disability (ID) had a higher percentage than those in the epilepsy without ID ($P = 1.92 \times 10^{-3}$).

Conclusion: This study suggested that *CACNA1A* mutations were potentially associated with pure epilepsy and the spectrum of epileptic phenotypes potentially ranged from the mild form of epilepsies such as absence epilepsy or partial epilepsy, to the severe form of developmental epileptic encephalopathy. The clinical phenotypes variability is potentially associated with the molecular sub-regional of the mutations.

Keywords: *CACNA1A*, partial epilepsy, childhood absence epilepsy, genotype-phenotype correlation, molecular sub-regional implication

INTRODUCTION

The voltage-gated calcium channel subunit alpha1 A gene (*CACNA1A*; MIM: 601011), located at chromosome locus19p13.13 and covering approximately 417 kb of genomic DNA with 47 exons, is predominantly expressed in the central nervous system (Kramer et al., 1995; Teh et al., 1995). It encodes the voltage-dependent P/Q-type calcium channel subunit alpha-1A (Cav2.1) that primarily distributed in nucleus, plasma membrane, neuronal cell body, and synapse (Ophoff et al., 1996). Cav2.1 is the alpha-1A subunit of the voltage-gated calcium channel (VGCC) that mediates the entry of calcium ions into excitable cells and are also involved in a variety of calcium-dependent processes, including muscle contraction, hormone or neurotransmitter release, and gene expression (Diriong et al., 1995). As a component of VGCC, Cav2.1 forms the pore region of the calcium channel and directs the channel activity (Tuluc et al., 2021).

Mutations in *CACNA1A* gene have been demonstrated to be associated with a wide range of paroxysmal diseases, such as episodic ataxia type 2 (EA2; MIM: 108500), familial hemiplegic migraine 1 (FHM1; MIM: 141500), spinocerebellar ataxia 6 (SCA6; MIM: 183086), and developmental epileptic encephalopathy 42 (DEE42; MIM: 617106). Cases with EA2 or FHM1 may be complicated by epilepsy or seizures that were generally mild phenotypes (Imbrici et al., 2004; Du et al., 2017). *CACNA1A* mutations have also been occasionally identified in patients with mild form of epilepsy, including absence epilepsy, juvenile myoclonic epilepsy, and idiopathic epilepsy (Klassen et al., 2011; Helbig et al., 2016; Lee et al., 2018). These findings suggest *CACNA1A* is possibly related to human epilepsies. However, the relationship between *CACNA1A* and epilepsies has not been defined and it is unknown the genotype-phenotype correlation in the spectrum of *CACNA1A*-associated disorders.

In this study, we performed trio-based whole-exome sequencing (WES) in a cohort of patients with epilepsy. Twelve *CACNA1A* mutations were identified in ten unrelated cases with phenotypic heterogeneity. We further systematically reviewed all *CACNA1A* mutations and analyzed their molecular heterogeneity, aiming to clarify the mechanism underlying phenotypical variation and the role of molecular sub-regional effect.

MATERIALS AND METHODS

Patients

The patients were recruited at the Epilepsy Center of the Second Affiliated Hospital of Guangzhou Medical University and the Affiliated Yuebei People's Hospital of Shantou University Medical College. Clinical phenotypes of epileptic seizures and epilepsy syndromes were assessed following the criteria of the Commission on Classification and Terminology of the International League Against Epilepsy (ILAE) (1981, 1989, 2001, 2010, 2017). Partial epilepsy was used to denote cases with partial seizures and EEG features of idiopathic epilepsy including shift, bilateral or multiple focal discharge. Generalized epilepsy was diagnosed on the basis of typical generalized seizures, such as absence, myoclonic, atonic, and generalized tonic-clonic seizures, supported by the results of generalized discharges on EEG. Participants with acquired causes like brain malformation, infection or metabolic disorders were excluded. We collected the comprehensive clinical materials, including gender, current age, seizure onset age, seizure type and frequency, outcome, response to antiepileptic drugs (AEDs), family history, and results from general and neurological examinations. Brain CT or MRI scans were performed to detect abnormalities in brain structure. Long-term (24 h) video EEGs that included open-close eyes test, hyperventilation, intermittent photic stimulation and sleep recording, were performed and the results were double-reviewed by two qualified researchers. All individuals enrolled were unrelated ethnic Han Chinese with four Han Chinese grandparents, and were born to non-consanguineous Chinese parents. All of subjects were followed up for at least 1 year at epilepsy centers. A total of 468 cases were recruited, including 318 cases with partial epilepsy and 150 cases with generalized epilepsy. Additionally, we recruited 296 healthy Chinese volunteers as a normal control group as our previous report (Wang et al., 2018, 2020, 2021).

All procedures in this study involving human participants have been approved by the ethics committee of the Second Affiliated Hospital of Guangzhou Medical University. Written informed consents have been obtained from all participants or their parents/legal guardians in the case of child or those with intellectual disability.

Whole-Exome Sequencing and Genetic Analysis

The genomic DNAs were extracted from the peripheral blood samples of the probands, their parents, and available family members using the FlexiGene DNA kit (Qiagen). Trio-based whole-exome sequencing was performed on an Illumina HiSeq 2000 sequencing platform as previously reported (Shi et al., 2019; Wang et al., 2021). To obtain high-quality reads, the massive parallel sequencing was performed with more than 125 times average depth and more than 98% coverage in the capture region of the chip. The original read data were aligned to the Genome Reference Consortium Human Genome build 37 (GRCh37) using Burrows-Wheeler alignment (BWA) with default parameters. Variant calling and quality filtration were conducted using the Genome Analysis Toolkit (DePristo et al., 2011).

To derive the whole candidate pathogenic variants in each trio, we adopted a case-by-case analytical approach as previously described (Zhou et al., 2018; Wang et al., 2021). Initially, we removed the common variants presenting a minor allele frequency ≥ 0.005 in the Genome Aggregation Database (gnomAD).[1] We then prioritized potentially pathogenic variants, including frameshift, nonsense, canonical splice site, initiation codon, and missense variants predicted as being damaging *in silico* tools (VarCards).[2] We screened *CACNA1A* mutations with origination of explainable for genetic diseases, including *de novo* mutation, mutation with segregations, and homozygous/compound heterozygous mutation. Additionally, I-Mutant 3.0 program was applied[3] to predict the effect of *CACNA1A* missense variants on protein stability, which was indicated by free energy change (DDG). Negative DDG value means that the mutated protein possesses less stability and vice versa. Eventually, the pathogenicity of the identified *CACNA1A* mutations was evaluated by American College of Medical Genetics and Genomics (ACMG) scoring (Richards et al., 2015). Polymerase chain reaction and sanger sequencing was performed

[1]http://gnomad.broadinstitute.org/

[2]http://varcards.biols.ac.cn/

[3]http://gpcr2.biocomp.unibo.it/cgi/predictors/I-Mutant3.0/I-Mutant3.0.cgi

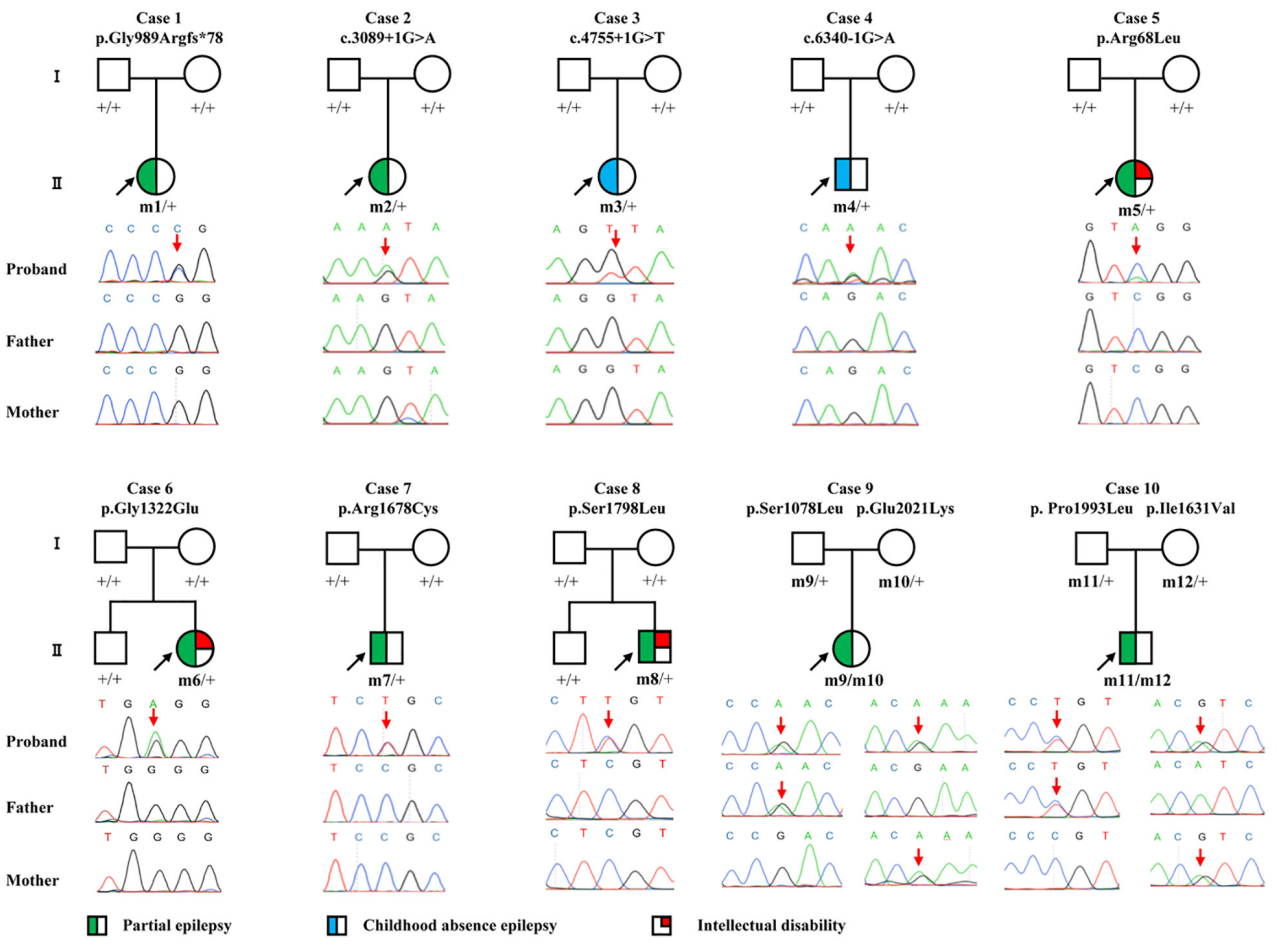

FIGURE 1 | Pedigrees and DNA sequencing chromatograms of the cases with *CACNA1A* mutations. Individuals with heterozygous mutation are indicated by m/ +, those with compound heterozygous mutation are indicated by m/m, and those negative for mutation are indicated by +/ +. The probands are indicated by black arrows. The positions of the mutations are indicated by red arrows. The phenotype of each case is indicated by different symbols in the figure.

to validate the identified potential pathogenic variations by using ABI 3730 sequencing platform (Applied Biosystems, Foster City, CA, United States). All *CACNA1A* mutations identified in this study were annotated to reference transcript NM_001127222.

Genotype-Phenotype Relationship

All *CACNA1A* mutations and related phenotypes were systematically retrieved from the professional edition of Human Gene Mutation Database (HGMD)[4] and the PubMed database[5] up to December 2021. To explore the relationship between genotype and phenotype, we divided the *CACNA1A* mutations into two categories, destructive (null) and missense mutations. Null mutations were those causing gross malformation of the gene/protein and leading to loss of function and haploinsufficiency (Richards et al., 2015; Liu et al., 2020), including truncating mutations (non-sense and frameshifting), splice site mutations (canonical ± 1 or 2), and mutations at initiation codon or with single/multi exon deletion. To facilitate analyzing the effect of molecular sub-regional on epileptic phenotypes, we collected the information on the distribution of *CACNA1A* missense mutations in various regions of the Cav2.1 channel. Considering that epileptic phenotype severity may be associated with mutation origin (*de novo* or inherited), we also collected the inheritance information of epilepsy associated *CACNA1A* mutations.

Statistical Analysis

Statistical analyses were performed in GraphPad Prism version 8.00. A two-tailed Fisher's exact test was used to compare the frequencies of null mutation, missense mutation, and *de novo* mutation between different phenotype groups. The recessive

[4]http://www.hgmd.cf.ac.uk/ac/index.php

[5]http://www.ncbi.nlm.nih.gov/pubmed/

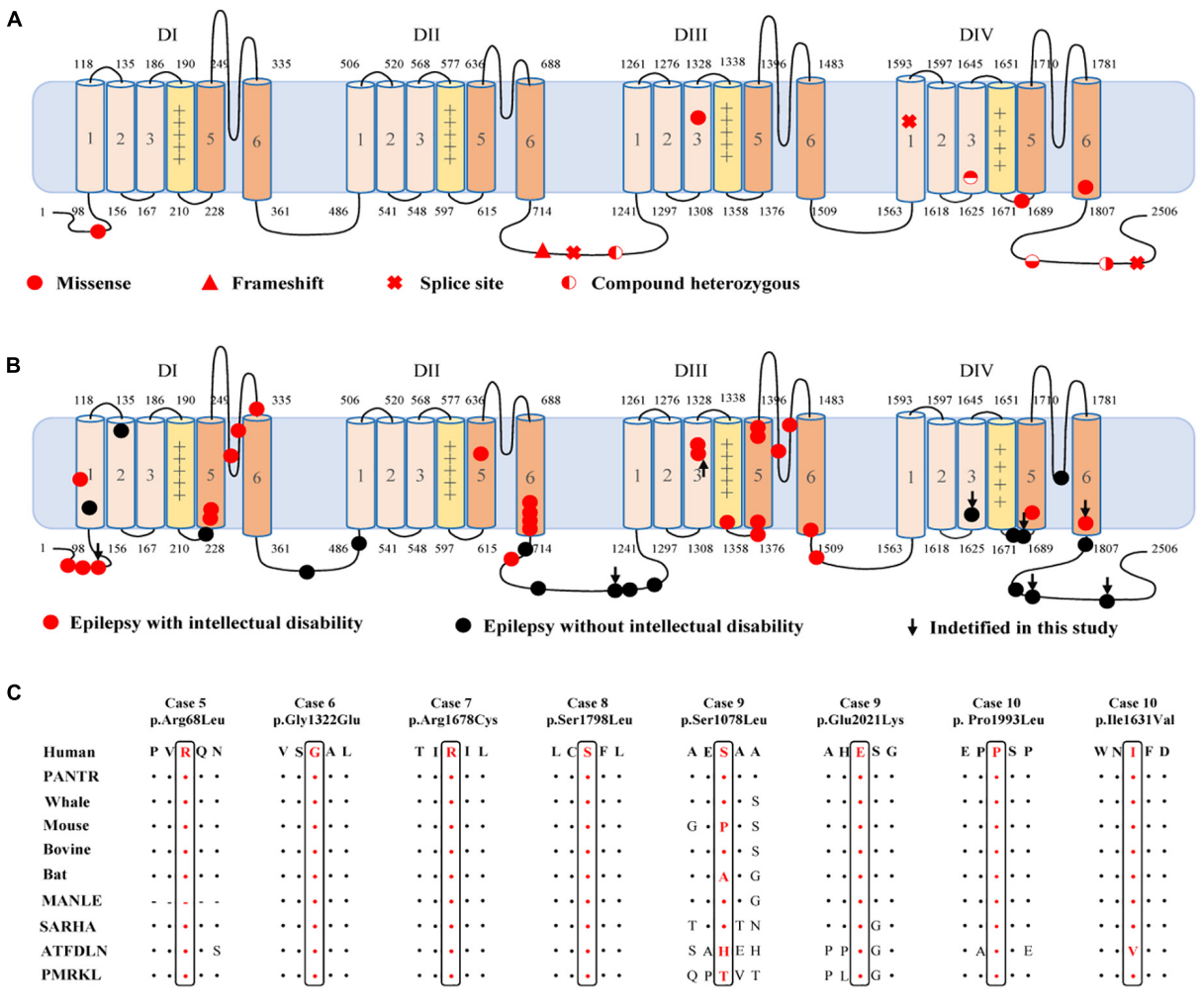

FIGURE 2 | Location of the identified *CACNA1A* mutations in Cav2.1 and amino acid sequence alignment of the missense mutations. **(A)** Schematic illustration of the Cav2.1 protein and the location of the *CACNA1A* mutations identified in this study. **(B)** Schematic illustration of the Cav2.1 protein and the location of the epilepsy-related *CACNA1A* missense mutations. **(C)** Amino acid sequence alignment of the eight missense mutations with protein substitutions show that Arg68, Gly1322, Arg1678, Ser1798, Pro1993, and Glu2021 are highly conserved across species. Ser1078 and Ile1631 show a low degree of conservation.

CACNA1A variants burden was also analyzed according to a recent research (Martin et al., 2018). The cutoff value for statistical significance is 0.05.

RESULTS

Identification of Novel *CACNA1A* Mutations

Twelve *CACNA1A* mutations were identified in ten unrelated cases of epilepsy, including four null mutations (c.2963_2964insG/p.Gly989Argfs*78, c.3089 + 1G > A, c.4755 + 1G > T, and c.6340-1G > A) and eight missense mutations (c.203G > T/p.Arg68Leu, c.3233C > T/p.Ser1078Leu, c.3965G > A/p.Gly1322Glu, c.4891A > G/p.Ile1631Val, c.5032C > T/p.Arg1678Cys, c.5393C > T/p.Ser1798Leu, c.5978C > T/p.Pro1993Leu, and c.6061G > A/p.Glu2021Lys). The Ser1798Leu mutation has previously been described as a *de novo* mutation in a case of EA2 (Ohba et al., 2013), whereas the remained 11 mutations have not been reported and were novel findings. Four of the missense mutations (c.3233C > T/p.Ser1078Leu&c.6061G > A/p.Glu2021Lys and c.4891A > G/p.Ile1631Val&c.5978C > T/p.Pro1993Leu) constituted two pairs of compound heterozygous mutations; the remaining four missense mutations and four null mutations were *de novo* (**Figures 1**, **2** and **Table 1**). The eight *de novo* mutations were neither in gnomAD populations nor in our 296 normal control subjects and were evaluated as pathogenic or likely pathogenic mutations according to the criteria of ACMG (**Table 2**). The two pairs of the compound heterozygous mutations were absent in our 296 normal control subjects and present in gnomAD with an extremely low frequency (**Table 2**). When the recessive variants burden was analyzed, a statistically significant difference of the compound heterozygous *CACNA1A* mutations in this cohort was observed comparing the excepted number by chance in

TABLE 1 | Clinical feature of the individuals with *CACNA1A* mutations.

Case	Mutation (NM_001127222)	Gender	Age	Onset age	Seizure course	Seizure-free duration	Effective AEDs	EEG	Brain imaging	Development	Diagnosis
Case 1	p.Gly989Argfs*78	Female	24 yr	3 yr	SPS, 1–2/mo and up to 2/wk for 9 yr	12 yr	VPA	Diffuse SW, irregular sharp and spike waves	Normal	Normal	PE
Case 2	c.3089 + 1G > A	Female	3 yr	1 yr	1–2/mo for 1 yr	1 yr	VPA	Bilateral occipital SSW	Normal	Normal	PE
Case 3	c.4755 + 1G > T	Female	9 yr	2 yr	FS twice at 2 yr, Ab, 10–20/d from 8 yr to 8.5 yr	0.5 yr	VPA	Ictal: 10 Ab; interictal: paroxysmal 3 HZ SSW.	Normal	Normal	CAE
Case 4	c.6340-1G > A	Male	10 yr	6 yr	Ab, 5–6/d for 2 yr	2 yr	VPA	Paroxysmal generalized 3 Hz SSW	Normal	Normal	CAE
Case 5	p.Arg68Leu	Female	21 yr	11 yr	sGTCS, 1–2/mo for 6 yr	4 yr	VPA, LTG	Right frontal and temporal spikes and FSW	Normal	ID	PE, ID
Case 6	p.Gly1322Glu	Female	4 yr	3 mo	sGTCS and CPS, 3–4/d for 1.5 yr	2 yr	VPA, LTG	Left parietal and temporal sharp waves and FSW	Normal	ID	PE, ID
Case 7	p.Arg1678Cys	Male	13 yr	10 yr	SPS, 1–2/mo for 2 yr	1 yr	OXC	Bilateral occipital sharp waves	Normal	Normal	PE
Case 8	p.Ser1798Leu	Male	5 yr	1.5 yr	sGTCS and CPS, 1–2/mo for 2.5 yr	1 yr	VPA	Bilateral occipital spikes and FSW	Normal	ID	PE, ID
Case 9	p.Ser1078Leu p.Glu2021Lys	Female	7 yr	4 yr	FS once at 4 yr, sGTCS and CPS, 1–4/wk for 2 yr	1 yr	VPA, OXC	Bilateral frontal and central sharp waves	Normal	Normal	PE
Case 10	p.Ile1631Val p.Pro1993Leu	Male	10 yr	1 yr	FS 1–2/yr for 4 yr, CPS once at 7 yr	3 yr	LEV	Left parietal and temporal spikes	Normal	Normal	PE

Ab, absence; AEDs, antiepileptic drugs; CAE, childhood absence epilepsy; CPS, complex partial seizure; d, days; EEG, electroencephalogram; FS, febrile seizure; FSW, focal sharp and slow wave; ID, intellectual disability; LEV, levetiracetam; LTG, lamotrigine; mo, months; OXC, oxcarbazepine; PE, partial epilepsy; sGTCS, secondary generalized tonic-clonic seizure; SPS, simple partial seizure; SSW, spike and slow wave; SW, slow waves; VPA, valproate; wk, weeks; yr, years.

the controls of East Asian and all populations in the Exome Aggregation Consortium ($P = 7.30 \times 10^{-4}$, $P = 2.53 \times 10^{-4}$) (Martin et al., 2018).

The c.2963_2964insG/p.Gly989Argfs*78 mutation was considered to potentially pathogenic by yielding a truncated transcript that gave rise to a non-functional Cav2.1 protein or haploinsufficiency. The three canonical splice site mutations (c.3089 + 1G > A, c.4755 + 1G > T, and c.6340-1G > A) could destroy the original splice donor or acceptor site that generally resulted in the skipping of the single exon or multiexon with consequent translational frameshift. All of the eight missense mutations were predicted to be damaging by at least one of the commonly used *in silico* prediction tools (**Table 2**). The amino acid sequence alignment indicated that Arg68Leu, Gly1322Glu, Arg1678Cys, Ser1798Leu, Pro1993Leu, and Glu2021Lys were located at residues that are highly conserved in various species; Ile1631Val are highly conserved in vertebrates but less so in lower animals (**Figure 2B**). The Ser1078Leu was located at a less conserved site but was predicted to be conserved by GERP (score = 5.17), phyloP (score = 5.429), and SiPhy (score = 17.443). Furthermore, I-Mutant 3.0 program showed that Arg68Leu, Gly1322Glu, Ile1631Val, and Arg1678Cys mutants have a strong influence on protein stability (**Table 2**).

None of the 10 patients had pathogenic or likely pathogenic mutations in the genes known to be associated with epileptic phenotypes (Wang et al., 2017) except *CACNA1A* mutations.

Clinical Features

In this study, we identified *CACNA1A* mutations in 10 unrelated cases. The seizure onset age of the ten cases ranged from 3 months to 11 years old, with a median age of onset of 3.5 years. Eight of the cases were diagnosed as partial epilepsy, including six cases with *de novo* missense/null mutations and two with compound heterozygous missense mutations. They had simple/complex partial seizures or secondarily generalized tonic-clonic seizures. They all had focal epileptic discharges with normal backgrounds or trends of generalization especially during sleep (**Figures 3A,C–E**). The remaining two cases were diagnosed as childhood absence epilepsy and carried two *de novo* canonical splice site mutations. They experienced frequent absence seizures and detected ictal or interictal generalized 3 HZ spike and slow waves on EEG recordings (**Figure 3B**). A patient (case 2) also carried a canonical splice site mutation (c.3089 + 1G > A) and was diagnosed as partial epilepsy, her EEGs presented bilateral occipital epileptic discharges with features of idiopathic epilepsies (**Figure 3A**). These findings indicated that splice site mutations of *CACNA1A* were potentially associated with generalized epilepsies or idiopathic epilepsies. All of the ten cases were ultimately seizure-free after antiepileptic treatment, although frequent epileptic seizures were observed in four cases (Cases 3, 4, 6, and 9; **Table 1**). One patient (Case 3) had antecedent febrile seizures. Three patients had mild intellectual abnormalities (Cases 5, 6, and 8; **Table 1**). All the ten cases were born by normal delivery, and the brain MRI findings were normal. No ataxia or migraine were observed in any of them.

TABLE 2 | Genetic characteristic and ACMG scoring of the *CACNA1A* mutations.

Case no.	Mutation	Inheritance	MAF	MAF-EAS	SIFT[a]	PP2_Var[a]	MutationTaster[a]	M_CAP[a]	DDG (kcal/mol)	ACMG scoring	ACMG pathogenicity
Case 1	p.Gly989Argfs*78	*De novo*	–	–	–	–	–	–	–	PVS1 + PS2 + PM2	Pathogenic
Case 2	c.3089 + 1G > A	*De novo*	–	–	–	–	–	–	–	PVS1 + PS2 + PM2	Pathogenic
Case 3	c.4755 + 1G > T	*De novo*	–	–	–	–	–	–	–	PVS1 + PS2 + PM2	Pathogenic
Case 4	c.6340-1G > A	*De novo*	–	–	–	–	–	–	–	PVS1 + PS2 + PM2	Pathogenic
Case 5	p.Arg68Leu	*De novo*	–	–	0.002 (D)	0.319 (B)	0.999 (D)	0.753 (D)	−0.73	PS2 + PM2 + PP3	Likely pathogenic
Case 6	p.Gly1322Glu	*De novo*	–	–	0.011 (D)	1 (D)	1 (D)	0.687 (D)	−1.47	PS2 + PM2 + PP3	Likely pathogenic
Case 7	p.Arg1678Cys	*De novo*	–	–	0 (D)	1 (D)	1 (D)	0.833 (D)	−0.89	PS2 + PM2 + PP3	Likely pathogenic
Case 8	p.Ser1798Leu	*De novo*	–	–	0 (D)	0.998 (D)	1 (D)	0.794 (D)	−0.15	PS2 + PM2 + PP3	Likely pathogenic
Case 9	p.Ser1078Leu	Paternal	1.4×10^{-5}	2.1×10^{-4}	0.09 (T)	0.057 (B)	1 (P) 1 (D)	0.619 (D)	0.44 0.28	PM2 + PP3 PM2 + PP3	Uncertain significance
	p.Glu2021Lys	Maternal	3.7×10^{-4}	4.8×10^{-3}	0.072 (T)	0.441 (B)		0.25 (D)			
Case 10	p.Pro1993Leu	Paternal	6.1×10^{-6}	-1.9×10^{-3}	0.304 (T)	0.738 (D)	1 (D) 0.997 (D)	0.221 (D)	0.19 −1.17	PM2 + PP3 PM2 + PP3	Uncertain significance
	p.Ile1631Val	Maternal	1.3×10^{-4}		0.58 (T)	0.262 (B)		0.076 (D)			

ACMG, American College of Medical Genetics and Genomics; B, benign; D, damaging; DDG, protein stability indicated by free energy change value; MAF, minor allele frequency from gnomAD; MAF-EAS, minor allele frequency from gnomAD-East Asian population; M_CAP, Mendelian Clinically Applicable Pathogenicity; P, polymorphism; PM2, absent in population databases; PP2_Var, Polyphen2_HVAR; PP3, multiple lines of computational evidence support a deleterious effect on the gene/gene product; PS2, De novo (paternity and maternity confirmed); PVS1, predicted null variant in a gene where loss of function (LOF) is a known mechanism of disease; SIFT, Sorting Intolerant From Tolerant; T, tolerable.

[a]*Typical results of damage effect prediction of the CACNA1A mutations in this table were selected from 23 algorithms in silico missense prediction (http://varcards.biols.ac.cn/).*

**means a premature termination of the protein caused by a frameshift mutation.*

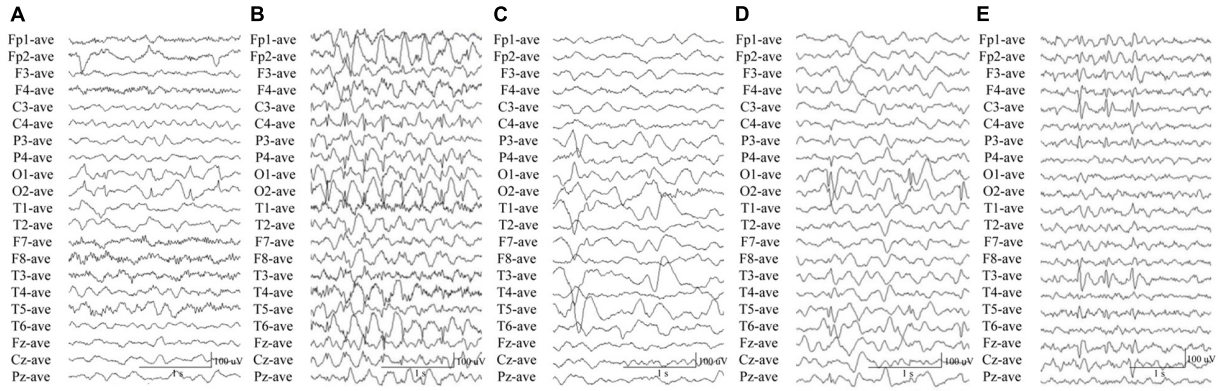

FIGURE 3 | Electroencephalography data of the cases with *CACNA1A* mutations. **(A)** Interictal EEG in case 2 showed bilateral occipital spike and slow waves. **(B)** Interictal EEG in case 4 showed generalized 3 Hz spike and slow waves. **(C)** Interictal EEG in case 6 showed left parietal and temporal sharp waves and focal spike and slow waves. **(D)** Interictal EEG in case 8 showed bilateral occipital spikes and focal spike and slow waves. **(E)** Interictal EEG in case 10 showed left parietal and temporal spikes.

Genotype-Phenotype Correlation

To explore the correlation between genotype and phenotype, we systematically reviewed all reported *CACNA1A* mutations. Previously, 312 mutations have been reported, including 115 null mutations, 183 missense mutations, 10 in-frame insertion/deletion mutations, and 4 (CAG)n dynamic mutations. These mutations were associated with a variety of clinical phenotypes that included EA2, FHM1, SCA6, CSVD (cerebral small vessel disease), and epilepsies. EA2 group present a significantly higher frequency of null mutation than the groups of epilepsy ($P = 7.92 \times 10^{-5}$), FHM1 ($P = 2.85 \times 10^{-5}$), SCA6 ($P = 5.69 \times 10^{-3}$), or CSVD ($P = 3.77 \times 10^{-6}$) (**Figure 4A**).

Cav2.1 encoded by *CACNA1A*, contains four homologous domains (DI-DIV) with six helical transmembrane segments (S1–S6). The S4 segments of each repeat serve as actual voltage sensors while S5 and S6 segments together with S5-S6 loop of each repeat form the channel pore (**Figure 2A**; Striessnig, 2021). In the present study, *de novo* missense mutations, except the Arg68Leu, were all located at pore region or near the voltage sensor region while compound heterozygous missense mutations were mainly located at linker region or C-terminal. We analyzed the data together with that from literature (**Figure 2B**). Previous studies have shown *CACNA1A* mutations potentially have an association with developmental abnormalities (Allen et al., 2013; Damaj et al., 2015; Epi4k Consortium, 2016). In this cohort, three cases of partial epilepsy also have ID. We then analyzed the epilepsies with ID and those without ID (**Supplementary Table 1**). No statistical difference in the frequency of missense was observed between the two epilepsy sub-groups (**Figure 4B**). However, it was found that missense mutations in the epilepsy with ID were more frequently located in the pore region than those in the epilepsy without ID ($P = 1.67 \times 10^{-4}$) (**Figure 4C**), suggesting a molecular sub-region effect. Moreover, the cases in the epilepsy with ID group had a higher percentage of *de novo* mutations than those in the epilepsy without ID ($P = 1.92 \times 10^{-3}$) (**Figure 4D**), suggesting a potential correlation between epileptic phenotype severity and mutation origins.

DISCUSSION

Previous studies have showed that the clinical phenotypes caused by *CACNA1A* mutations comprises a huge group of phenotypic heterogeneity, such as EA2, FHM1, SCA6, and DEE42 that was a severe form of epilepsy (Ophoff et al., 1996; Jodice et al., 1997; Zhuchenko et al., 1997; Terwindt et al., 2002; Jen et al., 2007; Rajakulendran et al., 2012; Allen et al., 2013; Epi4k Consortium, 2016). In the present study, we identified 12 *CACNA1A* mutations in ten cases of mild form of epilepsy, including four *de novo* null mutations, four *de novo* missense mutations, and two pairs of compound heterozygous missense mutations. The eight *de novo* mutations were evaluated as pathogenic or likely pathogenic mutations according to the criteria of ACMG (**Table 2**). Although both of the compound heterozygous missense mutations were evaluated as uncertain significance, the frequencies of the recessive *CACNA1A* mutations identified in this cohort were significantly higher than that in the controls of East Asian and all populations. This study suggested that *CACNA1A* gene is potentially associated with epilepsy. The patients with *CACNA1A* mutations may present epilepsy without ataxia or migraine. The spectrum of epileptic phenotypes potentially ranged from the mild form of epilepsies such as absence epilepsy or partial epilepsy, to the severe form of developmental epileptic encephalopathy.

The *CACNA1A* gene is predominantly expressed in neuron and plays a critical role in membrane excitability and neurotransmission release (Diriong et al., 1995; Kramer et al., 1995; Teh et al., 1995). *Cacna1a* knockout mouse model exhibited ataxia and epilepsy seizures.[6] The clinical phenotypes caused by *CACNA1A* mutations were highly concordant with that of *Cacna1a* knockout mouse model. Thus, *CACNA1A* loss of function may be the potentially pathogenic mechanism. *CACNA1A* mutations identified in this study included four null mutations and two compound heterozygous mutations

[6]http://www.informatics.jax.org/marker/MGI:109482

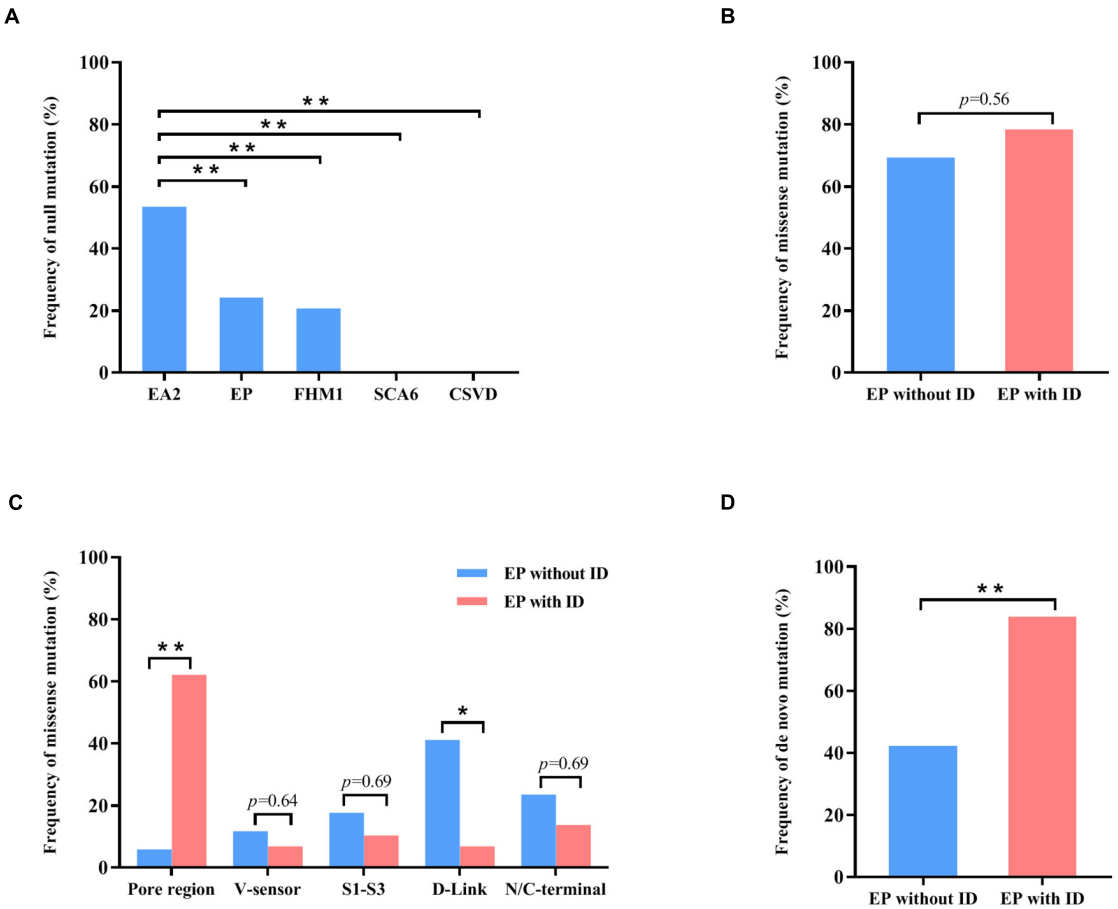

FIGURE 4 | Genotype–phenotype correlations of *CACNA1A* mutations. **(A)** The frequency of null mutations in *CACNA1A* for each phenotype. The values are expressed as the percentage of cases with null mutations (cases with null mutations/total cases) in each group. **(B)** The frequency of null mutations in *CACNA1A* for epilepsy without intellectual disability and epilepsy with intellectual disability. **(C)** The frequency of missense mutants in various regions of the Cav2.1 channel for epilepsy and epilepsy with intellectual disability. **(D)** The frequency of de novo mutations in *CACNA1A* for epilepsy and epilepsy with intellectual disability. Fisher's exact test was used for statistical analysis of the differences between each group. CSVD, cerebral small vessel disease (n = 18). EA2, episodic ataxia 2 (n = 155). EP, epilepsy (n = 63). EP without ID, epilepsy without intellectual disability (n = 26). EP with ID, epilepsy with intellectual disability (n = 37). FHM1, familial hemiplegic migraine 1 (n = 53). SCA6, spinocerebellar ataxia 6 (n = 7). * $P < 0.05$; ** $P < 0.01$.

that were potentially associated with a loss of function. The remaining four *de novo* missense mutations with protein substitution were located at the most highly conserved residue in the protein sequence alignments. The Gly1322Glu, Arg1678Cys, and Ser1798Leu mutants were located at pore region or near the voltage sensor region. The Arg68Leu and Gly1322Glu mutants have a strong influence on protein stability (**Table 2**). Therefore, the four *de novo* missense mutations were also considered to be potentially deleterious because of the possibility of giving rise to alteration of the structure of pore region/voltage sensor region or influencing the protein stability. However, the accurate functional consequence of the newly identified missense mutations was unknown. Previous studies have shown that *SCN1A* missense mutations in the pore region were characterized by loss of function (Meng et al., 2015). Currently, data on functional alteration of *CACNA1A* mutations is limited and did not permit a conclusion. Functional alteration of other type, such as gain of function, could not be excluded. Hence, the correlation between functional consequence and location of *CACNA1A* mutations warrants further studies.

Cav2.1 encoded by *CACNA1A*, is the pore-forming alpha-1A subunit of VGCC and contains four homologous domains (DI-DIV) with six helical transmembrane segments (S1–S6) (**Figure 2A**; Striessnig, 2021). Previously, *CACNA1A* have been established an association with DEE42 (Allen et al., 2013; Epi4k Consortium, 2016). In the present study, we identified *CACNA1A* mutations in the cases with relatively mild epilepsies. Most of the mutations were null mutations or in the pore-regions that would cause loss of function. The four missense mutations constituted two pairs of compound heterozygous mutations that were located at linker region or C-terminal. While single heterozygous variant was not pathogenic, the compound heterozygous mutations became potentially pathogenic. Our further analyses showed that missense mutations in the epilepsy with ID were more frequently located in the pore region than those in the epilepsy without ID. These findings potentially suggested a molecular sub-region

effect. This was also supported by a recent study that showed missense mutations located in the pore region were associated with severe epileptic encephalopathy, in spite of the difference in functional alteration (Jiang et al., 2019). Besides, two of splice site mutations were associated with generalized epilepsies characterized by absence seizures, suggesting a possible genotype-phenotype association that warrants further verification.

Previously, *CACNA1A* mutations were mainly associated with paroxysmal diseases such as EA2. The Ser1798Leu mutation identified in this study (case 8 with epilepsy) has been previously reported in a case of episodic ataxia 2 (EA2) (Ohba et al., 2013). Experiments in animals showed that *Cacna1a* knockout caused ataxia and epilepsy seizures (Pietrobon, 2005). The present study demonstrated that EA2 was more frequently associated with null mutations than epilepsy. However, it is unknown why the same mutation was associated with different phenotypes. Previous studies in *Cacna1a* knockout mice have indicated that loss of Cav2.1 channel would probably affect the function of other voltage-gated calcium channels (Reinson et al., 2016), which added one more factor on the expression of phenotype. Other mechanisms, such as genetic background and interactive genes, should be studied further.

In summary, we identified *CACNA1A* mutations in ten unrelated cases with relatively mild and pure epilepsy. All patients had favorable outcome with antiepileptic treatment without ataxia or migraine. Further analysis showed the clinical phenotypes variability is potentially associated with mutation type, molecular sub-regional effect, and inheritance pattern, which would help understanding the mechanism underlying phenotypical heterogeneity.

DATA AVAILABILITY STATEMENT

The datasets presented in this study can be found in online repositories. The names of the repository/repositories and accession number(s) can be found in the article/ **Supplementary Material**.

ETHICS STATEMENT

The studies involving human participants were reviewed and approved by Ethics Committee of the Second Affiliated Hospital of Guangzhou Medical University. Written informed consent to participate in this study was provided by the participants' legal guardian/next of kin. Written informed consent was obtained from the individual(s), and minor(s)' legal guardian/next of kin, for the publication of any potentially identifiable images or data included in this article.

AUTHOR CONTRIBUTIONS

X-LL and JW designed the study. Z-JL, X-YL, D-TL, C-FC, MJ, BL, NH, B-ML, W-JB, X-QT, HL, and Y-HY completed the recruitment of the patients and the analysis of the clinical data. L-DG, Y-WS, and JW completed the analysis of the genetic data. C-FC and Z-JL prepared the figures. X-LL and JW wrote the manuscript. Y-HY revised the manuscript. All authors have read and approved the final manuscript.

FUNDING

This work was funded by the National Natural Science Foundation of China (Grant Nos. 81971216, 81870903, and 82171439), the Guangdong Basic and Applied Basic Research Foundation (Grant Nos. 2020A1515011048, 2021A1515010986, and 2021A1515111064), and the Science and Technology Project of Guangzhou (Grant Nos. 201904010292, 202102021059, and 202102021063). The funders had no role in study design, data collection and analysis, and decision to publish or preparation of the manuscript.

ACKNOWLEDGMENTS

We are deeply grateful to the families who participated in this research.

SUPPLEMENTARY MATERIAL

The Supplementary Material for this article can be found online at: https://www.frontiersin.org/articles/10.3389/fnmol.2022.860662/full#supplementary-material

REFERENCES

Allen, A. S., Berkovic, S. F., Cossette, P., Delanty, N., Dlugos, D., Eichler, E. E., et al. (2013). De novo mutations in epileptic encephalopathies. *Nature* 501, 217–221. doi: 10.1038/nature12439

Damaj, L., Lupien-Meilleur, A., Lortie, A., Riou, É, Ospina, L. H., Gagnon, L., et al. (2015). CACNA1A haploinsufficiency causes cognitive impairment, autism and epileptic encephalopathy with mild cerebellar symptoms. *Eur. J. Hum. Genet.* 23, 1505–1512. doi: 10.1038/ejhg.2015.21

DePristo, M. A., Banks, E., Poplin, R., Garimella, K. V., Maguire, J. R., Hartl, C., et al. (2011). A framework for variation discovery and genotyping using next-generation DNA sequencing data. *Nat. Genet.* 43, 491–498. doi: 10.1038/ng.806

Diriong, S., Lory, P., Williams, M. E., Ellis, S. B., Harpold, M. M., and Taviaux, S. (1995). Chromosomal localization of the human genes for alpha 1A, alpha 1B, and alpha 1E voltage-dependent Ca2+ channel subunits. *Genomics* 30, 605–609. doi: 10.1006/geno.1995.1284

Du, X., Chen, Y., Zhao, Y., Luo, W., Cen, Z., and Hao, W. (2017). Dramatic response to pyridoxine in a girl with absence epilepsy with ataxia caused by a de novo CACNA1A mutation. *Seizure* 45, 189–191. doi: 10.1016/j.seizure.2016.12.020

Epi4k Consortium (2016). De novo mutations in SLC1A2 and CACNA1A are important causes of epileptic encephalopathies. *Am. J. Hum. Genet.* 99, 287–298. doi: 10.1016/j.ajhg.2016.06.003

Helbig, K. L., Farwell Hagman, K. D., Shinde, D. N., Mroske, C., Powis, Z., Li, S., et al. (2016). Diagnostic exome sequencing provides a molecular diagnosis for a significant proportion of patients with epilepsy. *Genet. Med.* 18, 898–905. doi: 10.1038/gim.2015.186

Imbrici, P., Jaffe, S. L., Eunson, L. H., Davies, N. P., Herd, C., Robertson, R., et al. (2004). Dysfunction of the brain calcium channel CaV2.1 in absence epilepsy

and episodic ataxia. *Brain* 127(Pt 12), 2682–2692. doi: 10.1093/brain/awh301

Jen, J. C., Graves, T. D., Hess, E. J., Hanna, M. G., Griggs, R. C., and Baloh, R. W. (2007). Primary episodic ataxias: diagnosis, pathogenesis and treatment. *Brain* 130(Pt 10), 2484–2493. doi: 10.1093/brain/awm126

Jiang, X., Raju, P. K., D'Avanzo, N., Lachance, M., Pepin, J., Dubeau, F., et al. (2019). Both gain-of-function and loss-of-function de novo CACNA1A mutations cause severe developmental epileptic encephalopathies in the spectrum of Lennox-Gastaut syndrome. *Epilepsia* 60, 1881–1894. doi: 10.1111/epi.16316

Jodice, C., Mantuano, E., Veneziano, L., Trettel, F., Sabbadini, G., Calandriello, L., et al. (1997). Episodic ataxia type 2 (EA2) and spinocerebellar ataxia type 6 (SCA6) due to CAG repeat expansion in the CACNA1A gene on chromosome 19p. *Hum. Mol. Genet.* 6, 1973–1978. doi: 10.1093/hmg/6.11.1973

Klassen, T., Davis, C., Goldman, A., Burgess, D., Chen, T., Wheeler, D., et al. (2011). Exome sequencing of ion channel genes reveals complex profiles confounding personal risk assessment in epilepsy. *Cell* 145, 1036–1048. doi: 10.1016/j.cell.2011.05.025

Kramer, P. L., Yue, Q., Gancher, S. T., Nutt, J. G., Baloh, R., Smith, E., et al. (1995). A locus for the nystagmus-associated form of episodic ataxia maps to an 11-cM region on chromosome 19p. *Am. J. Hum. Genet.* 57, 182–185.

Lee, C. G., Lee, J., and Lee, M. (2018). Multi-gene panel testing in Korean patients with common genetic generalized epilepsy syndromes. *PLoS One* 13:e0199321. doi: 10.1371/journal.pone.0199321

Liu, L., Chen, Z.-R., Xu, H.-Q., Liu, D.-T., Mao, Y., Liu, H.-K., et al. (2020). DEPDC5 variants associated malformations of cortical development and focal epilepsy with febrile seizure plus/febrile seizures: the role of molecular sub-regional effect. *Front. Neurosci.* 14:821. doi: 10.3389/fnins.2020.00821

Martin, H. C., Jones, W. D., McIntyre, R., Sanchez-Andrade, G., Sanderson, M., Stephenson, J. D., et al. (2018). Quantifying the contribution of recessive coding variation to developmental disorders. *Science* 362, 1161–1164. doi: 10.1126/science.aar6731

Meng, H., Xu, H. Q., Yu, L., Lin, G. W., He, N., Su, T., et al. (2015). The SCN1A mutation database: updating information and analysis of the relationships among genotype, functional alteration, and phenotype. *Hum. Mutat.* 36, 573–580. doi: 10.1002/humu.22782

Ohba, C., placeCityOsaka, H., Iai, M., Yamashita, S., Suzuki, Y., Aida, N., et al. (2013). Diagnostic utility of whole exome sequencing in patients showing cerebellar and/or vermis atrophy in childhood. *Neurogenetics* 14, 225–232. doi: 10.1007/s10048-013-0375-378

Ophoff, R. A., Terwindt, G. M., Vergouwe, M. N., van Eijk, R., Oefner, P. J., Hoffman, S. M., et al. (1996). Familial hemiplegic migraine and episodic ataxia type-2 are caused by mutations in the Ca2+ channel gene CACNL1A4. *Cell* 87, 543–552. doi: 10.1016/s0092-8674(00)81373-81372

Pietrobon, D. (2005). Function and dysfunction of synaptic calcium channels: insights from mouse models. *Curr. Opin. Neurobiol.* 15, 257–265. doi: 10.1016/j.conb.2005.05.010

Rajakulendran, S., Kaski, D., and Hanna, M. G. (2012). Neuronal P/Q-type calcium channel dysfunction in inherited disorders of the CNS. *Nat. Rev. Neurol.* 8, 86–96. doi: 10.1038/nrneurol.2011.228

Reinson, K., Õiglane-Shlik, E., Talvik, placeI., Vaher, U., Õunapuu, A., Ennok, M., et al. (2016). Biallelic CACNA1A mutations cause early onset epileptic encephalopathy with progressive cerebral, cerebellar, and optic nerve atrophy. *Am. J. Med. Genet. A* 170, 2173–2176. doi: 10.1002/ajmg.a.37678

Richards, S., Aziz, N., Bale, S., Bick, D., Das, S., Gastier-Foster, J., et al. (2015). Standards and guidelines for the interpretation of sequence variants: a joint consensus recommendation of the american college of medical genetics and genomics and the association for molecular pathology. *Genet. Med.* 17, 405–424. doi: 10.1038/gim.2015.30

Shi, Y. W., Zhang, Q., Cai, K., Poliquin, S., Shen, W., Winters, N., et al. (2019). Synaptic clustering differences due to different GABRB3 mutations cause variable epilepsy syndromes. *Brain* 142, 3028–3044. doi: 10.1093/brain/awz250

Striessnig, J. (2021). Voltage-Gated Ca(2+)-Channel α1-Subunit de novo missense mutations: gain or loss of function - implications for potential therapies. *Front. Synaptic Neurosci.* 13:634760. doi: 10.3389/fnsyn.2021.634760

Teh, B. T., Silburn, P., Lindblad, K., Betz, R., Boyle, R., Schalling, M., et al. (1995). Familial periodic cerebellar ataxia without myokymia maps to a 19-cM region on 19p13. *Am. J. Hum. Genet.* 56, 1443–1449.

Terwindt, G., Kors, E., Haan, J., Vermeulen, F., Van den Maagdenberg, A., Frants, R., et al. (2002). Mutation analysis of the CACNA1A calcium channel subunit gene in 27 patients with sporadic hemiplegic migraine. *Arch. Neurol.* 59, 1016–1018. doi: 10.1001/archneur.59.6.1016

Tuluc, P., Theiner, T., Jacobo-Piqueras, N., and Geisler, S. M. (2021). Role of high Voltage-Gated Ca(2+) channel subunits in pancreatic β-cell insulin release. from structure to function. *Cells* 10:2004. doi: 10.3390/cells10082004

Wang, J. Y., Zhou, P., Wang, J., Tang, B., Su, T., Liu, X. R., et al. (2018). ARHGEF9 mutations in epileptic encephalopathy/intellectual disability: toward understanding the mechanism underlying phenotypic variation. *Neurogenetics* 19, 9–16. doi: 10.1007/s10048-017-0528-522

Wang, J., Lin, Z. J., Liu, L., Xu, H. Q., Shi, Y. W., Yi, Y. H., et al. (2017). Epilepsy-associated genes. *Seizure* 44, 11–20. doi: 10.1016/j.seizure.2016.11.030

Wang, J., Poliquin, S., Mermer, F., Eissman, J., Delpire, E., Wang, J., et al. (2020). Endoplasmic reticulum retention and degradation of a mutation in SLC6A1 associated with epilepsy and autism. *Mol. Brain* 13:76. doi: 10.1186/s13041-020-00612-616

Wang, J., Qiao, J. D., Liu, X. R., Liu, D. T., Chen, Y. H., Wu, Y., et al. (2021). UNC13B variants associated with partial epilepsy with favourable outcome. *Brain* 144, 3050–3060. doi: 10.1093/brain/awab164

Zhou, P., He, N., Zhang, J. W., Lin, Z. J., Wang, J., Yan, L. M., et al. (2018). Novel mutations and phenotypes of epilepsy-associated genes in epileptic encephalopathies. *Genes Brain Behav.* 17:e12456. doi: 10.1111/gbb.12456

Zhuchenko, O., Bailey, J., Bonnen, P., Ashizawa, T., Stockton, D. W., Amos, C., et al. (1997). Autosomal dominant cerebellar ataxia (SCA6) associated with small polyglutamine expansions in the alpha 1A-voltage-dependent calcium channel. *Nat. Genet.* 15, 62–69. doi: 10.1038/ng0197-62

Conflict of Interest: The authors declare that the research was conducted in the absence of any commercial or financial relationships that could be construed as a potential conflict of interest.

Publisher's Note: All claims expressed in this article are solely those of the authors and do not necessarily represent those of their affiliated organizations, or those of the publisher, the editors and the reviewers. Any product that may be evaluated in this article, or claim that may be made by its manufacturer, is not guaranteed or endorsed by the publisher.

frontiers | Frontiers in Molecular Neuroscience

ORIGINAL RESEARCH
published: 06 May 2022
doi: 10.3389/fnmol.2022.889534

ATP6V0C Is Associated With Febrile Seizures and Epilepsy With Febrile Seizures Plus

Yang Tian[1†], Qiong-Xiang Zhai[2†], Xiao-Jing Li[1†], Zhen Shi[1], Chuan-Fang Cheng[3,4], Cui-Xia Fan[3,4], Bin Tang[3,4], Ying Zhang[5], Yun-Yan He[3,4], Wen-Bin Li[3,4], Sheng Luo[3,4], Chi Hou[1], Wen-Xiong Chen[1] Wei-Ping Liao[3,4] and Jie Wang[3,4]* for the China Epilepsy Gene 1.0 Project*

[1] Department of Neurology, Guangzhou Women and Children's Medical Center, Guangzhou Medical University, Guangzhou, China, [2] Department of Pediatrics, Guangdong Provincial People's Hospital, Guangdong Academy of Medical Sciences, Guangzhou, China, [3] Department of Neurology, Institute of Neuroscience, The Second Affiliated Hospital of Guangzhou Medical University, Guangzhou, China, [4] Key Laboratory of Neurogenetics and Channelopathies of Guangdong Province, Ministry of Education of China, Guangzhou, China, [5] The Seventh Affiliated Hospital, Sun Yat-sen University, Shenzhen, China

OPEN ACCESS

Edited by:
Rossella Di Giaimo, University of Naples Federico II, Italy

Reviewed by:
Gaetano Terrone, University of Naples Federico II, Italy
Joonhong Park, Chonbuk National University Hospital, South Korea

***Correspondence:**
Jie Wang
wangjie2014010@163.com
Wen-Xiong Chen
chenwenxiong@gwcmc.org

† These authors have contributed equally to this work

Specialty section:
This article was submitted to Molecular Signalling and Pathways, a section of the journal Frontiers in Molecular Neuroscience

Received: *04 March 2022*
Accepted: *12 April 2022*
Published: *06 May 2022*

Citation:
Tian Y, Zhai Q-X, Li X-J, Shi Z, Cheng C-F, Fan C-X, Tang B, Zhang Y, He Y-Y, Li W-B, Luo S, Hou C, Chen W-X, Liao W-P and Wang J (2022) ATP6V0C Is Associated With Febrile Seizures and Epilepsy With Febrile Seizures Plus. Front. Mol. Neurosci. 15:889534. doi: 10.3389/fnmol.2022.889534

Purpose: To identify novel genetic causes of febrile seizures (FS) and epilepsy with febrile seizures plus (EFS+).

Methods: We performed whole-exome sequencing in a cohort of 32 families, in which at least two individuals were affected by FS or EFS+. The probands, their parents, and available family members were recruited to ascertain whether the genetic variants were co-segregation. Genes with repetitively identified variants with segregations were selected for further studies to define the gene-disease association.

Results: We identified two heterozygous *ATP6V0C* mutations (c.64G > A/p.Ala22Thr and c.361_373del/p.Thr121Profs*7) in two unrelated families with six individuals affected by FS or EFS+. The missense mutation was located in the proteolipid c-ring that cooperated with a-subunit forming the hemichannel for proton transferring. It also affected the hydrogen bonds with surround residues and the protein stability, implying a damaging effect. The frameshift mutation resulted in a loss of function by yielding a premature termination of 28 residues at the C-terminus of the protein. The frequencies of *ATP6V0C* mutations identified in this cohort were significantly higher than that in the control populations. All the six affected individuals suffered from their first FS at the age of 7–8 months. The two probands later manifested afebrile seizures including myoclonic seizures that responded well to lamotrigine. They all displayed favorable outcomes without intellectual or developmental abnormalities, although afebrile seizures or frequent seizures occurred.

Conclusion: This study suggests that *ATP6V0C* is potentially a candidate pathogenic gene of FS and EFS+. Screening for *ATP6V0C* mutations would help differentiating patients with Dravet syndrome caused by *SCN1A* mutations, which presented similar clinical manifestation but different responses to antiepileptic treatment.

Keywords: *ATP6V0C*, loss of function, febrile seizures, epilepsy with febrile seizures plus, whole-exome sequencing

INTRODUCTION

ATP6V0C (OMIM*108745), located at chromosomal locus 16p13.3 and spans approximately 6 kb of genomic DNA, is highly expressed in the brain, predominantly in the brain cortex across whole lifespan.[1] It encodes a 155-amino acid H+ transport protein ATP6V0C that widely distributed in lysosomes, endosomes, Golgi-derived vesicles, secretory vesicles, and plasma membrane for some cell types (Toei et al., 2010). ATP6V0C is the c-subunit of the V0 domain of vacuolar ATPase (V-ATPase) that primarily mediates acidification of eukaryotic intracellular organelles and is necessary for numerous intracellular processes including protein sorting, zymogen activation, receptor-mediated endocytosis, and synaptic vesicle proton gradient generation (Morel, 2003). As a component of V0 domain of V-ATPase, ATP6V0C forms the proteolipid c-ring of the V-ATPase and plays a pivotal role in synaptic vesicle proton gradient generation and regulation of intra and extracellular *pH* value (Higashida et al., 2017; Xu et al., 2019). Experiments in zebrafish ortholog revealed that *ATP6V0C2* is associated with neurotransmitter storage/secretion and involved in the control of neuronal excitability (Chung et al., 2010). Homozygous *ATP6V0C* knockout mice exhibit neonatal lethality, abnormal embryonic tissue morphology, and failure of zygotic cell division.[2] However, the relationship between *ATP6V0C* variants and human disease remains to be explored.

Febrile seizures (FS) are the most frequent convulsion events in childhood and represent the majority of childhood seizures with an incidence as high as 4–10% (Hackett et al., 1997; Gupta, 2016; Smith et al., 2019). These patients have five to seven times higher risk of developing subsequent afebrile seizures (epilepsy with febrile seizures plus, EFS+), compared to the general population (Annegers et al., 1987; Hedera et al., 2006). Etiologically, FS and EFS+ cases are usually cryptogenic without any secondary causes, implying potential associations with genetic factors. Several genes have been reported to be associated with FS or EFS+, including *ADGRV1*, *CHD2*, *CPA6*, *DEPDC5*, *DYRK1A*, *FGF13*, *GABRA1*, *GABRB3*, *GABRD*, *GABRG2*, *HCN1*, *HCN2*, *IMPA2*, *NPRL3*, *PCDH19*, *PRRT2*, *SCN1A*, *SCN1B*, *SCN2A*, *SCN9A*, *SLC12A5*, *SLC32A1*, *SRP9*, *STX1B*, *STXBP1*, and *YWHAG* (OMIM[3]) (Carvill et al., 2014; Rigbye et al., 2016; Deng et al., 2018; Liu et al., 2020; Heron et al., 2021; Ye et al., 2021). However, the genetic causes in most of the patients with FS or EFS+ remain to be elucidated.

In this study, we employed a whole-exome sequencing approach for discovery novel genetic causes in a cohort of familial cases with FS or EFS+. We identified two heterozygous *ATP6V0C* mutations that co-segregated with the disease in two unrelated families with six individuals affected.

[1]https://www.gtexportal.org/home/

[2]http://www.informatics.jax.org/marker/MGI:88116

[3]https://www.omim.org/

MATERIALS AND METHODS

Patients

A cohort of 32 families, in which at least two individuals were affected by FS or EFS+, were recruited. The patients were from the Departments of Neurology, Guangzhou Women and Children's Medical Center and Guangdong Provincial People's Hospital since June 2018 to April 2021.

Clinical data of the affected individuals were comprehensively collected, including present age, gender, age at seizure onset, seizure course, complete family history, response to antiseizure medications, and general and neurological examination results. Brain Magnetic resonance imaging (MRI) scans were performed to exclude abnormalities in brain structure. Video-electroencephalography (EEG) monitoring records, including hyperventilation, intermittent photic stimulation, open-close eyes test, and sleeping recording, were collected and reviewed by two qualified investigators. Epileptic seizures and epilepsy syndromes were diagnosed and classified according to Commission on Classification and Terminology of the Commission on Classification and Terminology of the International League Against Epilepsy (2010, 1989), Engel and International League Against Epilepsy (ILAE) (2001), Berg et al. (2010), and Scheffer et al. (2017). FS and EFS+ was diagnosed as that previously study described (Ye et al., 2021). The patients, their parents, and other affected family members were screened for genetic variants by the whole-exome sequencing. A cohort of 296 healthy Chinese volunteers were recruited as a control group. This study was approved by the ethics committee of Guangzhou Women and Children's Medical Center and the ethics committee of Guangdong General Hospital. Written informed consent was obtained from the patient's guardian.

Whole-Exome Sequencing and Genetic Analysis

Whole blood samples were collected from the probands, their parents, and available family members to ascertain whether the genetic variants were co-segregation. Qiagen Flexi Gene DNA kit (Qiagen, Hilden, Germany) was used to extract genomic DNA from the whole blood samples. Whole-exome sequencing was performed on an Illumina HiSeq 2000 system by Beijing Genomics Institute (BGI) (Shenzhen, China) as previously described (Wang et al., 2018, 2021; Shi et al., 2019). The sequencing data were generated by massive parallel sequencing with more than 125 times average depth and more than 98% coverage in the capture region of the chip, which fulfills the high-quality criteria. Then, the raw data were aligned to the Genome Reference Consortium Human Genome build 37 (GRCh37) by Burrows–Wheeler alignment. Single-nucleotide point variants and indels were called with the Genome Analysis Toolkit. To obtain the comprehensive list of candidate pathogenic variants in each family, we adopted a case-by-case analytical pattern. We first removed the common variants with a minor allele frequency > 0.005 in Genome Aggregation

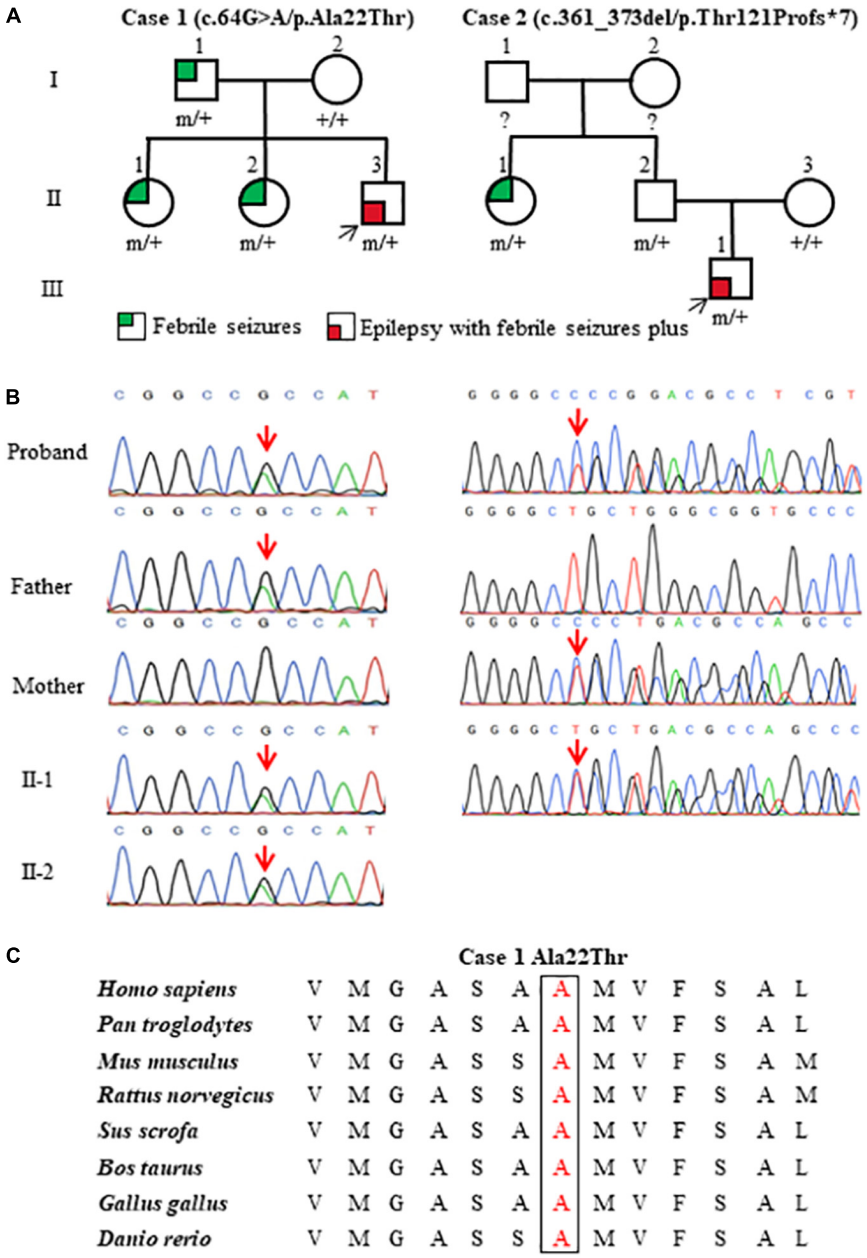

FIGURE 1 | Genetic data of cases with *ATP6V0C* mutations. **(A)** Pedigrees of the two families with *ATP6V0C* mutations and their corresponding phenotypes. Individuals with mutation are marked as m/+, and those without mutation are marked as +/+. **(B)** DNA sequencing chromatograms of the two families with *ATP6V0C* mutations. Red arrows indicate the positions of the mutations. **(C)** Amino acid sequence alignment of the missense mutation shows that residue Ala22 is highly conserved in various species.

Database (gnomAD). We then prioritized functional variants (protein-altering) including frameshift, nonsense, canonical splice site, initiation codon, and missense variants predicted as being damaging or probably damaging by *in silico* tools.[4] Finally, we applied a co-segregation analysis model to screen for possibly disease-causing variants in each family. To identify novel epilepsy-associated gene, we put the known epilepsy-associated genes aside. Genes with repetitively identified variants with segregations were selected for further studies to define the gene-disease association. *ATP6V0C* appeared as one of the candidate genes with recurrent variants in this cohort. PCR-Sanger sequencing was performed to validate the candidate pathogenic variants on ABI 3730 sequencer (Applied Biosystems, Foster City, CA, United States). All *ATP6V0C* variants identified in this study were annotated to reference transcript NM_001694.

[4]http://varcards.biols.ac.cn/

Molecular Structural Analysis

To explore the effect of the *ATP6V0C* missense variant on protein structure, we performed protein models using Phyre2[5] and AlphaFold.[6] The three-dimensional (3D) structures of protein model were analyzed and visualized by PyMOL 2.3.[7] In addition, we applied I-Mutant 3.0 program to predict the effect of the missense variant on protein stability.[8] The alteration of the protein stability was assessed by the free energy change value (DDG, Kcal/mol). Negative DDG value means that the mutated protein possesses less stability and vice versa.

Statistical Analysis

An aggregate analysis for *ATP6V0C* variants was performed in GraphPad Prism 7.00. The two-tailed Fisher's exact test was applied to compare the frequency of *ATP6V0C* variants in this cohort with that in the control populations of gnomAD and our 296 normal control subjects. The cutoff value for statistical significance is 0.05.

RESULTS

Identification of *ATP6V0C* Variants

Two heterozygous variants in the *ATP6V0C* gene (OMIM*108745) were identified in two unrelated families with FS or EFS+, including one missense variant (c.64G > A/p.Ala22Thr) and one frameshift variant (c.361_373del/p.Thr121Profs*7) (**Figures 1A,B**). The c.64G > A/p.Ala22Thr variant was identified in a family with four affected individuals, in which the variant co-segregated with the phenotypes. The c.361_373del/p.Thr121Profs*7 variant was detected in family 2 with two affected individuals. The missense variant (c.64G > A/p.Ala22Thr) was predicted to be damaging or probably damaging by 14 out of 21 commonly used *in silico* prediction tools (**Supplementary Table 1**). The amino acid sequence alignment indicated that the Ala22Thr variant was located at a residue that is highly conserved across various species (**Figure 1C**). The c.361_373del/p.Thr121Profs*7 variant was considered as potentially pathogenic, which introduced a translational frameshift transcript that gave rise to a non-functional ATP6V0C protein or haploinsufficiency.

The two *ATP6V0C* variants were not observed in any public databases (including 1000 Genomes Project, Exome Sequencing Project, and gnomAD), neither in our 296 normal control subjects. Statistical analyses were performed to compare the frequencies of *ATP6V0C* variants in this cohort and control populations of gnomAD and the 296 normal subjects. Two mutant alleles in a total of 64 alleles (32 cases) were identified in this cohort. Statistically significant differences were observed in aggregate frequencies of the mutant alleles between this cohort and the controls of gnomAD-East Asian, gnomAD-all population, and our 296-normal control cohort (2/64 vs. 0/19750, $p = 1.03 \times 10^{-5}$; 2/64 vs. 0/280788, $p = 5.11 \times 10^{-8}$; 2/64 vs. 0/592, $p = 9.38 \times 10^{-3}$, respectively) (**Table 1**).

In the two families, we did not identify pathogenic or likely pathogenic variants in the 977 genes known to be associated with epileptic seizures (Wang et al., 2017).

Effect of the Missense Mutation on Molecular Structure

ATP6V0C protein is the c-subunit of the V0 domain of V-ATPase that is composed of a cytosolic V1 domain and a transmembrane V0 domain and functions as an ATP-dependent proton pump (Higashida et al., 2017; Xu et al., 2019; Wang et al., 2020). The proteolipid c-ring that cooperated with a-subunit forming the hemichannel for proton transfer was comprised of nine c-subunits and one b-subunit (**Figures 2A,B**). The c-subunit, also known as V-ATPase 16 kDa proteolipid subunit and encoded by *ATP6V0C,* is composed of five topological domains and four transmembrane domains[9] (**Figures 2C,D**). Three topological domains (1–10, 77–92, and 153–155) are located within the lumen. The remaining two topological domains (34–55 and 115–131) are located within the cytoplasm. Four helical domains (11–33, 56–76, 93–114, and 132–152) are transmembrane. The Ala22Thr mutation was located in the first transmembrane segment of ATP6V0C protein (**Figures 2C,D**). The three-dimensional (3D) structure of the c-subunit was performed by Phyre2 and PyMOL (**Figures 2B,C** and **Supplementary Figure 1**). Considering that the Ala22Thr mutation was a heterozygote, so there should be at least four Ala22Thr mutants located in the proteolipid c-ring of V-ATPase. The molecular effect caused by the Ala22Thr mutation was further analyzed using available templates in Phyre2 and AlphaFold (**Figure 2E**). Residue Ala22 formed three hydrogen bonds with Gly18, Ala19, and Ser26 (Phyre2). AlphaFold showed that residue Ala22 formed three hydrogen bonds, one with Gly18 and two with Ser26. Both predictions showed that a novel hydrogen bond with Gly18 was formed when alanine at residue Ala22 was substituted by threonine (**Figure 2E**). Furthermore, the Ala22Thr lead to a new addition of hydroxide radical that potentially influence the proton transport in the hemichannel formed by proteolipid c-ring and a-subunit (**Figures 2C,E**). In addition, I-Mutant 3.0 program showed that the Ala22Thr cause a large decrease of the protein stability with a negative DDG value of 0.76 Kcal/mol.

Clinical Features

ATP6V0C mutations were identified in two families with six affected individuals (**Figures 1A,B**, and **Table 2**). All affected individuals presented FS. The major clinical characteristics of the six patients were listed in **Table 2**.

The missense mutation (c.64G > A/p.Ala22Thr) was identified in family 1 with four individuals affected. The proband was a 5-year-old boy who had his first seizure at the age of 8 months with a fever of 38.5°C. It was a GTCS and lasted for 2–3 min. The febrile GTCS occurred approximately once every 2 months and tended to occur at a lower temperature

[5]http://www.sbg.bio.ic.ac.uk/phyre2/html/page.cgi?id=index

[6]https://alphafold.ebi.ac.uk/entry/P27449

[7]http://pymol.org/2/

[8]http://gpcr2.biocomp.unibo.it/cgi/predictors/I-Mutant3.0/I-Mutant3.0.cgi

[9]https://www.uniprot.org

TABLE 1 | Analysis of the aggregate frequency of *ATP6V0C* variants identified in this study.

	Allele count/number in this study (%)	Allele count/number in gnomAD-all populations (%)	Allele count/number in gnomAD-East Asian population (%)	Allele count/number in 296 normal controls of Chinese population (%)
Identified *ATP6V0C* mutation				
c.64G > A/p.Ala22Thr	1/64 (1.56)	–/–	–/–	–/–
c.361_373del/p.Thr121Profs*7	1/64 (1.56)	–/–	–/–	–/–
Total	2/64 (3.12)	0/280788	0/19750	0/592
P value†		5.11×10^{-8}	1.03×10^{-5}	9.38×10^{-3}
OR (95% CI)		Inf (840.15-Inf)	Inf (58.51-Inf)	Inf (1.75-Inf)

†*P values and odds ratio were estimated with a 2-sided Fisher's exact test.*
CI, confidence interval; gnomAD, Genome Aggregation Database; OR, odds ratio.

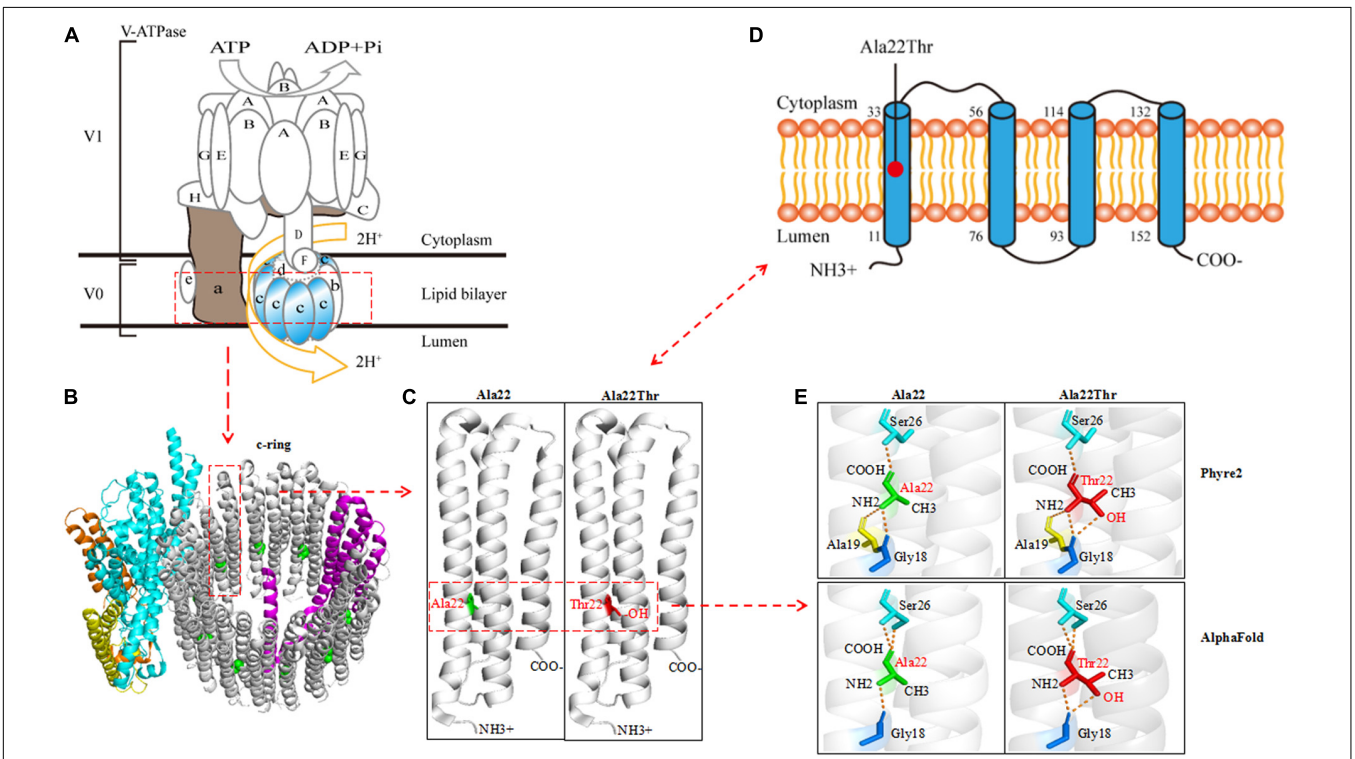

FIGURE 2 | Schematic illustration of the ATP6V0C protein and molecular effect of Ala22Thr on ATP6V0C protein. **(A)** Structure diagram of major molecular components of vacuolar ATPase (V-ATPase), which is composed of a cytosolic V1 domain and a transmembrane V0 domain. The V0 domain consists of five different subunits: a, b, c, d, and e. The proteolipid c-ring was comprised of nine c-subunits (ATP6V0C protein) and one b-subunit. The "c-ring" couples the energy generated by ATP hydrolysis to the translocation of protons from the cytosol to the lumen through the hemichannel formed between the a-subunit and the proteolipid c-ring. **(B)** Three-dimensional (3D) structure of the V0 domain. **(C)** The focal structure of ATP6V0C protein. Ala22Thr was located in the first transmembrane domain of ATP6V0C protein with an addition of hydroxide radical. **(D)** The commonly used topographical diagram showing the five topological domains and the four transmembrane domains. **(E)** Left: residue Ala22 formed three hydrogen bonds with Gly18, Ala19, and Ser26 in Phyre2; AlphaFold showed that residue Ala22 formed three hydrogen bonds, one with Gly18 and two with Ser26. Right: both predictions showed that a novel hydrogen bond with Gly18 was formed when alanine at residue Ala22 was substituted by threonine. Furthermore, the Ala22Thr lead to a new addition of hydroxide radical that potentially influence the proton transport in the proteolipid c-ring of the hemichannel.

(even at 37.3°C) later. Subsequently, afebrile GTCS occurred at the age of 1.5 years. Valproate (VPA) was then administered at a dose of 20 mg/kg/day. The seizure frequency decreased to around once every 4 months. At the age of 2 years and 2 months, the patient started to have myoclonic seizure with a frequency up to 1–2 times per day. Nitrazepam (NZP) was started (0.5 mg/kg/day) and the seizure frequency became 1 time per month within 4 months. At the age of 3 years and 8 months, lamotrigine (LTG) was added with a decrease of NZP, and the patient became seizure-free with VPA of 24.2 mg/kg/day, NZP of 0.3 mg/kg/day, and LTG of 1.2 mg/kg/day. Ictal video EEG recordings showed generalized polyspike-slow waves associated with myoclonic seizures (**Figure 3A**). Interictally, paroxysmal generalized 2∼4 Hz slow activities and irregular

TABLE 2 | Clinical features of individuals with *ATP6V0C* mutations.

Cases	Sex	Age	Seizure onset	Seizure course	Seizure-free duration	AEDs	EEG	Brain MRI	Development	Diagnosis
Case 1 (c.64G>A/p.Ala22Thr)										
I-1	M	44 yr	8 mo	GTCS (FS), 1–2 times/yr for 5 yr	38 yr	No	NA	NA	Normal	FS
II-1	F	14 yr	8 mo	GTCS (FS), 1–2 times/yr for 5 yr	8 yr	No	Normal	Normal	Normal	FS
II-2	F	12 yr	8 mo	GTCS (FS), 1–2 times/yr for 5 yr	6 yr	No	Normal	Normal	Normal	FS
II-3	M	5 yr	8 mo	GTCS (FS), 5–6 times/yr for 1.5 yr; myoclonic seizures, up to 1–2 times/d for 1.5 yr	1 yr	VPA, NZP, LTG	Ictal: generalized PSW; interictal: generalized 2˜4 Hz SW, irregular SSW and PSW	Normal	Normal	EFS+
Case 2 (c.361_373del/p.Thr121Profs*7)										
II-1	F	30 yr	8 mo	GTCS (FS), 0–2 times/yr for 4 yr	25 yr	No	Normal	NA	Normal	FS
III-1	M	3 yr	7 mo	GTCS (FS or aFS), 6–8 times/yr in cluster for 1.5 yr	1 yr	VPA	Generalized 2.5˜3.5 Hz SW	Normal	Normal	EFS+

AEDs, antiepileptic drugs; aFS, afebrile seizure; d, day; EEG, electroencephalogram; EFS+, epilepsy with febrile seizure plus; F, female; FS, febrile seizure; GTCS, generalized tonic–clonic seizure; LTG, lamotrigine; M, male; mo, months; MRI, magnetic resonance imaging; NA, not available; NZP, nitrazepam; PSW, polyspike-slow waves; SSW, spike-slow waves; SW, slow activities; VPA, valproate; wk, week; yr, years.

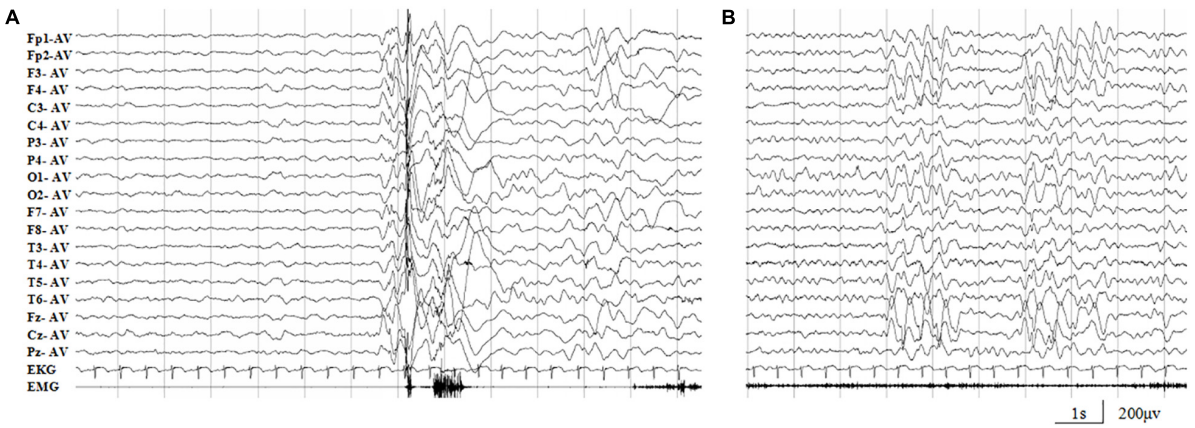

FIGURE 3 | Representative EEG recordings of the case 1. **(A)** Ictal EEG showed high-amplitude generalized polyspike-slow waves associated with myoclonic seizures. **(B)** Interictal paroxysmal generalized 2∼4 Hz slow activity, or irregular spike-slow waves with anterior predominance during wakefulness.

spike-slow waves (**Figure 3B**), or polyspike-slow waves with anterior predominance were recorded during wakefulness. The patient was born to non-consanguineous Chinese parents after a normal pregnancy and delivery. No positive signs in general and neurologic examinations were found. His intelligence, development, and growth were normal. His brain MRI scan, blood and cerebrospinal fluid routine biochemistry, metabolic, and pathogenic tests were normal. Three other members in this family, the father and two elder sisters, were affected by FS. They all had same seizure onset age and course from 8 months to 5 years old, normal intellectual and physical developments, and became seizure-free without antiepileptic therapy.

The proband in the family with Thr121Profs*7 was a 3-year-old boy who experienced FS at the age of 7 months. The FS then occurred every month in cluster, which consisted of 2–3 seizures. At the age of 1 year and 2 months, the patient suffered from afebrile GTCS. Valproate was then given at a dose of 21.2 mg/kg/day, and the seizure frequency reduced to once every 3 months. The patient became seizure-free with VPA of 23 mg/kg/day. The patient was born to non-consanguineous Chinese parents after a full-term pregnancy. He had an appropriate early developmental and had no physical malformations. His brain MRI and blood routine biochemical examination were normal. Video-EEG showed interictal paroxysmal generalized 2.5∼3.5 Hz slow activity. His paternal aunt carried the same mutation and was affected by FS in childhood. She had infrequent FS from 8 months to 4 years old and then became seizure free without medications. Both

the proband and his paternal aunt had normal intellectual and physical developments.

DISCUSSION

The *ATP6V0C* gene is ubiquitously expressed across the whole lifespan and highly expressed in the central nervous system, prominently in the brain cortex, cerebellum, hypothalamus, and hippocampus (see text footnote 1). It encodes a 155-amino acid H+ transport protein ATP6V0C that is the c-subunit of the V0 domain of V-ATPase. V-ATPase is composed of a peripheral V1 domain that consists of A, B, C, D, E, F, G, and H subunits, and an integral V0 domain that consists of five different subunits: a, b, c, d, and e (**Figures 2A,B**). As one component of the multi-subunit enzyme complex of V-ATPase, ATP6V0C forms the proteolipid c-ring of the V-ATPase (**Figures 2A,B**), which is critical for the transport of H+ flow and determines the intra and extracellular *pH* value of neurons (Tombaugh and Somjen, 1997; Bonnet and Wiemann, 1999; Mangieri et al., 2014). The ATPase H+ transporting V1 subunit A (*ATP6V1A*) gene that encodes V-ATPase subunit A, have been reported to be associated with developmental and epileptic encephalopathy 93 (DEE-93, MIM: 618012) (Fassio et al., 2018). However, the association between *ATP6V0C* gene variants and human disease has not been determined. In the present paper, we identified two *ATP6V0C* mutations that co-segregated with the disease in two unrelated families with six individuals affected. The two *ATP6V0C* mutations, including one missense mutation (c.64G > A/p.Ala22Thr) and one frameshift mutation (c.361_373del/p.Thr121Profs*7), were considered to be potentially deleterious because of the possibility of giving rise to alteration of the structure of proteolipid c-ring or producing a truncated transcript. The frequencies of the two *ATP6V0C* mutations in this cohort were statistically higher than that in the control groups of gnomAD and our 296 normal subjects. These data indicated that the *ATP6V0C* mutations were potentially associated with FS or FS related epilepsy.

Previous studies have described 16p13.3 microdeletions in several patients with epilepsy and microcephaly (Mucha et al., 2019; Tinker et al., 2020). The genetic abnormalities involved *ATP6V0C* and other genes such as *AMDHD2, CEMP1, PDPK1,* and *TBC1D24*. Two of the genes were suspected to be pathogenic, including *PDPK1* that was categorized as a highly constrained gene due to the pLI score > 0.95 (Samocha et al., 2014; Feng et al., 2019) and *TBC1D24* that had an established association with epilepsy (Duru et al., 2010; Falace et al., 2010; Luthy et al., 2019). An *ATP6V0C de novo* variant had been reported in a *SCN1A*-negative patient with Dravet syndrome while the patient simultaneously harbored *de novo* missense variants in the genes of *NKAIN3* and *SLC8A1* (Carvill et al., 2014). Recently, a *de novo* stop-loss variant in *ATP6V0C* had been identified in a patient with epilepsy and intellectual disability (Ittiwut et al., 2021). These data provided possible clues for the association between *ATP6V0C* and epilepsy, but the pathogenic role of *ATP6V0C* variants in those cases could not be determined due to the co-appearance of variants in other potentially pathogenic genes or the single affected case. In the present study, we identified *ATP6V0C* mutations in two families with six individuals affected; and the other possible pathogenic genes were excluded. Therefore, this study provided more direct evidence in supporting the association between *ATP6V0C* and epilepsy.

Experiments in zebrafish embryos showed that loss-of-function of *ATP6V0C2* led to a complete inhibition of depolarization-evoked Ca2+ influx in neurons (Chung et al., 2010). Homozygous *ATP6V0C* knockout mice exhibit neonatal lethality, abnormal embryonic tissue morphology, and failure of zygotic cell division (see text footnote 2), suggesting a pathogenic role of loss of function. In the present study, the *ATP6V0C* mutations included one frameshift mutation and one missense mutation. The frameshift mutation resulted in a loss of function by yielding a premature termination of 28 residues at the C-terminus of the protein. The missense mutation was located in the proteolipid c-ring that cooperated with a-subunit forming the hemichannel for proton transferring. It also affected the hydrogen bonds with surround residues and the protein stability, implying a damaging effect. Thus, loss of function was potentially the underlying mechanism of the pathogenicity of *ATP6V0C* mutations. However, the direct functional effects of the *ATP6V0C* mutations were not examined, on which further studies are needed.

All the six affected individuals suffered from their first FS at the age of 7–8 months. The two probands later manifested afebrile seizures including myoclonic seizures that were similar to Dravet syndrome caused by *SCN1A* mutations. However, the patients with *ATP6V0C* mutations displayed good prognosis without psychomotor development disorders, although afebrile seizures or frequent seizures occurred. The myoclonic seizures responded well to LTG, which potentially produce seizure aggravation in patients with *SCN1A* mutations. This study showed a significant difference in clinical prognosis between the epilepsy caused by *ATP6V0C* mutations and Dravet syndrome caused by *SCN1A* mutations. Screening for *ATP6V0C* mutations thus imply clinical significance.

CONCLUSION

In conclusion, this study identified *ATP6V0C* mutations in two unrelated families with six individuals affected by FS or EFS+. All affected patients suffered from their first FS at the age of 7–8 months and displayed good prognosis without psychomotor development abnormalities. The frequencies of *ATP6V0C* mutations identified in this cohort were significantly higher than that in the control populations. These findings suggested that *ATP6V0C* is potentially a causative gene in FS or EFS+. Screening for *ATP6V0C* mutations would help differentiating patients with Dravet syndrome, which presented similar clinical manifestation but different responses to antiepileptic treatment.

DATA AVAILABILITY STATEMENT

The datasets presented in this study can be found in online repositories. The names of the repository/repositories and accession number(s) can be found in the article/**Supplementary Material**.

ETHICS STATEMENT

The studies involving human participants were reviewed and approved by the Ethics Committee of Guangzhou Women and Children's Medical Center and the Ethics Committee of Guangdong General Hospital. Written informed consent to participate in this study was provided by the participants' legal guardian/next of kin. Written informed consent was obtained from the individual(s) and minor(s)' legal guardian/next of kin, for the publication of any potentially identifiable images or data included in this article.

AUTHOR CONTRIBUTIONS

YT, W-PL, and JW designed the study. YT, Q-XZ, X-JL, ZS, CH, W-BL, and W-XC recruited the patients and analyzed the clinical data. C-FC, C-XF, Y-YH, SL, W-PL, and JW analyzed the genetic data. YT, BT, and YZ performed the computational modeling. YT and JW wrote the manuscript. W-PL revised the manuscript. All authors have read and approved the final manuscript.

FUNDING

This work was supported by the Science and Technology Project of Guangdong Province (Grant Nos. 2017B030314159 and 2021A1515111064), Science and Technology Project of Guangzhou (Grant Nos. 201904020028, 202102021059, and 202102021063), and National Key R&D Program of China (Grant No. 2016YFC1306200).

ACKNOWLEDGMENTS

We thank the patients and their families for participating in this study.

SUPPLEMENTARY MATERIAL

The Supplementary Material for this article can be found online at: https://www.frontiersin.org/articles/10.3389/fnmol.2022.889534/full#supplementary-material

REFERENCES

Annegers, J. F., Hauser, W. A., Shirts, S. B., and Kurland, L. T. (1987). Factors prognostic of unprovoked seizures after febrile convulsions. *N. Engl. J. Med.* 316, 493–498. doi: 10.1056/NEJM198702263160901

Bonnet, U., and Wiemann, M. (1999). Ammonium prepulse: effects on intracellular pH and bioelectric activity of CA3-neurones in guinea pig hippocampal slices. *Brain Res.* 840, 16–22. doi: 10.1016/s0006-8993(99)01687-x

Berg, A. T., Berkovic, S. F., Brodie, M. J., Buchhalter, J., Cross, J. H, van Emde Boas, W., et al. (2010). Revised terminology and concepts for organization of seizures and epilepsies: report of the ILAE Commission on Classification and Terminology, 2005-2009. *Epilepsia* 51, 676–685. doi: 10.1111/j.1528-1167.2010.02522.x

Carvill, G. L., Weckhuysen, S., McMahon, J. M., Hartmann, C., Moller, R. S., Hjalgrim, H., et al. (2014). GABRA1 and STXBP1: novel genetic causes of Dravet syndrome. *Neurology* 82, 1245–1253. doi: 10.1212/WNL.0000000000000291

Chung, A. Y., Kim, M. J., Kim, D., Bang, S., Hwang, S. W., Lim, C. S., et al. (2010). Neuron-specific expression of atp6v0c2 in zebrafish CNS. *Dev. Dyn.* 239, 2501–2508. doi: 10.1002/dvdy.22383

Commission on Classification and Terminology of the International League Against Epilepsy (1981). Proposal for revised clinical and electroencephalographic classification of epileptic seizures. *Epilepsia* 22, 489–501. doi: 10.1111/j.1528-1157.1981.tb06159.x

Commission on Classification and Terminology of the International League Against Epilepsy (1989). Proposal for revised classification of epilepsies and epileptic syndromes. *Epilepsia* 30, 389–399. doi: 10.1111/j.1528-1157.1989.tb05316.x

Deng, H., Zheng, W., and Song, Z. (2018). The genetics and molecular biology of fever-associated seizures or epilepsy. *Expert Rev. Mol. Med.* 20:e3. doi: 10.1017/erm.2018.2

Duru, N., Iseri, S. A., Selcuk, N., and Tolun, A. (2010). Early-onset progressive myoclonic epilepsy with dystonia mapping to 16pter-p13.3. *J. Neurogenet.* 24, 207–215. doi: 10.3109/01677063.2010.514368

Engel, J. Jr., International League Against Epilepsy (ILAE). (2001). A proposed diagnostic scheme for people with epileptic seizures and with epilepsy: report of the ILAE Task Force on Classification and Terminology. *Epilepsia* 42, 796–803. doi: 10.1046/j.1528-1157.2001.10401.x

Falace, A., Filipello, F., La Padula, V., Vanni, N., Madia, F., De Pietri Tonelli, D., et al. (2010). TBC1D24, an ARF6-interacting protein, is mutated in familial infantile myoclonic epilepsy. *Am. J. Hum. Genet.* 87, 365–370. doi: 10.1016/j.ajhg.2010.07.020

Fassio, A., Esposito, A., Kato, M., Saitsu, H., Mei, D., Marini, C., et al. (2018). De novo mutations of the ATP6V1A gene cause developmental encephalopathy with epilepsy. *Brain* 141, 1703–1718. doi: 10.1093/brain/awy092

Feng, Y. C. A., Howrigan, D. P., Abbott, L. E., Tashman, K., Cerrato, F., Singh, T., et al. (2019). Ultra-Rare Genetic Variation in the Epilepsies: A Whole-Exome Sequencing Study of 17,606 Individuals. *Am. J. Hum. Genet.* 105, 267–282. doi: 10.1016/j.ajhg.2019.05.020

Gupta, A. (2016). Febrile Seizures. *Continuum* 22, 51–59.

Hackett, R., Hackett, L., and Bhakta, P. (1997). Febrile seizures in a south Indian district: incidence and associations. *Dev. Med. Child Neurol.* 39, 380–384. doi: 10.1111/j.1469-8749.1997.tb07450.x

Hedera, P., Ma, S., Blair, M. A., Taylor, K. A., Hamati, A., Bradford, Y., et al. (2006). Identification of a novel locus for febrile seizures and epilepsy on chromosome 21q22. *Epilepsia* 47, 1622–1628. doi: 10.1111/j.1528-1167.2006.00637.x

Heron, S. E., Regan, B. M., Harris, R. V., Gardner, A. E., Coleman, M. J., Bennett, M. F., et al. (2021). Association of SLC32A1 Missense Variants With Genetic Epilepsy With Febrile Seizures Plus. *Neurology* 96, e2251–e2260. doi: 10.1212/WNL.0000000000011855

Higashida, H., Yokoyama, S., Tsuji, C., and Muramatsu, S. I. (2017). Neurotransmitter release: vacuolar ATPase V0 sector c-subunits in possible gene or cell therapies for Parkinson's, Alzheimer's, and psychiatric diseases. *J. Physiol. Sci.* 67, 11–17. doi: 10.1007/s12576-016-0462-3

Ittiwut, C., Poonmaksatit, S., Boonsimma, P., Desudchit, T., Suphapeetiporn, K., Ittiwut, R., et al. (2021). Novel de novo mutation substantiates ATP6V0C as a gene causing epilepsy with intellectual disability. *Brain Dev.* 43, 490–494. doi: 10.1016/j.braindev.2020.10.016

Liu, L., Chen, Z. R., Xu, H. Q., Liu, D. T., Mao, Y., Liu, H. K., et al. (2020). DEPDC5 Variants Associated Malformations of Cortical Development and Focal Epilepsy With Febrile Seizure Plus/Febrile Seizures: The Role of Molecular Sub-Regional Effect. *Front. Neurosci*. 14:821. doi: 10.3389/fnins.2020.00821

Luthy, K., Mei, D., Fischer, B., De Fusco, M., Swerts, J., Paesmans, J., et al. (2019). TBC1D24-TLDc-related epilepsy exercise-induced dystonia: rescue by antioxidants in a disease model. *Brain* 142, 2319–2335. doi: 10.1093/brain/awz175

Mangieri, L. R., Mader, B. J., Thomas, C. E., Taylor, C. A., Luker, A. M., Tse, T. E., et al. (2014). ATP6V0C knockdown in neuroblastoma cells alters autophagy-lysosome pathway function and metabolism of proteins that accumulate in neurodegenerative disease. *PLoS One* 9:e93257. doi: 10.1371/journal.pone.0093257

Morel, N. (2003). Neurotransmitter release: the dark side of the vacuolar-H+ATPase. *Biol. Cell* 95, 453–457. doi: 10.1016/s0248-4900(03)00075-3

Mucha, B. E., Banka, S., Ajeawung, N. F., Molidperee, S., Chen, G. G., Koenig, M. K., et al. (2019). A new microdeletion syndrome involving TBC1D24, ATP6V0C, and PDPK1 causes epilepsy, microcephaly, and developmental delay. *Genet. Med*. 21, 1058–1064. doi: 10.1038/s41436-018-0290-3

Rigbye, K. A., van Hasselt, P. M., Burgess, R., Damiano, J. A., Mullen, S. A., Petrovski, S., et al. (2016). Is FGF13 a major contributor to genetic epilepsy with febrile seizures plus? *Epilepsy Res*. 128, 48–51. doi: 10.1016/j.eplepsyres.2016.10.008

Samocha, K. E., Robinson, E. B., Sanders, S. J., Stevens, C., Sabo, A., McGrath, L. M., et al. (2014). A framework for the interpretation of de novo mutation in human disease. *Nat. Genet*. 46, 944–950. doi: 10.1038/ng.3050

Scheffer, I. E., Berkovic, S., Capovilla, G., Connolly, M. B., French, J., Guilhoto, L., et al. (2017). ILAE classification of the epilepsies: position paper of the ILAE Commission for Classification and Terminology. *Epilepsia* 58, 512–521. doi: 10.1111/epi.13709

Shi, Y. W., Zhang, Q., Cai, K., Poliquin, S., Shen, W., Winters, N., et al. (2019). Synaptic clustering differences due to different GABRB3 mutations cause variable epilepsy syndromes. *Brain* 142, 3028–3044. doi: 10.1093/brain/awz250

Smith, D. K., Sadler, K. P., and Benedum, M. (2019). Febrile Seizures: Risks, Evaluation, and Prognosis. *Am. Fam. Phys*. 99, 445–450.

Tinker, R. J., Burghel, G. J., Garg, S., Steggall, M., Cuvertino, S., and Banka, S. (2020). Haploinsufficiency of ATP6V0C possibly underlies 16p13.3 deletions that cause microcephaly, seizures, and neurodevelopmental disorder. *Am. J. Med. Genet. A* [Epub Online ahead of print] doi: 10.1002/ajmg.a.61905

Toei, M., Saum, R., and Forgac, M. (2010). Regulation and isoform function of the V-ATPases. *Biochemistry* 49, 4715–4723. doi: 10.1021/bi100397s

Tombaugh, G. C., and Somjen, G. G. (1997). Differential sensitivity to intracellular pH among high- and low-threshold Ca2+ currents in isolated rat CA1 neurons. *J. Neurophysiol*. 77, 639–653. doi: 10.1152/jn.1997.77.2.639

Wang, J. Y., Zhou, P., Wang, J., Tang, B., Su, T., Liu, X. R., et al. (2018). ARHGEF9 mutations in epileptic encephalopathy/intellectual disability: toward understanding the mechanism underlying phenotypic variation. *Neurogenetics* 19, 9–16. doi: 10.1007/s10048-017-0528-2

Wang, J., Lin, Z. J., Liu, L., Xu, H. Q., Shi, Y. W., Yi, Y. H., et al. (2017). Epilepsy-associated genes. *Seizure* 44, 11–20.

Wang, J., Qiao, J. D., Liu, X. R., Liu, D. T., Chen, Y. H., Wu, Y., et al. (2021). UNC13B variants associated with partial epilepsy with favourable outcome. *Brain* 144, 3050–3060. doi: 10.1093/brain/awab164

Wang, L., Wu, D., Robinson, C. V., Wu, H., and Fu, T. M. (2020). Structures of a Complete Human V-ATPase Reveal Mechanisms of Its Assembly. *Mol. Cell*. 80, 501–511.e3.

Xu, Y., Zhou, P., Cheng, S., Lu, Q., Nowak, K., Hopp, A. K., et al. (2019). A Bacterial Effector Reveals the V-ATPase-ATG16L1 Axis that Initiates Xenophagy. *Cell* 178, 552–566.e20. doi: 10.1016/j.cell.2019.06.007

Ye, X. G., Liu, Z. G., Wang, J., Dai, J. M., Qiao, P. X., Gao, P. M., et al. (2021). YWHAG Mutations Cause Childhood Myoclonic Epilepsy and Febrile Seizures: Molecular Sub-regional Effect and Mechanism. *Front. Genet*. 12:632466. doi: 10.3389/fgene.2021.632466

Conflict of Interest: The authors declare that the research was conducted in the absence of any commercial or financial relationships that could be construed as a potential conflict of interest.

Publisher's Note: All claims expressed in this article are solely those of the authors and do not necessarily represent those of their affiliated organizations, or those of the publisher, the editors and the reviewers. Any product that may be evaluated in this article, or claim that may be made by its manufacturer, is not guaranteed or endorsed by the publisher.

frontiers | Frontiers in Molecular Neuroscience

ORIGINAL RESEARCH
published: 10 May 2022
doi: 10.3389/fnmol.2022.861159

Recessive *PKD1* Mutations Are Associated With Febrile Seizures and Epilepsy With Antecedent Febrile Seizures and the Genotype-Phenotype Correlation

*Jing-Yang Wang[1,2†], Jie Wang[1,2†], Xin-Guo Lu[3], Wang Song[1,2], Sheng Luo[1,2], Dong-Fang Zou[3], Li-Dong Hua[4], Qian Peng[5], Yang Tian[6], Liang-Di Gao[1,2], Wei-Ping Liao[1,2] and Na He[1,2]**

[1] Department of Neurology, Institute of Neuroscience, The Second Affiliated Hospital of Guangzhou Medical University, Guangzhou, China, [2] Key Laboratory of Neurogenetics and Channelopathies of the Ministry of Education of China, Guangzhou, China, [3] Epilepsy Center, Department of Neurology, Shenzhen Children's Hospital, Shenzhen, China, [4] Translational Medicine Center, Guangdong Women and Children Hospital, Guangzhou, China, [5] Department of Pediatrics, Dongguan City Maternal and Child Health Hospital, Southern Medical University, Dongguan, China, [6] Department of Neurology, Guangzhou Women and Children's Medical Center, Guangzhou Medical University, Guangzhou, China

Objective: The *PKD1* encodes polycystin-1, a large transmembrane protein that plays important roles in cell proliferation, apoptosis, and cation transport. Previous studies have identified *PKD1* mutations in autosomal dominant polycystic kidney disease (ADPKD). However, the expression of *PKD1* in the brain is much higher than that in the kidney. This study aimed to explore the association between *PKD1* and epilepsy.

Methods: Trios-based whole-exome sequencing was performed in a cohort of 314 patients with febrile seizures or epilepsy with antecedent febrile seizures. The damaging effects of variants was predicted by protein modeling and multiple *in silico* tools. The genotype-phenotype association of *PKD1* mutations was systematically reviewed and analyzed.

Results: Eight pairs of compound heterozygous missense variants in *PKD1* were identified in eight unrelated patients. All patients suffered from febrile seizures or epilepsy with antecedent febrile seizures with favorable prognosis. All of the 16 heterozygous variants presented no or low allele frequencies in the gnomAD database, and presented statistically higher frequency in the case-cohort than that in controls. These missense variants were predicted to be damaging and/or affect hydrogen bonding or free energy stability of amino acids. Five patients showed generalized tonic-clonic seizures (GTCS), who all had one of the paired missense mutations located in the PKD repeat domain, suggesting that mutations in the PKD domains were possibly associated with GTCS. Further analysis demonstrated that monoallelic mutations with haploinsufficiency of *PKD1* potentially caused kidney disease, compound heterozygotes with superimposed effects of two missense mutations were associated with epilepsy, whereas the homozygotes with complete loss of *PKD1* would be embryonically lethal.

OPEN ACCESS

Edited by:
Yuwu Jiang,
Peking University First Hospital, China

Reviewed by:
Saima Siddiqi,
Institute of Biomedical and Genetic Engineering (IBGE), Pakistan
Shuli Liang,
Capital Medical University, China
Ziyi Chen,
Sun Yat-sen University, China
Dezhi Cao,
Shenzhen Children's Hospital, China

***Correspondence:**
Na He
henachilli@163.com

† These authors have contributed equally to this work

Specialty section:
This article was submitted to Molecular Signalling and Pathways, a section of the journal Frontiers in Molecular Neuroscience

Received: *24 January 2022*
Accepted: *05 April 2022*
Published: *10 May 2022*

Citation:
Wang J-Y, Wang J, Lu X-G, Song W, Luo S, Zou D-F, Hua L-D, Peng Q, Tian Y, Gao L-D, Liao W-P and He N (2022) Recessive PKD1 Mutations Are Associated With Febrile Seizures and Epilepsy With Antecedent Febrile Seizures and the Genotype-Phenotype Correlation. Front. Mol. Neurosci. 15:861159. doi: 10.3389/fnmol.2022.861159

Conclusion: *PKD1* gene was potentially a novel causative gene of epilepsy. The genotype-phenotype relationship of *PKD1* mutations suggested a quantitative correlation between genetic impairment and phenotypic variation, which will facilitate the genetic diagnosis and management in patients with *PKD1* mutations.

Keywords: *PKD1* gene, epilepsy with antecedent febrile seizures, genotype-phenotype association, monoallelic mutation, compound heterozygous mutations

INTRODUCTION

PKD1 (MIM 601313) is a gene with 46 exons located on chromosome 16p13. The encoded protein polycystin-1 (PC1) forms a complex with polycystin-2 (PC2), which regulates calcium permeable cation channels and intracellular calcium homeostasis (Semmo et al., 2014; Kim et al., 2016; Su et al., 2018). PC1 is distributed widely in multiple tissues, especially highly in the brain (Fagerberg et al., 2014). Its expression is also developmentally regulated with the highest level in fetal life and maintained throughout adulthood (Geng et al., 1997). Homozygous *Pkd1* knockout mice have exhibited neural tube defects and embryonic or perinatal lethality (Lu et al., 2001; Lantinga-van Leeuwen et al., 2007). PC1 can also interact with homer 1/Vesl-1 and plays a role in synaptic plasticity in postnatal mouse hippocampus (Stokely et al., 2006). So far, *PKD1* mutations were reported to be associated with autosomal dominant polycystic kidney disease (ADPKD, MIM 173900), which was featured by dilatation of the renal tubules leading to cyst formation and progressive renal failure. The relationship between *PKD1* and diseases of the brain remains unknown.

Febrile seizures (FS) are the most common human convulsive event. Children with FS have a higher risk of developing spontaneous afebrile seizures (Baulac et al., 2004). Retrospective studies indicated that 10–15% of patients with epilepsy had antecedent FS (epilepsy with febrile seizures plus, EFS+) (Baulac et al., 2004). The gene associated with FS/EFS+ include *ADGRV1, CPA6, DYRK1A, FEB2, FEB5, FEB6, FEB7, FEB9, FEB10, FGF13, GABRB3, GABRD, GABRG2, GEFSP4, GEFSP6, GEFSP8, HCN1, NPRL3, SCN1A, SCN1B, SCN2A, SCN9A, and STX1B* (OMIM)[1]. In this study, we performed trios-based whole-exome sequencing (WES) in a cohort of patients of FS and epilepsy with antecedent FS. *PKD1* compound heterozygous mutations were identified in eight unrelated cases, among which seven probands presented epilepsy with antecedent FS. This study suggested that *PKD1* gene is potentially a candidate pathogenic gene of FS and epilepsy with antecedent FS.

MATERIALS AND METHODS

Patients

A total of 314 cases with febrile seizures and epilepsy with antecedent FS were recruited for genetic screening during January 2018–July 2021 from four hospitals, including The Second Affiliated Hospital of Guangzhou Medical University, Shenzhen Children's Hospital, Guangzhou Women and Children's Medical Center of Guangzhou Medical University, and Dongguan City Maternal and Child Health Hospital. Clinical characteristics of the affected individuals were collected, including present age, gender, age at seizure onset, seizure course, family history, state of development, effective antiepileptic drugs (AEDs). Magnetic resonance imaging (MRI) scans were performed to detect any brain structure abnormalities. Long-term video-EEG examination was obtained that included open-close eyes test, intermittent photic stimulation, hyperventilation, and sleeping recording. The results were reviewed by two qualified electroencephalographers. Epileptic seizures and epilepsies were diagnosed according to the criteria of the Commission on Classification and Terminology of the ILAE (1981, 1989, 2001, 2010, and 2017). FS was diagnosed with the criteria: (1) a seizure occurring in childhood after age of 1 month to 6 years accompanied by a fever, (2) the febrile illness not caused by central nervous system infection, (3) not meeting criteria for other acute symptomatic seizures. The patients and their parents (trios), and other available family members were screened for genetic variants by the whole-exome sequencing.

For the controls, a cohort of 296 healthy Chinese volunteers was recruited as a normal control group as our previous report (Wang et al., 2021). Frequencies of the identified variants were also compared with that in the other control populations, including East Asian and general populations in the Genome Aggregation Database (gnomAD)[2].

This study was approved by the Ethics Committee of The Second Affiliated Hospital of Guangzhou Medical University, and written informed consent was obtained from all patients and their parents.

Whole Exome Sequencing

Whole blood samples were collected from the probands, their parents, and other available family members. Qiagen Flexi Gene DNA kit (Qiagen, Hilden, Germany) was used to extract genomic DNA from the whole blood samples. Trio-based whole-exome sequencing was performed on an Illumina HiSeq 2000 system by BGI-Shenzhen (Shenzhen, China) as previously described (Wang et al., 2021). The sequencing data were generated by massively parallel sequencing with >125 times average depth and >98% coverage in the capture region of the chip to obtain high-quality reads that were mapped to the Genome Reference Consortium Human Genome build 37 (GRCh37) by Burrows-Wheeler alignment. Single-nucleotide point variants and indels were called with the Genome Analysis Toolkit. To obtain the

[1]https://www.omim.org/

[2]http://gnomad-sg.org/

comprehensive list of candidate pathogenic variants in each trio, we adopted a case-by-case analytical pattern. We first prioritized the rare variants with a minor allele frequency <0.005 in the 1000 Genomes Projects, Exome Aggregation Consortium, and gnomAD, and then screened for possibly disease-causing variants in each case under the following five models: (1) epilepsy-associated gene (Wang et al., 2017); (2) *de novo* variant dominant; (3) autosomal recessive inheritance, including homozygous and compound heterozygous variants; (4) X-linked; and (5) co-segregation analysis. To identify novel epilepsy-associated genes, we put the known epilepsy-associated genes aside (Wang et al., 2017). Genes with repetitively identified *de novo* variants, bi-allelic variants, hemizygous variants, or variants with segregations, were selected for further studies to define the gene-disease association. *PKD1* appeared as a candidate gene with recurrent compound heterozygous variants in this cohort. Sanger sequencing was used to validate the positive findings and the variant origination. All *PKD1* variants identified in this study were annotated to reference transcript NM_001009944.2.

Protein Modeling and Mutation Analysis

To evaluate the pathogenicity of candidate variants, the structure of PC1 was modeled to predict the effect of missense mutations on protein structure by using the Iterative Threading ASSEmbly Refinement software (I-TASSER)[3]. The confidence of models was quantitatively measured by a C-score in the range of [−5,2]. Three models were predicted and utilized in this study with C-scores of −0.64, −1.14, and −3.02, respectively. PyMOL 2.3 software was used for three-dimensional protein structure visualization and analysis.

To evaluate the protein stability changes upon single nucleotide mutations, the free energy change value ($\Delta\Delta G$, kcal/mol) was predicted by I-Mutant server[4] (Capriotti et al., 2005). Variants were divided into three classes: large increase of protein stability ($\Delta\Delta G > 0.5$ kcal/mol), large decrease of protein stability ($\Delta\Delta G < -0.5$ kcal/mol), and neutral stability (-0.5 kcal/mol $\leq \Delta\Delta G \leq 0.5$ kcal/mol). The consequences of all the missense variants were predicted by 21 *in silico* tools, including SIFT, PolyPhen2_HVAR, CADD, MutationTaster, Fathmm-MKL, fitCons, PhastCons, and GERP++.

Genotype-Phenotype Association Analysis

Previously, *PKD1* mutations were reported to be associated with ADPKD. To explore the genotype-phenotype association of *PKD1* mutations, we systematically reviewed all *PKD1* mutations in the HGMD database (version: HGMD Professional 2021.3)[5] and the ADPKD Variant database (version 4.0)[6]. The registered variants were reviewed from the references indexed in the databases. The literature was also searched on the PubMed database using the following search items: "biallelic mutation *PKD1*," "compound heterozygous mutation *PKD1*," and "homozygous mutation *PKD1*." Some biallelic *PKD1* mutations were reviewed from the cited references of publications from the initial search using the above-mentioned terms. Monoallelic and biallelic *PKD1* mutations identified in patients with ADPKD or sporadic PKD were systematically reviewed and classified.

Statistical Analysis

R statistical software (version 4.0.3) was used for data processing. The frequencies of the *PKD1* variants between the epilepsy cohort and the controls were compared by a two-sided Fisher exact test (Consortium, 2015). The burden of recessive variants was analyzed according to the method recommended recently (Martin et al., 2018). A p value of <0.05 was considered to be statistically significant.

Evaluating *PKD1* Gene as a Novel Candidate Epilepsy Gene

The Clinical Validity Framework that was developed by Clinical Genome Resource (ClinGen) was performed to evaluate *PKD1* as a novel candidate epilepsy gene (Strande et al., 2017).

RESULTS

Identification of *PKD1* Mutations

Eight pairs of compound heterozygous missense variants, including c.3362G > A/p.S1121N and c.8680G > A/p.A2894T, c.5401C > T/p.P1801S and c.6878C > T/p.P2293L c.8744A > G/p.N2915S and c.11689C > T/p.L3897F, c.10315C > T/p.R3439W and c.12391_12392delinsTT/p.E4131L, c.3587C > T/p.T1196M and c.10733C > T/p.A3578V, c.5212C > T/p.L1738F and c.10102G > A/p.D3368N, c.6706T > C/p.F2236L and c.10760C > T/p.A3587V, and c.1966C > G/p.L656V and c.4817C > G/p.T1606S, were identified in eight unrelated cases with FS or EFS+ (**Table 1** and **Figure 1**). The heterozygotes were inherited from their asymptomatic parents, indicating that *PKD1* variants in FS and EFS+ followed an autosomal recessive mode of inheritance.

All heterozygous variants presented no or low allele frequencies in the gnomAD database (**Table 2**). Homozygotes of these variants were not listed in any public databases. None of the variants were observed in the 296 normal controls. When the burden of recessive variants was analyzed (Martin et al., 2018), the *PKD1* variants in the present cohort were significantly more than the expected number by chance in the East Asian population [minor allele frequency (MAF) < 0.005, $p = 0.0004208$]. Furthermore, the aggregate frequency of the variants in this cohort was significantly higher than that in the five controls (**Table 2**), including the gnomAD-all population (16/628 vs. 248/221464, $p = 2.2 \times 10^{-16}$), the controls of gnomAD-all population (vs. 112/88270, $p = 1.43 \times 10^{-15}$), the gnomAD-East Asian population (vs. 162/16258, $p = 0.001014$), the controls of the gnomAD-East Asian population (vs. 76/7610, $p = 0.002089$), and the 296 normal controls (vs. 0/296, $p = 3.06 \times 10^{-5}$). None of the eight affected patients had pathogenic or likely pathogenic

[3]https://zhanglab.ccmb.med.umich.edu/I-TASSER/

[4]https://folding.biofold.org/i-mutant/i-mutant2.0.html

[5]http://www.hgmd.cf.ac.uk/ac/index.php

[6]http://pkdb.pkdcure.org

TABLE 1 | Clinical feature of the individuals with *PKD1* mutations.

Case	Variants	Sex	Age (year)	Onset (year)	Seizure course	EEG	Brain MRI	Development	Treatment (AEDs)	Seizure-free duration	Diagnosis
Case 1	c.3362G > A/p.S1121N c.8680G > A/p.A2894T	Male	10	6	FS, CPS, GTCS (twice a year)	Diffused spikes and spike-slow waves, obviously in the foreheads	Normal	Normal	LEV	1 year	EFS+
Case 2	c.5401C > T/p.P1801S c.6878C > T/p.P2293L	Male	3.5	2.5	FS, CPS, GTCS (twice a month)	Spikes in the bilateral frontal and central regions	Normal	Normal	–	6 months	EFS+
Case 3	c.8744A > G/p.N2915S c.11689C > T/p.L3897F	Male	10	4	FS, CPS (three times a year)	Spike-slow and slow waves in right frontal and temporal regions	Normal	Normal	OXC, LTG	1 year	EFS+
Case 4	c.10315C > T/p.R3439W c.12391_12392delinsTT/ p.E4131L	Male	11	1	FS, CPS (5–6 times a month)	Bilateral occipital spike-slow and slow waves; diffused spike-slow waves	Normal	Normal	CNZ, LEV	1 year	EFS+
Case 5	c.3587C > T/p.T1196M c.10733C > T/p.A3578V	Male	4.5	3	FS, GTCS (four times a month)	Irregular diffused spike-slow waves, obviously in the right areas	Normal	Normal	VPA	5 months	EFS+
Case 6	c.5212C > T/p.L1738F c.10102G > A/p.D3368N	Male	2.5	1	FS, CPS, GTCS (four times a month)	Spikes and spike-slow waves in the frontal, central, and temporal regions	Normal	Normal	VPA	3 months	EFS+
Case 7	c.6706T > C/p.F2236L c.10760C > T/p.A3587V	Female	9	2	FS (twice)	NA	NA	Normal	–	2 years	FS
Case 8	c.1966C > G/p.L656V c.4817C > G/p.T1606S	Male	6	3	FS, CPS, GTCS (once a month)	Spike-slow waves in the right frontal and temporal regions	Normal	Normal	LTG	3 months	EFS+

AEDs, antiepileptic drugs; FS, febrile seizure; CNZ, clonazepam; CPS, complex partial seizure; EEG, electroencephalogram; EFS+, epilepsy with antecedent FS; GTCS, generalized tonic-clonic seizure; LEV, levetiracetam; LTG, lamotrigine; MRI, magnetic resonance imaging; NA, not available; OXC, oxcarbazepine; VPA, valproate.

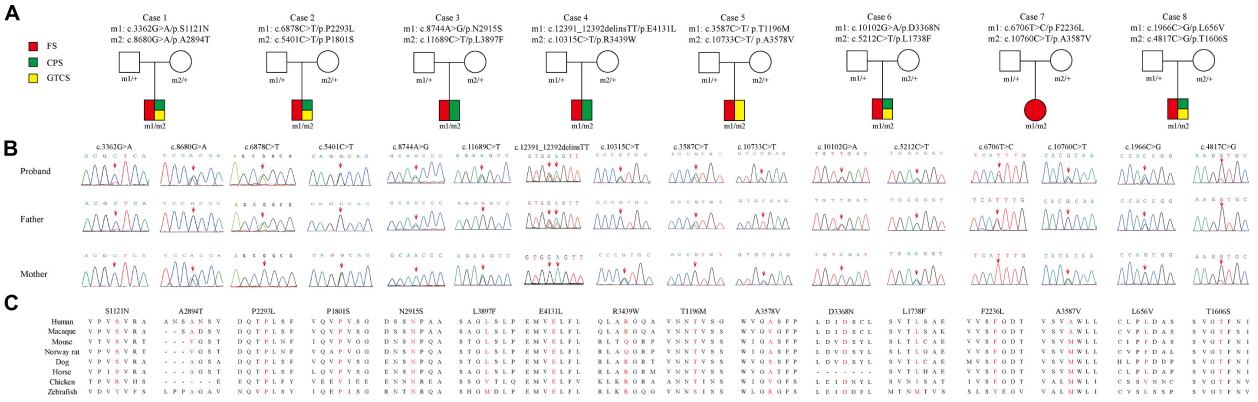

FIGURE 1 | Genetic data of cases with *PKD1* mutations. **(A)** Pedigrees of eight cases with compound heterozygous *PKD1* missense mutations and their corresponding phenotypes. FS, febrile seizure; CPS, complex partial seizure; GTCS, generalized tonic-clonic seizure. **(B)** DNA sequencing chromatogram of *PKD1* mutations. Arrows indicate the positions of the mutations. **(C)** Amino acid sequence alignment of the sixteen missense variants show that residues P2293L, N2915S, E4131L, D3368N, and T1606S are highly conserved in various species; S1121N, P1801S, L3897F, T1196M, L1738F, and F2236L were likely to be highly conserved across mammalian species; while L656V, A2894T, R3439W, A3578V, and A3587V are less conserved.

mutations in the 977 genes known to be associated with epileptic phenotypes (Wang et al., 2017).

The missense mutations P2293L, N2915S, E4131L, D3368N, and T1606S affected amino acid residues that are highly conserved in various species, and the residues S1121N, P1801S, L3897F, T1196M, L1738F, and F2236L were likely to be highly conserved across mammalian species, while the missense mutation L656V, A3578V, and A3587V were less conserved by sequence alignment, but were predicted to be conserved by *in silico* tools (**Supplementary Table 1**).

Molecular Location and Effect of *PKD1* Variants

The 4303-residue PC1 comprises a long N-terminal extracellular region, eleven transmembrane helices, and a C-terminal coiled-coil domain[7]. The N-terminal extracellular portion contains leucine-rich repeats (LRR), a C-type lectin domain, immunoglobulin (Ig)-like PKD repeat domains, a single low-density lipoprotein (LDL) receptor motif, the receptor for egg jelly (REJ) domain, and G protein-coupled receptor proteolysis site (GPS; Hughes et al., 1995; Rondeau, 1995; Gallagher et al., 2010; Arac et al., 2012; Ha et al., 2020). The majority (10/16) of missense mutations were located in the N-terminal extracellular region, among which five variants were located in the PKD repeat domains, including S1121N, T1196M, T1606S, L1738F, and P1801S. This region of PC1 likely plays an important role in cell-cell and cell-matrix interactions (Babich et al., 2004). The other six variants were located in transmembrane helices and C-terminal coiled-coil domain, including R3439W and L3368F in TM3–TM4 linker, A3578V in TM4 domain, A3587V in TM5 domain, L3897F in S1–S2 linker and E4131L in C-terminal (**Figure 2**). No hotspot variant or region was observed.

The molecular effect of the missense variants was further analyzed by protein modeling using I-TASSER (**Figure 3**). Two pairs of compound heterozygous variants (c.8744A > G/p.N2915S and c.11689C > T/p.L3897F, c.12391_12392delinsTT/p.E4131L and c.10315C > T/p.R3439W) had hydrogen bonding changes in both biallelic variants. Another three pairs (c.3362G > A/p.S1121N and c.8680G > A/p.A2894T, c.10102G > A/p.D3368N and c.5212C > T/p.L1738F, c.1966C > G/p.L656V and c.4817C > G/p.T1606S) had hydrogen bonding changes in one of the paired variants. The other three pairs (c.5401C > T/p.P1801S and c.6878C > T/p.P2293L, c.3587C > T/p.T1196M and c.10733C > T/p.A3578V, c.6706T > C/p.F2236L and c.10760C > T/p.A3587V) showed no hydrogen bond changes, but P1801S and F2236L were predicted to decrease the protein stability measured by $\Delta\Delta G$.

Clinical Features of the Cases With *PKD1* Mutations

The detailed clinical characteristics of the eight cases with compound heterozygous *PKD1* variants were summarized in **Table 1**. All patients began with FS, which started ranged from 1 to 6 years old, with a median onset age of 2.7 years. Seven patients developed afebrile seizures and were diagnosed as epilepsy with antecedent FS, and one patient (case 7) was affected by only FS. Six of the patients had complex partial seizures. Five patients showed generalized tonic-clonic seizures (GTCS), whom all had one of paired variants that was located in the PKD domains. All patients suffered infrequent seizures that ranged from several episodes to monthly seizures and became seizure-free finally, including two without AEDs treatment (case 2 and 7), four after monotherapy of AEDs (case 1, 5, 6, and 8), and two with combination of two AEDs (case 3 and 4). The EEGs in the seven patients with epilepsy showed focal discharges or diffused discharges with predominance in focal regions (**Table 1** and **Figure 4**). Brain MRI was normal in all cases. All the patients had normal development and showed no enlarged kidneys or kidney cysts.

[7]http://www.uniprot.org

TABLE 2 | A gene-based burden analysis for *PKD1* mutations identified in this study.

	Allele count/number in this study	Allele count/number in the gnomAD-all population	Allele count/number in the controls of gnomAD-all population	Allele count/number in the gnomAD-East Asian	Allele count/number in the controls of gnomAD-East Asian	Allele count/number in the controls of 296 healthy volunteers
Identified *PKD1* mutations						
chr16: 2161806 (c.3362G > A/p.S1121N)	1/628	–/–	–/–	–/–	–/–	0
chr16: 2153378 (c.8680G > A/p.A2894T)	1/628	17/267314 (0.00006360)	9/101036 (0.00008908)	1/19432 (0.00005146)	0/8668 (0)	0
chr16: 2159767 (c.5401C > T/p.P1801S)	1/628	8/239710 (0.00003337)	4/106082 (0.00003771)	4/17982 (0.0002224)	3/8750 (0.0003429)	0
chr16: 2158290 (c.6878C > T/p.P2293L)	1/628	33/275052 (0.0001200)	18/118012 (0.0001525)	19/19500 (0.0009744)	10/9576 (0.001044)	0
chr16: 2153314 (c.8744A > G/p.N2915S)	1/628	39/272678 (0.0001430)	18/116880 (0.0001540)	21/19496 (0.001077)	10/9604 (0.001041)	0
chr16: 2141447 (c.11689C > T/p.L3897F)*	1/628	4/4272 (0.0009363)	2/2036 (0.0009823)	0/62 (0)	0/40 (0)	0
chr16: 2147410 (c.10315C > T/p.R3439W)	1/628	51/275532 (0.0001851)	20/116618 (0.0001715)	39/19728 (0.001977)	18/9778 (0.001841)	0
chr16: 2140338, 2140339 (c.12391_12392delinsTT/ p.E4131L)	1/628	–/–	–/–	–/–	–/–	0
chr16: 2161581 (c.3587C > T/p.T1196M)*	1/628	4/181588 (0.00002203)	3/78930 (0.00003801)	3/13498 (0.0002223)	3/5936 (0.0005054)	0
chr16: 2143900 (c.10733C > T/p.A3578V)*	1/628	5/226808 (0.00002205)	2/80606 (0.00002481)	2/16796 (0.0001191)	1/7018 (0.0001425)	0
chr16: 2159956 (c.5212C > T/p.L1738F)	1/628	5/239702 (0.00002086)	5/105408 (0.00004743)	5/20568 (0.0002431)	5/13110 (0.0003814)	0
chr16: 2147934 (c.10102G > A/p.D3368N)	1/628	63/251880 (0.0002501)	24/108086 (0.0002220)	57/18150 (0.003140)	22/8750 (0.002514)	0
chr16: 2158462 (c.6706T > C/p.F2236L)	1/628	5/246952 (0.00002025)	2/108614 (0.00001841)	5/17974 (0.0002782)	2/8674 (0.0002306)	0
chr16: 2143873 (c.10760C > T/p.A3587V)	1/628	8/221464 (0.00003612)	3/88270 (0.00003399)	0/16258 (0)	0/7610 (0)	0
chr16: 2165510 (c.1966C > G/p.L656V)	1/628	–/–	–/–	–/–	–/–	0
chr16: 2160351 (c.4817C > G/p.T1606S)	1/628	6/249556 (0.00002404)	2/109386 (0.00001828)	6/18364 (0.0003267)	2/9044 (0.0002211)	0
Total	16/628	248/221464 (0.001120)	112/88270 (0.001269)	162/16258 (0.009964)	76/7610 (0.009987)	0
***P* value**		2.2×10^{-16}	1.43×10^{-15}	0.001014	0.002089	3.06×10^{-5}
OR (95% CI)		23.327 (13.042–38.887)	20.578 (11.300–35.177)	2.597 (1.441–4.382)	2.591 (1.401–4.518)	∞ (3.705–∞)

*OR, odd ratio; P values and odd ratio were estimated by two-sided Fisher's exact test. *The variants were excluded from statistical analysis because of the low-quality genotypes in gnomAD.*

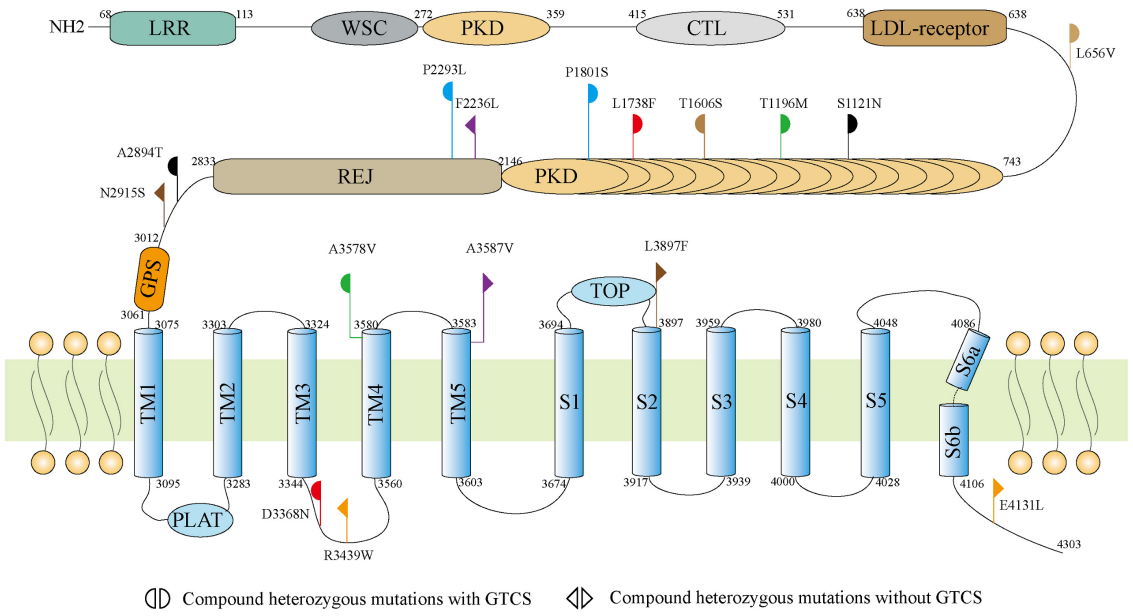

FIGURE 2 | Schematic illustration of the PC1 and locations of the *PKD1* mutations identified in this study.

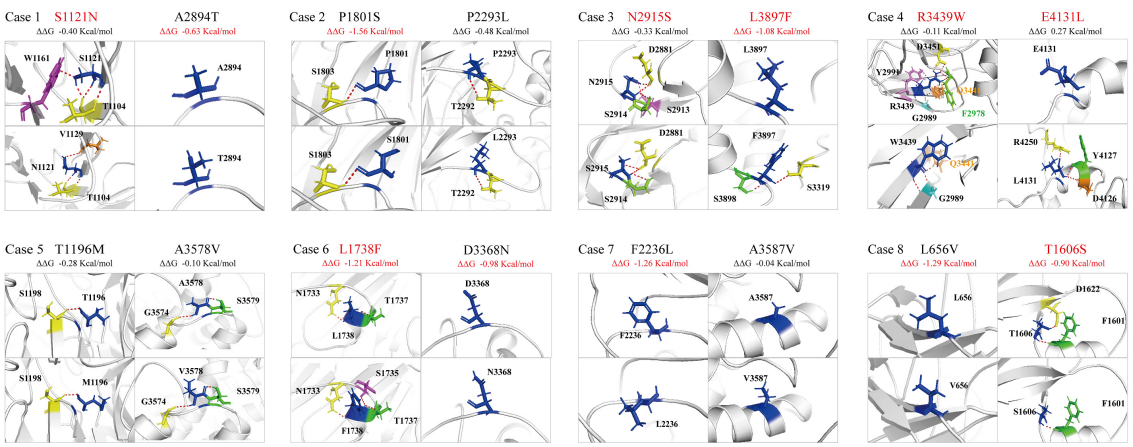

FIGURE 3 | Hydrogen bond changes of the *PKD1* mutants. Variants with changes on hydrogen bonding or free energy stability are highlighted in red.

In summary, the patients with compound heterozygous *PKD1* variants showed several common features: all began with febrile seizures; suffered infrequent seizures and became seizure-free; focal discharges in EEGs; and normal neurodevelopment.

The Expression Profile of *PKD1*

The expression of PC1 is ubiquitously distributed and developmentally regulated, predominantly during embryonic, infant, and adult stage. Tissue-specific expression is the basis of gene function and subsequently the clinical phenotype. We thus compared the expression of *PKD1* in the human brain and the kidney. In UniGene database, *PKD1* in the brain is expressed 1.79 times as much as that in the kidney (**Figure 5A**)[8]. Furthermore, data from the GTEx database showed that *PKD1* was highly and widely expressed in all sub-regions of the brain, including the cortex, hypothalamus and hippocampus. Expression of *PKD1* in these sub-regions of the brain was higher than that in the kidney, for example, the expression in the brain cortex was 6.10 times higher than that in the kidney cortex (**Figure 5B**)[9].

Genotype-Phenotype Association of *PKD1* Variants

To explore the mechanism underlying phenotypic variations, we systematically reviewed *PKD1* mutations and analyzed correlations between genotypes and phenotypes. To date, a total

[8]https://www.ncbi.nlm.nih.gov/gene/5310

[9]https://www.gtexportal.org/home/index.html

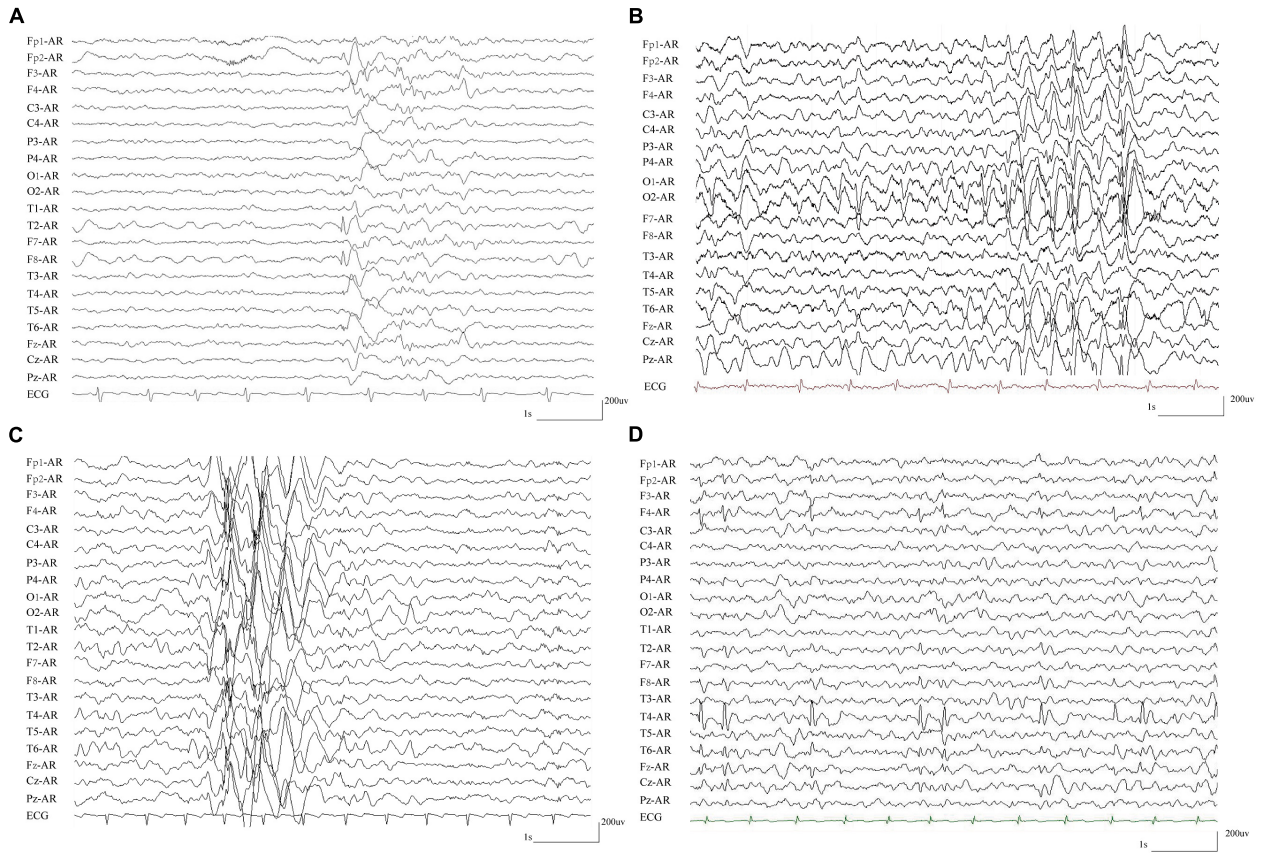

FIGURE 4 | Representative EEG recordings from patients with compound heterozygous *PKD1* mutations. **(A)** Interictal EEG in case 3 showed spike-slow and slow waves in the right anterior frontal and temporal regions. **(B)** Interictal EEG in case 4 showed spike-slow and slow waves in the bilateral occipital lobes and diffused spike-slow waves. **(C)** Interictal EEG in case 5 showed irregular diffused spike-slow waves with predominance in the right areas. **(D)** Interictal EEG in case 8 showed spike-slow waves in the right frontal and temporal regions.

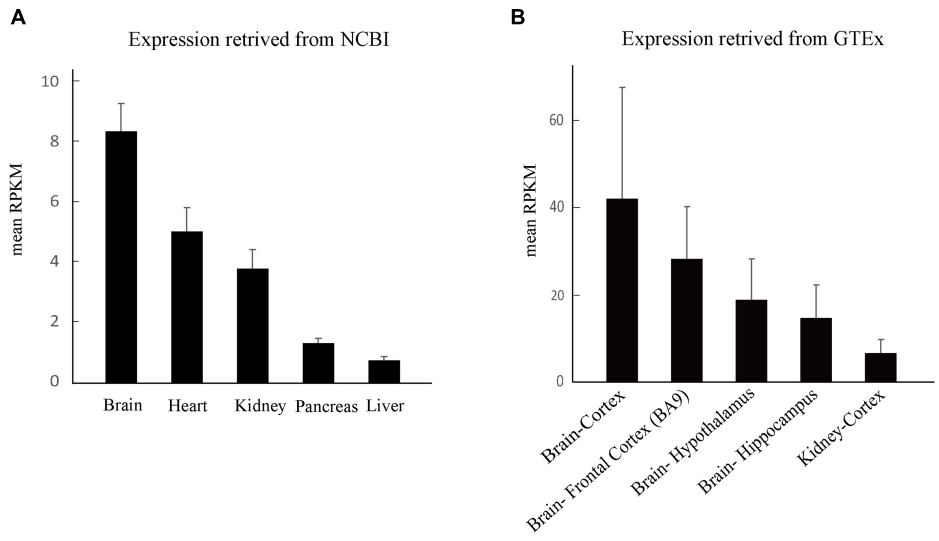

FIGURE 5 | Tissue expression of *PKD1*. **(A)** The overall expression of *PKD1* in different tissues retrieved from NCBI. **(B)** Comparison of *PKD1* expression in the sub-regions of human brain and kidney retrieved from GTEx.

of 2599 mutations have been registered to be associated with ADPKD or sporadic PKD in the HGMD database and ADPKD Mutation Database. ADPKD/PKD-associated *PKD1* mutations were mainly monoallelic mutations (90.9%, 2360/2599), among which majority (72.3%, 1706/2360) were destructive mutations, including nonsense, splicing defects, frameshifting, in frame deletion/insertions, and large rearrangements. A small portion (9.1%) of the 2599 mutations were reported as biallelic mutations in ADPKD/PKD, including 114 pairs of compound heterozygotes and nine pairs of homozygotes. It was noticed that the nine pairs of *PKD1* homozygotes were associated with a severe phenotype in 14 individuals, and 21.4% of the patients with homozygotes (3/14) were premature neonate died and others (71.4%, 10/14) exhibited *in utero* onset ADPKD (Cornec-Le Gall et al., 2018; Al-Hamed et al., 2019; Garel et al., 2019; Durkie et al., 2021).

In contrast, in the present study, FS/EFS+ associated *PKD1* mutations were all compound heterozygous missense mutations (100%, 16/16).

Evaluation of Epilepsy as a Novel Phenotype of *PKD1* Variants

We evaluated the *PKD1*-epilepsy correlation by using ClinGen Clinical-Validity Framework. The total allowable points from clinical-genetic aspect were 7.5 points and that from experimental aspect were 6 points. The results of clinical validity summary matrix were 13.5 points that was categorized as "Strong," supporting the association between *PKD1* variants and FS/EFS+ (**Table 3**).

DISCUSSION

PKD1 encodes PC1, a large transmembrane protein that plays multiple roles in cell proliferation, apoptosis, cell polarity, and cation transport (Paul and Vanden Heuvel, 2014). Previous studies have demonstrated that *PKD1* is the major causative gene of ADPKD, of which mutations are responsible for 85% of ADPKD cases (Paul and Vanden Heuvel, 2014; Kim and Park, 2016). However, the expression of PC1 in the brain is much higher than that in the kidney (**Figures 5A,B**), suggesting a role in the function of the brain. In the present study, compound heterozygous *PKD1* mutations were identified in eight unrelated cases with FS and epilepsy with antecedent FS. The frequency of the *PKD1* variants in the cohort of epilepsy was significantly higher than that in control populations in gnomAD. These findings suggested that *PKD1* was potentially associated with epilepsy. The evaluation from ClinGen Clinical-Validity Framework also supports a strong association between *PKD1* mutations and epilepsy.

The transmembrane protein PC1 comprises a large extracellular N terminus, eleven membrane-spanning domains, and a short cytoplasmic C terminus. It functions as a channel subunit, cell surface receptor, and G-protein coupled receptor (Hu and Harris, 2020). PC1 may form ion channel pore by itself or contribute to channel pore *via* formation of heteromultimeric channels with PC2 (Babich et al., 2004). Generally, PC1 interacts with PC2 through the C-terminal tail to form a voltage-regulated Ca^{2+} channel, which regulates intracellular calcium influx. The simultaneous presence of both PC1 and PC2 amplify the inositol trisphosphate-induced Ca^{2+} release (Mekahli et al., 2012). Expression of PC1 can also regulate channel activity independent of the channel activity of PC2 (Babich et al., 2004). As a constitutive activator of G-proteins, PC1 activates endogenous voltage-activated Ca^{2+} channels and G protein-activated inward rectifying K^+ channels in sympathetic neurons (Delmas et al., 2002). Deletion of PC1 caused complete loss of ionic currents (Babich et al., 2004). The calcium homeostasis is critical for neuronal stability and excitation, and the intracellular Ca^{2+} is essential for many basic cellular processes of neurons. Besides, PC1 is extensively expressed in the brain, especially in the cortex and hippocampus. These findings provide an electrophysiological and an anatomical basis for epileptogenesis.

As a receptor, PC1 is involved in multiple signaling pathways, such as Wnt signaling pathway, AP-1, PI3kinase/Akt, GSK3β, STAT6, and the mammalian target of rapamycin (mTOR) pathway (Boca et al., 2007; Boletta, 2009; Holditch et al., 2019). PC1 inhibits mTOR activity by stabilizing the tuberous sclerosis 1-tuberous sclerosis 2 (TSC1–TSC2) complex, which is known as a negative regulator of the mTOR complex (Boletta, 2009; Distefano et al., 2009). Through mediating signaling, PC1 regulates cell proliferation, differentiation, and apoptosis (Paul and Vanden Heuvel, 2014). Homozygous *Pkd1* knockout mice have exhibited neural tube defects and embryonic lethality (Lu et al., 2001; Lantinga-van Leeuwen et al., 2007), indicating that *PKD1* is important for the development of the brain. In the present study, the seven patients with EFS+ and *PKD1* mutations had complex partial seizures and/or focal discharges in EEGs, suggesting potential neurodevelopmental abnormalities. However, whether the *PKD1* variants were associated with brain malformation warrants further studies with large cohorts and advanced neuroimaging techniques.

It was noticed that five patients with GTCS had one of the paired missense variants that was located in the Ig-like PKD repeat domains of the N terminus. The PKD repeat domains play an important role in the PC1-dependent channel activity (Babich et al., 2004), possibly through regulating homophilic cell-cell/cell-matrix interactions (Ibraghimov-Beskrovnaya et al., 2000). Extracellular application of antibodies against the Ig-like PKD domains disrupted cell-cell adhesion, and reduces PC1-dependent ionic currents (Ibraghimov-Beskrovnaya et al., 2000; Babich et al., 2004). These data suggested that mutations in the PKD domains were possibly associated with GTCS, which warrants further validation by large cohorts and functional studies.

Previously reported *PKD1* mutations were mainly associated with ADPKD. From the genotype aspect, ADPKD-associated *PKD1* mutations were mainly monoallelic, and majority of the mutations were destructive (Sandford, 2009; Cornec-Le Gall et al., 2014; Lanktree et al., 2021), implying that monoallelic mutations with haploinsufficiency of *PKD1* potentially caused kidney disease. Less commonly, truncating *PKD1* mutations

TABLE 3 | Evaluating the clinical validity of *PKD1*-epilepsy associations based on the framework developed by the clinical genome resource.

Case-level data	Evidence type		Case information			Suggested points/case		Points given	Max score
						Default	Range		
	Variant evidence	Autosomal dominant OR X-linked disorder	Variant is *de novo*			2	0–3	0	12
			Proband with predicted or proven null variant			1.5	0–2	0	10
			Proband with other variant type with some evidence of gene impact			0.5	0–1.5	0	7
		Autosomal recessive	Two variants in trans and at least one *de novo* or a predicted/proven null variant			2	0–3	0	12
			Two variants (not predicted/proven null) with some evidence of gene impact in trans			1	0–1.5	7.5[a]	
	Segregation evidence		Evidence of segregation in one or more families	LOD score example	3	5	0–7	0	7
					2	4			
					1.5	3			
					1	0.5			
Case-control data	**Case-control study type**		**Case-control quality criteria**			**Suggested points/study**		**Points given**	**Max score**
	Single variant analysis		• Variant detection methodology • Power • Bias and confounding factors • Statistical significance			0–6			12
	Aggregate variant analysis					0–6		6[b]	

(Continued)

TABLE 3 | (Continued)

Total allowable points for genetic evidence				7.5	12
Evidence category	**Evidence type**	**Suggested points**		**Points given**	**Max score**
		Default	**Range**		
Function	Biochemical function	0.5	0–2	0.5[c]	2
	Protein interaction		0–2	0.5[d]	
	Expression		0–2	1[e]	
Functional alteration	Cells from affected individual	1	0–2	0	2
	Engineered cells	0.5	0–1	0	
Models and rescue	Animal model	2	0–4	3[f]	4
	Cell culture model system	1	0–2	1[g]	
	Rescue in animal model	2	0–4	0	
	Rescue in engineered equivalent	1	0–2	0	
Total allowable points for experimental evidence		6		6	6
Clinical validity summary matrix				13.5	Strong

[a] *Two pairs of compound heterozygous variants had hydrogen bonding changes and were predicted to be damaging in both biallelic variants; three pairs had hydrogen bonding changes in one variant and free energy stability changes (ΔΔG) or predicted damaging effect in the other paired variant; three pairs had free energy stability changes (ΔΔG) or predicted damaging effect in one of the paired variants (1.5 pt × 2 cases + 1.0 pt × 3 cases + 0.5 pt × 3 case = 7.5 pts).*

[b] *This is an aggregate analysis. Comparing to allele number in gnomAD-control populations and in controls of gnomAD-East Asian populations, the frequency of the variants in the present cohort is significant higher (**Table 2**) (Assigned 6 pts). The points are not included in total allowable points for genetic evidence.*

[c] *PC1plays multiple roles in cell proliferation, apoptosis, cell polarity, and cation transport, which is involved in neuronal excitation and synaptic plasticity (Assigned 0.5 pt).*

[d] *PC1 interacts with PC2 to form a voltage-regulated Ca^{2+} channel that regulates calcium homeostasis. As a receptor, PC1 is involved in multiple signaling pathways, such as Wnt signaling pathway, AP-1, PI3kinase/Akt, GSK3β, STAT6, and mTOR pathway, regulating cell proliferation, differentiation, and apoptosis (Assigned 0.5 pt).*

[e] *PC1 is ubiquitously distributed and highly expressed in the brain (Assigned 1 pt).*

[f] *Homozygous Pkd1 knockout mice have exhibited neural tube defects and embryonic or perinatal lethality (Assigned 3 pt).*

[g] *In human cells, mitochondrial abnormalities were identified both in the cells with homozygous PKD1 mutation and in those carrying heterozygous PKD1 mutation (Assigned 1 pt).*

were identified in families ADPKD (Lanktree et al., 2021). Homozygotes of *PKD1* mutations caused severe phenotype with *in utero* onset ADPKD or premature neonate death (Cornec-Le Gall et al., 2018; Al-Hamed et al., 2019; Garel et al., 2019; Durkie et al., 2021), consistent with the embryonic lethality in homozygous *Pkd1* knockout mice (Lu et al., 2001; Lantinga-van Leeuwen et al., 2007). A quantitative correlation between genetic impairment and phenotypic severity was suggested. In the present study, the *PKD1* mutations identified in our patients with FS/EFS+ were all compound heterozygous missense mutations. All patients showed infrequent seizures and became seizure-free without AEDs treatment or after treatments of one or two AEDs. All the children showed no enlarged kidney or kidney cysts at present. Whether they will develop kidney abnormalities in later adulthood needs further follow-up. On the other hand, attention should be paid to whether the PKD patients with compound heterozygous variants had self-limited FS or mild seizures in their early life.

This study has several limitations. The direct functional effects of the mutations were not examined. The whole spectrum of phenotype of *PKD1* mutations warrants further determination with large cohorts.

CONCLUSION

This study identified eight pairs of compound heterozygous missense mutations in patients with FS/EFS+. These mutations presented significantly higher frequency in case cohort than that in the control populations. Taken together the data from gene expression profile, gene functions, and *PKD1* deficiency animal model, it is suggested that *PKD1* was potentially a novel cause of epilepsy. Further analysis revealed that monoallelic mutations with haploinsufficiency of *PKD1* were associated with PKD, homozygotes with complete loss of PC1 would be embryonically lethal, whereas compound heterozygotes with superimposed effects of two missense mutations were potentially associated with epilepsy with good prognosis. The genotype-phenotype correlation helps explaining phenotypical variations.

DATA AVAILABILITY STATEMENT

The original contributions presented in the study are publicly available. This data can be found here: NCBI, OM969823, and OM969870.

ETHICS STATEMENT

The studies involving human participants were reviewed and approved by the Ethics Committee of The Second Affiliated Hospital of Guangzhou Medical University. Written informed consent to participate in this study was provided by the participants' legal guardian/next of kin. Written informed consent was obtained from the minor(s)' legal guardian/next of kin for the publication of any potentially identifiable images or data included in this article.

AUTHOR CONTRIBUTIONS

NH, J-YW, and JW contributed to the conception of the study, interpretation of clinical data, and drafting of the manuscript. X-GL, WS, SL, D-FZ, L-DH, QP, YT, L-DG, and W-PL examined the patients and participated in drafting of the manuscript. W-PL provided critical review and substantially revised the manuscript. All authors read and approved the manuscript before sending the manuscript to the journal for publication.

FUNDING

This work was funded by the National Natural Science Foundation of China (Grant No. 81971216 to NH), Science and Technology Project of Guangdong Province (Grant No. 2017B030314159 to W-PL), Guangdong Basic and Applied Basic Research Foundation (Grant No. 2020A1515011048 to NH), Science and Technology Project of Guangzhou (Grant Nos. 201904010292 to NH and 201904020028 to W-PL), and UCB Pharma Ltd., Joint Science Research Foundation of China Association Against Epilepsy (Grant No. 2020006B to NH). The funders had no role in study design, data collection and analysis, and decision to publish or preparation of the manuscript.

ACKNOWLEDGMENTS

The help of patients and clinicians participating in this work are greatly appreciated.

SUPPLEMENTARY MATERIAL

The Supplementary Material for this article can be found online at: https://www.frontiersin.org/articles/10.3389/fnmol.2022.861159/full#supplementary-material

REFERENCES

Al-Hamed, M. H., Alsahan, N., Rice, S. J., Edwards, N., Nooreddeen, E., Alotaibi, M., et al. (2019). Bialleleic PKD1 mutations underlie early-onset autosomal dominant polycystic kidney disease in Saudi Arabian families. *Pediatr. Nephrol.* 34, 1615–1623. doi: 10.1007/s00467-019-04267-x

Arac, D., Boucard, A. A., Bolliger, M. F., Nguyen, J., Soltis, S. M., Sudhof, T. C., et al. (2012). A novel evolutionarily conserved domain of cell-adhesion GPCRs mediates autoproteolysis. *EMBO J.* 31, 1364–1378. doi: 10.1038/emboj.2012.26

Babich, V., Zeng, W. Z., Yeh, B. I., Ibraghimov-Beskrovnaya, O., Cai, Y., Somlo, S., et al. (2004). The N-terminal extracellular domain is required for polycystin-1-dependent channel activity. *J. Biol. Chem.* 279, 25582–25589. doi: 10.1074/jbc.M402829200

Baulac, S., Gourfinkel-An, I., Nabbout, R., Huberfeld, G., Serratosa, J., Leguern, E., et al. (2004). Fever, genes, and epilepsy. *Lancet Neurol.* 3, 421–430. doi: 10.1016/S1474-4422(04)00808-7

Boca, M., D'Amato, L., Distefano, G., Polishchuk, R. S., Germino, G. G., and Boletta, A. (2007). Polycystin-1 induces cell migration by regulating phosphatidylinositol 3-kinase-dependent cytoskeletal rearrangements and GSK3beta-dependent cell cell mechanical adhesion. *Mol. Biol. Cell* 18, 4050–4061. doi: 10.1091/mbc.e07-02-0142

Boletta, A. (2009). Emerging evidence of a link between the polycystins and the mTOR pathways. *Pathogenetics* 2:6. doi: 10.1186/1755-8417-2-6

Capriotti, E., Fariselli, P., and Casadio, R. (2005). I-Mutant2.0: predicting stability changes upon mutation from the protein sequence or structure. *Nucleic Acids Res.* 33, W306–W310. doi: 10.1093/nar/gki375

Consortium, C. (2015). Sparse whole-genome sequencing identifies two loci for major depressive disorder. *Nature* 523, 588–591. doi: 10.1038/nature14659

Cornec-Le Gall, E., Audrezet, M. P., Le Meur, Y., Chen, J. M., and Ferec, C. (2014). Genetics and pathogenesis of autosomal dominant polycystic kidney disease: 20 years on. *Hum. Mutat.* 35, 1393–1406. doi: 10.1002/humu.22708

Cornec-Le Gall, E., Torres, V. E., and Harris, P. C. (2018). Genetic complexity of autosomal dominant polycystic Kidney and Liver Diseases. *J. Am. Soc. Nephrol.* 29, 13–23. doi: 10.1681/ASN.2017050483

Delmas, P., Nomura, H., Li, X., Lakkis, M., Luo, Y., Segal, Y., et al. (2002). Constitutive activation of G-proteins by polycystin-1 is antagonized by polycystin-2. *J. Biol. Chem.* 277, 11276–11283. doi: 10.1074/jbc.M110483200

Distefano, G., Boca, M., Rowe, I., Wodarczyk, C., Ma, L., Piontek, K. B., et al. (2009). Polycystin-1 regulates extracellular signal-regulated kinase-dependent phosphorylation of tuberin to control cell size through mTOR and its downstream effectors S6K and 4EBP1. *Mol. Cell Biol.* 29, 2359–2371. doi: 10.1128/MCB.01259-08

Durkie, M., Chong, J., Valluru, M. K., Harris, P. C., and Ong, A. C. M. (2021). Biallelic inheritance of hypomorphic PKD1 variants is highly prevalent in very early onset polycystic kidney disease. *Genet. Med.* 23, 689–697. doi: 10.1038/s41436-020-01026-4

Fagerberg, L., Hallstrom, B. M., Oksvold, P., Kampf, C., Djureinovic, D., Odeberg, J., et al. (2014). Analysis of the human tissue-specific expression by genome-wide integration of transcriptomics and antibody-based proteomics. *Mol. Cell Proteomics* 13, 397–406. doi: 10.1074/mcp.M113.035600

Gallagher, A. R., Germino, G. G., and Somlo, S. (2010). Molecular advances in autosomal dominant polycystic kidney disease. *Adv. Chronic Kidney Dis.* 17, 118–130. doi: 10.1053/j.ackd.2010.01.002

Garel, J., Lefebvre, M., Cassart, M., Della Valle, V., Guilbaud, L., Jouannic, J. M., et al. (2019). Prenatal ultrasonography of autosomal dominant polycystic kidney disease mimicking recessive type: case series. *Pediatr. Radiol.* 49, 906–912. doi: 10.1007/s00247-018-4325-3

Geng, L., Segal, Y., Pavlova, A., Barros, E. J., Lohning, C., Lu, W., et al. (1997). Distribution and developmentally regulated expression of murine polycystin. *Am. J. Physiol.* 272, F451–F459. doi: 10.1152/ajprenal.1997.272.4.F451

Ha, K., Nobuhara, M., Wang, Q., Walker, R. V., Qian, F., Schartner, C., et al. (2020). The heteromeric PC-1/PC-2 polycystin complex is activated by the PC-1 N-terminus. *eLife* 9:e60684. doi: 10.7554/eLife.60684

Holditch, S. J., Brown, C. N., Atwood, D. J., Lombardi, A. M., Nguyen, K. N., Toll, H. W., et al. (2019). A study of sirolimus and mTOR kinase inhibitor in a hypomorphic Pkd1 mouse model of autosomal dominant polycystic kidney disease. *Am. J. Physiol. Renal Physiol.* 317, F187–F196. doi: 10.1152/ajprenal.00051.2019

Hu, J., and Harris, P. C. (2020). Regulation of polycystin expression, maturation and trafficking. *Cell Signal* 72:109630. doi: 10.1016/j.cellsig.2020.109630

Hughes, J., Ward, C. J., Peral, B., Aspinwall, R., Clark, K., San Millan, J. L., et al. (1995). The polycystic kidney disease 1 (PKD1) gene encodes a novel protein with multiple cell recognition domains. *Nat. Genet.* 10, 151–160. doi: 10.1038/ng0695-151

Ibraghimov-Beskrovnaya, O., Bukanov, N. O., Donohue, L. C., Dackowski, W. R., Klinger, K. W., and Landes, G. M. (2000). Strong homophilic interactions of the Ig-like domains of polycystin-1, the protein product of an autosomal dominant polycystic kidney disease gene. PKD1. *Hum. Mol. Genet.* 9, 1641–1649. doi: 10.1093/hmg/9.11.1641

Kim, D. Y., and Park, J. H. (2016). Genetic Mechanisms of ADPKD. *Adv. Exp. Med. Biol.* 933, 13–22. doi: 10.1007/978-981-10-2041-4_2

Kim, S., Nie, H., Nesin, V., Tran, U., Outeda, P., Bai, C. X., et al. (2016). The polycystin complex mediates Wnt/Ca(2+) signalling. *Nat. Cell Biol.* 18, 752–764. doi: 10.1038/ncb3363

Lanktree, M. B., Guiard, E., Akbari, P., Pourafkari, M., Iliuta, I. A., Ahmed, S., et al. (2021). Patients with Protein-Truncating PKD1 Mutations and Mild ADPKD. *Clin. J. Am. Soc. Nephrol.* 16, 374–383. doi: 10.2215/CJN.11100720

Lantinga-van Leeuwen, I. S., Leonhard, W. N., van der Wal, A., Breuning, M. H., de Heer, E., and Peters, D. J. (2007). Kidney-specific inactivation of the Pkd1 gene induces rapid cyst formation in developing kidneys and a slow onset of disease in adult mice. *Hum. Mol. Genet.* 16, 3188–3196. doi: 10.1093/hmg/ddm299

Lu, W., Shen, X., Pavlova, A., Lakkis, M., Ward, C. J., Pritchard, L., et al. (2001). Comparison of Pkd1-targeted mutants reveals that loss of polycystin-1 causes cystogenesis and bone defects. *Hum. Mol. Genet.* 10, 2385–2396. doi: 10.1093/hmg/10.21.2385

Martin, H. C., Jones, W. D., McIntyre, R., Sanchez-Andrade, G., Sanderson, M., Stephenson, J. D., et al. (2018). Quantifying the contribution of recessive coding variation to developmental disorders. *Science* 362, 1161–1164. doi: 10.1126/science.aar6731

Mekahli, D., Sammels, E., Luyten, T., Welkenhuyzen, K., van den Heuvel, L. P., Levtchenko, E. N., et al. (2012). Polycystin-1 and polycystin-2 are both required to amplify inositol-trisphosphate-induced Ca2+ release. *Cell Calcium* 51, 452–458. doi: 10.1016/j.ceca.2012.03.002

Paul, B. M., and Vanden Heuvel, G. B. (2014). Kidney: polycystic kidney disease. *Wiley Interdiscip. Rev. Dev. Biol.* 3, 465–487. doi: 10.1002/wdev.152

Rondeau, E. (1995). Polycystic kidney: complete structure of the PKD1 gene and its protein. *Nephrologie* 16, 338–339.

Sandford, R. N. (2009). The diversity of PKD1 alleles: implications for disease pathogenesis and genetic counseling. *Kidney Int.* 75, 765–767. doi: 10.1038/ki.2009.17

Semmo, M., Kottgen, M., and Hofherr, A. (2014). The TRPP subfamily and polycystin-1 proteins. *Handb. Exp. Pharmacol.* 222, 675–711. doi: 10.1007/978-3-642-54215-2_27

Stokely, M. E., Hwang, S. Y., Hwang, J. Y., Fan, B., King, M. A., Inokuchi, K., et al. (2006). Polycystin-1 can interact with homer 1/Vesl-1 in postnatal hippocampal neurons. *J. Neurosci. Res.* 84, 1727–1737. doi: 10.1002/jnr.21076

Strande, N. T., Riggs, E. R., Buchanan, A. H., Ceyhan-Birsoy, O., DiStefano, M., Dwight, S. S., et al. (2017). Evaluating the clinical validity of gene-disease associations: an evidence-based framework developed by the clinical genome resource. *Am. J. Hum. Genet.* 100, 895–906. doi: 10.1016/j.ajhg.2017.04.015

Su, Q., Hu, F., Ge, X., Lei, J., Yu, S., Wang, T., et al. (2018). Structure of the human PKD1-PKD2 complex. *Science* 361:eaat9819. doi: 10.1126/science.aat9819

Wang, J., Lin, Z. J., Liu, L., Xu, H. Q., Shi, Y. W., Yi, Y. H., et al. (2017). Epilepsy-associated genes. *Seizure* 44, 11–20. doi: 10.1016/j.seizure.2016.11.030

Wang, J., Qiao, J. D., Liu, X. R., Liu, D. T., Chen, Y. H., Wu, Y., et al. (2021). UNC13B variants associated with partial epilepsy with favourable outcome. *Brain* 144, 3050–3060. doi: 10.1093/brain/awab164

Conflict of Interest: The authors declare that the research was conducted in the absence of any commercial or financial relationships that could be construed as a potential conflict of interest.

Publisher's Note: All claims expressed in this article are solely those of the authors and do not necessarily represent those of their affiliated organizations, or those of the publisher, the editors and the reviewers. Any product that may be evaluated in this article, or claim that may be made by its manufacturer, is not guaranteed or endorsed by the publisher.

frontiers | Frontiers in Molecular Neuroscience

ORIGINAL RESEARCH
published: 17 May 2022
doi: 10.3389/fnmol.2022.862480

SHROOM4 Variants Are Associated With X-Linked Epilepsy With Features of Generalized Seizures or Generalized Discharges

Wen-Jun Bian†‡, Zong-Jun Li‡, Jie Wang, Sheng Luo, Bing-Mei Li, Liang-Di Gao, Na He and Yong-Hong Yi†*

Institute of Neuroscience and Department of Neurology, Key Laboratory of Neurogenetics and Channelopathies of Guangdong Province and the Ministry of Education of China, The Second Affiliated Hospital of Guangzhou Medical University, Guangzhou, China

OPEN ACCESS

Edited by:
Qian Chen, Massachusetts Institute of Technology, United States

Reviewed by:
Xiaofeng Yang, Bioland Laboratory, China
Nigel CK Tan, National Neuroscience Institute (NNI), Singapore

***Correspondence:**
Yong-Hong Yi
yyh168@sina.com

†ORCID:
Wen-Jun Bian
orcid.org/0000-0002-7175-1210
Yong-Hong Yi
orcid.org/0000-0002-6075-2015

‡These authors have contributed equally to this work

Specialty section:
This article was submitted to Molecular Signalling and Pathways, a section of the journal Frontiers in Molecular Neuroscience

Received: *26 January 2022*
Accepted: *25 April 2022*
Published: *17 May 2022*

Citation:
Bian W-J, Li Z-J, Wang J, Luo S, Li B-M, Gao L-D, He N and Yi Y-H (2022) SHROOM4 Variants Are Associated With X-Linked Epilepsy With Features of Generalized Seizures or Generalized Discharges. Front. Mol. Neurosci. 15:862480. doi: 10.3389/fnmol.2022.862480

Objective: *SHROOM4* gene encodes an actin-binding proteins, which plays an important role in cytoskeletal architecture, synaptogenesis, and maintaining gamma-aminobutyric acid receptors-mediated inhibition. *SHROOM4* mutations were reported in patients with the Stocco dos Santos type of X-linked syndromic intellectual developmental disorder (SDSX; OMIM# 300434). In this study, we investigated the association between *SHROOM4* and epilepsy.

Methods: Trios-based whole-exome sequencing was performed in a cohort of 320 cases with idiopathic generalized epilepsy or idiopathic partial epilepsy. Protein modeling was used to assess the damaging effects of variations.

Results: Six hemizygous missense *SHROOM4* variants, including c.13C > A/p.Pro5Thr, c.3236C > T/p.Glu1079Ala, c.3581C > T/p.Ser1194Leu, c.4288C > T/p.Arg1430Cys, c.4303G > A/p.Val1435Met, c.4331C > T/p.Pro1444Leu, were identified in six cases with idiopathic epilepsy without intellectual disability. All patients presented with features of generalized seizures or generalized discharges. These hemizygous variants had no or extremely low allele frequencies in controls and showed statistically higher frequency in the case cohort than controls. All variants were predicted to alter hydrogen bond with surrounding amino acids or decreased protein stability. The *SHROOM4* variants reported in patients with SDSX were mostly destructive or duplicative variants; in contrast, the *SHROOM4* variants were all missense variants, suggesting a potential genotype-phenotype correlation. The two missense variants associated with SDSX were located in the middle of SHROOM4 protein, whereas variants associated with idiopathic epilepsy were located around the N-terminal PDZ domain and the C-terminal ASD2 domain.

Significance: *SHROOM4* was potentially a candidate pathogenic gene of idiopathic epilepsy without intellectual disability. The genotype-phenotype correlation and sub-regional effect helps understanding the mechanism underlying phenotypic variation.

Keywords: epilepsy, *SHROOM4* gene, whole-exome sequencing, intellectual disability, genotype-phenotype correlation, sub-regional effect

INTRODUCTION

SHROOM4 gene (OMIM* 300579) (also known as *KIAA1202* gene) resides on Xp11.22 and encodes a member of the actin-binding proteins of shroom family (Hagens et al., 2006), which contain a PDZ and an ASD2 domain. The SHROOM4 protein is broadly distributed, including the brain and predominantly during embryonic and adult period. SHROOM4 and members of this protein family have been shown to localize at the cytoskeleton, and play a role in neurulation, cellular architecture, actin remodeling, ion channel function, and synaptogenesis (Hagens et al., 2006; Zapata et al., 2017). *SHROOM4* mutations have been demonstrated to be associated with Stocco dos Santos type of X-linked syndromic intellectual developmental disorder (SDSX; OMIM# 300166) (Froyen et al., 2007; Honda et al., 2010; Armanet et al., 2015; Farwell et al., 2015). Knockdown of *SHROOM4* in rat severely impairs gamma-aminobutyric acid (GABA) receptors activity causing increased anxiety-like behavior and susceptibility to seizures (Zapata et al., 2017). However, the relationship between *SHROOM4* gene mutations and epilepsy is not determined.

In this study, we performed trio-based whole-exome sequencing (WES) in a cohort of patients with idiopathic epilepsy. Six novel hemizygous missense variants of *SHROOM4* were identified in six unrelated cases with epilepsy with generalized seizures or generalized discharges on electroencephalography (EEG). To understand the mechanism of phenotypic variation, we analyzed the genotype-phenotype correlation and the sub-regional effect of *SHROOM4* variants.

MATERIALS AND METHODS

Patients

A total of 320 cases (trios) with epilepsy without acquired causes (idiopathic epilepsies) were recruited in this study from the Epilepsy Center of the Second Affiliated Hospital of Guangzhou Medical University in China between January 2013 and December 2020. The complete pedigree and clinical data of the probands were collected, including age, gender, age of seizure onset, type, course, and frequency of seizure, family history, therapy, prognosis, general and neurological examination, long-term video EEG, and brain magnetic resonance imaging (MRI). Epilepsy syndromes and epileptic seizures were diagnosed according to the criteria of the Commission on Classification and Terminology of the ILAE (1981, 1989, 2001, 2010, and 2017). Idiopathic generalized epilepsy were diagnosed based on a range of seizure types including absence, spasms, myoclonus, clonic, atonic, tonic, and tonic-clonic seizures, supported by typically generalized discharges on EEG. Idiopathic partial epilepsy had partial seizures and features of bilateral discharge or tendency of generalized discharge. EEG examinations showed focal abnormalities with features of idiopathic epilepsies, including shifting, bilateral, or multiple focal discharges with normal backgrounds. Patients with acquired causes were excluded. All subjects were followed up for at least one year.

This project was approved by the Ethics Committee of the Second Affiliated Hospital of Guangzhou Medical University and was conducted according to the guidelines of the International Committee of Medical Journal Editors regarding patients' consent for research or participation. Written informed consent was obtained from the patients and their legal guardians.

Whole-Exome Sequencing and Genetic Analysis

Peripheral blood samples were obtained from the probands, parents, and other available family members to determine the origin of the identified genetic variants. Genomic DNA was extracted as previously reported (Wang et al., 2018; Shi et al., 2019). Trio-based Whole-Exome Sequencing (WES) was performed with the Illumina HiSeq 2500/4000 platform by BGI-Shenzhen (Shenzhen, China). Deep sequencing data were aligned to the reference GRCh37 build (hg19) and variants were called according to the standard procedures as previously reported (Shi et al., 2019). A case-by-case analytical approach was used to identify candidate causative variants in each trio. Generally, the rare variants with a minor allele frequency < 0.005 were first prioritized in the 1000 Genomes Projects, Exome Aggregation Consortium, and Genome Aggregation Database (gnomAD) (Genomes Project et al., 2015; Karczewski et al., 2020). Next, potentially pathogenic mutations were retained, including frameshift, nonsense, canonical splice site, initiation codon, and missense mutations predicted as being damaging by *in silico* tools[1]. Finally, potential disease-causing variants were screened under following five models: (1) epilepsy-associated gene model; (2) *de novo* dominant inheritance model; (3) autosomal recessive inheritance model, including compound heterozygous and homozygous variants; (4) X-linked inheritance model; (5) co-segregation model. To identify novel epilepsy-associated genes, the known epilepsy-associated genes (Wang et al., 2017) were not analyzed in the present study. Genes with repetitively identified *de novo* variants, bi-allelic variants, hemizygous variants, or variants with segregations, were selected for further studies to define the gene-disease association. *SHROOM4* appeared as one of the candidate genes with recurrent hemizygous variants in this cohort. All variants in *SHROOM4* were annotated based on transcript NM_020717.5. Positive findings and the variant origination were validated by Sanger sequencing.

Mutation Analysis

Protein modeling was conducted *via* Iterative Threading ASSEmbly Refinement (I-TASSER) software to predict the effect of candidate variants on molecular structure (Zhang, 2008; Yang and Zhang, 2015). Three-dimensional protein structure and hydrogen bonds alteration were visualized and analyzed by using PyMOL 1.7.

I-Mutant server was used to predict protein stability alteration caused by single nucleotide mutations-related amino acid change (Capriotti et al., 2005). Protein stability was measured with free energy change value (DDG, kcal/mol).

[1] http://varcards.biols.ac.cn/

To evaluate the genotype–phenotype correlation, *SHROOM4* variants were systematically reviewed through PubMed database and human gene mutation database up to December 2021.

Statistical Analysis

IBM SPSS Statistics 19 was used for statistical analysis. Fisher's exact test was applied to access the allele frequencies of *SHROOM4* variants in the cohort of this study and the control populations, and the proportions of missense variants between epilepsy and intellectual disability. A p value of < 0.05 was considered to be statistically significant.

RESULTS

Identification of *SHROOM4* Variants

Six hemizygous missense variants in *SHROOM4*, including c.13C > A/p.Pro5Thr, c.3236C > T/p.Glu1079Ala, c.3581C > T/p.Ser1194Leu, c.4288C > T/p.Arg1430Cys, c.4303G > A/p.Val1435Met, and c.4331C > T/p.Pro1444Leu, were identified in six unrelated cases with idiopathic epilepsy (**Figure 1** and **Table 1**). All of the hemizygous missense variants were inherited from their asymptomatic mothers, consisted with a classical X-linked recessive (XLR) inheritance pattern (**Figures 1A,B**).

No hemizygote of these variants were found in the controls of gnomAD-all populations, except the variant Ser1194Leu with an extremely low frequency (1/87,776) (**Table 2**). All of the hemizygous variants were not found in the controls of gnomAD-East Asian populations.

The aggregate frequency of the hemizygous variants in this cohort was significantly higher than that in controls (**Table 2**), including the gnomAD-all population (6/448 vs. 2/180,876; $p = 6.134 \times 10^{-15}$), the controls of gnomAD-all population (vs. 1/79,656; $p = 4.273 \times 10^{-13}$), the gnomAD-East Asian population (vs. 0/13,792, $p = 9.386 \times 10^{-10}$), and the controls of the gnomAD-East Asian population (vs. 0/6,901, $p = 9.462 \times 10^{-8}$).

All *SHROOM4* variants identified in this study were predicted to be damaging by one of the silico tools (**Supplementary Table 1**). Protein sequence alignment indicated that five of six variants are located at residues that are highly conserved across species (**Figure 1C**). The Arg1430 was less conserved but was

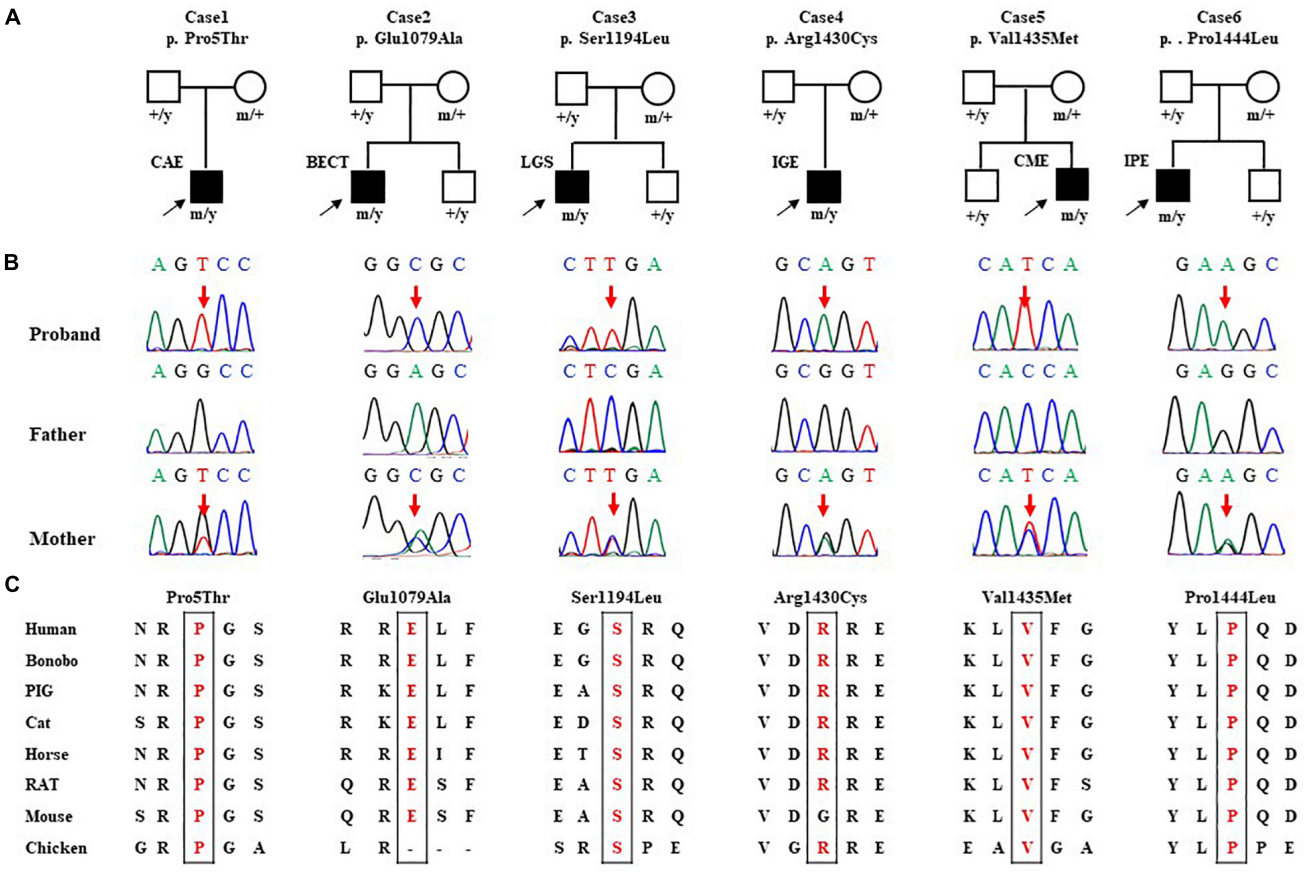

FIGURE 1 | Genetic data of cases with *SHROOM4* variants. **(A)** Pedigrees of the six cases with *SHROOM4* mutations and their corresponding phenotypes. **(B)** DNA sequence chromatogram of the *SHROOM4* mutations. Arrows indicate the positions of the mutations. **(C)** The amino acid sequence alignment of the six missense mutations shows that the residues Pro5, Glu1079, Ser1194, Arg1430, Val1435, and Pro1444 are highly conserved across species.

predicted to be conserved by GERP (score = 4.15) and phyloP (score = 2.907) (**Supplementary Table 2**). None of the six affected patients had pathogenic or likely pathogenic variants in genes known to be associated with epileptic phenotypes (Wang et al., 2017).

Clinical Features

The clinical features of the six cases with *SHROOM4* variants were summarized in **Table 1**. The onset age of seizures ranged from 3 years to 16 years old, with a median age of onset of 5.5 years. The patient of case 1 was diagnosed as childhood absence epilepsy (CAE) characterized by absence seizure and 3 Hz generalized spike-slow waves on EEGs (**Figure 2A**). The patients of case 3, case 4, and case 5 were diagnosed as generalized epilepsy, including Lennox-Gastaut syndrome (LGS), idiopathic generalized epilepsy (IGE), and childhood myoclonic epilepsy (CME); and the three cases had both generalized and focal discharge features on EEGs (**Figures 2C−E**). The patients of case 2 and case 6 were diagnosed as partial epilepsy, i.e., benign childhood epilepsy with centrotemporal EEG spikes (BECTS) and idiopathic partial epilepsy (IPE), but their EEGs had generalized discharges (asymmetric) (**Figures 2B,F**). In a word, these patients mainly present with generalized epilepsy, or idiopathic partial epilepsy with generalized seizures or generalized discharge on EEGs. All patients showed normal development. Their brain MRI were normal. These patients all presented good responses to antiepileptic drug and achieved seizure-free.

Molecular and Molecular Sub-Regional Effects of the *SHROOM4* Variants

The SHROOM4 protein contains two evolutionarily conserved domains, i.e., an N-terminal PDZ domain, and a C-terminal ASD2 domain (Hagens et al., 2006; Yoder and Hildebrand, 2007). In the present study, variant Pro5Thr was located in the N-terminal PDZ domain, while Glu1079Ala, Ser1194Leu, Arg1430Cys, Val1435Met, and Pro1444Leu were located in or near to the C-terminal ASD2 domain (**Figure 3A**).

The molecular effect of the missense variants was analyzed by using I-TASSER for protein modeling and PyMOL 1.7 for visualization (**Figure 3B**). Three of the variants, including Glu1079Ala, Ser1194Leu, and Arg1430Cys, changed hydrogen bonds with the surrounding residues. Originally, Glu1079 formed two hydrogen bonds with residues Leu1080 and Lys1083, respectively. When glutamine was replaced by alanine, the hydrogen bonds with Leu1080 was destroyed. Ser1194 formed two hydrogen bonds with His1190. When serine was replaced by leucine, one of the hydrogen bond was destroyed. Arg1430 formed seven hydrogen bonds with residues Asp1371, Glu1423, His1427, Asp1429, and Arg1431, respectively. When arginine was replaced by cystine, five hydrogen bonds with Asp1371, Glu1423, and Asp1429 were destroyed, and only the hydrogen bonds with His1427 and Arg1431 were kept.

The other three variants, including Pro5Thr, Pro1444Leu, and Val1435Met, have no changed in hydrogen bonds, but they were predicted to decrease the protein stability significantly ($\Delta\Delta G$ values < -0.5 kcal/mol) (**Figure 3B**).

Genotype-Phenotype Correlation

Previously, 12 *SHROOM4* variants have been reported, including 3 missense (Hagens et al., 2006; Farwell et al., 2015; Routier et al., 2019), 2 duplications (Froyen et al., 2007; Isrie et al., 2012), and 7 destructive variants (1 nonsense, 3 gross deletion variants (Honda et al., 2010; Armanet et al., 2015; Danyel et al., 2019; Heide et al., 2020), and 3 complex rearrangements (Hagens et al., 2006; Dong et al., 2021)) (**Supplementary Table 2**). Eleven of the variants associated with intellectual disability (ID), of which 9 were destructive mutations or duplications (**Figure 3C**). Among the three missense variants, one missense variant was associated with ID (Farwell et al., 2015) and one missense variant was associated with ID and seizures (Hagens et al., 2006). Additional one missense variant (His401Tyr) was reported to be associated with myoclonic-atonic epilepsy (MAE) (Routier et al., 2019). These variants are all hemizygous. In this study, all hemizygous variants were missense variants, which were associated with idiopathic epilepsy without ID (**Figure 3A**). The proportion of missense variants in epilepsy (7/7) was significantly higher than that in ID (1/10) ($p < 0.001$) (**Figure 3C**), suggesting a genotype-phenotype correlation.

DISCUSSION

SHROOM4 gene encodes an actin-binding proteins, which plays an important role in cytoskeletal architecture, synaptogenesis, and maintaining $GABA_B$ receptor-mediated inhibition. Hemizygous missense variants were identified in six cases with idiopathic epilepsy without intellectual disability (**Figure 1A**). All patients presented with features of generalized seizures or generalized discharges. These hemizygous variants had no or extremely low allele frequencies in controls and showed statistically higher frequency in the case cohort than controls (**Table 2**). All variants were predicted to alter hydrogen bond with surrounding amino acids or decreased protein stability. This study suggests that *SHROOM4* is potentially a candidate causative gene of X-link epilepsy with features of generalized seizures or generalized discharges.

The *SHROOM4* gene is widely expressed in the brain[2]. It plays a critical role in regulating dendritic spine morphology and controls the cell surface expression and intracellular trafficking of $GABA_B$ receptor (Zapata et al., 2017), which inhibit neuronal activity through G protein-coupled second-messenger systems (Euro, 2014; Yoo et al., 2017). In rat, *Shrm4* were found to influence hippocampal excitability by modulating tonic inhibition in dentate gyrus granule cells. Knockdown of *Shrm4* cause increased susceptibility to seizures (Zapata et al., 2017). Previously, a study identified a hemizygous missense variant in a family with ID and seizures (Hagens et al., 2006). Recently, a missense variant with unknown origin was also found in a male with MAE (Routier et al., 2019). However, the relationship

[2]https://www.gtexportal.org/home/gene/SHROOM4

TABLE 1 | Clinical features of the individuals with *SHROOM4* variants.

Case	Variants (NM_020717.5)	Gender	Age	Seizure onset	Seizure course	Effective AEDs	Seizure-free duration	EEG	Brain MRI	Development	Diagnosis
Case 1	c.13C > A/p.Pro5Thr	Male	9 yr	7 yr	Absence, 4-5 times/day	VPA	1 yr	3 Hz generalized spike-slow waves	Normal	Normal	CAE
Case 2	c.3236A > C/p.Glu1079Ala	Male	11 yr	7 yr	GTCS, 2 times in 2 years	LTG	3 yr	Bilateral central-temporal independent sharp waves and spikes	Normal	Normal	BECTS
Case 3	c.3581C > T/p.Ser1194Leu	Male	16 yr	3 yr	Tonic seizure, 4-5 times/day in the first three years, CPS 1-2 times/month	VPA,OXC,CNZ	2 yr	Childhood: not available Present: generalized slow waves and left temporal spike-slow waves	Normal	Normal	LGS
Case 4	c.4288C > T/p.Arg1430Cys	Male	17 yr	16 yr	GTCS 1-2 times/month	VPA	1 yr	Irregular generalized spike-slow waves	Normal	Normal	IGE
Case 5	c.4303G > A/p.Val1435Met	Male	5 yr	4 yr	Myoclonic seizure, 5-6 times/day	LTG	2 yr	Irregular polyspike-slow waves and bilateral temporal independent spike-slow waves	Normal	Normal	CME
Case 6	c.4331C > T/p.Pro1444Leu	Male	17 yr	3 yr	GTCS or CPS 2-3 times/day	VPA,OXC	1.5 yr	Right predominant generalized spike-slow waves, bilateral temporal independent spike-slow waves Ictal: GTCS with generalized origination	Normal	Normal	IPE

AEDs, antiepileptic drugs; BECTS, benign childhood epilepsy with centrotemporal EEG spikes; CAE, childhood absence epilepsy; CME: Childhood myoclonic epilepsy; CPS, complex partial seizure; EEG, electroencephalogram; GTCS, generalized tonic-clonic seizure; LGS, Lennox-Gastaut syndrome; LTG, lamotrigine; MRI, magnetic resonance imaging; IGE, idiopathic generalized epilepsy; IPE, idiopathic partial epilepsy; VPA, valproate.

TABLE 2 | Analysis of the aggregate frequency of *SHROOM4* variants identified in this study.

Variants (NM_020717.5)	Position	Allele count/number in hemizygotes in this study (%)	Allele count/number in hemizygotes of gnomAD-all populations (%)	Allele Count/number in hemizygotes in controls of gnomAD-all populations (%)	Allele Count/number in hemizygotes of gnomAD-East Asian populations (%)	Allele Count/Number in the controls of gnomAD-East Asian populations (%)
c.13C > A/p.Pro5Thr	chrX:50557006	1/448 (0.2232)	-	-	-	-
c.3236A > C/p.Glu1079Ala	chrX:50350906	1/448 (0.2232)	-	-	-	-
c.3581C > T/p.Ser1194Leu	chrX:50350561	1/448 (0.2232)	1/204,757	1/87,776	-	-
c.4288C > T/p.Arg1430Cys	chrX:50339889	1/448 (0.2232)	1/180,876	-	-	-
c.4303G > A/p.Val1435Met	chrX:50339874	1/448 (0.2232)	-	-	-	-
c.4331C > T/p.Pro1444Leu	chrX:50339846	1/448 (0.2232)	0/181,847	0/79,656	-	-
Total		6/448 (1.3392)	2/180,876	1/79,656	0/13,792	0/6,901
P value			6.134×10^{-15}	4.273×10^{-13}	9.386×10^{-10}	9.462×10^{-8}
OR			1,227.652	1,081.289	405.203	202.756
(95%CI)			(247.11−6,099.01)	(129.91−8,999.96)	(22.72−7,225.75)	(11.37−3,615.63)

p values and odds ratio were estimated with 2-sided Fisher's exact test.
CI, confidence interval; gnomAD, Genome Aggregation Database; OR, odd ratio.

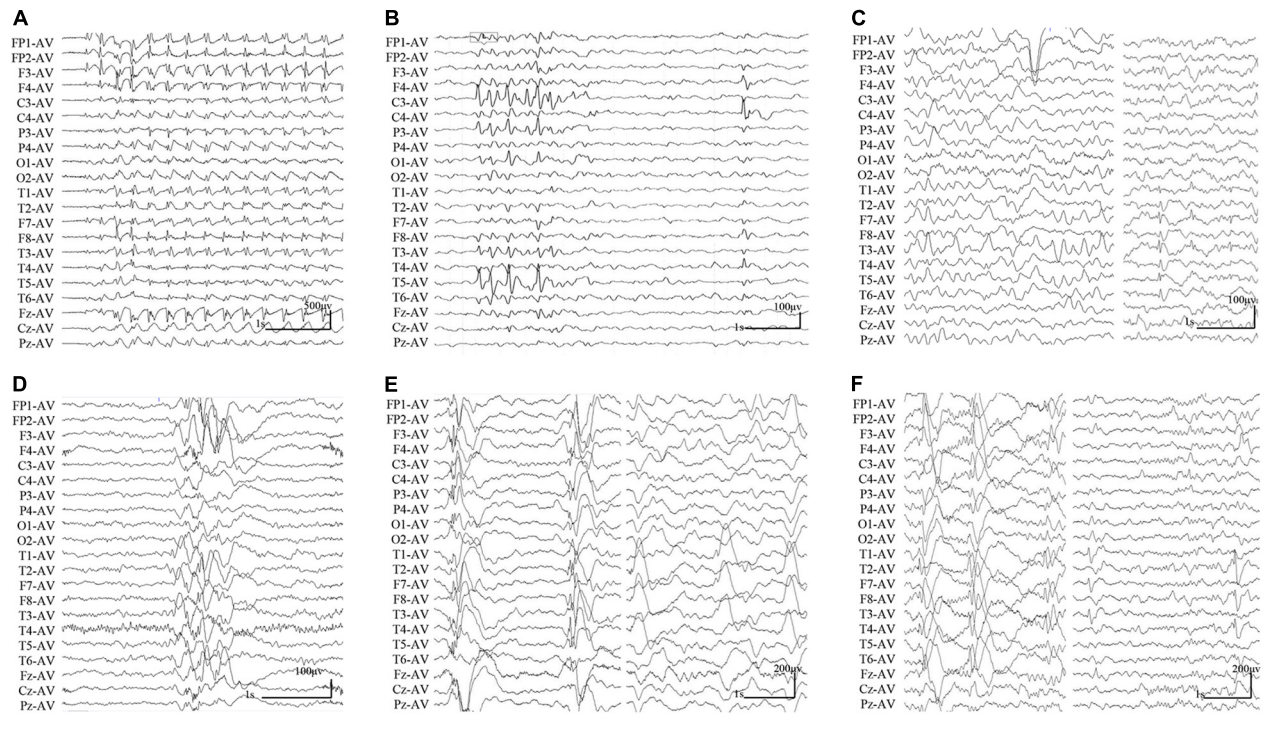

FIGURE 2 | Changes of interictal EEGs and MRI in the cases with *SHROOM4* variants. **(A)** Interictal EEG of case 1 showed 3 Hz generalized spike-slow waves (obtained at the age of 7 years). **(B)** Interictal EEG of case 2 showed bilateral central-temporal independent sharp waves and spikes (obtained at the age of 7 years). **(C)** Interictal EEG of case 3 showed generalized slow waves and left temporal spike-slow waves (obtained at the age of 14 years). **(D)** Interictal EEG of case 4 showed irregular generalized spike-slow waves (obtained at the age of 16 years). **(E)** Interictal EEG of case 5 showed irregular polyspike-slow waves and bilateral temporal independent spike-slow waves (obtained at the age of 4 years). **(F)** Interictal EEG of case 6 showed right predominant generalized spike-slow waves, bilateral temporal independent spike-slow waves (obtained at the age of 3 years).

between *SHROOM4* mutations and epilepsy remains uncertain. In this study, we identified six novel hemizygous missense variants in six unrelated cases with idiopathic epilepsy but without ID, suggesting that *SHROOM4* is potentially a candidate gene of epilepsy.

Previous studies have shown that mutations of the GABA receptors, such as, *GABRA1*, *GABRA5*, *GABRA6, GABRB3, GABRD*, *GABRG2*, were associated with idiopathic generalized epilepsy (Cossette et al., 2002; Hirose, 2006; Moller et al., 2017; Lee et al., 2018; May et al., 2018). Mutations of the $GABA_B$

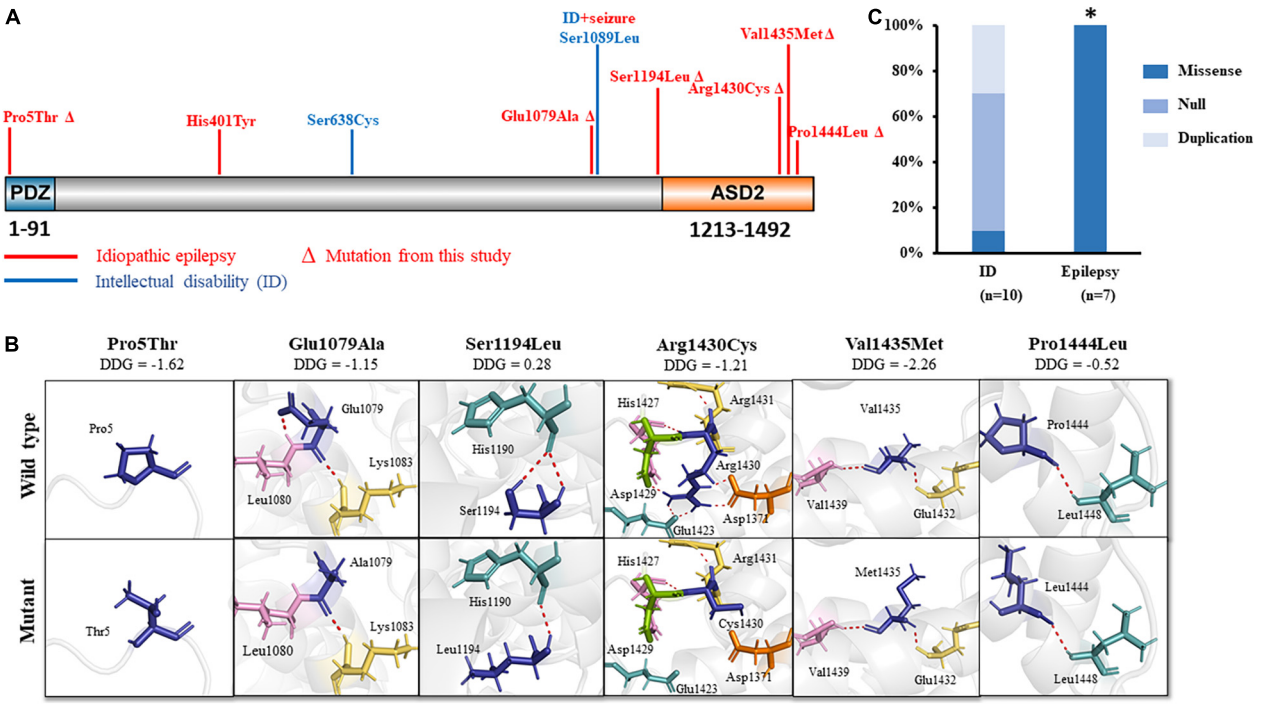

FIGURE 3 | Schematic illustration of *SHROOM4* variants. **(A)** Linear schematic of missense *SHROOM4* mutations and their locations on SHROOM4 protein. Mutations associated with epilepsy were shown in red color. Mutations associated with ID were shown in blue. ΔThe mutation was found in this study **(B)** Changes of hydrogen bonds and free energy change value (DDG) of the mutations. **(C)** The proportion of missense mutations in epilepsy and ID. *The proportion of missense mutations in epilepsy is significantly higher than that in ID.

receptor cause generalized epilepsy by impairing inhibitory network neurodevelopment (Samarut et al., 2018). Recent study found that knockdown of *Shrm4* severely impairs $GABA_B$ receptor-mediated inhibition and thus potentially associated with generalized epilepsy. In the present study, patients with *SHROOM4* variants presented mainly generalized epilepsy, such as CAE, MAE, LGS, IGE, and those with partial seizures also had bilateral or generalized discharge or generalized seizures (**Table 1** and **Figure 1**), potentially suggesting an association between *SHROOM4* variants and generalized epilepsy. The patients with *SHROOM4* mutations showed good responses to proper antiepileptic treatment and got seizure free, in spite of frequent daily seizures in several cases. These findings suggested that the establishment of *SHROOM4*-epilepsy association would be potentially significant in management of the patients with *SHROOM4* mutations.

Previously, 11 variants were reported in patients with ID (Ng et al., 2004), 9 of which were destructive mutations or duplications (**Figure 3C** and **Supplementary Table 2**). Only two of those variants were missense variants. In contrast, epilepsy-associated variants were all missense variants (**Figure 3C**), suggesting a genotype-phenotype correlation.

SHROOM4 gene encodes a member of the Shroom family, which contains an N-terminal PDZ domain and a C-terminally positioned motif termed ASD2 (Hagens et al., 2006; Yoder and Hildebrand, 2007). The PDZ domain interacts with C terminus of $GABA_B$ receptors, while the ASD2 domain is capable of inducing myosin II-dependant changes in cell shape. The central portion of the protein appears to be an actin targeting sequence and mediated Shrm4 localization (Yoder and Hildebrand, 2007). The current data demonstrated that two missense variants located in or closed to N-terminal PDZ domain were associated with generalized epilepsy; two missense variants located in the middle of protein were associated with ID, one of which was located near to C-terminal ASD2 domain and associated with epilepsy (Hagens et al., 2006; Farwell et al., 2015); missense variants located in or near to C-terminal ASD2 domain were associated with epilepsy with both focal and generalized seizures or discharges. These evidences suggested a possible molecular sub-regional effect of *SHROOM4* variants, as that in several genes reported previously (Wang et al., 2018; Liu et al., 2020; Tang et al., 2020). However, further studies are required to determine the function details of each region and their association with different phenotypes.

This study has several limitations. Knockdown, i.e., LOF of Shrm4, in rat resulted in severely impaired synaptogenesis and reduced $GABA_B$ receptor-mediated inhibition, causing susceptibility to seizures. The probability of being LOF intolerant (pLI) score was high for *SHROOM4* (pLI = 0.997), suggesting that *SHROOM4* is intolerant to LOF variants. However, the specific mechanism of epileptogenesis of the *SHROOM4* variants remains unknown; and further experimental studies are required to determine the functional consequence of the variants. Additionally, although these

missense variants were associated with generalized epilepsy, the patients presented different epilepsy syndromes. The mechanism of phenotype variation warrants further studies.

In conclusion, we identified six novel *SHROOM4* hemizygous missense variants in epilepsy patients with features of generalized seizures or generalized discharges. Further analysis revealed that a potential genotype-phenotype correlation and sub-regional molecular implication of *SHROOM4* variants. This study potentially extends the spectrum of diseases phenotype associated with *SHROOM4* variants and helps to understand the mechanisms of phenotypic variation.

DATA AVAILABILITY STATEMENT

The original contributions presented in the study are included in the article/**Supplementary Material**, further inquiries can be directed to the corresponding author/s.

ETHICS STATEMENT

The studies involving human participants were reviewed and approved by the Ethics Committee of The Second Affiliated Hospital of Guangzhou Medical University. Written informed consent to participate in this study was provided by the participants' legal guardian/next of kin.

AUTHOR CONTRIBUTIONS

Y-HY designed the study, administered the project, and revised the manuscript. W-JB completed collection of the clinical data, analyzed the data, and draft of the manuscript. Z-JL analyzed the data and drafted of the manuscript. SL, NH, L-DG, B-ML, and JW contributed to data analysis and interpretation. B-ML and L-DG performed data analysis and provided technical assistance. All authors have read and approved the final manuscript.

FUNDING

This work was funded by the National Natural Science Foundation of China (Grant No. 81870903 to Y-HY), the National Natural Science Foundation of China (Grant No. 81971216 to NH), Guangdong Basic and Applied Basic Research Foundation (Grant No. 2020A1515011048 to NH), Science and Technology Project of Guangzhou (Grant No. 201904010292 to NH), and UCB Pharma Ltd. Joint Science Research Foundation of China Association Against Epilepsy (Grant Nos. 2020006B to NH and CU-2022-027 to W-JB). The funders had no role in study design, data collection and analysis, and decision to publish or preparation of the manuscript.

ACKNOWLEDGMENTS

Our sincere thanks to Professor Wei-Ping Liao for editing this manuscript.

SUPPLEMENTARY MATERIAL

The Supplementary Material for this article can be found online at: https://www.frontiersin.org/articles/10.3389/fnmol.2022.862480/full#supplementary-material

REFERENCES

Armanet, N., Metay, C., Brisset, S., Deschenes, G., Pineau, D., Petit, F. M., et al. (2015). Double Xp11.22 deletion including SHROOM4 and CLCN5 associated with severe psychomotor retardation and Dent disease. *Mol. Cytogenet.* 8:8. doi: 10.1186/s13039-015-0107-x

Capriotti, E., Fariselli, P., and Casadio, R. (2005). I-Mutant2.0: predicting stability changes upon mutation from the protein sequence or structure. *Nucleic Acids Res.* 33, W306–W310. doi: 10.1093/nar/gki375

Cossette, P., Liu, L., Brisebois, K., Dong, H., Lortie, A., Vanasse, M., et al. (2002). Mutation of GABRA1 in an autosomal dominant form of juvenile myoclonic epilepsy. *Nat. Genet.* 31, 184–189. doi: 10.1038/ng885

Danyel, M., Suk, E. K., Raile, V., Gellermann, J., Knaus, A., and Horn, D. (2019). Familial Xp11.22 microdeletion including SHROOM4 and CLCN5 is associated with intellectual disability, short stature, microcephaly and Dent disease: a case report. *BMC Med. Genom.* 12:6. doi: 10.1186/s12920-018-0471-6

Dong, Z., Chau, M. H. K., Zhang, Y., Dai, P., Zhu, X., Leung, T. Y., et al. (2021). Deciphering the complexity of simple chromosomal insertions by genome sequencing. *Hum. Genet.* 140, 361–380. doi: 10.1007/s00439-020-02210-x

Euro, E.-R. E. S. C. (2014). De novo mutations in synaptic transmission genes including DNM1 cause epileptic encephalopathies. . *Am. J. Hum. Genet.* 95, 360–370. doi: 10.1016/j.ajhg.2014.08.013

Farwell, K. D., Shahmirzadi, L., El-Khechen, D., Powis, Z., Chao, E. C., Tippin Davis, B., et al. (2015). Enhanced utility of family-centered diagnostic exome sequencing with inheritance model-based analysis: results from 500 unselected families with undiagnosed genetic conditions. *Genet. Med.* 17, 578–586. doi: 10.1038/gim.2014.154

Froyen, G., Van Esch, H., Bauters, M., Hollanders, K., Frints, S. G., Vermeesch, J. R., et al. (2007). Detection of genomic copy number changes in patients with idiopathic mental retardation by high-resolution X-array-CGH: important role for increased gene dosage of XLMR genes. *Hum. Mutat.* 28, 1034–1042. doi: 10.1002/humu.20564

Genomes Project, C., Auton, A., Brooks, L. D., Durbin, R. M., Garrison, E. P., Kang, H. M., et al. (2015). A global reference for human genetic variation. *Nature* 526, 68–74. doi: 10.1038/nature15393

Hagens, O., Dubos, A., Abidi, F., Barbi, G., Van Zutven, L., Hoeltzenbein, M., et al. (2006). Disruptions of the novel KIAA1202 gene are associated with X-linked mental retardation. *Hum. Genet.* 118, 578–590. doi: 10.1007/s00439-005-0072-2

Heide, S., Spentchian, M., Valence, S., Buratti, J., Mach, C., Lejeune, E., et al. (2020). Prenatal exome sequencing in 65 fetuses with abnormality of the corpus callosum: contribution to further diagnostic delineation. *Genet. Med.* 22, 1887–1891. doi: 10.1038/s41436-020-0872-8

Hirose, S. (2006). A new paradigm of channelopathy in epilepsy syndromes: intracellular trafficking abnormality of channel molecules. *Epilepsy Res.* 70(Suppl. 1), S206–S217. doi: 10.1016/j.eplepsyres.2005.12.007

Honda, S., Hayashi, S., Imoto, I., Toyama, J., Okazawa, H., Nakagawa, E., et al. (2010). Copy-number variations on the X chromosome in Japanese patients with mental retardation detected by array-based comparative genomic hybridization analysis. *J. Hum. Genet.* 55, 590–599. doi: 10.1038/jhg.2010.74

Isrie, M., Froyen, G., Devriendt, K., de Ravel, T., Fryns, J. P., Vermeesch, J. R., et al. (2012). Sporadic male patients with intellectual disability: contribution of X-chromosome copy number variants. *Eur. J. Med. Genet.* 55, 577–585. doi: 10.1016/j.ejmg.2012.05.005

Karczewski, K. J., Francioli, L. C., Tiao, G., Cummings, B. B., Alfoldi, J., Wang, Q., et al. (2020). The mutational constraint spectrum quantified from variation in 141,456 humans. *Nature* 581, 434–443. doi: 10.1038/s41586-020-2308-7

Lee, C. G., Lee, J., and Lee, M. (2018). Multi-gene panel testing in Korean patients with common genetic generalized epilepsy syndromes. *PLoS One* 13:e0199321. doi: 10.1371/journal.pone.0199321

Liu, L., Chen, Z. R., Xu, H. Q., Liu, D. T., Mao, Y., Liu, H. K., et al. (2020). DEPDC5 Variants Associated Malformations of Cortical Development and Focal Epilepsy With Febrile Seizure Plus/Febrile Seizures: the Role of Molecular Sub-Regional Effect. *Front. Neurosci.* 14:821. doi: 10.3389/fnins.2020.00821

May, P., Girard, S., Harrer, M., Bobbili, D. R., Schubert, J., Wolking, S., et al. (2018). Rare coding variants in genes encoding GABAA receptors in genetic generalised epilepsies: an exome-based case-control study. *Lancet Neurol.* 17, 699–708. doi: 10.1016/S1474-4422(18)30215-1

Moller, R. S., Wuttke, T. V., Helbig, I., Marini, C., Johannesen, K. M., Brilstra, E. H., et al. (2017). Mutations in GABRB3: from febrile seizures to epileptic encephalopathies. *Neurology* 88, 483–492. doi: 10.1212/WNL.0000000000003565

Ng, D., Thakker, N., Corcoran, C. M., Donnai, D., Perveen, R., Schneider, A., et al. (2004). Oculofaciocardiodental and Lenz microphthalmia syndromes result from distinct classes of mutations in BCOR. *Nat. Genet.* 36, 411–416. doi: 10.1038/ng1321

Routier, L., Verny, F., Barcia, G., Chemaly, N., Desguerre, I., Colleaux, L., et al. (2019). Exome sequencing findings in 27 patients with myoclonic-atonic epilepsy: is there a major genetic factor? *Clin. Genet.* 96, 254–260. doi: 10.1111/cge.13581

Samarut, E., Swaminathan, A., Riche, R., Liao, M., Hassan-Abdi, R., Renault, S., et al. (2018). gamma-Aminobutyric acid receptor alpha 1 subunit loss of function causes genetic generalized epilepsy by impairing inhibitory network neurodevelopment. *Epilepsia* 59, 2061–2074. doi: 10.1111/epi.14576

Shi, Y. W., Zhang, Q., Cai, K., Poliquin, S., Shen, W., Winters, N., et al. (2019). Synaptic clustering differences due to different GABRB3 mutations cause variable epilepsy syndromes. *Brain* 142, 3028–3044. doi: 10.1093/brain/awz250

Tang, B., Li, B., Gao, L. D., He, N., Liu, X. R., Long, Y. S., et al. (2020). Optimization of in silico tools for predicting genetic variants: individualizing for genes with molecular sub-regional stratification. *Brief Bioinform.* 21, 1776–1786. doi: 10.1093/bib/bbz115

Wang, J., Lin, Z. J., Liu, L., Xu, H. Q., Shi, Y. W., Yi, Y. H., et al. (2017). Epilepsy-associated genes. *Seizure* 44, 11–20. doi: 10.1016/j.seizure.2016.11.030

Wang, J. Y., Zhou, P., Wang, J., Tang, B., Su, T., Liu, X. R., et al. (2018). ARHGEF9 mutations in epileptic encephalopathy/intellectual disability: toward understanding the mechanism underlying phenotypic variation. *Neurogenetics* 19, 9–16. doi: 10.1007/s10048-017-0528-2

Yang, J., and Zhang, Y. (2015). I-TASSER server: new development for protein structure and function predictions. *Nucleic Acids Res.* 43, W174–W181. doi: 10.1093/nar/gkv342

Yoder, M., and Hildebrand, J. D. (2007). Shroom4 (Kiaa1202) is an actin-associated protein implicated in cytoskeletal organization. *Cell Motil. Cytoskel.* 64, 49–63. doi: 10.1002/cm.20167

Yoo, Y., Jung, J., Lee, Y. N., Lee, Y., Cho, H., Na, E., et al. (2017). GABBR2 mutations determine phenotype in rett syndrome and epileptic encephalopathy. *Ann. Neurol.* 82, 466–478. doi: 10.1002/ana.25032

Zapata, J., Moretto, E., Hannan, S., Murru, L., Longatti, A., Mazza, D., et al. (2017). Epilepsy and intellectual disability linked protein Shrm4 interaction with GABABRs shapes inhibitory neurotransmission. *Nat. Commun.* 8:14536. doi: 10.1038/ncomms14536

Zhang, Y. (2008). I-TASSER server for protein 3D structure prediction. *BMC Bioinform.* 9:40. doi: 10.1186/1471-2105-9-40

Conflict of Interest: The authors declare that the research was conducted in the absence of any commercial or financial relationships that could be construed as a potential conflict of interest.

Publisher's Note: All claims expressed in this article are solely those of the authors and do not necessarily represent those of their affiliated organizations, or those of the publisher, the editors and the reviewers. Any product that may be evaluated in this article, or claim that may be made by its manufacturer, is not guaranteed or endorsed by the publisher.

frontiers | Frontiers in Molecular Neuroscience

ORIGINAL RESEARCH
published: 19 May 2022
doi: 10.3389/fnmol.2022.825390

Recessive *LAMA5* Variants Associated With Partial Epilepsy and Spasms in Infancy

Sheng Luo[1†‡], Zhi-Gang Liu[2,3‡], Juan Wang[1], Jun-Xia Luo[4], Xing-Guang Ye[2,3], Xin Li[5], Qiong-Xiang Zhai[6], Xiao-Rong Liu[1], Jie Wang[1], Liang-Di Gao[1], Fu-Li Liu[7], Zi-Long Ye[1], Huan Li[1], Zai-Fen Gao[4], Qing-Hui Guo[5], Bing-Mei Li[1], Yong-Hong Yi[1] and Wei-Ping Liao[1†]*

[1] Key Laboratory of Neurogenetics and Channelopathies of Guangdong Province and the Ministry of Education of China, Department of Neurology, Institute of Neuroscience, Second Affiliated Hospital of Guangzhou Medical University, Guangzhou, China, [2] The Second School of Clinical Medicine, Southern Medical University, Guangzhou, China, [3] Department of Pediatrics, Affiliated Foshan Maternity & Child Healthcare Hospital, Southern Medical University, Foshan, China, [4] Epilepsy Center, Qilu Children's Hospital of Shandong University, Jinan, China, [5] Department of Pediatrics, The Second Hospital, Cheeloo College of Medicine, Shandong University, Jinan, China, [6] Department of Neurology, Guangdong General Hospital, Guangdong Academy of Medical Sciences, Guangzhou, China, [7] Department of Neurology, The First People's Hospital of Foshan, Foshan, China

Objective: The *LAMA5* gene encodes the laminin subunit α5, the most abundant laminin α subunit in the human brain. It forms heterotrimers with the subunit β1/β2 and γ1/γ3 and regulates neurodevelopmental processes. Genes encoding subunits of the laminin heterotrimers containing subunit α5 have been reported to be associated with human diseases. Among *LAMAs* encoding the laminin α subunit, *LAMA1-4* have also been reported to be associated with human disease. In this study, we investigated the association between *LAMA5* and epilepsy.

Methods: Trios-based whole-exome sequencing was performed in a cohort of 118 infants suffering from focal seizures with or without spasms. Protein modeling was used to assess the damaging effects of variations. The *LAMAs* expression was analyzed with data from the GTEX and VarCards databases.

Results: Six pairs of compound heterozygous missense variants in *LAMA5* were identified in six unrelated patients. All affected individuals suffered from focal seizures with mild developmental delay, and three patients presented also spasms. These variants had no or low allele frequencies in controls and presented statistically higher frequency in the case cohort than in controls. The recessive burden analysis showed that recessive *LAMA5* variants identified in this cohort were significantly more than the expected number in the East Asian population. Protein modeling showed that at least one variant in each pair of biallelic variants affected hydrogen bonds with surrounding amino acids. Among the biallelic variants in cases with only focal seizures, two variants of each pair were located in different structural domains or domains/links, whereas in the

OPEN ACCESS

Edited by:
Sampath Rangasamy,
Translational Genomics Research Institute (TGen), United States

Reviewed by:
Laurence Goutebroze,
Institut National de la Santé et de la Recherche Médicale (INSERM), France
Fei Yin,
Xiangyang Central Hospital, China

***Correspondence:**
Wei-Ping Liao
wpliao@163.net

†ORCID:
Sheng Luo
orcid.org/0000-0002-7184-1267
Wei-Ping Liao
orcid.org/0000-0001-9929-9185

‡These authors have contributed equally to this work and share first authorship

Specialty section:
This article was submitted to Molecular Signalling and Pathways, a section of the journal Frontiers in Molecular Neuroscience

Received: 30 November 2021
Accepted: 19 April 2022
Published: 19 May 2022

Citation:
Luo S, Liu Z-G, Wang J, Luo J-X, Ye X-G, Li X, Zhai Q-X, Liu X-R, Wang J, Gao L-D, Liu F-L, Ye Z-L, Li H, Gao Z-F, Guo Q-H, Li B-M, Yi Y-H and Liao W-P (2022) Recessive *LAMA5* Variants Associated With Partial Epilepsy and Spasms in Infancy. Front. Mol. Neurosci. 15:825390. doi: 10.3389/fnmol.2022.825390

cases with spasms, the biallelic variants were constituted by two variants in the identical functional domains or both with hydrogen bond changes.

Conclusion: Recessive *LAMA5* variants were potentially associated with infant epilepsy. The establishment of the association between *LAMA5* and epilepsy will facilitate the genetic diagnosis and management in patients with infant epilepsy.

Keywords: *LAMA5* gene, infant-onset epilepsy, laminins, trios-based WES, spasms

INTRODUCTION

The *LAMA5* gene (OMIM* 601033) encodes the laminin subunit α5, expressed in the human brain, especially in the cortex and during the early stages of life (Durkin et al., 1997). The laminin subunit α5 forms heterotrimers with subunits β1/β2 and γ1/γ3 and regulates neurodevelopmental biological processes, including epiblast polarization, neurite outgrowth, neuronal migration, synaptic stability, and cell adhesion, differentiation, migration, and signaling (Liang and Crutcher, 1992; Luckenbill-Edds, 1997; Domogatskaya et al., 2012; Mukherjee et al., 2020). In mice, homozygous knock-out of *LAMA5* caused lethality throughout fetal growth and development, and led to exencephaly, megalencephaly, and other neural tube defects (Miner et al., 1998; Kikkawa and Miner, 2006). Genes encoding subunits of the laminin heterotrimers containing subunit α5 have been reported to be associated with human diseases. Among *LAMAs* encoding the laminin α subunit, *LAMA1-4* have also been reported to be associated with human disease. The association between the *LAMA5* gene, which encodes the most abundant laminin α subunit in the human brain, and human diseases, has not been determined.

Epilepsy is one of the most common neurological disorders in children with an estimated prevalence of 4–5 per 10,000. Infancy is the critical period of brain development, and epilepsy presents the highest incidence in infancy (Wirrell et al., 2011; Eltze et al., 2013; Hirose, 2013). Multiple seizures may appear in infancy epilepsy, such as focal (partial), myoclonic, spasms seizures, and spasms typically occur in infancy (Bayat et al., 2021). Clinically, both spasms and focal seizures are common in infancy. A proportion of infants with epilepsy have acquired causes, such as trauma, infection, and immune, but the etiologies in the majority are unknown. Previous studies have shown that genetic factors play an important role in the etiology of infant epilepsy (Gan et al., 2019; Kang et al., 2019). The established causative genes include *PRRT2, KCNQ2, SCN1A, SCN2A, STXBP1, CDKL5,* and *ARX,* which contribute to approximately 19% of patients with infant-onset epilepsy (Song et al., 2021).

In this study, trios-based whole-exome sequencing (WES) was performed in a cohort of infants with epilepsy. Six pairs of compound heterozygous missense variants in *LAMA5* were detected in six unrelated cases. The present study suggests that recessive *LAMA5* variants were potentially associated with infant epilepsy.

MATERIALS AND METHODS

Subjects

One hundred and eighteen infants who suffered from focal seizures without any acquired causes were recruited from four hospitals, including the Second Affiliated Hospital of Guangzhou Medical University, Foshan Maternal and Child Health Hospital, the Second Affiliated Hospital of Shandong University, and Children's Hospital of Shandong University, from June 2019 to July 2021. Clinical information of the affected individuals was collected, including age at onset, type and frequency of seizures, family history, systemic and neurological findings, and effective antiepileptic drugs. The structural abnormalities were detected by brain magnetic resonance imaging (MRI) scans. Long-term (24 h) video electroencephalography (EEG) monitoring records were performed with electrodes being arranged according to the international standard of 10–20 reduced montage system. The procedures of open-close eyes test, hyperventilation, intermittent photic stimulation, and sleeping recording were obtained. The EEG results were reviewed by at least two qualified electroencephalographers. The Chinese version of the Gesell development scales was utilized in the neurodevelopment evaluation of the participants according to their ages. Its scores were evaluated using tests for gross motor, fine motor, adaptive behavior, language, and personal-social behavior. Epileptic seizures and epilepsy syndromes were diagnosed according to the criteria of the Commission on Classification and Terminology of the International League Against Epilepsy (1981, 1989, 2001, 2010, and 2017). All patients were followed up for more than 1 year.

For the controls, WES was performed on 296 healthy Chinese volunteers who served as a normal control group as our previous report (Wang et al., 2018). Frequencies of the identified variants were also compared with that in the other control populations, including East Asian and general populations in the Genome Aggregation Database (gnomAD[1]), and the 8,364 persons without known neuropsychiatric conditions in the Epi25 WES Browser[2] (Epi25 Collaborative, 2019; Karczewski et al., 2020).

This study adhered to the principles of the International Committee of Medical Journal Editors concerning patient consent for research or participation and received approval

[1]gnomad.broadinstitute.org

[2]https://epi25.broadinstitute.org/

from the Ethics Committee of the Second Affiliated Hospital of Guangzhou Medical University. Written informed consents were provided by the patient's legal guardians.

Whole Exon Sequencing

Blood samples of the probands, their parents, and other available family members were collected to identify the source of the genetic variation and to aid in the analysis of the pathogenicity of variants. Genomic DNAs were extracted from blood samples using the Qiagen Flexi Gene DNA kit (Qiagen, Hilden, Germany). WES was performed using a NextSeq500 sequencing instrument (Illumina, San Diego, CA, United States) following the standard procedures previously described (Wang et al., 2018). The sequencing data were generated by massively parallel sequencing with an average depth of $>125\times$ and $>98\%$ coverage of the capture region on the chip for obtaining high-quality reads that were mapped to the Genome Reference Consortium Human genome build 37 by Burrows–Wheeler alignment. Single-nucleotide point variants and indels were called with the Genome Analysis Toolkit.

Genetic Analysis

A case-by-case analytical approach was adopted to identify candidate causative variants in each trio. Primarily, the rare variants were prioritized with a minor allele frequency <0.005 in the Genome Aggregation Database (see Text Footnote 1). Then, potentially pathogenic variants were retained, including frameshift, nonsense, canonical splice site, initiation codon, and missense variants predicted as being damaging *in silico* tools. Lastly and importantly, the potentially disease-causing variants in each trio were analyzed with an individualized protocol. The variants in each trio were sorted according to the following five models: (1) epilepsy-associated gene model (Wang et al., 2017); (2) *de novo* variant dominant model; (3) autosomal recessive inheritance model, including homozygous and compound heterozygous variants; (4) X-linked model; (5) co-segregation analysis model. To identify novel epilepsy-associated genes, the known epilepsy-associated genes were put aside. Genes with *de novo* variants, bi-allelic variants, hemizygous variants, or variants with segregations, which represent the genetic difference between the patients and normal individuals in a family and potentially explain the occurrence of disease, were selected for further studies to define the gene-disease association. *LAMA5* emerged as one of the candidate genes with recurrent bi-allelic variants in this cohort of infancy epilepsy. Sanger sequencing was used to validate the candidate variants. All *LAMA5* variants identified in this study were annotated into the reference transcript NM_005560.4.

Bioinformatic Analyses

Protein modeling was performed by using the Iterative Threading ASSEmbly Refinement software (I-TASSER[3]) to evaluate the damaging effect of candidate variants (Yang and Zhang, 2015). The confidence of each model was quantitatively measured by a *C*-score in the range of [−5, 2]. PyMOL Molecular Graphics System (Version 2.3.2; Schrödinger, LLC; New York, NY, United States) was used for three-dimensional protein structure visualization and analysis. I-Mutant Suite server was used for the prediction of protein stability changes upon single-nucleotide variants that lead to changes in the amino acid[4] (Capriotti et al., 2005). The alteration of the protein stability was assessed by the free energy change value ($\Delta\Delta G$, kcal/mol). Values greater than 0.5 kacl/mol imply a large increase in protein stability, values less than −0.5 kacl/mol are considered to be a large decrease in protein stability, and others imply neutral stability. The consequences of all the missense variants were predicted by several common tools, including SIFT, PolyPhen2_HVAR, CADD, MutationTaster, GenoCanyon, fitCons, M_CAP, and GERP.

Statistical Analysis

R (version 4.0.3) was used for data processing. The frequencies of the *LAMA5* variants between the epilepsy cohort and the controls were compared by a two-sided Fisher exact test (CONVERGE Consortium, 2015). The burden of recessive variants was analyzed according to the method recommended recently (Martin et al., 2018). P-value < 0.05 was considered statistically significant.

RESULTS

Identification of *LAMA5* Variants

Six pairs of compound heterozygous missense variants, i.e., (c.1337G > A/p.Arg446Gln and c.10699C > T/p.Pro3567Ser), (c.1418G > A/p.Pro473Leu and c.3608C > T/p.Arg1203Gln), (c.5426G > A/p.Arg1809His and c.7394G > A/p.Arg2465Gln), (c.3170C > T/p.Ser1057Leu and c.6388C > T/p.Arg2130Cys), (c.9448G > A/p.Gly3150Ser and c.10744C > T/p.Arg3582Trp), and (c.1963G > A/p.Gly655Ser and c.2192C > G/p.Ala731Gly), were identified in six unrelated cases with focal seizures, including three infants with also spasms (**Figures 1A,B** and **Table 1**). The compound heterozygous variants originated from their asymptomatic mothers and fathers, consistent with a classical recessive inheritance pattern.

These variants presented no or low frequencies (MAF < 0.005) in the gnomAD databases (**Table 2**). Nine of the variants did not present in the normal control of Epi25 WES Brower, and the other three variants presented extremely low frequencies (MAF < 0.0005). None of the variants, except p.Ala731Gly, were presented in the 296 normal controls.

When the burden of recessive variants was analyzed, (Martin et al., 2018) the *LAMA5* variants in the present cohort were significantly more than the expected number by chance in the East Asian population (MAF < 0.005, $P = 6.4654 \times 10^{-6}$). Furthermore, the aggregate frequency of the variants in this cohort was significantly higher than that in the six controls (**Table 2**), including the controls of 296 normal individuals (12/236 vs. 1/592, $p = 2.243 \times 10^{-6}$), the normal control of Epi25 WES Browser (vs. 6/16844, $p < 2.2 \times 10^{-16}$), the

[3]https://zhanglab.ccmb.med.umich.edu/I-TASSER/

[4]https://folding.biofold.org/i-mutant/i-mutant2.0.html

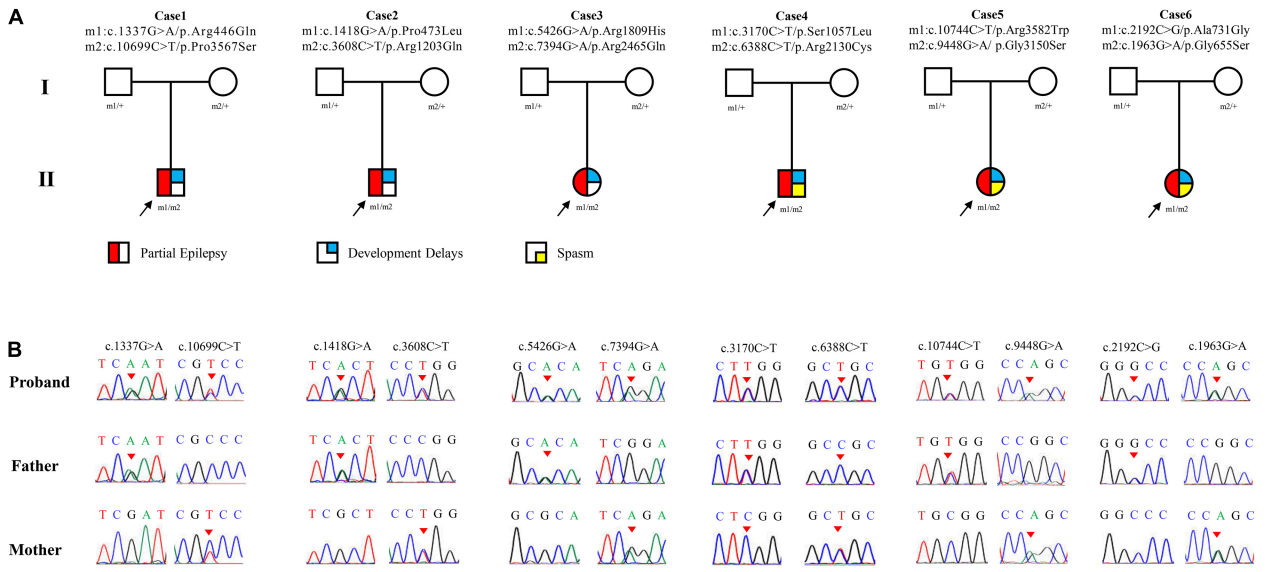

FIGURE 1 | Genetic data of cases with *LAMA5* variants. **(A)** Pedigrees of the six cases with *LAMA5* mutations and their corresponding phenotypes. **(B)** DNA sequence chromatogram of the *LAMA5* mutations. Arrows indicate the positions of the variants.

gnomAD-all population (vs. 472/248,058; $p = 8.306 \times 10^{-14}$), the controls of gnomAD-all population (vs. 218/100,060; $p = 4.728 \times 10^{-13}$), the gnomAD-East Asian population (vs. 167/18250, $p = 3.36 \times 10^{-6}$), and the controls of the gnomAD-East Asian population (vs. 71/8836, $p = 1.749 \times 10^{-6}$).

All *LAMA5* variants identified in this study were predicted to be damaging by at least two *in silico* tools (**Supplementary Table 1**). The probability that transcript falls into distribution of recessive genes (pRec) is 0.99353 for the *LAMA5* gene, indicating that it is very likely intolerant to recessive loss-of-function variations (Karczewski et al., 2020). None of the six affected individuals had pathogenic or likely pathogenic variants in genes known to be associated with epilepsy (Wang et al., 2017).

Clinical Features of the Cases With *LAMA5* Variants

The main clinical features of the six patients with *LAMA5* variants were summarized in **Table 1**. All patients showed infant-onset epilepsy with onset ages ranging from 1 to 9 months. The patients of cases 1, case 2, and case 3 suffered from infrequent focal seizures or secondary tonic-clonic seizures (monthly or yearly) and became seizure-free after treatment with valproate monotherapy or valproate in combination with levetiracetam. Their EEGs showed bilateral, unilateral, and multiple discharges, predominantly at the frontal, central, and temporal lobe, mainly during sleep (**Figure 2A**). The patients of case 4 and case 5 had daily focal seizures with spasms. Seizure-free was achieved after treatment with a combination of adrenocorticotropic hormones and topiramate. The patient of case 6 also had focal seizures and spasms (daily). The spasms and focal seizures disappeared after treatment, but myoclonic seizures appeared, which were infrequent (3–4 times/month). Interictal multifocal and generalized discharges were recorded in the three cases with spasms (**Figure 2B**).

These patients were full-term and delivered without abnormalities. Brain MRI was normal in the six cases. All patients showed mild global developmental delays.

Molecular Alteration of Laminin Subunit α5

The laminin subunit α5 contains one signal peptide, one Laminin N terminal domain, 22 Laminin EGF-like domains, one Laminin IV type A domain, and five Laminin G-like domains (Uniport-id: O15230) (**Figure 3A**). Five of the variants were located in Laminin EGF-like domains, including p.Arg446Gln, p.Pro473Leu, p.Gly655Ser, p.Ala731Gly, and p.Arg2130Cys. Three variants, p.Glu3150Ser, p.Pro3567Ser, and p.Arg3582Trp, were located in the Laminin G-like domains. Variant p.Val1809His was located in the Laminin IV type A domain. The other three variants p.Ser1057Leu, p.Arg1203Gln, and p.Arg2465Gln are located between structural domains (**Figure 3A**).

The molecular effects of the variants were analyzed by using I-TASSER for protein modeling and PyMOL for visualization. Eight of the variants, including p.Arg446Gln, p.Pro3567Ser, p.Arg1203Gln, p.Arg2465Gln, p.Ser1057Leu, p.Arg2130Cys, p.Arg3582Trp, and p.Ala731Gly changed their hydrogen bonds with surrounding residues. The other four variants, p.Pro473Leu, p.Gly655Ser, p.Arg1809His, and p.Gly3150Ser, did not change their hydrogen bonds but were predicted to decrease the protein stability significantly with $\Delta\Delta G$ values less than −0.5 kcal/mol. In each pair of compound heterozygous variants, at least one variant had hydrogen bonds change (**Figure 3B**).

It is notable that among the compound heterozygous variants in the three cases with only focal seizures (case 1, case 2, and

TABLE 1 | Clinical features of the patients with *LAMA5* variants.

	Variants (NM_005560.4)	Sex	Age	Seizure onset	Seizure course	Seizure timing	Seizure-free duration	AEDs	EEG	Brain MRI	Development delay
Case 1	c.1337G > A/p.Arg446Gln c.10699C > T/p.Pro3567Ser	M	4 yr.	9 mo.	sGTCS ∼7/yr. FS once in 3 yrs.	Nocturnal mostly	3 yr	LEV, VPA	Spike-slow waves in middle and posterior temporal areas.	Normal	Mild
Case 2	c.1418G > A/p.Pro473Leu c.3608C > T/p.Arg1203Gln	M	4 yr.	5 mo.	sGTCS 1-2 time/wk.	Diurnal and nocturnal	3 yr	VPA	Sharp and spike waves in frontal, central, and pretemporal areas.	Normal	Mild
Case 3	c.5426G > A/p.Arg1809His c.7394G > A/p.Arg2465Gln	F	4 yr.	1 mo.	1–2 time/wk.	Diurnal and nocturnal	4 yr	VPA	Spikes in the frontal and central areas.	Normal	Mild
Case 4	c.3170C > T/p.Ser1057Leu c.6388C > T/p.Arg2130Cys	M	1.5 yr.	3 mo.	Spasms and CPS, 1–3 times/days	Diurnal mostly	1 yr	TPM, ATCH	Spike-slow waves in the anterior area and generalized spikes and spike-slow waves.	Normal	Mild
Case 5	c.9448G > A/p.Gly3150Ser c.10744C > T/p.Arg3582Trp	F	1.5 yr.	5 mo.	Spasms and CPS, 1–2 times/day.	Nocturnal mostly	1 yr	TPM, ATCH	Spike-slow and sharp-slow waves in the bilateral posterior area and generalized spikes and spike-slow waves.	Normal	Mild
Case 6	c.2192C > G/p.Ala731Gly c.1963G > A/p.Gly655Ser	F	2.5 yr.	3 mo.	Spasms and CPS, 2–3 times/day.	Diurnal and nocturnal	–	CNZ, LEV, TPM, LTG	Spikes and spike-slow waves in bilateral temporal, frontal and central areas.	Normal	Mild

AEDs, antiepileptic drug; ATCH, adrenocorticotropic hormone; CPS, complex partial seizure; EEG, electroencephalogram; F, female; FS, febrile seizure; LEV, levetiracetam; LTG, lamotrigine; M, male; mo, month; MRI, magnetic resonance imaging; sGTCS, secondary generalized tonic-clonic seizure; TPM, topiramate; VPA, valproate; wk, week; yr, year.

case 3), two variants of each pair were located in different structural domains or domains/links (**Figure 3A**). Case 1 had the compound heterozygous variants with two variants located furthest apart (p.Arg446Gln and p.Pro3567Ser); the patient showed a milder phenotype than the others, e.g., the latest onset age (8-month-old) and infrequent seizure frequency (yearly). In the three cases with spasms, two pairs of compound heterozygous variants (case 5 and case 6) were constituted by two variants in the identical functional domains. The two variants of case 4 were in non-identical structural domains but presented the most pronounced hydrogen bonding changes (a total of eight hydrogen bonds disrupted).

The Expression Profile of *LAMAs*

The functional laminins are cruciform heterotrimers that consist of three short arms formed by the N-terminal portion of α, β, and γ subunits, respectively, and a long arm polymerized by the C-terminal parts of the three subunits (**Figure 4A**). The laminin short arms (N-terminus) are involved in laminin's ability to polymerize with those of other laminins to form a polygonal network, while the laminin long arm interacts with the extracellular matrix components to regulate biological processes (Hohenester, 2019). Laminin subunit α5 appears in laminin-511 (with β1 and γ1), laminin-521 (with β2 and γ1), and laminin-523 (with β2 and γ3). Previous studies show that laminins containing subunit α5 play an essential role in embryonic development and are intensely expressed on the surface of the ectoderm (Copp et al., 2011). Tissue-specific expression is the basis of gene function and subsequently the clinical phenotype. We thus compared the expression of *LAMAs* in the human brain from the data in VarCards and Genotype-Tissue Expression databases (GTEx Consortium, 2013). The *LAMA5* gene presented the highest expression in the human brain (**Figure 4B**). Furthermore, it was more abundant in the

TABLE 2 | Analysis of the aggregate frequency of *LAMA5* variants identified in this study.

Variants (NM_005560.4)	Allele count/number in this study	Allele count/number in the six controls						Homozygotes in the controls of gnomAD
		The controls of 296 healthy volunteers	The controls of Epi25 WES Brower	GnomAD-all population	The controls of gnomAD-all population	GnomAD-East Asian	The controls of gnomAD-East Asian	
c.1337C > T/p.Arg446Gln	1/236	–/–	1/16864	6/280278	1/109070	2/19918	0/9034	0
c.1418G > A/p.Pro473Leu	1/236	–/–	3/16870	15/263638	2/100060	0/19346	0/8626	0
c.1963G > A/p.Gly655Ser	1/236	–/–	–/–	7/248058	2/108800	0/18250	0/8948	0
c.2192C > G/p.Ala731Gly	1/236	1/592	–/–	14/281176	6/109254	14/19938	6/9046	0
c.3170C > T/p.Ser1057Leu	1/236	–/–	–/–	–/–	–/–	–/–	–/–	–
c.3608G > A/p.Arg1203Gln	1/236	–/–	–/–	28/270370	8/104670	7/19516	1/8836	0
c.5426G > A/p.Arg1809His	1/236	–/–	2/16860	1/251170	1/109360	0/18378	0/9038	0
c.6388C > T/p.Arg2130Cys	1/236	–/–	–/–	125/261646	65/110372	10/19184	6/9426	0
c.7394G > A/p.Arg2465Gln	1/236	–/–	–/–	108/253406	50/108836	78/19018	35/9738	0
c.9448G > A/p.Gly3150Ser	1/236	–/–	–/–	108/272790	56/117014	17/19536	7/9698	0
c.10699C > T/p.Pro3567Ser	1/236	–/–	–/–	1/248280	–/–	1/18254	–/–	–
c.10744C > T/Arg3582Trp	1/236	–/–	0/16844	59/277032	27/118346	38/19806	16/9870	0
Total	12/236(5.08 × 10^{-2})	1/592(1.69 × 10^{-3})	6/16844(3.56 × 10^{-4})	472/248058(1.9 × 10^{-3})	218/100060(2.18 × 10^{-3})	167/18250(9.15 × 10^{-3})	71/8626(8.04 × 10^{-3})	0
P-value		2.243 × 10^{-6}	<2.2 × 10^{-16}	8.306 × 10^{-14}	4.728 × 10^{-13}	3.36 × 10^{-6}	1.749 × 10^{-6}	–
OR (95% CI)		31.589(4.628–1348.630)	149.545(61.506–484.264)	28.104(14.202–50.423)	24.538(12.299–44.594)	5.799(2.894–10.599)	6.452(3.139–12.204)	–

P-values and odds ratio were estimated with 2-sided Fisher's exact test.
CI, confidence interval; gnomAD, Genome Aggregation Database; OR, odd ratio; WES, whole-exome sequencing.

cerebral cortex, substantia nigra, frontal cortex, hippocampus, and anterior cingulate cortex (**Figure 4C**).

DISCUSSION

The *LAMA5* gene, predominantly expressed in the early stage of life, plays a vital role in neurodevelopmental biological processes such as neurite outgrowth, epiblast polarization, neuronal migration, synaptic stability, and cell adhesion, differentiation, migration, and signaling. A functional study suggested that the laminin subunit α5 was deposited at synapses in the brain and was essential for dendritic spine structural regulation and synapse stability (Omar et al., 2017). Experimentally, mutant protein of *LAMA5* resulted in decreased binding to the synaptic vesicle protein encoded by *SV2A* (Maselli et al., 2018). Abnormalities in the central nervous system were monitored in the conditional allele knockout *LAMA5* mice (Omar et al., 2017). In this study, six pairs of biallelic variants in *LAMA5* were identified in patients with infant-onset epilepsy. All variants presented no or low allele frequencies in controls. The aggregate frequency of the *LAMA5* variants identified in the case cohort was significantly higher than that in controls. The recessive burden analysis also showed that the *LAMA5* variants in the present cohort were significantly more than the expected number in the East Asian population. These findings suggest a potential association between *LAMA5* variants and epilepsy.

Previously, a *de novo* canonical splice site variant (c.10828 + 1G > A) was identified in a patient with developmental delays and epilepsy (Han et al., 2018). In a patient with cortical developmental malformations, a pair of compound heterozygous variants (p.Glu3567Lys and p.Asp2372Asn) were identified (Wiszniewski et al., 2018). One pair of homozygous variants in *LAMA5* (p.Arg2659Trp) and one homozygous variant in *LAMA1* were identified in a patient with the presynaptic congenital myasthenic syndrome who has non-classified facial tics or tics (Maselli et al., 2018). A heterozygous variant in *LAMA5* (p.Val3140Met) was identified in a family with a complex multisystem syndrome, in which several family members with the *LAMA5* variant had seizures (Sampaolo et al., 2017). These data provided clues for the possible association between *LAMA5* and epilepsy, but the pathogenic role of *LAMA5* variants in epilepsy could not be determined due to the variable phenotype, co-appearance of variants in other potentially pathogenic genes, or the single affected case. In the present study, we identified *LAMA5* variants in six unrelated cases, and the other possible pathogenic genes were excluded. Therefore, this study provided direct evidence in supporting the association between *LAMA5* and epilepsy.

In animals, the homozygous *LAMA5* knockout mice model showed preweaning lethality with complete penetrance[5], while the heterozygous knockout mice showed fewer abnormalities, suggesting a dose-effect. The pRec, a metric for intolerant of biallelic loss-of-function variants, is 0.99353 for the *LAMA5*

[5]http://www.informatics.jax.org/allele/MGI:1934917

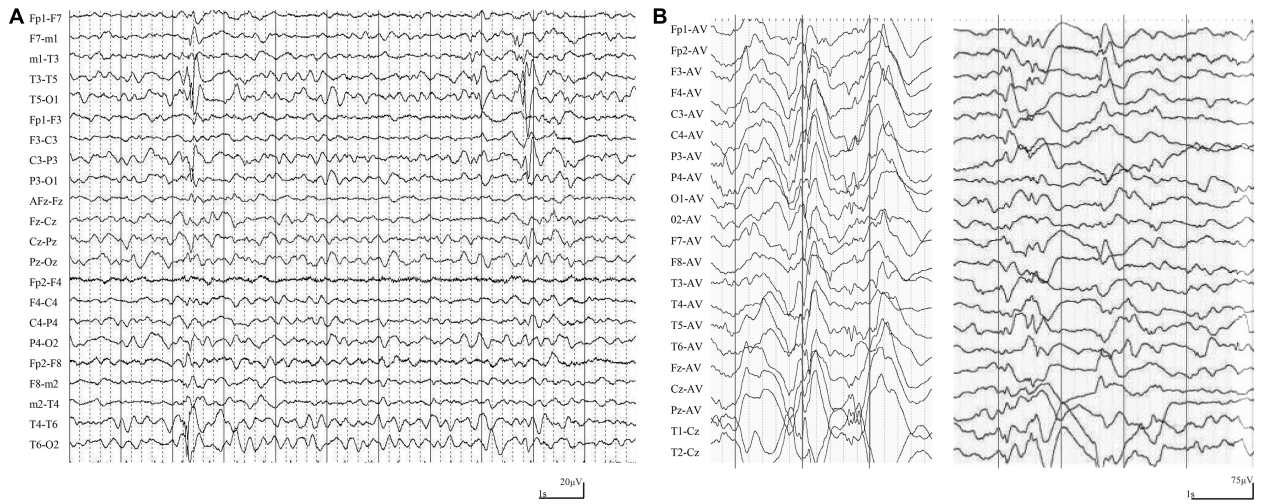

FIGURE 2 | Ictal and interictal EEG in the cases with *LAMA5* variants. **(A)** Interictal EEG in case 1 at the age of 8 months showed irregular spike-slow waves in the middle and posterior temporal region. **(B)** Interictal EEG in case 4 at the age of 3 months showed diffuse high amplitude spike and spike-slow waves, and focal spike-slow waves in the anterior region.

gene, indicating that it is highly intolerant for recessive loss-of-function variations (Karczewski et al., 2020). The *LAMA5* variants identified in the present study were all biallelic variants. It was noted that among the compound heterozygous variants in the three cases with only focal seizures, two variants of each pair variant were located in different structural domains or domains/links. In the three cases with spasms, two pairs of variants were constituted by two variants in the identical functional domains, and another pair of variants presented the most pronounced hydrogen bonding changes. Taken together that homozygous *LAMA5* knockout mice displayed preweaning lethality with complete penetrance, it was considered that homozygous variants in *LAMA5* would cause the most severe damage effect and resulted in the most severe phenotype or even early death; the compound heterozygous variants with two variants located in identical functional domains potentially created relatively severe damage effect and caused severe epilepsy such as spasms; and the compound heterozygous variants with two variants located in non-identical functional domains potentially caused relatively mild damage effects and led to mild phenotypes. It is suggested that the location of variants in compound heterozygous variants was potentially associated with the phenotype severity, providing one of the explanations for the phenotype variation.

Structurally, the laminin subunit α5 forms heterotrimers with laminin subunits β1/β2 and γ1/γ3, which were encoded by *LAMB1*, *LAMB2*, *LAMC1*, and *LAMC3* that were associated with neurodevelopmental diseases and epilepsy. The *LAMB1* gene is the responsible gene of lissencephaly 5 (OMIM #615191) characterized by focal and spasmodic seizures and psychomotor development delay (Radmanesh et al., 2013; Tonduti et al., 2015). The *LAMB2* gene is the causative gene of Pierson syndrome (OMIM #609049), with which the majority of patients died early and the survivors presented severe neurodevelopmental delays (Pierson et al., 1963; Zenker et al., 2004). The *LAMC1* gene has been repeatedly reported in Dandy–Walker malformation with occipital cephalocele, and most of the affected individuals had an infant-onset intellectual disability with or without seizures (Carvalho et al., 2006; Darbro et al., 2013). Variants in *LAMC3* were the causes of occipital cortical malformations (OMIM #614115), and the affected individuals experienced seizures (Barak et al., 2011). Experimentally, these genes caused neurological abnormalities through a common mechanism of disrupted function of laminin heterotrimers in regulating neuronal migration and other biological processes (Pierson et al., 1963; Zenker et al., 2004; Carvalho et al., 2006; Darbro et al., 2013; Radmanesh et al., 2013; Tonduti et al., 2015). However, the *LAMA5* gene, which encodes one of the indispensable parts of the heterotrimers, has not been confirmed to be associated with neurological disorders. In this study, the patients with biallelic *LAMA5* variants presented focal seizures and developmental delays, suggesting a potential role of *LAMA5* in epilepsy with the involvement of neurodevelopment.

Regarding *LAMA*s that encode the laminin α subunits, the associations between *LAMA1-4* and human diseases have been established. Variants in *LAMA1* cause Poretti–Boltshauser syndrome (OMIM #615960), characterized by delayed motor development, speech delay, and cognitive function; and seizures, tics, and spasticity have also been observed (Aldinger et al., 2014; Elmas et al., 2020). *LAMA2* is the causative gene of autosomal recessive limb-girdle muscular dystrophy-23 (OMIM #618138) and congenital merosin deficient or partially deficient muscular dystrophy (OMIM #607855), in which epilepsy was regarded as one of the core features (Chan et al., 2014; Xiong et al., 2015; Salvati et al., 2021). The *LAMA3* gene is the responsible gene of Herlitz type junctional epidermolysis bullosa (OMIM #226700), generalized atrophic benign epidermolysis bullosa (OMIM #226650), and laryngo-onycho-cutaneous syndrome

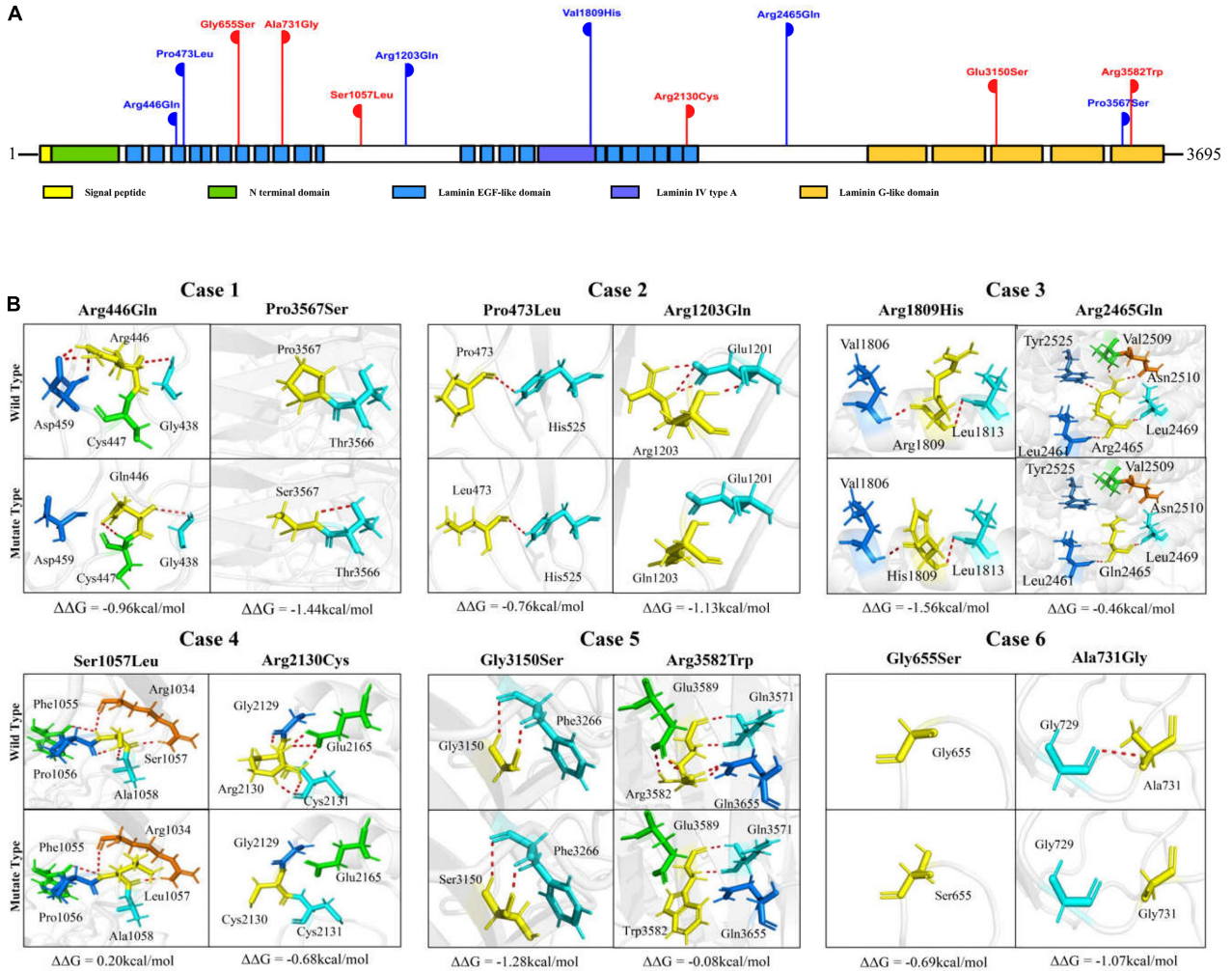

FIGURE 3 | Schematic illustration of *LAMA5* variants. **(A)** Schematic illustration of the laminin subunit α5 and the location of the *LAMA5* variants identified in this study. Two variants of the same height represent a pair of biallelic mutations. The variants of red-colored represent cases with both spasms and focal seizures; those of blue-colored represent cases with only focal seizures. **(B)** Hydrogen bond changes and free energy stability changes (Δ Δ*G*, Kcal/mol) value of the variants from the present study.

(OMIM #245660) (Kivirikko et al., 1995; McGrath et al., 1995; Vidal et al., 1995; Nakano et al., 2002; McLean et al., 2003). The *LAMA4* gene is the causative gene of dilated cardiomyopathy 1JJ (OMIM #615235) (Knoll et al., 2007). Compared with the other *LAMA*s genes, the *LAMA5* gene had the highest expression in the human brain and was abundant in the cerebral cortex, substantia nigra, frontal cortex, hippocampus, and anterior cingulate cortex. Generally, tissue-specific expression is the basis of gene function and subsequently the clinical phenotype. The highest expression of *LAMA5* in the human brain provided an anatomical basis for the association between *LAMA5* and neurological diseases.

The proteins encoded by *LAMAs* are of tissue-specific expression and independent function, while the protein encoded by *LAMA5* interacts with that encoded by *LAMBs* and *LAMCs*. Therefore, the possibility of digenic or polygenic mechanisms could not be excluded. No pathogenetic or likely pathogenetic variants in *LAMBs*, *LAMCs*, or other epilepsy genes were identified in these patients, suggesting a potential monogenic role of *LAMA5*. However, the patients with *LAMA5* variants presented a relatively moderate phenotype, and several variants presented in the population with low frequency. Thus, a modifier role of *LAMA5* could not be excluded. Further studies with large cohorts are needed to validate the pathological nature of *LAMA5* variants.

Among the disease-causing genes in humans (OMIM[6]), 1,008 genes were associated with disease in a dominant inheritance pattern, whereas 1,936 genes were in a recessive inheritance pattern. Considering that the genome in humans is diploid, it is possible that recessive variants were more common than dominant variants in the etiology of human diseases. Currently, most infantile spasms-related genes (36/47) (Bayat et al., 2021) and all focal epilepsy-associated genes were of autosomal

[6]www.omim.org

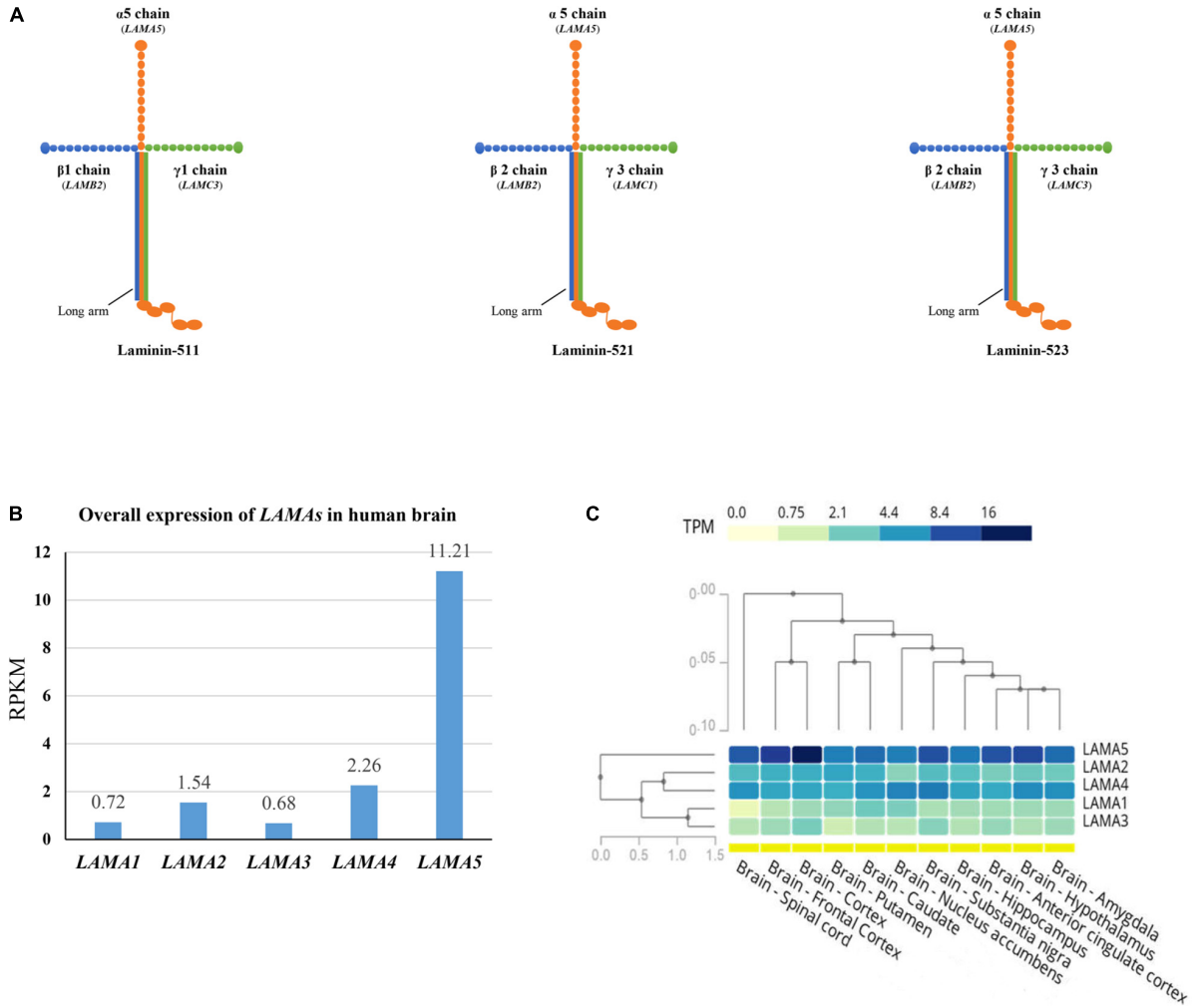

FIGURE 4 | Schematic illustration of laminin heterotrimers and the expression profile of *LAMAs*. **(A)** Schematic illustration of the heterotrimers containing laminin subunit α5. Laminin subunit α5 formed laminin-511 with subunit β1 and γ1, laminin-521 with subunit β2 and γ1, and laminin-523 with subunit β2 and γ3. **(B)** The overall expression of *LAMAs* in the human brain. RPKM, Reads Per Kilobase per Million mapped reads. **(C)** Heatmap and hierarchical clustering of *LAMAs* expression in the sub-regions of human brain. Columns represent individual sub-region and rows represent individual genes. The darker the color, the higher the expression. The lines represent cluster analysis. More details were presented in the GTEx database (www.gtexportal.org).

dominant inheritance. Thus, more attention should be paid to recessive variants in epilepsy. This study revealed *LAMA5* as a potential novel autosomal recessive gene in infant epilepsy, enriching the genetic etiology of epilepsy.

This study has several limitations. The direct functional effects of the variants were not examined. The consequences of the variants on the interactions of the alpha subunit with its partners warrant further studies. Besides point variants, whether CNV in the *LAMA5* gene was pathogenic should also be considered.

CONCLUSION

The association between *LAMA5* and epilepsy was supported by multiple pieces of evidence, such as common clinical features, unique gene functions, and statistical evidence. The establishment of the association between *LAMA5* and epilepsy will facilitate the genetic diagnosis and management in patients with infant epilepsy.

DATA AVAILABILITY STATEMENT

The datasets presented in this study can be found in online repositories. The names of the repository/repositories and accession number(s) can be found below: NCBI GenBank: OM994299 – OM994307 and OM994308 – OM994334.

ETHICS STATEMENT

This study adhered to the principles of the International Committee of Medical Journal Editors concerning patient

consent for research or participation and received approval from the Ethics Committee of the Second Affiliated Hospital of Guangzhou Medical University. Written informed consent was provided by the patients' legal guardians.

AUTHOR CONTRIBUTIONS

SL, Z-GL, and W-PL designed the experiments. JuW, J-XL, X-GY, XL, Q-XZ, X-RL, JiW, L-DG, F-LL, B-ML, Z-FG, Q-HG, and Y-HY collected and analyzed the clinical data and patient samples. Z-LY and HL performed the computational modeling. SL, Z-GL, and W-PL wrote the manuscript, with contributions from all the authors.

FUNDING

This work was supported by the National Natural Science Foundation of China (Grant Nos. 81971216 and 81871015), Natural Science Foundation of Guangdong Province (2020A1515010108), Science and Technology Project of Guangzhou (Grant Nos. 201904010292 and 201904020028), Science and Technology Project of Guangdong Province (Grant No. 2017B030314159), Shandong Medical and Health Science and Technology Development Plan (Grant No. 202106010271), and Multi-Center Clinical Research Fund Project of the Second Affiliated Hospital of Guangzhou Medical University (2020-LCYJ-DZX-03).

ACKNOWLEDGMENTS

The help of patients and clinicians participating in this work are greatly appreciated.

SUPPLEMENTARY MATERIAL

The Supplementary Material for this article can be found online at: https://www.frontiersin.org/articles/10.3389/fnmol.2022.825390/full#supplementary-material

REFERENCES

Aldinger, K. A., Mosca, S. J., Tetreault, M., Dempsey, J. C., Ishak, G. E., Hartley, T., et al. (2014). Mutations in LAMA1 cause cerebellar dysplasia and cysts with and without retinal dystrophy. *Am. J. Hum. Genet.* 95, 227–234. doi: 10.1016/j.ajhg.2014.07.007

Barak, T., Kwan, K. Y., Louvi, A., Demirbilek, V., Saygi, S., Tuysuz, B., et al. (2011). Recessive LAMC3 mutations cause malformations of occipital cortical development. *Nat. Genet.* 43, 590–594. doi: 10.1038/ng.836

Bayat, A., Bayat, M., Rubboli, G., and Moller, R. S. (2021). Epilepsy syndromes in the first year of life and usefulness of genetic testing for precision therapy. *Genes (Basel)* 12:1051. doi: 10.3390/genes12071051

Capriotti, E., Fariselli, P., and Casadio, R. (2005). I-Mutant2.0: predicting stability changes upon mutation from the protein sequence or structure. *Nucleic Acids Res.* 33, W306–W310. doi: 10.1093/nar/gki375

Carvalho, D. R., Giuliani, L. R., Simao, G. N., Santos, A. C., and Pina-Neto, J. M. (2006). Autosomal dominant atretic cephalocele with phenotype variability: report of a Brazilian family with six affected in four generations. *Am. J. Med. Genet. A* 140, 1458–1462. doi: 10.1002/ajmg.a.31255

Chan, S. H., Foley, A. R., Phadke, R., Mathew, A. A., Pitt, M., Sewry, C., et al. (2014). Limb girdle muscular dystrophy due to LAMA2 mutations: diagnostic difficulties due to associated peripheral neuropathy. *Neuromuscul. Disord.* 24, 677–683. doi: 10.1016/j.nmd.2014.05.008

GTEx Consortium (2013). The genotype-tissue expression (GTEx) project. *Nat. Genet.* 45, 580–585. doi: 10.1038/ng.2653

CONVERGE Consortium (2015). Sparse whole-genome sequencing identifies two loci for major depressive disorder. *Nature* 523, 588–591. doi: 10.1038/nature14659

Copp, A. J., Carvalho, R., Wallace, A., Sorokin, L., Sasaki, T., Greene, N. D., et al. (2011). Regional differences in the expression of laminin isoforms during mouse neural tube development. *Matrix Biol.* 30, 301–309. doi: 10.1016/j.matbio.2011.04.001

Darbro, B. W., Mahajan, V. B., Gakhar, L., Skeie, J. M., Campbell, E., Wu, S., et al. (2013). Mutations in extracellular matrix genes NID1 and LAMC1 cause autosomal dominant Dandy-Walker malformation and occipital cephaloceles. *Hum. Mutat.* 34, 1075–1079. doi: 10.1002/humu.22351

Domogatskaya, A., Rodin, S., and Tryggvason, K. (2012). Functional diversity of laminins. *Annu. Rev. Cell Dev. Biol.* 28, 523–553. doi: 10.1146/annurev-cellbio-101011-155750

Durkin, M. E., Loechel, F., Mattei, M. G., Gilpin, B. J., Albrechtsen, R., and Wewer, U. M. (1997). Tissue-specific expression of the human laminin alpha5-chain, and mapping of the gene to human chromosome 20q13.2-13.3 and to distal mouse chromosome 2 near the locus for the ragged (Ra) mutation. *FEBS Lett.* 411, 296–300. doi: 10.1016/s0014-5793(97)00686-8

Elmas, M., Gogus, B., and Solak, M. (2020). Understanding what you have found: a family with a mutation in the LAMA1 gene with literature review. *Clin. Med. Insights Case Rep.* 13:1179547620948666. doi: 10.1177/1179547620948666

Eltze, C. M., Chong, W. K., Cox, T., Whitney, A., Cortina-Borja, M., Chin, R. F., et al. (2013). A population-based study of newly diagnosed epilepsy in infants. *Epilepsia* 54, 437–445. doi: 10.1111/epi.12046

Epi25 Collaborative (2019). Ultra-rare genetic variation in the epilepsies: a whole-exome sequencing study of 17,606 individuals. *Am. J. Hum. Genet.* 105, 267–282. doi: 10.1016/j.ajhg.2019.05.020

Gan, J., Cai, Q., Galer, P., Ma, D., Chen, X., Huang, J., et al. (2019). Mapping the knowledge structure and trends of epilepsy genetics over the past decade: a co-word analysis based on medical subject headings terms. *Medicine (Baltimore)* 98:e16782. doi: 10.1097/MD.0000000000016782

Han, J. Y., Jang, J. H., Park, J., and Lee, I. G. (2018). Targeted next-generation sequencing of korean patients with developmental delay and/or intellectual disability. *Front. Pediatr.* 6:391. doi: 10.3389/fped.2018.00391

Hirose, G. (2013). [An overview of epilepsy: its history, classification, pathophysiology and management]. *Brain Nerve* 65, 509–520.

Hohenester, E. (2019). Structural biology of laminins. *Essays Biochem.* 63, 285–295. doi: 10.1042/EBC20180075

Kang, K. W., Kim, W., Cho, Y. W., Lee, S. K., Jung, K. Y., Shin, W., et al. (2019). Genetic characteristics of non-familial epilepsy. *PeerJ* 7:e8278. doi: 10.7717/peerj.8278

Karczewski, K. J., Francioli, L. C., Tiao, G., Cummings, B. B., Alfoldi, J., Wang, Q., et al. (2020). The mutational constraint spectrum quantified from variation in 141,456 humans. *Nature* 581, 434–443. doi: 10.1038/s41586-020-2308-7

Kikkawa, Y., and Miner, J. H. (2006). Molecular dissection of laminin alpha 5 in vivo reveals separable domain-specific roles in embryonic development and kidney function. *Dev. Biol.* 296, 265–277. doi: 10.1016/j.ydbio.2006.04.463

Kivirikko, S., McGrath, J. A., Baudoin, C., Aberdam, D., Ciatti, S., Dunnill, M. G., et al. (1995). A homozygous nonsense mutation in the alpha 3 chain gene of laminin 5 (LAMA3) in lethal (Herlitz) junctional epidermolysis bullosa. *Hum. Mol. Genet.* 4, 959–962. doi: 10.1093/hmg/4.5.959

Knoll, R., Postel, R., Wang, J., Kratzner, R., Hennecke, G., Vacaru, A. M., et al. (2007). Laminin-alpha4 and integrin-linked kinase mutations cause human cardiomyopathy via simultaneous defects in cardiomyocytes and endothelial cells. *Circulation* 116, 515–525. doi: 10.1161/CIRCULATIONAHA.107.689984

Liang, S., and Crutcher, K. A. (1992). Neuronal migration on laminin in vitro. *Brain Res. Dev. Brain Res.* 66, 127–132. doi: 10.1016/0165-3806(92)90148-p

Luckenbill-Edds, L. (1997). Laminin and the mechanism of neuronal outgrowth. *Brain Res. Brain Res. Rev.* 23, 1–27. doi: 10.1016/s0165-0173(96)00013-6

Martin, H. C., Jones, W. D., McIntyre, R., Sanchez-Andrade, G., Sanderson, M., Stephenson, J. D., et al. (2018). Quantifying the contribution of recessive coding variation to developmental disorders. *Science* 362, 1161–1164. doi: 10.1126/science.aar6731

Maselli, R. A., Arredondo, J., Vazquez, J., Chong, J. X., Bamshad, M. J., Nickerson, D. A., et al. (2018). A presynaptic congenital myasthenic syndrome attributed to a homozygous sequence variant in LAMA5. *Ann. N Y Acad. Sci.* 1413, 119–125. doi: 10.1111/nyas.13585

McGrath, J. A., Kivirikko, S., Ciatti, S., Moss, C., Dunnill, G. S., Eady, R. A., et al. (1995). A homozygous nonsense mutation in the alpha 3 chain gene of laminin 5 (LAMA3) in Herlitz junctional epidermolysis bullosa: prenatal exclusion in a fetus at risk. *Genomics* 29, 282–284. doi: 10.1006/geno.1995.1246

McLean, W. H., Irvine, A. D., Hamill, K. J., Whittock, N. V., Coleman-Campbell, C. M., Mellerio, J. E., et al. (2003). An unusual N-terminal deletion of the laminin alpha3a isoform leads to the chronic granulation tissue disorder laryngo-onycho-cutaneous syndrome. *Hum. Mol. Genet.* 12, 2395–2409. doi: 10.1093/hmg/ddg234

Miner, J. H., Cunningham, J., and Sanes, J. R. (1998). Roles for laminin in embryogenesis: exencephaly, syndactyly, and placentopathy in mice lacking the laminin alpha5 chain. *J. Cell Biol.* 143, 1713–1723. doi: 10.1083/jcb.143.6.1713

Mukherjee, C., Saleem, S., Das, S., Biswas, S. C., and Bhattacharyya, D. (2020). Human placental laminin: role in neuronal differentiation, cell adhesion and proliferation. *J. Biosci.* 45:93.

Nakano, A., Chao, S. C., Pulkkinen, L., Murrell, D., Bruckner-Tuderman, L., Pfendner, E., et al. (2002). Laminin 5 mutations in junctional epidermolysis bullosa: molecular basis of Herlitz vs. non-Herlitz phenotypes. *Hum. Genet.* 110, 41–51. doi: 10.1007/s00439-001-0630-1

Omar, M. H., Kerrisk Campbell, M., Xiao, X., Zhong, Q., Brunken, W. J., Miner, J. H., et al. (2017). CNS neurons deposit laminin alpha5 to stabilize synapses. *Cell Rep.* 21, 1281–1292. doi: 10.1016/j.celrep.2017.10.028

Pierson, M., Cordier, J., Hervouuet, F., and Rauber, G. (1963). [An unusual congenital and familial congenital malformative combination involving the eye and kidney]. *J. Genet. Hum.* 12, 184–213.

Radmanesh, F., Caglayan, A. O., Silhavy, J. L., Yilmaz, C., Cantagrel, V., Omar, T., et al. (2013). Mutations in LAMB1 cause cobblestone brain malformation without muscular or ocular abnormalities. *Am. J. Hum. Genet.* 92, 468–474. doi: 10.1016/j.ajhg.2013.02.005

Salvati, A., Bonaventura, E., Sesso, G., Pasquariello, R., and Sicca, F. (2021). Epilepsy in LAMA2-related muscular dystrophy: a systematic review of the literature. *Seizure* 91, 425–436. doi: 10.1016/j.seizure.2021.07.020

Sampaolo, S., Napolitano, F., Tirozzi, A., Reccia, M. G., Lombardi, L., Farina, O., et al. (2017). Identification of the first dominant mutation of LAMA5 gene causing a complex multisystem syndrome due to dysfunction of the extracellular matrix. *J. Med. Genet.* 54, 710–720. doi: 10.1136/jmedgenet-2017-104555

Song, T. Y., Deng, J., Fang, F., Chen, C. H., Wang, X. H., Wang, X., et al. (2021). [The etiology of 340 infants with early-onset epilepsy]. *Zhonghua Er Ke Za Zhi* 59, 387–392. doi: 10.3760/cma.j.cn112140-20201016-00947

Tonduti, D., Dorboz, I., Renaldo, F., Masliah-Planchon, J., Elmaleh-Berges, M., Dalens, H., et al. (2015). Cystic leukoencephalopathy with cortical dysplasia related to LAMB1 mutations. *Neurology* 84, 2195–2197. doi: 10.1212/WNL.0000000000001607

Vidal, F., Baudoin, C., Miquel, C., Galliano, M. F., Christiano, A. M., Uitto, J., et al. (1995). Cloning of the laminin alpha 3 chain gene (LAMA3) and identification of a homozygous deletion in a patient with Herlitz junctional epidermolysis bullosa. *Genomics* 30, 273–280. doi: 10.1006/geno.1995.9877

Wang, J., Lin, Z. J., Liu, L., Xu, H. Q., Shi, Y. W., Yi, Y. H., et al. (2017). Epilepsy-associated genes. *Seizure* 44, 11–20. doi: 10.1016/j.seizure.2016.11.030

Wang, J. Y., Zhou, P., Wang, J., Tang, B., Su, T., Liu, X. R., et al. (2018). ARHGEF9 mutations in epileptic encephalopathy/intellectual disability: toward understanding the mechanism underlying phenotypic variation. *Neurogenetics* 19, 9–16. doi: 10.1007/s10048-017-0528-2

Wirrell, E. C., Grossardt, B. R., Wong-Kisiel, L. C., and Nickels, K. C. (2011). Incidence and classification of new-onset epilepsy and epilepsy syndromes in children in Olmsted County, Minnesota from 1980 to 2004: a population-based study. *Epilepsy Res.* 95, 110–118. doi: 10.1016/j.eplepsyres.2011.03.009

Wiszniewski, W., Gawlinski, P., Gambin, T., Bekiesinska-Figatowska, M., Obersztyn, E., Antczak-Marach, D., et al. (2018). Comprehensive genomic analysis of patients with disorders of cerebral cortical development. *Eur. J. Hum. Genet.* 26, 1121–1131. doi: 10.1038/s41431-018-0137-z

Xiong, H., Tan, D., Wang, S., Song, S., Yang, H., Gao, K., et al. (2015). Genotype/phenotype analysis in Chinese laminin-alpha2 deficient congenital muscular dystrophy patients. *Clin. Genet.* 87, 233–243. doi: 10.1111/cge.12366

Yang, J., and Zhang, Y. (2015). I-TASSER server: new development for protein structure and function predictions. *Nucleic Acids Res.* 43, W174–W181. doi: 10.1093/nar/gkv342

Zenker, M., Tralau, T., Lennert, T., Pitz, S., Mark, K., Madlon, H., et al. (2004). Congenital nephrosis, mesangial sclerosis, and distinct eye abnormalities with microcoria: an autosomal recessive syndrome. *Am. J. Med. Genet. A* 130A, 138–145. doi: 10.1002/ajmg.a.30310

Conflict of Interest: The authors declare that the research was conducted in the absence of any commercial or financial relationships that could be construed as a potential conflict of interest.

Publisher's Note: All claims expressed in this article are solely those of the authors and do not necessarily represent those of their affiliated organizations, or those of the publisher, the editors and the reviewers. Any product that may be evaluated in this article, or claim that may be made by its manufacturer, is not guaranteed or endorsed by the publisher.

frontiers | Frontiers in Molecular Neuroscience

ORIGINAL RESEARCH
published: 23 June 2022
doi: 10.3389/fnmol.2022.864074

ADGRV1 Variants in Febrile Seizures/Epilepsy With Antecedent Febrile Seizures and Their Associations With Audio-Visual Abnormalities

Peng Zhou[1†‡], Heng Meng[2‡], Xiaoyu Liang[1], Xiaoyun Lei[2], Jingwen Zhang[3], Wenjun Bian[1], Na He[1], Zhijian Lin[4], Xingwang Song[1], Weiwen Zhu[1], Bin Hu[1], Bingmei Li[1], Limin Yan[5], Bin Tang[1], Tao Su[1], Hankui Liu[6], Yong Mao[6], Qiongxiang Zhai[3] and Yonghong Yi[1*†] for the China Epilepsy Gene 1.0 Project*

[1] Key Laboratory of Neurogenetics and Channelopathies of Guangdong Province and the Ministry of Education of China, Department of Neurology, Institute of Neuroscience, The Second Affiliated Hospital, Guangzhou Medical University, Guangzhou, China, [2] Department of Neurology, The First Affiliated Hospital of Jinan University, Clinical Neuroscience Institute of Jinan University, Guangzhou, China, [3] Department of Pediatrics, Guangdong Provincial People's Hospital, Guangdong Academy of Medical Sciences, Guangzhou, China, [4] Department of Neurology, Affiliated Hospital of Putian University, Putian, China, [5] Department of Neurology, The Second Affiliated Hospital of Hainan Medical University, Haikou, China, [6] BGI-Shenzhen, Shenzhen, China

Objective: *ADGRV1* gene encodes adhesion G protein-coupled receptor-V1 that is involved in synaptic function. *ADGRV1* mutations are associated with audio-visual disorders. Although previous experimental studies suggested that *ADGRV1* variants were associated with epilepsy, clinical evidence is limited and the phenotype spectrum is to be defined.

Methods: Trio-based targeting sequencing was performed in a cohort of 101 cases with febrile seizure (FS) and epilepsy with antecedent FS. Protein modeling was used to assess the damaging effects of variants. The genotype-phenotype correlations of the *ADGRV1* variants in epilepsy and audio-visual disorders were analyzed.

Results: *ADGRV1* variants were identified in nine unrelated cases (8.91%), including two heterozygous frameshift variants, six heterozygous missense variants, and a pair of compound heterozygous variants. These variants presented a statistically higher frequency in this cohort than that in control populations. Most missense variants were located at CalX-β motifs and changed the hydrogen bonds. These variants were inherited from the asymptomatic parents, indicating an incomplete penetrance. We also identified *SCN1A* variants in 25 unrelated cases (24.75%) and *SCN9A* variants in 3 unrelated cases (2.97%) in this cohort. Contrary to *SCN1A* variant-associated epilepsy that revealed seizure was aggravated by sodium channel blockers, *ADGRV1* variants were associated with mild epilepsy with favorable responses to antiepileptic drugs. The patients denied problems with audio-visual-vestibular abilities in daily life. However, audio-visual tests revealed auditory and visual impairment in the patient with compound heterozygous variants, auditory or vestibular impairment in the patients with heterozygous frameshift,

OPEN ACCESS

Edited by:
Qian Chen,
Massachusetts Institute of Technology, United States

Reviewed by:
Saima Siddiqi,
Institute of Biomedical and Genetic Engineering (IBGE), Pakistan
Elena Dmitrievna Belousova,
Pirogov Russian National Research Medical University, Russia

***Correspondence:**
Qiongxiang Zhai
zhaiqiongxiang@sina.com
Yonghong Yi
yyh168@sina.com

†ORCID:
Peng Zhou
orcid.org/0000-0002-5503-1774
Yonghong Yi
orcid.org/0000-0002-6075-2015

‡These authors share first authorship

Specialty section:
This article was submitted to Molecular Signalling and Pathways, a section of the journal Frontiers in Molecular Neuroscience

Received: 28 January 2022
Accepted: 25 April 2022
Published: 23 June 2022

Citation:
Zhou P, Meng H, Liang X, Lei X, Zhang J, Bian W, He N, Lin Z, Song X, Zhu W, Hu B, Li B, Yan L, Tang B, Su T, Liu H, Mao Y, Zhai Q and Yi Y (2022) ADGRV1 Variants in Febrile Seizures/Epilepsy With Antecedent Febrile Seizures and Their Associations With Audio-Visual Abnormalities. Front. Mol. Neurosci. 15:864074. doi: 10.3389/fnmol.2022.864074

or hydrogen-bond changed missense variants but no abnormalities in the patients with missense variants without hydrogen-bond changes. Previously reported *ADGRV1* variants that were associated with audio-visual disorders were mostly biallelic/destructive variants, which were significantly more frequent in the severe phenotype of audio-visual disorders (Usher syndrome 2) than in other mild phenotypes. In contrast, the variants identified in epilepsy were monoallelic, missense mainly located at CalX-β, or affected isoforms VLGR1b/1c.

Significance: *ADGRV1* is potentially associated with FS-related epilepsy as a susceptibility gene. The genotype, submolecular implication, isoforms, and damaging severity of the variants explained the phenotypical variations. *ADGRV1* variant-associated FS/epilepsy presented favorable responses to antiepileptic drugs, implying a clinical significance.

Keywords: *ADGRV1*, febrile seizures, audio-visual disorders, genotype-phenotype correlation, submolecular effect

INTRODUCTION

The human adhesion G protein-coupled receptor V1 (*ADGRV1*) gene (OMIM: 602,851) encodes a very large G protein-coupled receptor-1 (VLGR1), which is localized at synaptic junctions and acts in concert to regulate synaptic function (Neubig and Siderovski, 2002; Togashi et al., 2002). It has also been termed the monogenic audiogenic seizures-susceptibility 1 (*MASS1*) gene, G protein-coupled receptor 98 (*GPR98*) gene, or *VLGR1* gene. Three VLGR1 mRNA isoforms, namely VLGR1a, VLGR1b, and VLGR1c, are expressed in the brain, cochlea, eyes, and connective tissues. VLGR1b, the largest full-length isoform, has a large extracellular domain, encompassing a signal peptide, seven epilepsy-associated repeats (i.e., epitempin repeats), and 35 calcium exchanger β (CalX-β) motifs (Beckmann et al., 1998; Scheel et al., 2002; Staub et al., 2002; Pons et al., 2003; McMillan and White, 2010). Its cytoplasmic domain contains a class I PDZ (i.e., PSD95, Dlg, and ZO-1/ZO-2) binding motif, which is recognized as a ligand for several proteins and is involved in maintaining the structural integrity of hair bundles in the inner ears (Sun et al., 2013). Variants in *ADGRV1* gene are associated with audio-visual disorders, typically Usher syndrome type 2 (USH2), which is characterized by moderate-to-severe congenital sensorineural hearing loss and postnatal retinitis pigmentosa.

Previous studies suggested a potential association between *ADGRV1* gene and epilepsy. The seven epitempin repeats were first identified in the leucine-rich glioma-inactivated 1 gene (Staub et al., 2002), which is associated with autosomal dominant lateral temporal lobe epilepsy with auditory features (Kalachikov et al., 2002). Experimental studies have demonstrated associations between the *Adgrv1/Mass1/Vlgr1* genes and audiogenic seizures in mice. A truncating variant (c.7009delG) of the *Mass1* gene was determined to cause audiogenic seizures in *Frings* mice (Skradski et al., 2001). *Vlgr1*-knockout mice presented a much higher susceptibility to audiogenic seizures (Yagi et al., 2009). Recombinant mutant mice with the deletion of VLGR1 transmembrane and cytoplasmic domains were susceptible to audiogenic seizures (McMillan and White, 2004). A previous study on 48 families with epilepsy with febrile seizures (FSs) identified a nonsense *ADGRV1* variant in a family with two affected siblings, which provided initial clinical evidence on the association between *ADGRV1* and epilepsy (Nakayama et al., 2002). Recent studies have identified ultra-rare *ADGRV1* missense variants in patients with myoclonic epilepsy, FS, genetic generalized epilepsy, and atypical Rolandic epilepsy (Myers et al., 2018; Han et al., 2020; Dahawi et al., 2021; Liu et al., 2022). However, the clinical evidence is generally limited, and the phenotype spectrum of epilepsy is to be defined.

In this study, we screened epilepsy-related genes in 101 unrelated cases with FS or epilepsy with antecedent FS (EFS+) using a targeted sequencing approach and identified eight heterozygous variants and a pair of compound heterozygous variants of *ADGRV1* in nine unrelated cases. The possible impairments of auditory, visual, and vestibular function were also evaluated. We reviewed all reported *ADGRV1* variants and analyzed the correlation between genotype and phenotype, aimed to determine the roles of *ADGRV1* variants in epilepsy and its relationships with audio-visual abnormalities.

SUBJECTS AND METHODS

Subjects

Patients were recruited from the Epilepsy Center of the Second Affiliated Hospital of Guangzhou Medical University and Guangdong Provincial People's Hospital from 2015 to 2021. The cohort consisted of 101 cases with FS-related epilepsy, including 19 cases with FS and 82 cases with EFS+. The detailed clinical information was collected, which contains seizure onset age, seizure type and frequency, course of seizure, response to antiepileptic treatment, family history, and general and neurological examination. Brain magnetic resonance imaging (MRI) scan was conducted to identify structure abnormality. Video electroencephalography (EEG) was performed, and the results were reviewed using two qualified electroencephalographers. Epileptic seizures and epilepsies were

diagnosed according to the criteria of the Commission on Classification and Terminology of the ILAE (1981, 1989, 2001, 2010, and 2017). We used the term FS plus (FS+), as in previous reports (Scheffer and Berkovic, 1997; Singh et al., 1999), to denote individuals with FS extending outside the age range definition of 3 months to 6 years or with afebrile generalized tonic-clonic seizures. The activities of the daily life of the patients with *ADGRV1* variants and their parents (asymptomatic carriers) were evaluated to reflect the subjective characteristics of hearing loss, nyctalopia, constriction of the visual fields, and decreased visual acuity. Further audiometric, ophthalmologic, and vestibular tests were performed to detect any subclinical abnormalities. An audiologic evaluation included pure tone audiometry, transient-evoked otoacoustic emission, and auditory brain stem-evoked response recording using the standard protocol. The ophthalmic test included a general ophthalmic examination, Goldmann perimetry, funduscopy, and full-field electroretinography (ERG). The vestibular function was evaluated using infrared video nystagmography, positional nystagmography, and binaural bithermal caloric testing (Smith et al., 1994).

For the controls, whole-exome sequencing (WES) was performed on 296 healthy Chinese volunteers who served as a normal control group as in our previous report (Consortium, 2013). Frequencies of the identified variants were also compared with that in the other control populations, including East Asian and general populations in the Genome Aggregation Database (gnomAD, gnomad.broadinstitute.org) (Karczewski et al., 2020).

This study adhered to the guidelines of the International Committee of Medical Journal Editors with regard to patient consent for research or participation and received approval from the ethics committee of the hospitals. Written informed consents were provided by the patient's legal guardians.

Targeted Sequencing

All cases were recruited in trios. Blood samples of the probands, their parents, and other available family members were collected to ascertain the source of the variants. Genomic DNA was extracted from blood using the Qiagen Flexi Gene DNA Kit. A gene panel was designed for targeted sequencing on 480 epilepsy-related genes to uncover disease-causing variants (**Supplementary Table 1**). These genes include 62 epilepsy genes, 34 neurodevelopmental epilepsy genes, 159 epilepsy-related genes, 52 potential epilepsy-associated genes, and 173 genes that are suspected to be related to epilepsy, according to the classification of epilepsy-associated genes (Wang et al., 2017).

Raw read data were aligned on the human assembly genome reference consortium human genome build 37 (GRCh37, also known as hg19) using the Burrows-Wheeler Alignment (Li and Durbin, 2010). The single nucleotide variant and indel calling and filtering were performed using the Genome Analysis Toolkit as previously described (DePristo et al., 2011). According to the guidelines for investigating causality of sequence variants in human disease proposed by the U.S. National Human Genome Research Institute (MacArthur et al., 2014) and the interpretation methods in a previous study (Torkamani et al., 2014), a series of filters were applied to derive a set of candidate disease-causing variants in this study. First, population-based filtration removed variants presenting a minor allele frequency (MAF) $\geq$0.005 in the Genome Aggregation Database (gnomad.broadinstitute.org), except for those variants previously reported in the Human Gene Variant Database (HGMD) and/or OMIM database. Second, annotation-based filtration removed variants in segmental duplication regions that are prone to produce false-positive variant calls due to mapping errors. Third, functional impact-based filtration retained frame-shift and nonsense variants. Missense variants were included when predicted to be deleterious in sequence conservation or damaging in protein function by one or more *in silico* tools (http://varcards.biols.ac.cn/). Splice-site variants were included when predicted to have altered splicing using the Human Splicing Finder. Fourth, phenotype-based filtration retained variants based on clinical concordance between the phenotypes of patients and previously reported phenotypes of the mutated genes. Following filtering, Sanger sequencing was employed to validate the potential pathogenic variants. The position number for the variants has been obtained from the start codon, i.e., ATG, of the full-length *ADGRV1* isoform sequence (RefSeq accession number: NG_007083.2).

Molecular Modeling of VLGR1b

Protein modeling was performed by using the Iterative Threading ASSEmbly Refinement (I-TASSER) (Roy et al., 2010) software to evaluate the damaging effect of the amino acid substitution on the VLGR1b protein structure. The confidence of each model was quantitatively measured by a C-score in the range of [−5,2]. The PyMOL Molecular Graphics System (Version 2.3.2; Schrödinger, LLC; New York, USA) was used for three-dimensional protein structure visualization and analysis.

Analysis of Genotype-Phenotype Correlation and Statistics

We reviewed all *ADGRV1* variants from the HGMD (http://www.hgmd.cf.ac.uk/ac/index.php) and PubMed (http://www.ncbi.nlm.nih.gov/pubmed/) up to December 2021.

The audio-visual disorders associated with *ADGRV1* variants were classified into clinical subtypes as Usher type 2 (USH2), Usher type 3 (USH3), nonsyndromic hearing loss, and nonsyndromic retinitis pigmentosa based on the representations in the original reports. USH2 is characterized by moderate to severe congenital sensorineural hearing loss and later development of retinitis pigmentosa. USH3 is relatively milder and characterized by postlingual hearing loss and variable retinitis pigmentosa and vestibular dysfunction (Millan et al., 2011).

Variants are generally classified into destructive and missense variants. Destructive variants are referred to as those causing gross protein malformations and haploinsufficiency, including truncating variants (i.e., nonsense and frameshifting), splice-site variants, and variants with genomic rearrangement (Wei et al., 2017).

The statistical analysis was performed using SPSS version 22.0 (SPSS Inc., Chicago, IL). The frequencies of the *ADGRV1* variants between the epilepsy cohort and the controls were compared by

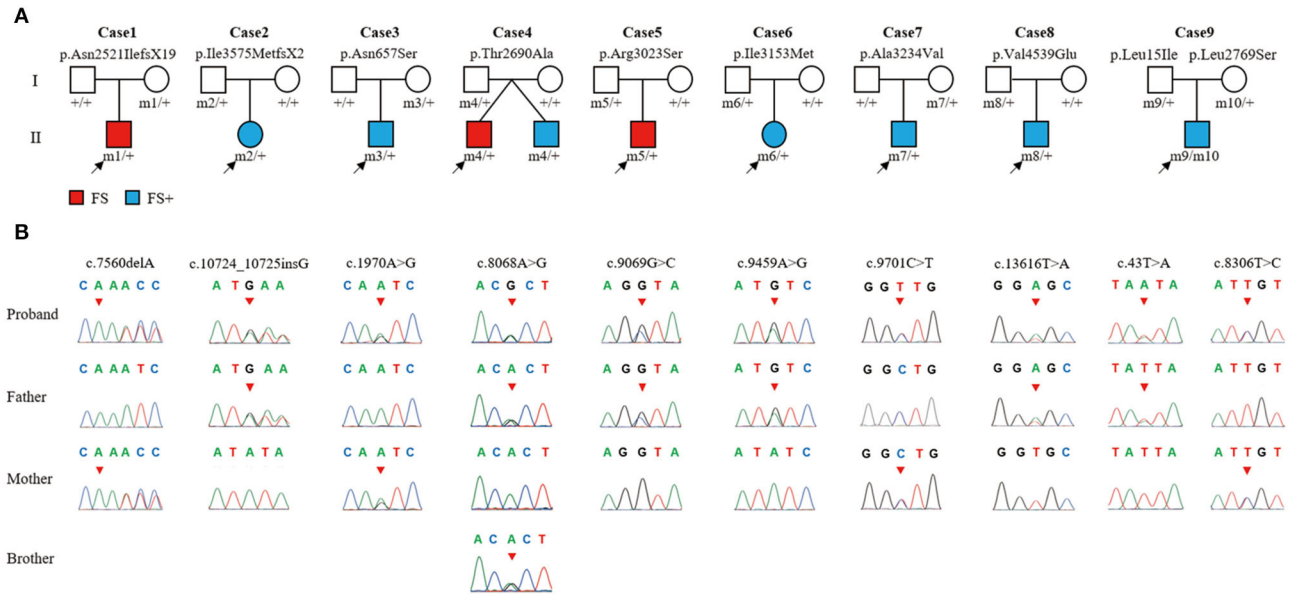

FIGURE 1 | The *ADGRV1* variants identified in the nine cases of febrile seizures or epilepsy with antecedent febrile seizures. **(A)** Pedigrees of the nine cases with *ADGRV1* variants and their corresponding phenotypes. **(B)** DNA sequence chromatograms of the *ADGRV1* variants. Arrows indicate the positions of the nucleotide changes.

a two-sided Fisher's exact test. Fisher's exact test and the chi-square test were used to analyze the variants between epilepsy and audio-visual disorders. Values of $p < 0.05$ (two-sided) were considered significant.

RESULTS

ADGRV1 Variants

In this cohort, 10 *ADGRV1* variants were identified in 9 unrelated cases with FS or FS+ (**Figure 1** and **Table 1**). *ADGRV1* variants identified in this study included two heterozygous frameshift variants (i.e., c.7560delA/p.Asn2521IlefsX19 and c.10724_10725insG/p.Ile3575MetfsX2), six heterozygous missense variants (i.e., c.1970A>G/p.Asn657Ser, c.8086A>G/p.Thr2690Ala, c.9096G>C/p.Arg3023Ser, c.9459A>G/p.Ile3153Met, c.9701C>T/p.Ala3234Val, and c.13616T>A/p.Val4539Glu), and a pair of compound heterozygous variants (i.e., c.43T>A/p.Leu15Ile and c.8306T>C/p.Leu2769Ser). The variant p.Thr2690Ala was identified in a pair of affected twins (Case 4). These variants were inherited from their asymptomatic parents.

The 8 missense variants were absent or presented as rare (MAF <0.005) in the gnomAD database (**Table 2**). The aggregate frequency of these variants in this cohort was significantly higher than that in the controls of 296 normal individuals (11/202 vs. 2/592; $p = 1.10\times10^{-5}$), the gnomAD-all population (vs. 89/203,608; $p < 2.20\times10^{-16}$), the controls of the gnomAD-all population (vs. 43/81,262; $p < 2.20\times10^{-16}$), the gnomAD-East Asian population (vs. 87/14,282, $p = 1.15\times10^{-7}$), and the controls of the gnomAD-East Asian population (vs. 42/6,074, $p = 6.82\times10^{-7}$).

We also identified 25 *SCN1A* variants (including 18 *de novo*) in 25 unrelated cases (24.75%) and 3 *SCN9A* variants in three unrelated cases (2.97%) in this cohort (**Supplementary Table 2**). We did not detect variants in the other potential FS-associated genes (such as *SCN1B*, *GABRG2*, *GABRD*, and *CPA6*) (Wang et al., 2017) in this cohort.

Clinical Features of Epilepsy

Clinical data of the nine cases with *ADGRV1* variants are shown in **Table 1**. Onset ages of FS ranged from the third day of life to 5 years. All cases experienced a few febrile or afebrile generalized tonic-clonic seizures or secondarily generalized tonic-clonic seizures per year.

The representative abnormal EEGs of these cases are shown in **Figure 2**. Initial interictal EEGs were normal in two cases (i.e., cases 4 and 7). A variety of EEG abnormalities was found in the other seven cases. Interictal EEGs of four cases (i.e., cases 2, 5, 6, and 9) showed generalized spike-slow wave discharges, which were less regular or asymmetric in cases 2, 6, and 9 (**Figures 2B,D,E**). Focal sharp, spike, or spike-slow waves were observed in three cases (i.e., cases 1, 3, and 8). The epileptiform waves of cases 1 and 3 were apparently aggravated during slow sleep (**Figures 2A,C**).

All cases presented favorable outcomes. Cases 4, 5, and 7 became seizure-free without any antiepileptic treatment. The other five cases with heterozygous variants had been seizure-free on monotherapy of valproate or oxcarbazepine or lamotrigine. The case with compound heterozygous variants also responded well to antiepileptic drugs (AEDs), but the seizures occasionally recurred, induced by fatigue mostly. The EEGs of all cases

TABLE 1 | Clinical features of individuals with *ADGRV1* variants.

Case	Variant (NM_032119)	Gender	Age	FS onset	aFS onset	Seizure course	Seizure-free duration	Effective AEDs	EEG	Diagnosis
1	c.7560delA (p.Asn2521IlefsX19)	Male	6 yr	3 d	-	GTCS, 2∼4 times/mo	5 yr	LTG	Right central spikes or slow waves	FS
2	c.10724_10725insG (p.Ile3575MetfsX2)	Female	11 yr	4 yr	4 yr	GTCS, 1∼3 times/yr	5 yr	VPA	Generalized spikes and spike-slow waves	FS+
3	c.1970A>G (p.Asn657Ser)	Male	15 yr	8 mo	10 yr	sGTCS, 1 time/yr	3 yr	VPA	Right temporal sharp-slow waves	FS+
4-1	c.8068A>G (p.Thr2690Ala)	Male	12 yr	2 yr	-	GTCS, 1∼2 times/yr	3 yr	-	Normal	FS
4-2		Male	12 yr	2 yr	-	GTCS, 1∼2 times/yr	4 yr	-	Normal	FS+
5	c.9069G>C (p.Arg3023Ser)	Male	12 yr	4 yr	-	GTCS, 1 time/yr	6 yr	-	Generalized spikes and spike-slow waves	FS
6	c.9459A>G (p.Ile3153Met)	Female	11 yr	2 yr	-	GTCS, 1∼2 times/yr	4 yr	VPA	Generalized 2.5-3.0 Hz spike-slow waves and multiple focal spike-slow waves	FS
7	c.9701C>T (p.Ala3234Val)	Male	9 yr	9 mo	3 yr	GTCS, sGTCS, 1∼2 times/yr	4 yr	-	Normal	FS+
8	c.13616T>A (p.Val4539Glu)	Male	11 yr	1 yr	5 yr	GTCS, 1∼2 times/yr	3 yr	VPA	Bilateral parietal single sharp waves	FS+
9	c.43T>A (p.Leu15Ile) c.8306T>C (p.Leu2769Ser)	Male	14 yr	5 yr	6 yr	sGTCS, 1∼3 times/yr	4 yr	OXC, VPA, LTG	Asymmetric generalized spike-slow waves	FS+

AEDs, antiepileptic drugs; aFS, afebrile seizures; d, day; EEG, electroencephalogram; FS, febrile seizures; FS+, febrile seizures plus; GTCS, generalized tonic-clonic seizures; LTG, lamotrigine; mo, month; OXC, oxcarbazepine; sGTCS, secondary generalized tonic–clonic seizure; VPA, valproate; yr, year.

TABLE 2 | Analysis of the aggregate frequency of *ADGRV1* variants identified in this study.

	Allele count/ number in this study	Allele count/number in controls of 296 healthy volunteers	Allele count/number in gnomAD-all populations	Allele count/number in gnomAD-East Asian	Allele count/number in controls of gnomAD-all populations	Allele count/number in controls of gnomAD-East Asian populations
Identified *ADGRV1* variants (NM_032119)						
c.7560delA/p.Asn2521IlefsX19	1/202	-/-	-/-	-/-	-/-	-/-
c.10724_10725insG/p.Ile3575MetfsX2	1/202	-/-	-/-	-/-	-/-	-/-
c.1970A>G/p.Asn657Ser	1/202	-/-	2/247306	0/17910	1/107964	0/8638
c.8068A>G/p.Thr2690Ala	2/202	-/-	13/280314	13/19530	5/119390	5/9552
c.9069G>C/p.Arg3023Ser	1/202	1/592	8/203608	8/14282	4/81262	4/6074
c.9459A>G/p.Ile3153Met	1/202	-/-	-/-	-/-	-/-	-/-
c.9701C>T/p.Ala3234Val	1/202	1/592	52/280398	52/19522	28/119346	28/9546
c.13616T>A/p.Val4539Glu	1/202	-/-	1/247234	1/17890	0/107948	0/8586
c.43T>A/p.Leu15Ile	1/202	-/-	-/-	-/-	-/-	-/-
c.8306T>C/p.Leu2769Ser	1/202	-/-	13/229608	13/16202	5/94586	5/7246
Total	11/202 (0.054)	2/592 (0.0034)	89/203608 (0.0025)	87/14282 (0.032)	43/81262 (0.0029)	42/6074 (0.036)
P value[†]		1.10×10^{-5}	$< 2.20 \times 10^{-16}$	1.15×10^{-7}	$< 2.20 \times 10^{-16}$	6.82×10^{-7}
OR (95% CI)		16.91 (3.65–158.29)	132.13 (62.42–250.90)	9.39 (4.45–18.02)	108.60 (49.78–216.96)	8.26 (3.78–16.65)

[†] *p-values and odds ratio were estimated with a 2-sided Fisher's exact test.*

CI, confidence interval; gnomAD, Genome Aggregation Database; OR, odds ratio.

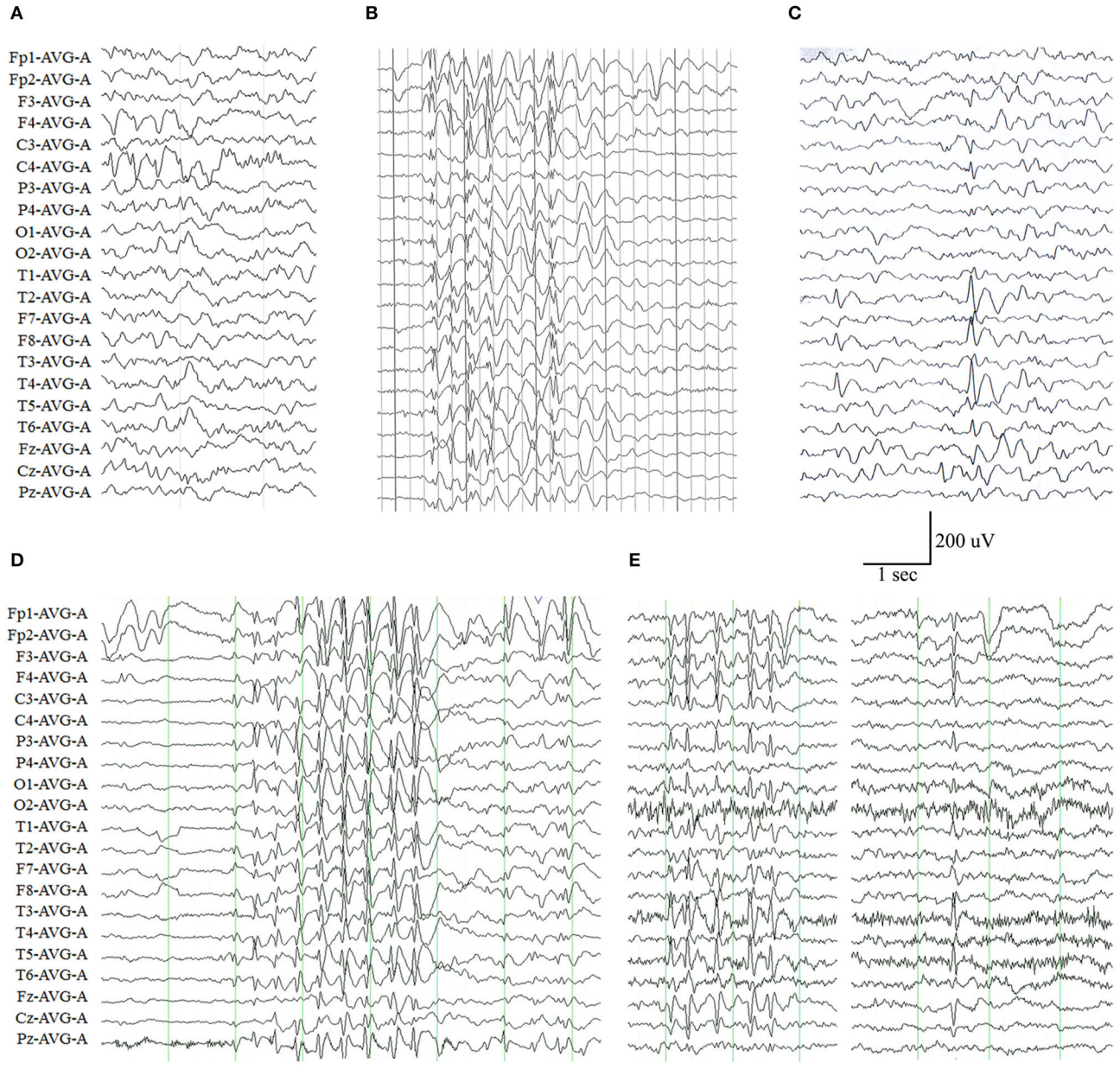

FIGURE 2 | Electroencephalography (EEG) changes in the cases with *ADGRV1* variants. **(A)** Interictal EEG of case 1 at the age of 4 months showed spike-slow waves in the posterior right frontal and central lobes. **(B)** Interictal EEG of case 2 at the age of 6 years showed irregular generalized spike-slow waves. **(C)** Interictal EEG of case 3 at the age of 11 years showed spike-slow waves in the right temporal lobe. **(D)** Interictal EEG of case 6 at the age of 5 years showed asymmetric generalized spike-slow waves. **(E)** Interictal EEG of case 9 at the age of 8 years showed irregular and asymmetric generalized spike-slow waves.

became normal with the achievement of seizure control until the last follow-up.

Clinical Features of Audio-Visual Abnormalities

All cases and the unaffected variant carriers denied problems of audio-visual-vestibular abilities in daily life. A total of six cases (i.e., cases 1, 2, 3, 4, 7, and 9) received audiometric, ophthalmologic, and vestibular tests (**Table 3**). Both cases 4 and 7 did not present any auditory or visual problems. Case 2 revealed mild hearing impairment of the right ear. Case 3 revealed mildly decreased sensitivity of the right horizontal semicircular canal in the caloric test. Case 9, who had compound heterozygous variants, presented both subclinical auditory and visual abnormalities, including mild hearing impairment of the right ear, abnormal visual field, moderately reduced cone function of bilateral eyes, and mildly

reduced rod function of the right eye. His father, who carried variant p.Leu15Ile, revealed mildly reduced cone function of bilateral eyes.

Molecular Alteration of VLGR1

Variants p.Asn2521IlefsX19 and p.Ile3575MetfsX2 resulted in frame shifting and premature termination codons. The two mutants were expected to lack not only the functional domains of epitempin and CalX-β but also the entire membrane-spanning region. Among the 8 missense variants, p.Leu15Ile was located in the signal peptide, and p.Ala3234Val was located in epilepsy-associated repeat 1. The remaining six variants were located in CalX-β domains, namely p.Asn657Ser (CalX-β 5), p.Thr2690Ala (CalX-β 19), p.Leu2769Ser (CalX-β 19), p.Arg3023Ser (CalX-β 21), p.Ile3153Met (CalX-β 22), and p.Val4539Glu (CalX-β 31) (**Supplementary Table 3**). In short, the majority of these missense variants potentially affect the function of CalX-β domains.

To evaluate the potentially damaging effect of the missense variants, protein modeling was performed to analyze the protein structure affected by the substitutions (**Figure 3**). Variants p.Thr2690Ala (from case 4) and p.Ala3234Val (from case 7) did not change their hydrogen bonds. Both cases 4 and 7 presented normal EEGs, were seizure-free without any treatment, and had a normal audio-visual function. Four variants, namely, p.Asn657Ser, p.Arg3023Ser, p.Ile3153Met, and p.Val4539Glu, resulted in new hydrogen bonds with surrounding amino acid residues. Among the compound heterozygous variants, p.Leu15Ile resulted in an extended α-helix structure of the signal peptide, and p.Leu2769Ser formed a new hydrogen bond.

Genotype-Phenotype Correlation

To date, a total of 268 variants in 155 unrelated cases have been reported (**Supplementary Table 3**). Most variants have been identified in patients with audio-visual disorders (240 variants in 130 cases); additional 28 variants have been identified in 25 cases with epilepsy, including 10 variants in this study.

Among the cases with audio-visual abnormalities, USH2 was the most common phenotype with 98 cases reported. There were 23 cases with nonsyndromic hearing loss, four cases with nonsyndromic retinitis pigmentosa, and three cases with USH3. Additionally, two cases with *ADGRV1* variants were reported as unclassified USH, which were not included for further analysis due to the lack of clinic details. The majority of patients with audio-visual disorders (85.16%, 109/128) had biallelic variants (i.e., homozygous and compound heterozygous). In contrast, monoallelic variants were more common in patients with epilepsy (88.00%, 22/25) (**Figure 4A**).

CalX-β motifs are the most recurrent function domains in the ectodomain of VLGR1b. To explore the correlation between the dysfunction of CalX-β motifs and diseases, we analyzed the location of the missense variants identified in different phenotypes (**Supplementary Table 3**). Compared with audio-visual disorders (51.32%, 39/76), the frequency of missense variants located at the CalX-β motif was significantly higher in epilepsy (80.00%, 20/25) (**Figure 4B**).

To explore the relationship between genotype and phenotypic severity among audio-visual disorders, we analyzed the variant constituents of USH2, nonsyndromic deafness, nonsyndromic retinitis pigmentosa, and USH3. Missense variants accounted for 18.38% (34/185) of the variants in USH2, whereas it was 78.05% (32/41) in nonsyndromic hearing loss, and it occurred as the unique variant type in nonsyndromic retinitis pigmentosa (8/8) and USH3 (3/3). There was a significant difference in the frequencies of missense variants between USH2 and nonsyndromic hearing loss or nonsyndromic retinitis pigmentosa or USH3 (**Figure 4C**).

Three main mRNA isoforms, namely VLGR1a, VLGR1b, and VLGR1c, are expressed in humans. Variants at the N-terminal segment (residues 1–2,295) potentially affect isoforms VLGR1b and 1c. Variants at the central segment (residues 2,296–4,339) affect only isoform VLGR1b. Variants at the C-terminal segment (residues 4,340–6,306) affect isoforms VLGR1b and 1a (**Figure 4D**). The frequency of the variants located at the C-terminal segment was significantly higher in audio-visual disorders (38.91%, 93/239) than that in epilepsy (17.85%, 5/28) (**Figure 4D**). Subsequently, the variants associated with epilepsy mainly affected VLGR1b and 1c rather than VLGR1a.

DISCUSSION

This study identified *ADGRV1* variants in nine unrelated cases with FS-related epilepsy, including two heterozygous frameshift variants, six heterozygous missense variants, and a pair of compound heterozygous missense variants. The aggregate frequency of these variants in the case-cohort was significantly higher than that in control populations. The missense variants were located in the functional domains and were predicted to affect the molecular structures by changing the original hydrogen bonds. These clues suggested that *ADGRV1* variants were potentially associated with epilepsy. However, these variants were inherited from their asymptomatic parents, and the affected patients presented few seizures and responded well to AEDs. The incomplete penetrance and mild phenotype indicated that *ADGRV1* variants potentially caused changes in susceptibility.

Febrile seizures are the most common convulsive events in childhood, which may be accompanied by unprovoked seizures and epilepsy. Previously, five genetic loci have been reported to be responsible for FS including *FEB1* on chromosome 8q13–21, *FEB2* on chromosome 19p13.3, *FEB3* on chromosome 2q23–24, *FEB4* on chromosome 5q14-15, and *FEB5* on chromosome 6q22–24 (Johnson et al., 1998; Peiffer et al., 1999; Nakayama et al., 2000). Genes potentially associated with FS-related epilepsy include *SCN1A*, *ADGRV1*, *SCN1B*, *SCN9A*, *GABRG2*, *GABRD*, and *CPA6* (Wang et al., 2017). *SCN1A* variants are the most common causes of FS-related epilepsy, with more than 1,200 variants identified (www.gzneurosci.com/scn1a/database/) (Meng et al., 2015). In this cohort, 24.75% of patients had *SCN1A* variants, which confirmed the causative role of *SCN1A* in FS-related epilepsy. *ADGRV1* variants were identified in 8.91% of the cases and listed as the second, suggesting that *ADGRV1* was one of the candidate genes associated with FS or FS-related epilepsy. The incomplete penetrance suggests that *ADGRV1* variants caused a relatively lower pathogenicity (susceptibility)

TABLE 3 | Audio-visual examination of six patients and their variant-carried parent(s).

Family		Variant (NM_032119)	Pure tone audiometry	Transient evoked otoacoustic emission	ABR	General ophthalmic examination	Fundo-scopy	ERG	Caloric test
1	P	c.7560delA (p.Asn2521IlefsX19)	N	N	N	UA	UA	UA	UA
	M	c.7560delA (p.Asn2521IlefsX19)	N	N	N	-	-	-	-
2	P	c.10724_10725insG (p.Ile3575MetfsX2)	R mild abnormal at low frequency	N	N	N	N	-	N
	F	c.10724_10725insG (p.Ile3575MetfsX2)	-	-	-	-	-	-	-
3	P	c.1970 A>G (p.Asn657Ser)	N	N	N	N	N	N	R horizontal semicircular canal weakness
	M	c.1970 A>G (p.Asn657Ser)	-	-	-	-	-	-	-
4	P	c.8068A>G (p.Thr2690Ala)	N	N	N	N	N	N	-
	B	c.8068A>G (p.Thr2690Ala)	N	N	N	N	N	N	-
	F	c.8068A>G (p.Thr2690Ala)	N	N	N	-	-	-	-
7	P	c.9701C>T (p.Ala3234Val)	N	N	N	N	N	N	-
	F	c.9701C>T (p.Ala3234Val)	N	N	N	N	N	N	-
9	P	c.43T>A (p.Leu15Ile)	R mild abnormal at low frequency	N	N	N	N	Mild-moderate bilateral Cone/R rod degeneration	N
	F	c.8306T>C (p.Leu2769Ser)	N	N	N	N	N	Mild bilateral Cone	N
	M	c.43T>A (p.Leu15Ile) c.8306T>C (p.Leu2769Ser)	N	N	N	N	N	N	N

ABR, auditory brain stem evoked response; B, brother; ERG, full-field electroretinography; F, father; M, mother; N, normal; P, proband; R, right; UA, unavailable (for the age was too young to do the test).

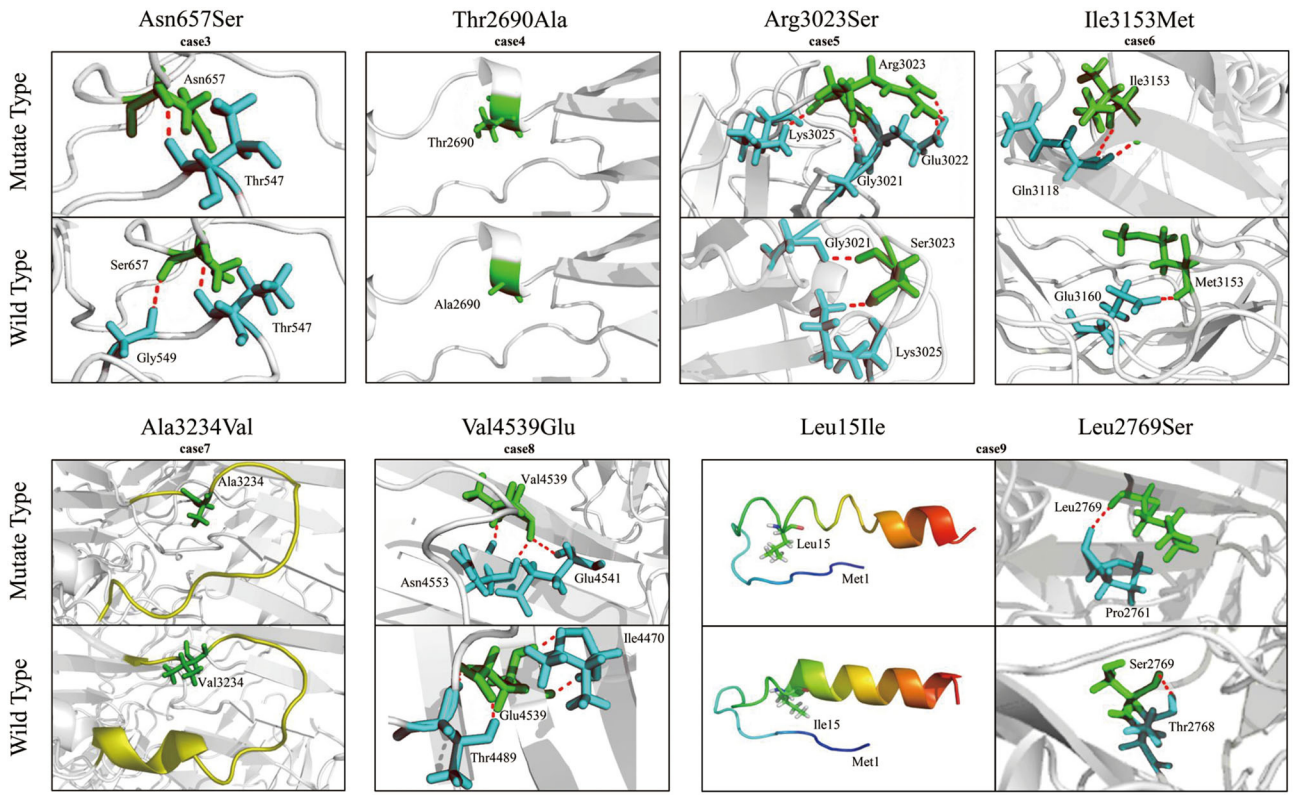

FIGURE 3 | Molecular modeling of VLGR1b and the mutants. Hydrogen bonds were changed in four heterozygous missense variants, namely, Asn657Ser, Arg3023Ser, Ile3153Met, and Val4539Glu. Mutant Thr2690Ala and Ala3234Val did not change any hydrogen bond. Among the compound heterozygous variants, Leu15 is located near an α-helix structure of the signal peptide, and the α-helix structure was extended in the L15I mutant. A new hydrogen bond was formed in the mutant Leu2769Ser. The hydrogen bonds are indicated by dotted red lines.

to epilepsy, coincident with the relatively mild phenotype of FS-related epilepsy shown in this study.

The patients with *ADGRV1* variants presented favorable responses to AEDs, including sodium channel blocker AEDs. In contrast, most patients with FS and FS-related epilepsy caused by *SCN1A* variants, such as Dravet syndrome (Brunklaus et al., 2012) and partial epilepsy with FS plus (Liao et al., 2010), were at risk of seizure aggravation induced by sodium channel blocker AEDs. Therefore, the present findings implied the significance of genetic testing in clinical treatment and management.

ADGRV1 variants p.Asn2521IlefsX19 and p.Ile3575MetfsX2 resulted in the massive deletion of the main functional domains of the VLGR1 protein. Similarly, a nonsense variant p.S2832X of *ADGRV1* (p.S2652X in the *MASS1* isoform) was identified in two FS-affected siblings (Nakayama et al., 2002). Taken together with the evidence from genetic experiments that *Mass1* truncating mutation caused audiogenic seizures in the Frings mouse (Skradski et al., 2001; McMillan and White, 2004; Yagi et al., 2009), it is suggested that the loss of function or haploinsufficiency of *ADGRV1* potentially contributed to the epileptogenesis. Except for p.Leu15Ile and p.Ala3234Val, the remaining twelve missense variants, including six possible pathogenic variants reported previously (Myers et al., 2018), were located at or close to CalX-β motifs and proposed to affect the structures. This evidence suggested that CalX-β motifs were critical for VLGR1 function, and missense variants ruining the CalX-β motif were potentially associated with epilepsy. Indeed, the maintenance and the existence of a highly repeated structure of the VLGR1 protein, such as the multiple CalX-β motifs, were suggested to be essential for protein function (McMillan et al., 2002). The variant p.Ala3234Val was located at epilepsy-associated repeat 1, which is a common domain that existed in proteins encoded by epilepsy-associated genes such as *LGI1* and was proposed to play an important role in the pathogenesis of epilepsy (Staub et al., 2002). Further functional studies are required to determine the impacts of the variants on these functional domains and their roles in epileptogenesis.

On the contrary, most of the currently reported *ADGRV1* variants have been identified in audio-visual disorders. Further analysis demonstrated that biallelic variants were more common in audio-visual disorders than epilepsy (**Figure 4A**). For audio-visual disorders, a destructive variant was the major genotype of the severe phenotype (USH2). In contrast, missense variants were identified in most cases with relatively mild phenotypes, including nonsyndromic hearing loss, nonsyndromic retinitis pigmentosa, and USH3 (**Figure 4C**). These findings suggest that the genetic impairment of *ADGRV1* was associated with the phenotypic severity of audio-visual disorders, particularly concerning hearing loss.

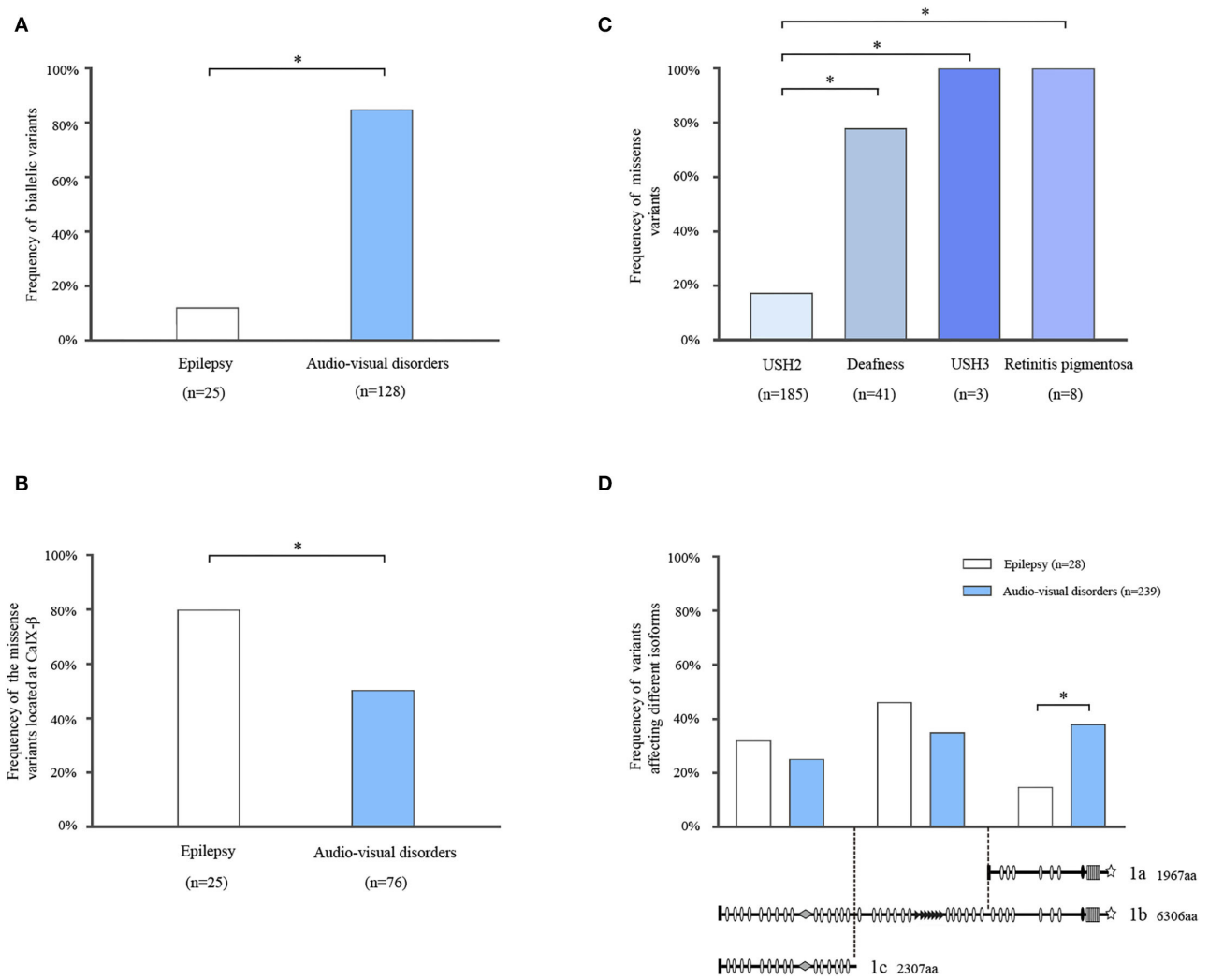

FIGURE 4 | Systematic analysis of *ADGRV1* variants in epilepsy and audio-visual disorders. **(A)** The frequency of biallelic variants in epilepsy and audio-visual disorders. **(B)** The frequency of the missense variants located at the CalX-β motif in epilepsy and audio-visual disorders. **(C)** The frequency of missense variants in different phenotypes of audio-visual disorders. **(D)** The location distribution of the variants in epilepsy and audio-visual disorders. The values are expressed as the percentage of the variants located at the N-terminal segment (residues 1–2,295), central segment (residues 2,296–4,339), and C-terminal segment (residues 4,340–6,306). Fisher's exact test and chi-square test were used for statistical analysis. *means $P < 0.05$.

The patients with FS-related epilepsy in this study did not appear any obvious audio-visual symptoms. Subclinical auditory and visual abnormalities were observed in further tests. Mild hearing impairment was detected in the patient with the heterozygous frameshift variant. Both mild hearing impairment and moderate retinitis pigmentosa were detected in the patient with compound heterozygous variants. Among the patients with the heterozygous missense variant, the patient with the hydrogen bond-changed variant presented horizontal semicircular canal weakness, while the patients carrying the variant without a hydrogen bond change did not suffer from any auditory or visual abnormality. These observations were consistent with the genotype-phenotype correlation between *ADGRV1* and audio-visual disorders. There was the possibility that the hearing impairment and retinitis pigmentosa would aggregate later, like the patients with USH2 or USH3, and the auditory and visual abnormalities might influence the learning and social abilities. It is, therefore, recommended to follow up the patients with *ADGRV1* variants with auditory and visual tests.

A correlation between the severity of the epilepsy phenotype and *ADGRV1* impairment was also suggested in this study. Cases with heterozygous variants presented relatively mild seizures and a good response to AEDs than the patient with compound heterozygous variants, who experienced relatively refractory seizures, and seizure-free was achieved after the combination treatment of AEDs. Additionally, cases 4 and 7 presented normal EEGs and became seizure-free without any treatment, in whom the variants (i.e., p.Thr2690Ala and p.Ala3234Val) did not change the hydrogen bonds in protein modeling. However, the severe phenotype of epilepsy had not been observed in the USH2 cases that carried *ADGRV1* variants of severe genetic impairment. The

mechanism underlying the perplexing phenomenon is unknown, for which two clues from this study may be helpful to explain.

First, the isoforms involved may differ in audio-visual disorders and epilepsy. This study showed that the variants in isoforms VLGR1b and VLGR1c rather than that in VLGR1a appeared more frequently in patients with epilepsy (**Figure 4D**). A previous study suggested that *ADGRV1* variants in USH2 involved isoforms VLGR1b and 1a (Weston et al., 2004). The tissue-specific expression of isoforms is potentially the pathogenic bases of the diverse phenotypic spectrum associated with *ADGRV1*. The RT-PCR study on the mouse embryo demonstrated that Vlgr1b and Vlgr1c were expressed predominantly in the brain ventricular zone and participated in the neurogenesis process (McMillan et al., 2002). Both *Vlgr1*-knockout and recombinant mutant mice presented high susceptibility to audiogenic seizures. This experimental evidence suggested that the isoforms VLGR1b and VLGR1c were associated with the pathogenesis of epilepsy. In contrast, several experimental studies demonstrated that VLGR1a and VLGR1b were critical for the pathogenesis of audio-visual disorders. In hair cells of cochlea, VLGR1 mainly localizes at the ankle region of the stereocilia (McGee et al., 2006). The PDZ domain-binding motifs at the C-terminal end of VLGR1a and VLGR1b have been identified to mediate the interaction with several proteins, the majority of which are members of the ankle-link complex in stereocilia of hair cells. The ankle-link complex plays crucial roles in maintaining the stereociliary integrity and stability and in the hearing signal transduction process (Goodyear et al., 2005). Therefore, the structures and function of VLGR1a and VLGR1b supported their roles in hair cells and auditory disorders.

Second, this study showed that the epilepsy-associated missense variants occurred more frequently in the CalX-β motif than that in audio-visual disorders (**Figure 4B**). The extracellular domain of VLGR1b contains 35 CalX-β motifs, which resemble the regulatory domains of Na^+/Ca^{2+} exchangers (Nikkila et al., 2000). In the central nervous system, Na^+-Ca^{2+} exchanges play a fundamental role in controlling changes in the intracellular concentrations of Na^+ and Ca^{2+} ions that occur in physiologic conditions such as neurotransmitter release, cell migration and differentiation, and gene expression, as well as neurodegenerative processes (Canitano et al., 2002). Therefore, the disrupted function caused by variants in the CalX-β motif was potentially involved with epileptogenesis.

This study has several limitations. Functional studies are needed to determine the damage effects of the variants. The relationships between the functional domains of VLGR1 and epilepsy also warrant further studies. The audio-visual abnormalities in patients with *ADGRV1* variants should be followed up.

In conclusion, we identified 10 *ADGRV1* variants in nine unrelated cases with FS or epilepsy with antecedent FS. The incomplete penetrance and mild phenotype indicated that *ADGRV1* variants potentially caused changes in susceptibility. The genotype, submolecular implication, isoforms, and damaging severity of the variants explained the phenotypical variations. *ADGRV1* variants associated with FS/epilepsy presented favorable responses to AEDs, implying a clinical significance.

DATA AVAILABILITY STATEMENT

The datasets presented in this study can be found in online repositories. The names of the repository/repositories and accession number(s) can be found at: https://www.ncbi.nlm.nih.gov/nuccore/, ON156994-ON157024.

ETHICS STATEMENT

The studies involving human participants were reviewed and approved by the Ethics Committee of the Second Affiliated Hospital of Guangzhou Medical University and Guangdong Provincial People's Hospital. Written informed consent to participate in this study was provided by the participants' legal guardian/next of kin. Written informed consent was obtained from the individual(s), and minor(s)' legal guardian/next of kin, for the publication of any potentially identifiable images or data included in this article.

AUTHOR CONTRIBUTIONS

The study was conceived by YY. The case collection was carried out by BL, PZ, HM, LY, JZ, QZ, YY, NH, XS, WZ, and BH. Variant screening and data analysis were performed by PZ, HM, XLi, WB, ZL, XLe, BT, and TS. The manuscript was written by PZ, HM, and YY. Protein structure modeling was carried out by HL and YM. All authors contributed to the article and approved the submitted version.

FUNDING

This study was supported by grants from the National Natural Science Foundation of China (Grant Nos. 81870903, 81971216, and 82071548), National Key Research and Development Program of China (Grant No. 2016YFC1306200), Natural Science Foundation of Guangdong Province (Grant No. 2020A1515010108), Science and Technology Project of Guangzhou (Grant Nos. 201904010292 and 201904020028), Science and Technology Project of Guangdong Province (Grant No. 2017B030314159), and Multi-Center Clinical Research Fund Project of the Second Affiliated Hospital of Guangzhou Medical University (Grant No. 2020-LCYJ-DZX-03). The funders had no role in the study design, data collection and analysis, and decision to publish or preparation of the manuscript.

ACKNOWLEDGMENTS

The authors are very much grateful to the families who participated in this research.

SUPPLEMENTARY MATERIAL

The Supplementary Material for this article can be found online at: https://www.frontiersin.org/articles/10.3389/fnmol.2022.864074/full#supplementary-material

REFERENCES

Beckmann, G., Hanke, J., Bork, P., and Reich, J. G. (1998). Merging extracellular domains: fold prediction for laminin G-like and amino-terminal thrombospondin-like modules based on homology to pentraxins. *J. Mol. Biol.* 275, 725–730. doi: 10.1006/jmbi.1997.1510

Brunklaus, A., Ellis, R., Reavey, E., Forbes, G. H., and Zuberi, S. M. (2012). Prognostic, clinical and demographic features in SCN1A mutation-positive Dravet syndrome. *Brain* 135, 2329–2336. doi: 10.1093/brain/aws151

Canitano, A., Papa, M., Boscia, F., Castaldo, P., Sellitti, S., Taglialatela, M., et al. (2002). Brain distribution of the Na+/Ca2+ exchanger-encoding genes NCX1, NCX2, and NCX3 and their related proteins in the central nervous system. *Ann. N. Y. Acad. Sci.* 976, 394–404. doi: 10.1111/j.1749-6632.2002.tb04766.x

Consortium, G. (2013). The Genotype-Tissue Expression (GTEx) project. *Nat. Genet.* 45, 580–585. doi: 10.1038/ng.2653

Dahawi, M., Elmagzoub, M. S., Ahmed, E. A., Baldassari, S., Achaz, G., et al. (2021). Involvement of gene in familial forms of genetic generalized epilepsy. *Front. Neurol.* 12, 738272. doi: 10.3389/fneur.2021.738272

DePristo, M. A., Banks, E., Poplin, R., Garimella, K. V., Maguire, J. R., Hartl, C., et al. (2011). A framework for variation discovery and genotyping using next-generation DNA sequencing data. *Nat. Genet.* 43, 491–498. doi: 10.1038/ng.806

Goodyear, R. J., Marcotti, W., Kros, C. J., and Richardson, G. P. (2005). Development and properties of stereociliary link types in hair cells of the mouse cochlea. *J. Comp. Neurol.* 485, 75–85. doi: 10.1002/cne.20513

Han, J. Y., Lee, H. J., Lee, Y.-M., and Park, J. (2020). Identification of missense mutation as a candidate genetic cause of familial febrile seizure 4. *Children (Basel, Switzerland)* 7, 144. doi: 10.3390/children7090144

Johnson, E. W., Dubovsky, J., Rich, S. S., O'Donovan, C. A., Orr, H. T., Anderson, V. E., et al. (1998). Evidence for a novel gene for familial febrile convulsions, FEB2, linked to chromosome 19p in an extended family from the Midwest. *Hum. Mol. Genet.* 7, 63–67. doi: 10.1093/hmg/7.1.63

Kalachikov, S., Evgrafov, O., Ross, B., Winawer, M., Barker-Cummings, C., Martinelli Boneschi, F., et al. (2002). Mutations in LGI1 cause autosomal-dominant partial epilepsy with auditory features. *Nat. Genet.* 30, 335–341. doi: 10.1038/ng832

Karczewski, K. J., Francioli, L. C., Tiao, G., Cummings, B. B., Alfoldi, J., Wang, Q., et al. (2020). The mutational constraint spectrum quantified from variation in 141,456 humans. *Nature* 581, 434–443. doi: 10.1038/s41586-020-2308-7

Li, H., and Durbin, R. (2010). Fast and accurate long-read alignment with Burrows-Wheeler transform. *Bioinformatics* 26, 589–595. doi: 10.1093/bioinformatics/btp698

Liao, W.-P., Shi, Y.-W., Long, Y.-S., Zeng, Y., Li, T., Yu, M.-J., et al. (2010). Partial epilepsy with antecedent febrile seizures and seizure aggravation by antiepileptic drugs: associated with loss of function of Na(v)1.1. *Epilepsia* 51, 1669–1678. doi: 10.1111/j.1528-1167.2010.02645.x

Liu, Z., Ye, X., Zhang, J., Wu, B., Dong, S., and Gao, P. (2022). Biallelic ADGRV1 variants are associated with Rolandic epilepsy. *Neurol. Sci.* 43, 1365–1374. doi: 10.1007/s10072-021-05403-y

MacArthur, D. G., Manolio, T. A., Dimmock, D. P., Rehm, H. L., Shendure, J., Abecasis, G. R., et al. (2014). Guidelines for investigating causality of sequence variants in human disease. *Nature* 508, 469–476. doi: 10.1038/nature13127

McGee, J., Goodyear, R. J., McMillan, D. R., Stauffer, E. A., Holt, J. R., Locke, K. G., et al. (2006). The very large G-protein-coupled receptor Vlgr1: a component of the ankle link complex required for the normal development of auditory hair bundles. *J. Neurosci.* 26, 6543–6553. doi: 10.1523/jneurosci.0693-06.2006

McMillan, D. R., Kayes-Wandover, K. M., Richardson, J. A., and White, P. C. (2002). Very large G protein-coupled receptor-1, the largest known cell surface protein, is highly expressed in the developing central nervous system. *J. Biol. Chem.* 277, 785–792. doi: 10.1074/jbc.M108929200

McMillan, D. R., and White, P. C. (2004). Loss of the transmembrane and cytoplasmic domains of the very large G-protein-coupled receptor-1 (VLGR1 or Mass1) causes audiogenic seizures in mice. *Mol. Cell. Neurosci.* 26, 322–329. doi: 10.1016/j.mcn.2004.02.005

McMillan, D. R., and White, P. C. (2010). Studies on the very large G protein-coupled receptor: from initial discovery to determining its role in sensorineural deafness in higher animals. *Adv. Exp. Med. Biol.* 706, 76–86. doi: 10.1007/978-1-4419-7913-1_6

Meng, H., Xu, H.-Q., Yu, L., Lin, G.-W., He, N., Su, T., et al. (2015). The SCN1A mutation database: updating information and analysis of the relationships among genotype, functional alteration, and phenotype. *Hum. Mutat.* 36, 573–580. doi: 10.1002/humu.22782

Millan, J. M., Aller, E., Jaijo, T., Blanco-Kelly, F., Gimenez-Pardo, A., and Ayuso, C. (2011). An update on the genetics of usher syndrome. *J. Ophthalmol.* 2011, 417217–417217. doi: 10.1155/2011/417217

Myers, K. A., Nasioulas, S., Boys, A., McMahon, J. M., Slater, H., Lockhart, P., et al. (2018). ADGRV1 is implicated in myoclonic epilepsy. *Epilepsia* 59, 381–388. doi: 10.1111/epi.13980

Nakayama, J., Fu, Y.-H., Clark, A. M., Nakahara, S., Hamano, K., Iwasaki, N., et al. (2002). A nonsense mutation of the MASS1 gene in a family with febrile and afebrile seizures. *Ann. Neurol.* 52, 654–657. doi: 10.1002/ana.10347

Nakayama, J., Hamano, K., Iwasaki, N., Nakahara, S., Horigome, Y., Saitoh, H., et al. (2000). Significant evidence for linkage of febrile seizures to chromosome 5q14-q15. *Hum. Mol. Genet.* 9, 87–91. doi: 10.1093/hmg/9.1.87

Neubig, R. R., and Siderovski, D. P. (2002). Regulators of G-protein signalling as new central nervous system drug targets. *Nat. Rev. Drug. Discov.* 1, 187–197. doi: 10.1038/nrd747

Nikkila, H., McMillan, D. R., Nunez, B. S., Pascoe, L., Curnow, K. M., and White, P. C. (2000). Sequence similarities between a novel putative G protein-coupled receptor and Na+/Ca2+ exchangers define a cation binding domain. *Mol. Endocrinol.* 14, 1351–1364. doi: 10.1210/mend.14.9.0511

Peiffer, A., Thompson, J., Charlier, C., Otterud, B., Varvil, T., Pappas, C., et al. (1999). A locus for febrile seizures (FEB3) maps to chromosome 2q23-24. *Ann. Neurol.* 46, 671–678. doi: 10.1002/1531-8249(199910)46:4<671::Aid-ana20>3.0.Co;2-5

Pons, T., Gomez, R., Chinea, G., and Valencia, A. (2003). Beta-propellers: associated functions and their role in human diseases. *Curr. Med. Chem.* 10, 505–524. doi: 10.2174/0929867033368204

Roy, A., Kucukural, A., and Zhang, Y. (2010). I-TASSER: a unified platform for automated protein structure and function prediction. *Nat. Protoc.* 5, 725–738. doi: 10.1038/nprot.2010.5

Scheel, H., Tomiuk, S., and Hofmann, K. (2002). A common protein interaction domain links two recently identified epilepsy genes. *Hum. Mol. Genet.* 11, 1757–1762. doi: 10.1093/hmg/11.15.1757

Scheffer, I. E., and Berkovic, S. F. (1997). Generalized epilepsy with febrile seizures plus. A genetic disorder with heterogeneous clinical phenotypes. *Brain* 120 (Pt 3), 479–490. doi: 10.1093/brain/120.3.479

Singh, R., Scheffer, I. E., Crossland, K., and Berkovic, S. F. (1999). Generalized epilepsy with febrile seizures plus: a common childhood-onset genetic epilepsy syndrome. *Ann. Neurol.* 45, 75–81. doi: 10.1002/1531-8249(199901)45:1<75::Aid-art13>3.0.Co;2-w

Skradski, S. L., Clark, A. M., Jiang, H., White, H. S., Fu, Y. H., and Ptacek, L. J. (2001). A novel gene causing a mendelian audiogenic mouse epilepsy. *Neuron* 31, 537–544. doi: 10.1016/s0896-6273(01)00397-x

Smith, R. J., Berlin, C. I., Hejtmancik, J. F., Keats, B. J., Kimberling, W. J., Lewis, R. A., et al. (1994). Clinical diagnosis of the Usher syndromes. Usher syndrome consortium. *Am. J. Med. Genet.* 50, 32–38. doi: 10.1002/ajmg.1320500107

Staub, E., Perez-Tur, J., Siebert, R., Nobile, C., Moschonas, N. K., Deloukas, P., et al. (2002). The novel EPTP repeat defines a superfamily of proteins implicated in epileptic disorders. *Trends Biochem. Sci.* 27, 441–444. doi: 10.1016/s0968-0004(02)02163-1

Sun, J.-P., Li, R., Ren, H.-Z., Xu, A.-T., Yu, X., and Xu, Z.-G. (2013). The very large G protein coupled receptor (Vlgr1) in hair cells. *J. Mol. Neurosci.* 50, 204–214. doi: 10.1007/s12031-012-9911-5

Togashi, H., Abe, K., Mizoguchi, A., Takaoka, K., Chisaka, O., and Takeichi, M. (2002). Cadherin regulates dendritic spine morphogenesis. *Neuron* 35, 77–89. doi: 10.1016/s0896-6273(02)00748-1

Torkamani, A., Bersell, K., Jorge, B. S., Bjork, R. L. Jr., Friedman, J. R., Bloss, C. S., et al. (2014). De novo KCNB1 mutations in epileptic encephalopathy. *Ann. Neurol.* 76, 529–540. doi: 10.1002/ana.24263

Wang, J., Lin, Z.-J., Liu, L., Xu, H.-Q., Shi, Y.-W., Yi, Y.-H., et al. (2017). Epilepsy-associated genes. *Seizure* 44, 11–20. doi: 10.1016/j.seizure.2016.11.030

Wei, F., Yan, L.-M., Su, T., He, N., Lin, Z.-J., Wang, J., et al. (2017). Ion channel genes and epilepsy: functional alteration, pathogenic potential, and mechanism of epilepsy. *Neurosci. Bull.* 33, 455–477. doi: 10.1007/s12264-017-0134-1

Weston, M. D., Luijendijk, M. W. J., Humphrey, K. D., Moller, C., and Kimberling, W. J. (2004). Mutations in the VLGR1 gene implicate G-protein signaling in

the pathogenesis of Usher syndrome type II. *Am. J. Hum. Genet.* 74, 357–366. doi: 10.1086/381685

Yagi, H., Noguchi, Y., Kitamura, K., and Sato, M. (2009). Deficiency of Vlgr1 resulted in deafness and susceptibility to audiogenic seizures while the degree of hearing impairment was not correlated with seizure severity in C57BL/6-and 129-backcrossed lines of Vlgr1 knockout mice. *Neurosci. Lett.* 461, 190–195. doi: 10.1016/j.neulet.2009.06.012

Conflict of Interest: HL and YM were employed by BGI-Shenzhen.

The remaining authors declare that the research was conducted in the absence of any commercial or financial relationships that could be construed as a potential conflict of interest.

Publisher's Note: All claims expressed in this article are solely those of the authors and do not necessarily represent those of their affiliated organizations, or those of the publisher, the editors and the reviewers. Any product that may be evaluated in this article, or claim that may be made by its manufacturer, is not guaranteed or endorsed by the publisher.

Advantages of publishing in Frontiers

OPEN ACCESS
Articles are free to read for greatest visibility and readership

FAST PUBLICATION
Around 90 days from submission to decision

HIGH QUALITY PEER-REVIEW
Rigorous, collaborative, and constructive peer-review

TRANSPARENT PEER-REVIEW
Editors and reviewers acknowledged by name on published articles

Frontiers
Avenue du Tribunal-Fédéral 34
1005 Lausanne | Switzerland

Visit us: www.frontiersin.org
Contact us: frontiersin.org/about/contact

REPRODUCIBILITY OF RESEARCH
Support open data and methods to enhance research reproducibility

DIGITAL PUBLISHING
Articles designed for optimal readership across devices

FOLLOW US
@frontiersin

IMPACT METRICS
Advanced article metrics track visibility across digital media

EXTENSIVE PROMOTION
Marketing and promotion of impactful research

LOOP RESEARCH NETWORK
Our network increases your article's readership